Solving the Mysteries of the Solid Elements (From the Origin of Elements to Machine Parts)

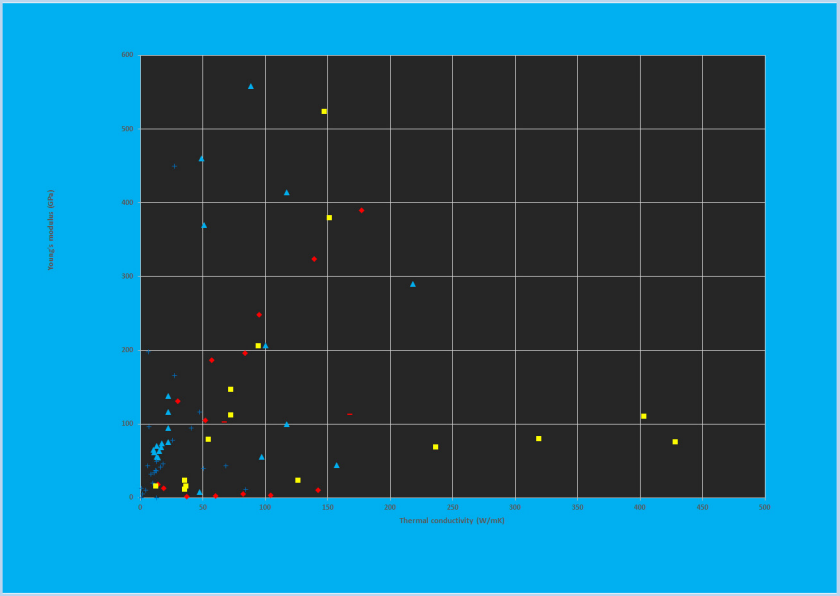

Yoshiharu Mae

Solving the Mysteries of the Solid Elements (From the Origin of Elements to Machine Parts)

Solving the Mysteries of the Solid Elements (From the Origin of Elements to Machine Parts)

By

Yoshiharu Mae

Cambridge
Scholars
Publishing

Solving the Mysteries of the Solid Elements
(From the Origin of Elements to Machine Parts)

By Yoshiharu Mae

This book first published 2019

Cambridge Scholars Publishing

Lady Stephenson Library, Newcastle upon Tyne, NE6 2PA, UK

British Library Cataloguing in Publication Data
A catalogue record for this book is available from the British Library

ISBN (10): 1-5275-4004-9
ISBN (13): 978-1-5275-4004-0

TABLE OF CONTENTS

PREFACE

Most of the elements on the periodic table are solid elements. The solid elements have various properties, respectively. Frequently, the properties of the elements are listed at the end of books on materials science or metallurgy. But they are only shown as a matter of form. The reasons why each element has such properties are not shown.

The periodic table is the only one which shows the relative relationship to each other among elements. But it is a pity that it shows only the similarities of chemical properties in the same group.

It shows very little about the atomic radius, crystal structure, melting point, Young's modulus, thermal conductivity and so on.

Furthermore, the similarity of the chemical properties is only valid at the elements in the 1^{st}, 2^{nd}, 18^{th} group – alkali metals, alkaline earth metals and halogen.

For example, the elements in the 14^{th} group – C, Si, Ge, Sn, and Pb – show very different chemical properties. Shortly, the periodic table shows very little about the solid elements.

Taking these situations into consideration, a new representation of the elements is desired.

This author has set two assumptions.

In general, the main characteristics of the solid elements are their crystal structures and their possession of free electrons.

Among many physical properties, lattice strength, as represented by Young's modulus, and free electron mobility, as represented by thermal conductivity, were therefore selected for their characterization.

Consequently, a diagram was made with the thermal conductivity on the abscissa and the Young's modulus on the ordinate, and each element was plotted on the diagram. This diagram was referred to as the **"thermal conductivity-Young's modulus" (TC-YM) diagram.**

On the other hand, there are many mysteries in the solid elements. For instance, most of the solid elements adopt various crystal structures. But it is not known whether there is a rule which determines the crystal structures of the elements. There are many other mysteries left unsolved in the solid elements.

Here, the results of the studies having applied the TC-YM diagram to these mysteries will be shown.

This book is full of many original figures which mankind has never seen about the basic properties of elements.

1. PREPARATION OF THE KEY FOR SOLVING THE MYSTERIES OF THE SOLID ELEMENTS

Looking at books on the solid elements, the various properties of the elements such as atomic number, atomic mass, density, atomic volume, melting point, boiling point, specific heat, fusion heat, linear expansion coefficient, thermal conductivity, electrical resistance, Young's modulus, crystal structures, lattice constant, etc., are listed in a table. They are shown equally.

In the properties of the elements, there are **base quantities** and **derived quantities**. The density of the element is clearly a derived quantity, because it is determined by the atomic mass, atomic radius and the crystal structure. The base quantity is a quantity which cannot be determined by other quantities. But, in practice, it is difficult to judge which are the base quantities and derived quantities in the material properties of the elements. For instance, the melting temperature and the Young's modulus are considered to be base quantities and independent of each other. But it can be speculated that the melting temperatures of elements are determined by the Young's modulus. Fig. 1-1 shows the relationship between the melting temperatures of elements and the Young's moduli of elements.

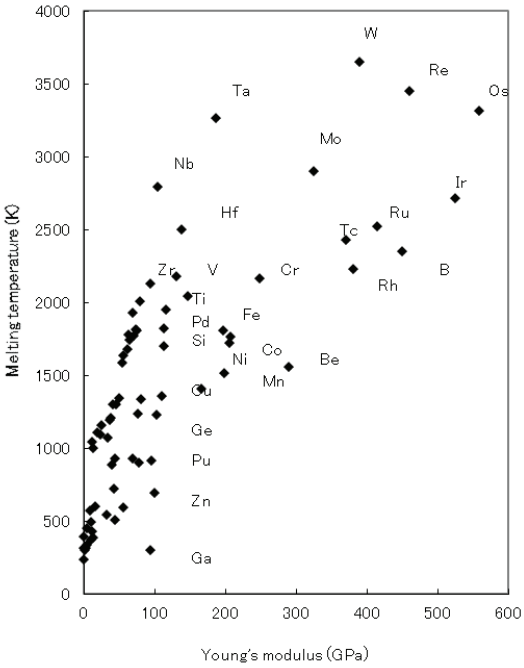

Fig. 1-1 – Melting temperatures of elements as a parameter of Young's modulus

A rough tendency that the melting temperature is proportional to the Young's modulus is recognized. But, W having the highest melting temperature does not have the largest Young's modulus. In addition, the elements possessing a similar Young's modulus of about 100 GPa – Ga, Zn, Pu, Ge, Cu, Si, Pd, Ti, and Zr – show a very large range of melting temperature.

Therefore, it can be speculated that it is impossible to represent one property with one base quantity such as Young's modulus, and at least one more base quantity would be necessary. Two base quantities and one property form

three-dimensional space, and can be displayed on the plane, if the property is shown by layers. More than two base quantities cannot be displayed on a plane. Therefore, two base quantities were sought in this study.

As a result, the Young's modulus and thermal conductivity were selected as two base quantities.

The reason why the elements possessing a similar Young's modulus of about 100 GPa – Ga, Zn, Pu, Ge, Cu, Si, Ti, and Zr – show a very wide range of melting temperatures will be shown in Chapter 4.

1.1 Introduction of the TC-YM diagram

This author has introduced a new diagram to explain the behaviors of elements. In general, the main characteristics of the metallic elements are metallic bonding of atoms and the existence of free electrons.

Among many physical properties, the Young's modulus was selected as a representative index for the strength of the lattice; thermal conductivity was selected as a representative index for the characteristics of free electrons.

Young's modulus is a gradient of the stress-strain curve in the region of elasticity in the tensile test, as shown in Fig. 1-2.

The Young's modulus relates also to the atomic structures of the materials. Fig. 1-3 shows the interatomic force between two atoms. [1]

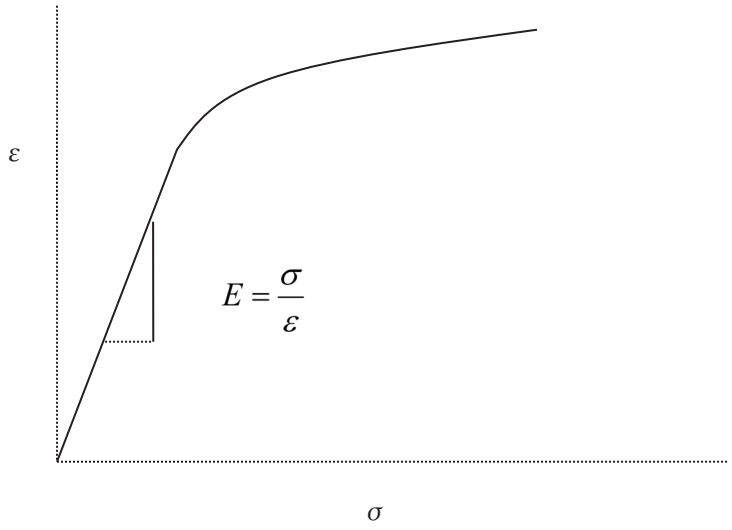

Fig. 1-2 – Stress-strain curve of a tensile specimen and its Young's modulus

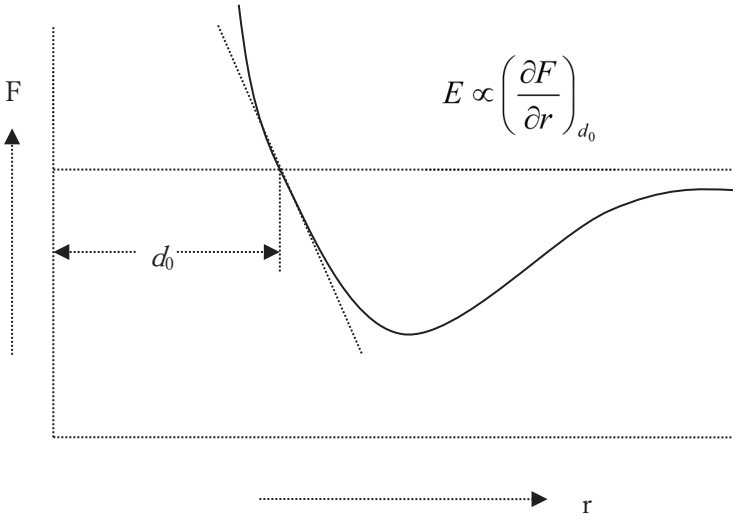

Fig. 1-3 – Interatomic force versus interatomic distance

The repulsive force acts within d_0, and the attractive force acts outside d_0. The gradient of the tangent at d_0 is proportional to the Young's modulus. Therefore, the Young's modulus is a substantial factor which represents the state of atoms.

Consequently, a diagram was made with the thermal conductivity on the abscissa and the Young's modulus on the ordinate, and each element was plotted on the diagram. This diagram will be referred to as the "thermal conductivity-Young's modulus" (TC-YM) diagram.

Young's modulus is generally thought to be an engineering factor, but it is a physically fundamental factor: The Young's modulus is proportional to the gradient of the tangent of the curve of the Condon-Morse force between atoms at an equivalent atomic distance [1] i.e., proportional to the second-order differential of the binding potential between two atoms at equivalent atomic distance. [2] Young's modulus is therefore a good index to represent the binding state of atoms.

Thermal conductivity can be considered to be related to the mobility of free electrons in atoms. This is also a physically fundamental factor.

A diagram with thermal conductivity on the abscissa and Young's modulus on the ordinate (TC–YM diagram) can therefore reflect the essential properties of atoms of the metallic and semi-metallic elements.

The thermal conductivity is said to come from both the free electron transfer and the lattice vibration. [3] The ratio of the thermal conductivity to the electrical conductivity is constant at room temperature and is called the Wiedemann-Franz law. [4] Fig. 1-4 shows the relationship of solid elements

between the thermal conductivity and the electrical conductivity.

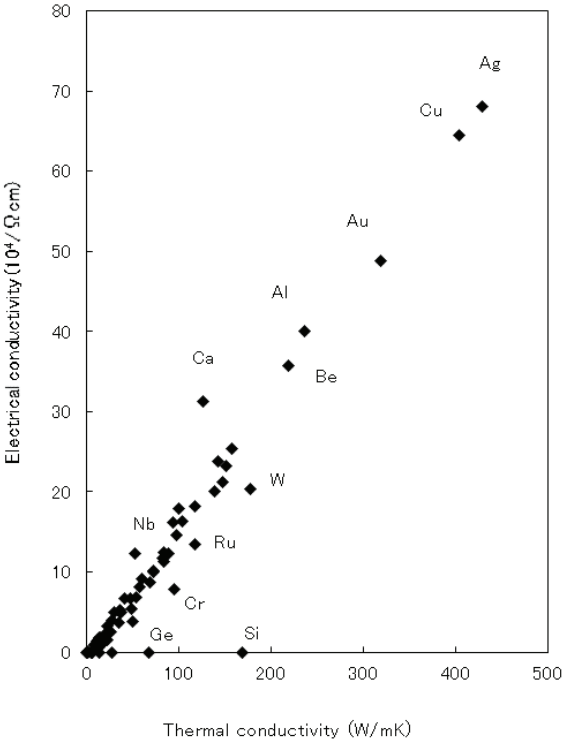

Fig. 1-4 – Relationship in the elements between the thermal conductivity and the electrical conductivity

Except for the semi-conductor elements Ge and Si, the thermal conductivity is proportional to the electrical conductivity in all solid elements. Fig. 1-4 shows that the thermal conductivity is covered by the free electrons in the solid elements.

Then, how about the contribution of the lattice vibration to the thermal conductivity?

To examine this, the result of taking the correlation between the thermal conductivity and the Young's modulus as the factor of lattice vibration is this TC-YM diagram. The result is shown in Fig. 1-5. [5]

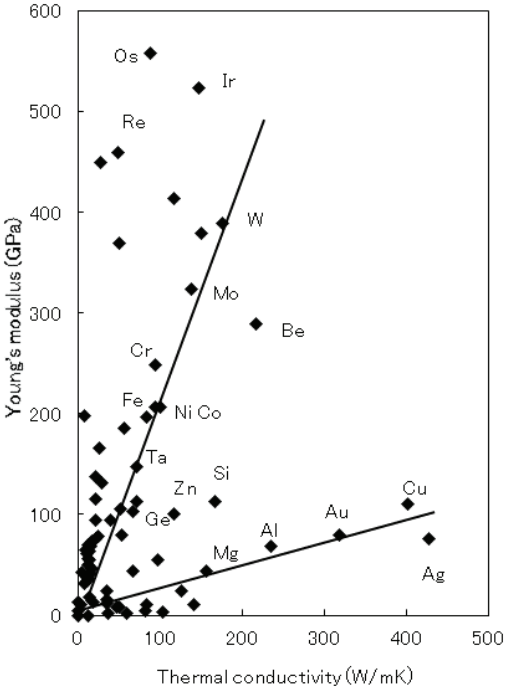

Fig. 1-5 – Relationship in the elements between the thermal conductivity and the Young's modulus

At first glance at this figure, this author felt that there were some patterns hidden in it. **It was felt as if it were a starry sky of elements viewed from**

the window of a house. Some constellations can be seen. What does each constellation mean? This is the subject of this book.

In this case, the semiconductor elements – Ge and Si – are contained in the figure. Moreover, Ge and Si show behaviors similar to the nearby elements such as the alloying elements, as shown subsequently. Further, the half metallic elements, such as As, Se, Te, and I, show the intrinsic characteristics according to their positions in the TC-YM diagram. In this way, the TC-YM diagram shows the characteristics of most solid elements, including metallic, semiconductor and half metallic elements.

As shown in Fig. 1-5, there is an element group of Mg, Al, Au, and Cu in which the thermal conductivity abruptly increases with only a slight increase of the Young's modulus, and there is an element group of Ta, Fe, Ni, Co, Cr, Mo, and W in which the thermal conductivity increases modestly with the increase of the Young's modulus. However, there are many additional elements that are randomly distributed in the TC-YM diagram.

As shown in Fig. 1-4, the thermal conductivity is covered by the transfer of the free electrons; therefore, the Young's modulus is freed from the contribution to the thermal conductivity, and is able to take free values, enabling the elements of high thermal conductivity and low Young's modulus and those of low thermal conductivity and high Young's modulus.

To confirm the validity of this diagram, firstly, it was tested if the diagram could show the crystal structures of elements significantly.

Fig. 1-6 shows the distribution of the crystal structures of various elements in a TC-YM diagram.

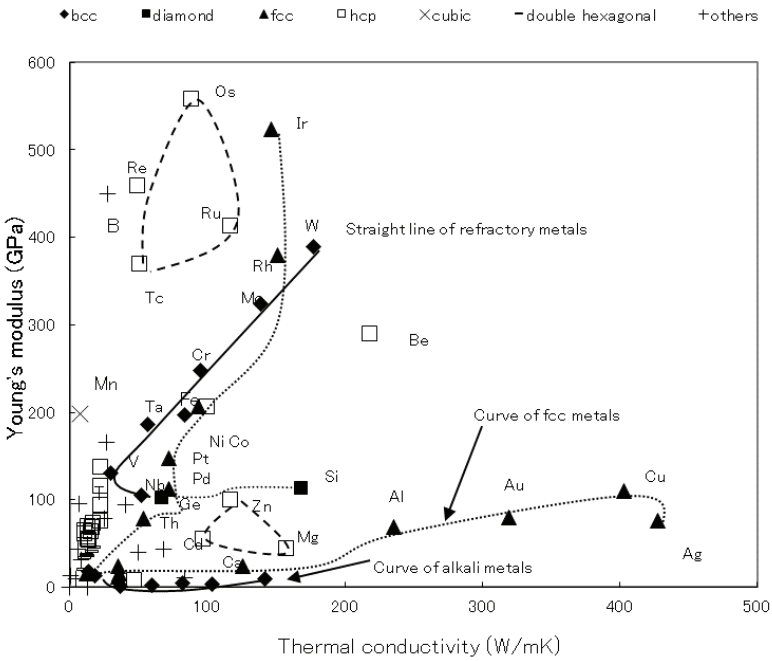

Fig. 1-6 – Crystal structures of elements shown on the TC-YM diagram

The crystal structures are classified as body-centered-cubic (bcc), face-centered-cubic (fcc), hexagonal-close-packed (hcp), diamond structured, and “others” for miscellaneous structures. [6] The most remarkable feature of Fig. 1-6 is that the bcc-structured elements mostly lie on a straight line, connecting V, Ta, Cr, Mo, and W, which can be called *the straight line of refractory metals*. At the moment this author looked at this, he was convinced of the validity of the diagram. Iron is located near this line.

Additionally, elements with fcc structures lie on a clear curve, which can be called *the curve of fcc metals*. It took some time for this author to find the

curve of fcc metals. When he did, he was convinced further of the validity of the diagram.

In contrast, bcc-structured alkali metals lie on a curve near the abscissa (*the curve of alkali metals*). Elements with hcp and other structures are distributed elsewhere. Lanthanides gather tightly in the low Young's modulus and low thermal conductivity region. In the periodic table, the lanthanides are shown outside the table, and the relationships with other elements are lost.

The TC-YM diagram, therefore, shows clear patterns with respect to the crystal structures of elements. Other elemental properties, such as atomic radius, melting temperature, thermal expansion, boiling point, heat of fusion, vapor pressure, heat capacity, electronegativity, and ionization energy, also show clear patterns in TC-YM diagrams.

The details of the crystal structures will be discussed in Chapter 2.

1.2 Distribution of elements on the TC-YM diagram per period in the periodic table

There was an examination of the kind of relationship that exists between the TC-YM diagram and the periodic table.

Fig. 1-7 shows the distribution of elements of the 2^{nd}, 3^{rd}, and 4^{th} periods on the TC-YM diagram, respectively. The elements of the same period draw a cycle. It starts from the bottom of the diagram, and goes up toward the high thermal conductivity and high Young's modulus region. And then, it decreases the thermal conductivity and finally decreases the Young's

modulus and goes down to the origin of the diagram. With the increasing period number, the form of the cycle becomes complicated.

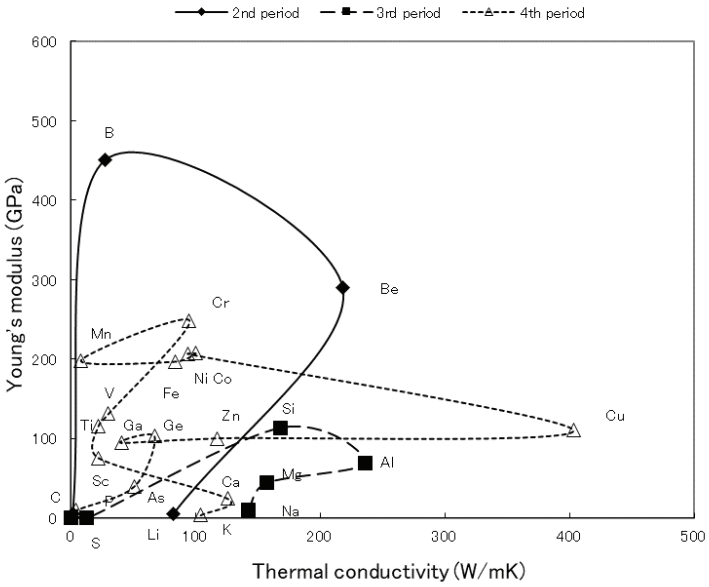

Fig. 1-7 – Distribution of elements of the 2nd, 3rd, and 4th periods on the TC-YM diagram

Fig. 1-8 shows the distribution of elements of the 5th, 6th, and 7th periods on the TC-YM diagram, respectively. The elements of each period draw a complicated cycle. It starts from the bottom, goes up with decreasing conductivity, and then goes up further with increasing conductivity. After reaching the peak, it goes down with decreasing conductivity. And then, it increases the conductivity abruptly. After that, it again decreases the conductivity abruptly and ends near the origin.

Young's modulus of Tc: Tc is an unstable and radioactive element. It is

said that Tc is the first man-made element. Data on its Young's modulus are missing. As shown in Fig. 1-8, the forms of the cycles of the 5th period and the 6th period are similar to each other. The thermal conductivity of Tc is reported to be 50.6 W/mK. Therefore, the Young's modus of Tc can be speculated to be around 370 GPa from the similarity of the forms of the cycles. The speculated position of Tc is plotted on Fig. 1-8. This position of Tc on the TC-YM diagram will be proved to be valid in other properties of Tc.

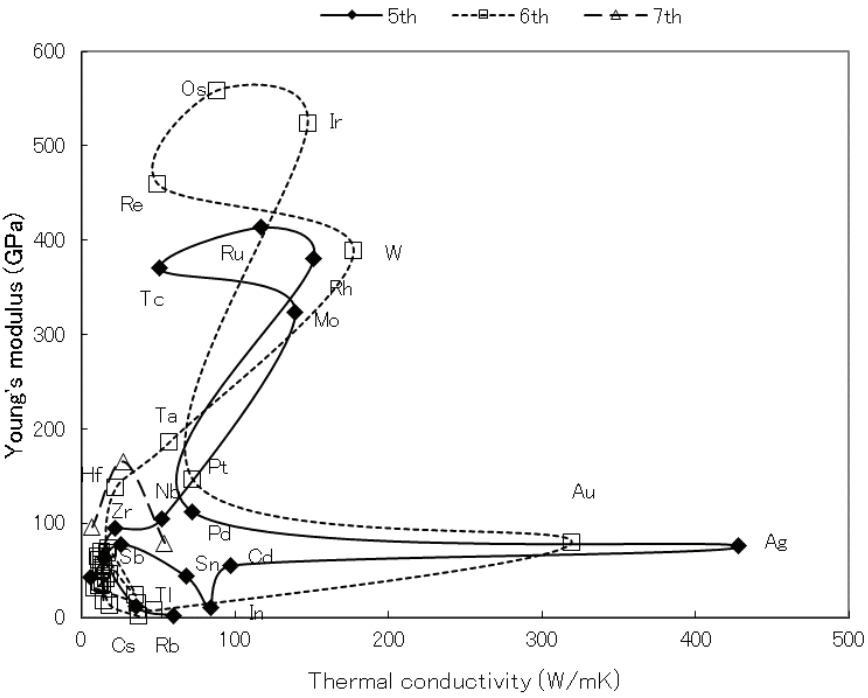

Fig. 1-8 – Distribution of elements of the 5th, 6th, and 7th periods on the TC-YM diagram

1.3 Distribution of elements on the TC-YM diagram per group in the periodic table

One of the greatest characteristics of the periodic table is that elements of the same group have similar properties, especially in chemical properties. But elements of group 13 – B, Al, Ga, In, and Tl – and those of group 14 – C, Si, Ge, Sn, and Pb – cannot be said to have similar properties.

Fig. 1-9 shows the distribution of elements on the TC-YM diagram per group (from group 1 to group 10). The elements of the same group show each line.

Fig. 1-10 shows the distribution of elements on the TC-YM diagram per group (from group 11 to group 16).

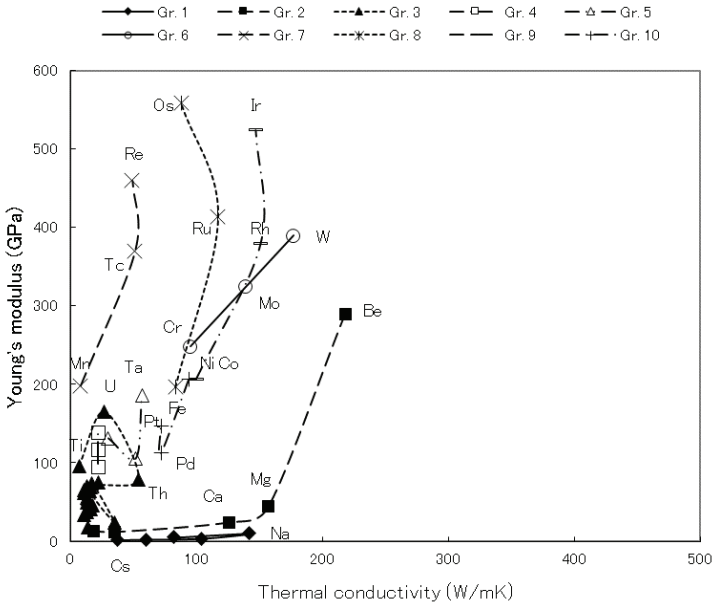

Fig. 1-9 – Distribution of elements on the TC-YM diagram per group (from group 1 to group 10)

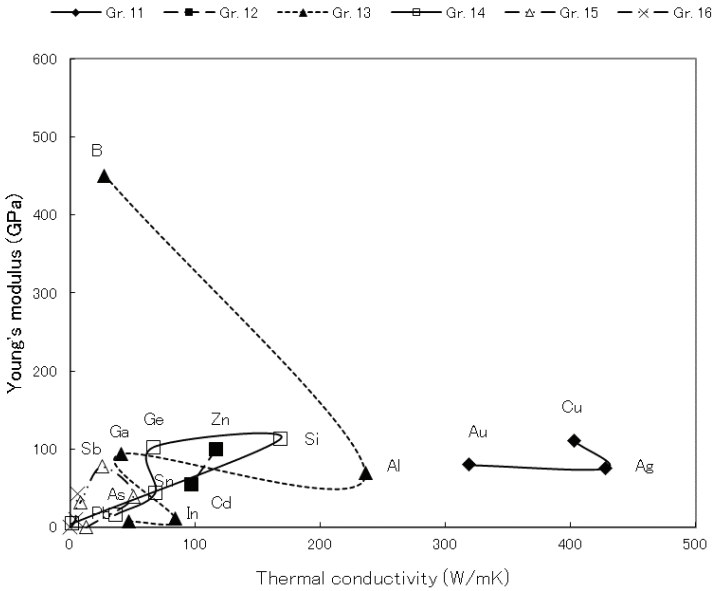

Fig. 1-10 – Distribution of elements on the TC-YM diagram per group (from group 11 to group 16)

The elements of group 1 (alkali metals) commonly show very low Young's modulus. Only the thermal conductivity varies with different inner electron shells.

The elements in group 2 (alkaline earth metals) commonly show also very low Young's modulus except for Be. Only the thermal conductivity varies with varying inner electron shell.

The trend changes in group 3.

The elements of group 3 – Sc, Y, lanthanides and actinides – commonly show very low thermal conductivity except Th, U and Pu. Only the Young's

modulus varies with varying inner electron shell in the low Young's modulus range.

The elements of group 4 – Ti, Zr and Hf – also commonly show very low thermal conductivity. Only the Young's modulus varies with varying inner electron shell.

The trend changes in group 5.

The elements of group 5 – V, Nb and Ta – show the Young's modulus proportional to the thermal conductivity except for Nb. Both the Young's modulus and the thermal conductivity vary with varying inner electron shell.

The elements of group 6 – Cr, Mo and W – also show the Young's modulus proportional to the thermal conductivity. Both the Young's modulus and the thermal conductivity vary with varying inner electron shell. With increasing inner electron shell, both the Young's modulus and the thermal conductivity increase.

The trend changes in group 7.

The elements of group 7 – Mn, Tc and Re – commonly show low thermal conductivity. The Young's modulus varies with varying inner electron shell.

The elements of group 8 – Fe, Re and Os – commonly show a little larger thermal conductivity. The Young's modulus varies with varying inner electron shell. Os has the largest Young's modulus among elements.

The elements of group 9 – Co, Rh and Ir – commonly show a little larger thermal conductivity. The Young's modulus varies with inner electron shell.

The elements of group 10 – Ni, Pd and Pt – commonly show medium thermal conductivity. The Young's modulus varies with varying inner electron shell, but these values are smaller than in the former groups.

The trend changes in group 11.

The elements in group 11 – Cu, Ag and Au – commonly show low Young's modulus. The thermal conductivity varies with varying inner electron shell. The values of the thermal conductivity commonly are large.

The elements in group 12 – Zn, Cd and Hg – commonly show low Young's modulus except for Hg. The thermal conductivity varies with varying inner electron shell.

The elements in group 13 – B, Al, Ga, In and Tl – commonly show low Young's modulus, except for B. The thermal conductivity varies with varying inner electron shell.

The elements in group 14 – C, Si, Ge, Sn and Pb – commonly show low Young's modulus. The thermal conductivity varies with varying inner electron shell.

The elements in group 15 – P, As, Sb and Bi – commonly show very low Young's modulus. The thermal conductivity varies with varying inner electron shell. But the varying range is small.

The elements in group 16 – S, Se and Te – commonly show very small Young's modulus. The thermal conductivity doesn't vary any more, and commonly adopts very small values.

In conclusion, the following can be said:

The binding force between atoms represented by the Young's modulus and the mobility of free electrons represented by the thermal conductivity is roughly decided by the electron configuration in the outer shell, and thereafter, it is decided by the structure of the inner shell.

It has been said that the properties of elements are decided solely by the electron configuration in the outer shell. This assumption must be corrected.

1.4 Distribution of the lanthanides on the TC-YM diagram

As shown in Fig. 1-8, the lanthanides of the 6^{th} period are crowded in the region of low thermal conductivity and low Young's modulus. Fig. 1-11 shows the distribution of the lanthanides at the range of low thermal conductivity and low Young's modulus of the TC-YM diagram. The 6^{th} period starts from Cs on the bottom. It goes up with decreasing thermal conductivity through Ba to La. The lanthanides begin from La. It goes up in a winding way. It reaches finally Lu, and Lu connects to Hf. But on the way, anomalies happen, namely, Eu and Yb drop abruptly. This will be discussed in Chapter 6.

The lanthanides have been displayed separately from the main elements in the periodic table. But in the TC-YM diagram, they are displayed together with other elements. Their locations are variable on the diagram, and their properties are variable according to their locations.

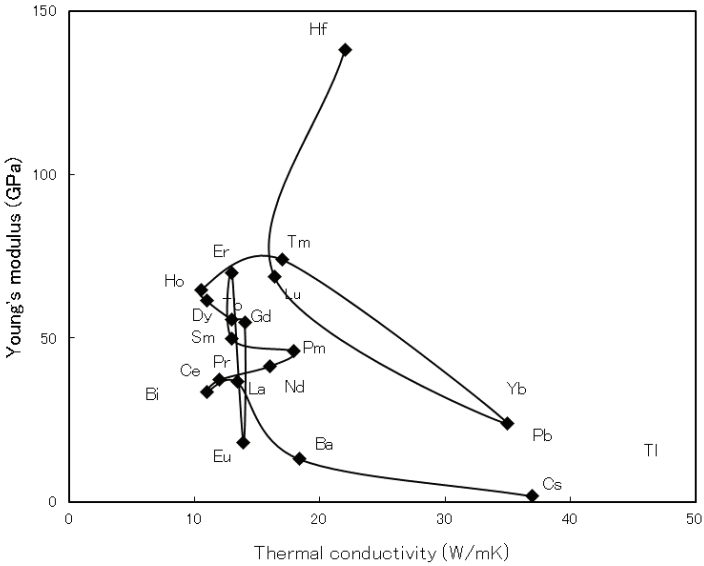

Fig. 1-11 - Distribution of the lanthanides on the TC-YM diagram

1.5 Young's modulus and thermal conductivity of elements on the periodic table

To be sure, the distributions of both the Young's modulus and thermal conductivity of elements on the periodic table are shown in Figs. 1-12 and 1-13, respectively.

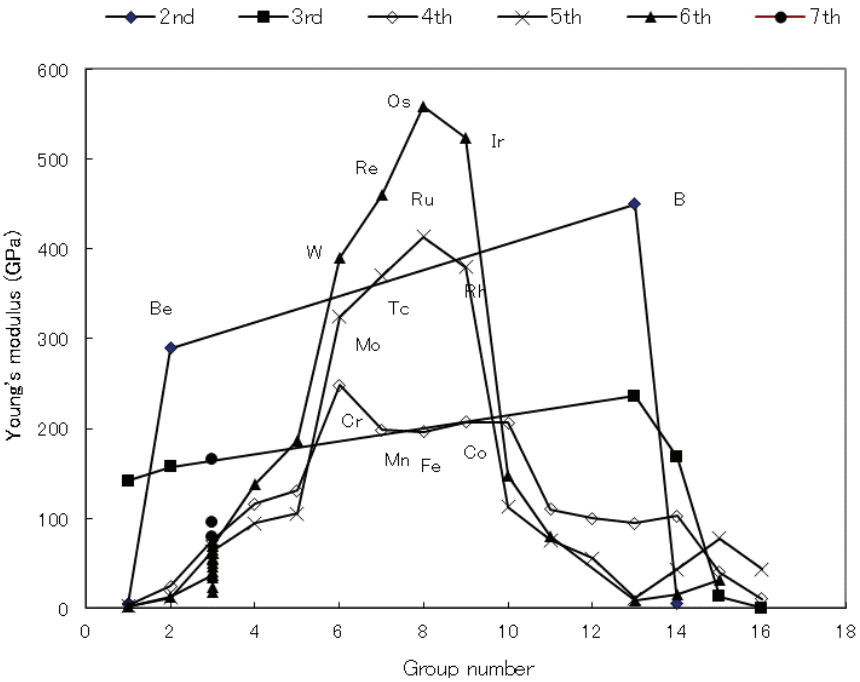

Fig. 1-12 – Young's moduli of elements as a parameter of the group number in the periodic table

The Young's moduli of elements show, as a whole, mountain-like patterns with the peaks at group 8. These patterns are similar to those of the melting temperatures of elements shown in Figure 4.1. But the positions of their peaks are different to each other. Melting temperatures adopt their peaks at group 6, but Young's moduli adopt their peaks at group 8. Therefore, there is no linear relationship between melting temperatures and Young's moduli of elements, as shown in Fig. 1-1.

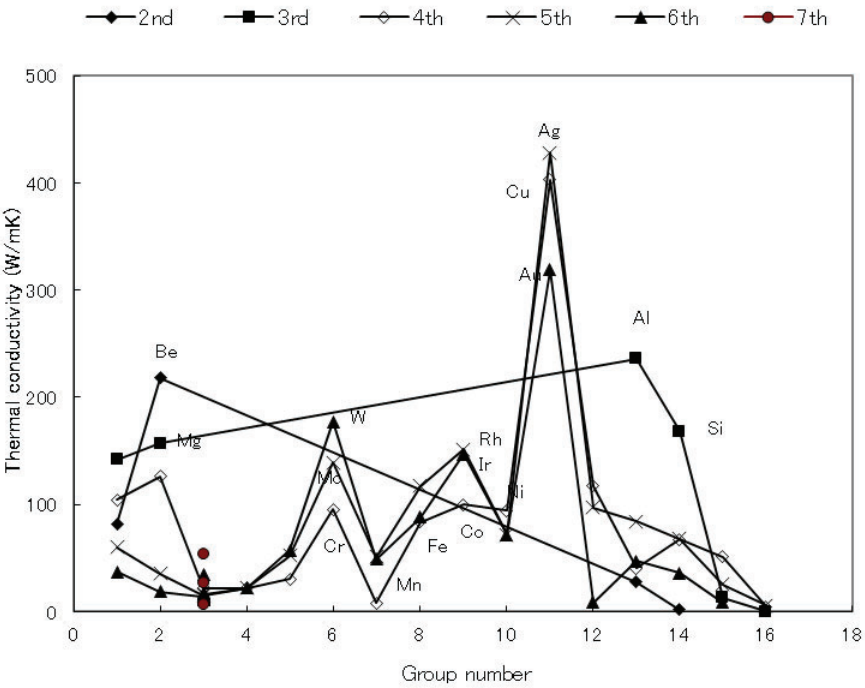

Fig. 1-13 Values of the thermal conductivity of elements as a parameter of the group number in the periodic table

In contrast to the Young's modulus, the thermal conductivity of elements shows complicated patterns on the periodic table, as shown in Fig. 1.13. It goes up and down with increasing atomic number. It is impossible to read a tendency from this figure.

Fig. 1-14 shows the variation of the Young's modulus of the lanthanides as a parameter of the atomic number, and Fig. 1-15 shows the variation of the thermal conductivity of the lanthanides as a parameter of the atomic number, respectively.

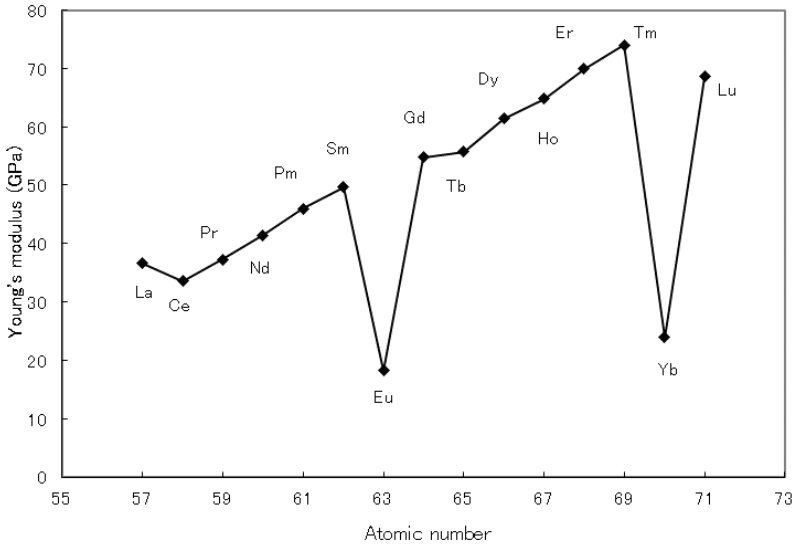

Fig. 1-14 – Young's moduli of the lanthanides as a parameter of the atomic number in the periodic table

The Young's modulus increases with increasing atomic number. But it drops abruptly at Eu and Yb.

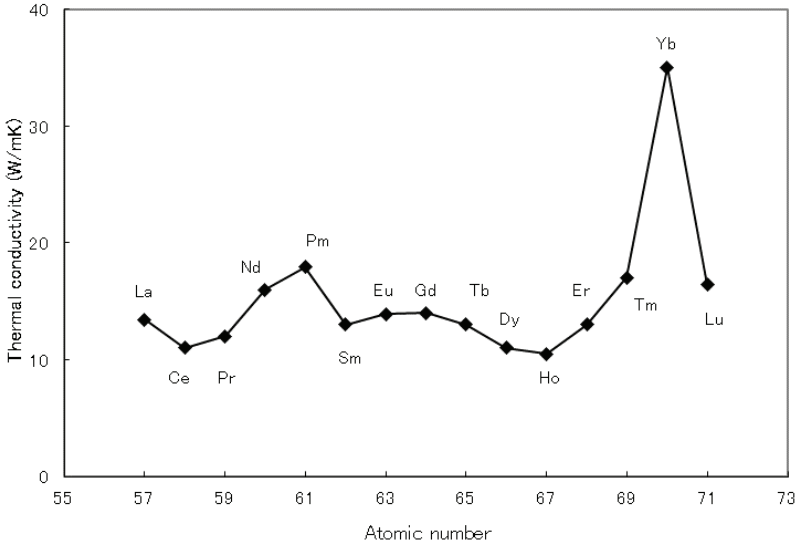

Fig. 1.15 – Values of thermal conductivity of the lanthanides as a parameter of the atomic number in the periodic table

The thermal conductivity of the lanthanides is constant with the atomic number. But it adopts a large value at Yb.

These anomalies can be explained on the TC-YM diagram, as discussed in Chapter 6.

Fig. 1-16 shows the variation of the Young's modulus of the actinides as a parameter of the atomic number, and Fig. 1-17 shows the variation of the thermal conductivity of the actinides as a parameter of the atomic number, respectively.

Data are scarce regarding the actinides. The tendency cannot be read from these figures. Details will be discussed in Chapter 7.

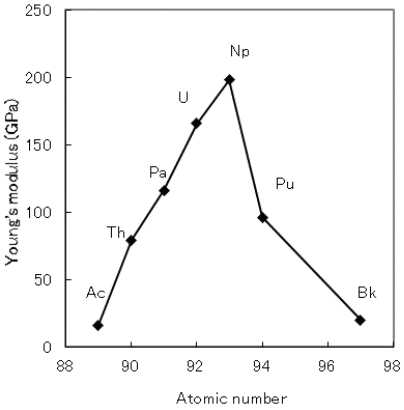

Fig. 1-16 – Young's moduli of the actinides as a parameter of the atomic number in the periodic table

Young's moduli of Ac, Pa, Np, and Bk were speculated from other data, as described in Chapter 7. In contrast to the lanthanides, the actinides adopt large Young's moduli. The reasons will be discussed in Chapter 7.

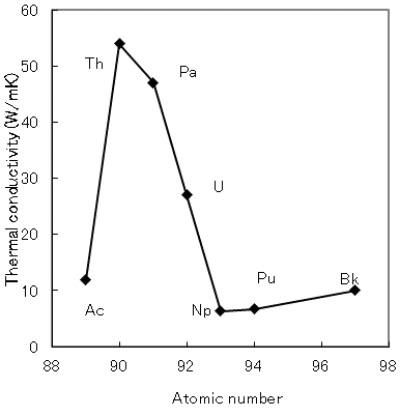

Fig. 1-17 – Values of the thermal conductivity of the actinides as a parameter of the atomic number in the periodic table

In contrast to the lanthanides, the actinides adopt large values of thermal conductivity. The reasons will be discussed in Chapter 7.

1.6 Distribution of other properties of elements on the TC-YM diagram

Other properties of elements, such as atomic radius, melting point, thermal expansion, boiling point, heat of fusion, vapor pressure, heat capacity, electronegativity, and ionization energy, also show clear patterns on the TC-YM diagram. The distributions of melting temperature and atomic radius are shown in Figs. 4-3 and 4-4, respectively. The distributions of electronegativity and ionization energy are shown in Figs. 5-3 and 5-4, respectively.

They all show regular patterns on the TC-YM diagram.

References

1. W. Hayden, W. G. Moffat and J. Wulff, The Structure and Properties of Materials, Iwanami, Tokyo, 1965, vol. III Mechanical Behavior, p. 26.
2. W. Hayden, W. G. Moffat and J. Wulff, The Structure and Properties of Materials, Iwanami, Tokyo, 1965, vol. III Mechanical Behavior, p. 31.
3. D. R. Askeland, The Science and Engineering of Materials, PWS, Boston, 1994, 3rd ed., p. 709.
4. U. Mizutani, Introduction to the Electron Theory of Metals, Cambridge University Press, Cambridge, 2001, p. 299.
5. Y. Mae, What the Darken-Gurry plot means about the solubility of elements in metals, Met. Mater. Trans, A, 47A, 2016, pp. 6498-6506.

6. Japan Institute of Metals, Metals Data Book, Maruzen, Tokyo, 1993, 3rd ed., pp. 36-43.

2. CRYSTAL STRUCTURES OF ELEMENTS

Metallic elements adopt crystal structures such as face-centered cubic (fcc), body-centered-cubic (bcc), hexagonal-closed-packed (hcp), and so on. Which crystal structure it adopts determines the fate of the metal. Metals with fcc and bcc structures have good formability (plasticity) due to their many slip systems. But metals with hcp structures have poor formability due to their limited slip systems.

his author studied titanium in his youth. Commercially pure titanium (CP Ti) has good formability owing to its deformation twins. But, when it is alloyed, the deformation twin is suppressed and room temperature ductility is lost. Consequently, hot working is essential for the forming of Ti alloys. Hot working the fine products of Ti alloys requires special procedures. It is hard work.

In contrast to this, iron (bcc and fcc) and copper (fcc) have large ductility and can be formed easily. As a result, iron and copper have large markets.

How are the crystal structures of elements determined?

As to the kinds of crystal structures, please refer to the literature. [1, 2]

The stacking sequence for fcc is ABC, and that for hcp is ABAB. The stacking sequence for the double hexagonal structures, which are often observed in the lanthanides, is ABAC. [3]

First, the crystal structures of elements plotted on the periodic table are shown in Fig. 2-1.

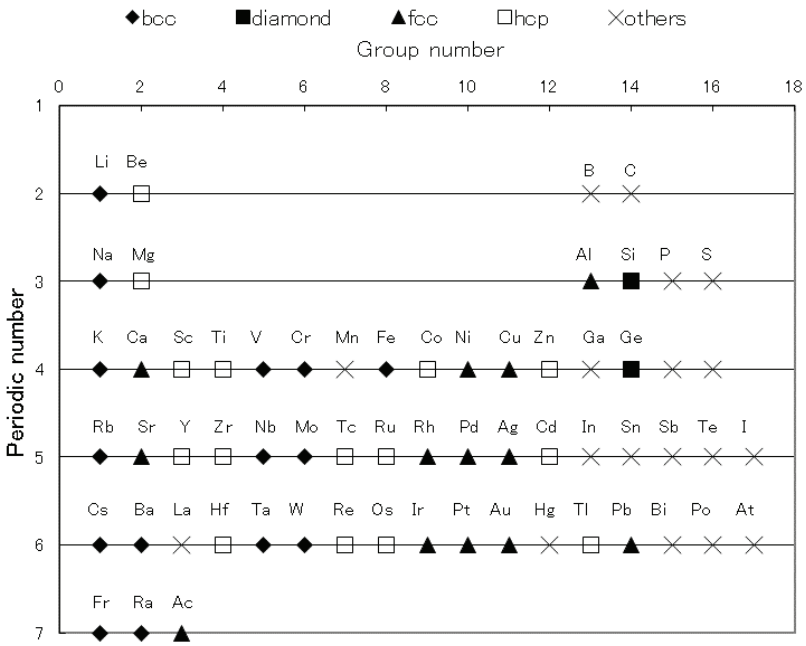

Fig. 2-1 – Crystal structures of elements on the periodic table

The alkali metals in the 1st group are all bcc-structured. But the alkaline-earth metals in the 2nd group show hcp, fcc, and bcc structures with increasing period.

Other bcc metals are located in the 5th and 6th groups.

The elements of fcc structures gather in the center but scatter in other areas.

The metals of hcp structures are located between them.

The elements of other crystal structures are located mainly in the right side of the periodic table.

Totally, the elements show agglomerations of the same crystal structures, but it is hard to read the tendency of the crystal structures from the periodic table.

This figure has been quoted many times in books, but no author could find the tendency.

The lanthanides and actinides are shown outside the periodic table. It is also difficult to interpret their crystal structures on the periodic table.

Then, the crystal structures of elements were plotted on the TC-YM diagram, and shown in Fig. 2-2.

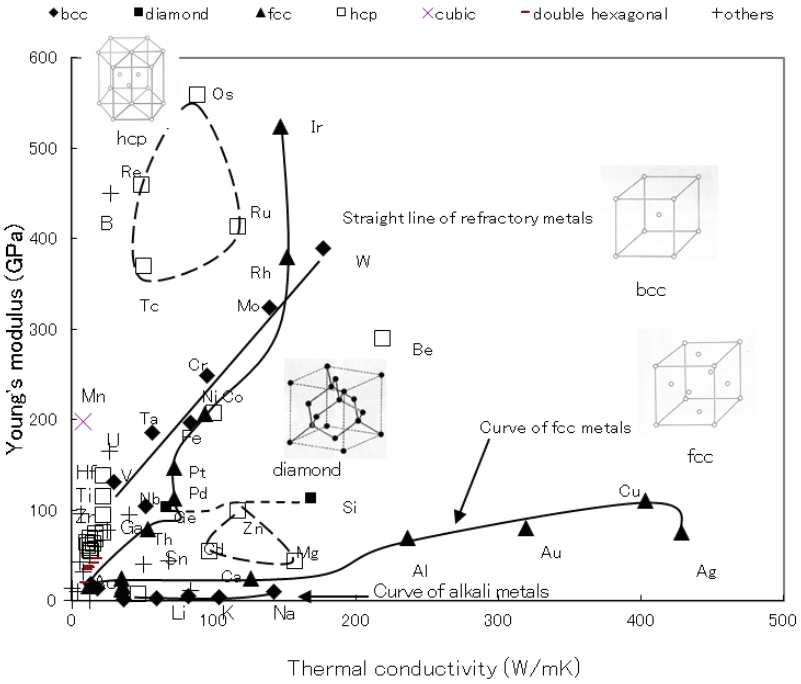

Fig. 2-2 – Crystal structures of elements shown on the TC-YM diagram

This is the same figure as Fig. 1-6. All of the metallic elements show clear tendencies. This is very surprising, isn't it? We have been taught that this element is fcc-structured, and that element is bcc-structured, and so on.

But the plots of crystal structures of elements on the TC-YM diagram give us clues for remembering.

(1) The bcc elements – W, Mo, Cr, Ta, and V – lie on a straight line, called **the straight line of refractory metals**.

Only Nb (bcc) is off the line, but it connects to the Ge and Si (diamond

structure). Both the bcc structure and the diamond structure are non-closed packed structures.

(2) The alkali metals (bcc) – Na, K, Li, Rb, and Cs – are lying on **the curve of alkali metals** from right to left.

(3) The fcc elements lie on **the curve of fcc metals**. All of the fcc elements – Ag, Cu, Al, Ca, Pb, Sr, Yb, Th, Pd, Pt, Ni, Rh, and Ir – lie on a specific curve which can be referred to as the curve of fcc metals. It runs through the wide range of the diagram. Therefore, the fcc metals show a wide variety of properties.

(4) The hcp metals are located in the corners between the bcc metals and the fcc metals. From such a viewpoint, they give minor impressions.

The hcp elements of low melting temperatures – Zn, Cd, and Mg – form a triangle in the lower portion of the diagram.

Those of high melting temperatures – Os, Re, Tc, Ru, and Os – form a square in the upper portion of the diagram.

Some lanthanides which have larger Young's moduli among the lanthanides also have hcp structures.

Co adopts an hcp structure though it is very adjacent to Ni. It transforms into an fcc structure at high temperature in accordance with Ni.

Tl near Rb adopts an hcp structure far from other hcp elements. It transforms into a bcc structure at high temperature in accordance with alkali metals nearby.

(5) The elements of miscellaneous crystal structures are distributed in the niche of low Young's modulus and low thermal conductivity. Some elements which have smaller Young's moduli among the lanthanides have double-hexagonal structures.

(6) As shown in Figure 2.1, the alkaline-earth metals adopt various crystal structures. This cannot be explained on the periodic table. But, on the TC-YM diagram, it can be explained as follows: Be and Mg are located at the area of the hcp structures; therefore, they adopt hcp structures. Ca and Sr are lying on the straight line of fcc metals, therefore, they adopt fcc structures. Ba lies on the extension of the curve of alkali metals, therefore, it adopts a bcc structure. The Young's modulus of Ra is unknown, but it is speculated to lie on the same extension of the curve of alkali metals.

(7) The elements in Group 13 in the periodic table – B, Al, Ga, In, and Tl – adopt various crystal structures. They can be explained on the TC-YM diagram. B adopts a minor structure (rhombohedral), because it is away from other elements on the diagram. Al adopts an fcc structure, because it is located on the curve of fcc metals. Ga is located near Zr and Th. It adopts a minor structure (orthorhombic) because it is away from both the elements of hcp structures and the curve of fcc metals. In (indium) adopts a minor structure (tetragonal), because it is located near Li, but away from both the curve of fcc metals and the curve of alkali metals. Tl adopts an hcp structure, because it is located near Rb, but a little away from the curve of alkali metals. It transforms into a bcc structure at high temperature.

(8) The elements in Group 14 in the periodic table – C, Si, Ge, Sn, and Pb – adopt various crystal structures. But it can be said that they commonly adopt

diamond structures somewhere except for Pb. Si and Ge are located near the center of the diagram, and connect to Nb. The bcc structure and the diamond structure are not close-packed. It means that these elements have directional and strong bonding forces. These elements form the back-bone of the diagram. Sn is located under Ge on the diagram. It adopts a tetragonal structure at room temperature, but transforms into a diamond structure at low temperature. Pb is located on the curve of fcc metals. It is an authentic fcc-structured element.

In this way, the mysteries of the crystal structures of elements on the periodic table can be explained on the TC-YM diagram. The crystal structures of the lanthanides and the actinides will be discussed in Chapters 6 and 7, respectively.

Where are the major elements on the diagram?

Fe: This is in the 8th group of the 4th period, and is surrounded by non-bcc elements on the periodic table, as shown in Fig. 2-1. It is difficult to speculate from the periodic table why it adopts a bcc structure. In contrast, on the TC-YM diagram, Fe is located just right and on the upper side of Ta and near Cr on the straight line of refractory metals, as shown in Fig. 2-2. Fe adopts a bcc structure at room temperature, because it is near the straight line of the refractory metals. Ni is located just on the right side of Fe. Ni is an fcc metal lying on the curve of fcc metals. Therefore, Fe transforms into an fcc structure at high temperature. This brings Fe a great advantage. Co is located just on the right side of Ni and off the curve of fcc metals. Therefore, Co adopts an hcp structure at room temperature. But, it transforms into an fcc structure at high temperature, affected by Ni, similarly to Fe.

Iron is located at the point of the medium Young's modulus and medium thermal conductivity. This brings many practical advantages to iron. Above all, iron is included in those elements which have greatest abundance in the universe, as shown in Fig. 3-3.

Cu: Cu is in the 11th group of the 4th period, and belongs to the group of fcc metals on the periodic table.

On the TC-YM diagram, Cu is located on the right-most side of the diagram, adjacent to Ag. Cu lies on the curve of fcc metals and adopts an fcc structure.

Al: Al is in the 13th group of the 3rd period and is the only fcc metal in the 13th group. There are no fcc metals around it. It is difficult to speculate from the periodic table why it adopts an fcc structure. In contrast, on the TC-YM diagram, Al is located at the medium thermal conductivity and low Young's modulus. It lies on the curve of fcc metals.

Therefore, Al is a soft and ductile metal with medium conductivity. The greatest advantage of Al is its lightness. The density is a derived quantity; therefore, it doesn't show a trend on the TC-YM diagram, but for reference, it was shown in Fig. 2-3.

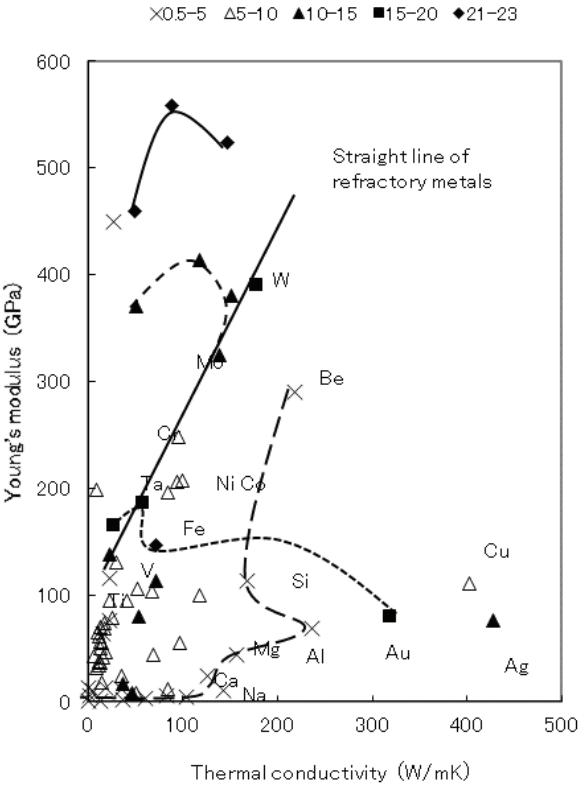

Fig. 2-3 – Distribution of the density of elements on the TC-YM diagram

Ti: Ti is in group 4 of the 4th period. It belongs to the group of hcp metals on the periodic table. On the TC-YM diagram, Ti is located at the low thermal conductivity and medium Young's modulus. It is located at the downward extension of the straight line of refractory metals. Therefore, it adopts an hcp structure at room temperature and transforms into a bcc structure at high temperature. It has a high melting temperature in spite of its low Young's modulus, affected by the refractory metals. It has a relatively low density. Therefore, it is used for aerospace application.

Unfortunately, it adopts an hcp structure, therefore; its formability is not good.

Pb: Pb is in group 14 of the 6th period, and is surrounded by the non-fcc metals on the periodic table. It is difficult to speculate from the periodic table why it adopts an fcc structure. In contrast, on the TC-YM diagram, Pb is located on the curve of fcc metals. Pb has low thermal conductivity and low Young's modulus. Therefore, Pb is a very soft metal with large density.

When this author began to learn metallurgy, he could not remember the crystal structures of elements. There were no clues to connect each element to each crystal structure. But if the crystal structures were plotted on the TC-YM diagram, people could connect them to their values of Young's modulus and thermal conductivity. Consequently, people can understand the crystal structures of the elements systematically.

The area near the lanthanides in Fig. 2-2 is crowded with elements. The details in that area are shown in Chapters 6 and 7, respectively. The crystal structures in the area near the lanthanides are also distributed regularly.

The relationship with the existing theories

It is said that the bcc structure has an electron-to-atom (e/a) ratio near 1 and forms the spherical s orbital, the hcp structure has an e/a ratio near 2 and forms the sp hybrid orbital, the fcc structure has an e/a ratio near 3 and forms the sp^2 hybrid orbital, and the diamond structure has an e/a ratio near 4 and forms the sp^3 hybrid orbital. This is typically valid from Na, Mg, Al and Si in the third period of the periodic table. Na forms the spherical s orbital, its e/a ratio is 1, and it adopts a bcc structure. Mg forms the sp hybrid orbital,

its e/a ratio is 2, and it adopts an hcp structure. Al forms the sp^2 hybrid structure, its e/a ratio is 3, and it adopts an fcc structure. Si forms the sp^3 hybrid orbital, its e/a ratio is 4, and it adopts a diamond structure. [4]

What is the correlation between this knowledge and the orderings of the crystal structure of elements shown in Fig. 2-2?

The elements – Li, Na, K, Cs, Fr, Ba, Ra, Eu, V, Nb, Ta, Cr, Mo, W and Fe – adopt bcc structures.

The alkali metals – Li, Na, K, Cs and Fr – are monovalent. The spherical orbital theory is valid.

But the elements – Ba, Ra and Eu – are divalent.

The refractory metals – V, Nb, Ta, Cr, Mo, and W – are multivalent. Fe is also multivalent.

It is said that the vacant d orbitals in the refractory metals drain off electrons from s and p orbitals. As a result, the refractory metals may be monovalent and adopt bcc structures. [4] But they are multivalent practically. The spherical s orbital theory seems to be invalid in bcc metals.

The elements – Be, Mg, Sc, Y, Gd, Tb, Dy, Ho, Er, Tm, Lu, Ti, Zr, Hf, Tc, Re, Ru, Os, Co, Zn, Cd and Tl – adopt hcp structures. According to the hybrid orbital theory, they must be divalent. Be, Mg, Cd, and Zn are divalent. The hybrid orbital theory is valid in Be, Mg, and Cd. But the other elements are hardly considered to be divalent. In general, the sp hybrid theory seems to be invalid.

The elements – Ca, Sr, Yb, Ac, Th, Rh, Ir, Ni, Pd, Pt, Cu, Ag, Au, Al and Pb – adopt fcc structures. Al is trivalent. The sp^2 hybrid theory is valid in Al. But elements such as Ag, Cu, and Au cannot be considered to be trivalent. Many other elements cannot be considered to be trivalent either. The sp^2 hybrid orbital theory fails.

In this way, the hybrid orbital theory explains only the limited situations. The total view over the crystal structure of elements is available only on the TC-YM diagram. The atoms of each element gather and bond to each other. At that time, the binding force and free electrons are generated. As a result, the thermal conductivity and Young's modulus are determined. Finally, the crystal structures of elements are decided according to each position of the element on the TC-YM diagram. Simultaneously, other properties are decided according to each position of the element on the TC-YM diagram. The graphical representation of the properties of elements is the largest characteristic of the TC-YM diagram.

References

1. R. E. Hummel, Understanding materials science, Springer, 1997, pp. 33-34.
2. D. R. Askeland, The science and engineering of materials, 1989, p. 42.
3. Japan Institute of Metals, Metals Data Book, 3rd ed., Maruzen, Tokyo, 1993, pp. 36-43.
4. Susan Trolier-McKinstry and Robert E. Newnham, Materials Engineering, Bonding, Structure, and Structure-Property Relationship, Cambridge University Press, Section 10.2 Bonding and Crystal Structure, 2018.

3. ABUNDANCE OF ELEMENTS IN THE UNIVERSE

The usefulness of a metal is determined mainly by its price. Many factors affect the price of a metal, but the abundance on the earth is one of the greatest factors. The abundance of a metal on the earth is affected by the abundance in the universe. It is generally said that the elements up to iron in the periodic table were produced after the big bang, and the elements after iron were produced after the supernova.

The abundance of elements in the universe is often shown in books. [1] The Oddo-Harkins plot is famous with respect to the abundance of elements.

Fig. 3-1 shows the Oddo-Harkins plot. The abundance is defined as the existing ratio of elements when the content of Si is normalized to 1,000,000.

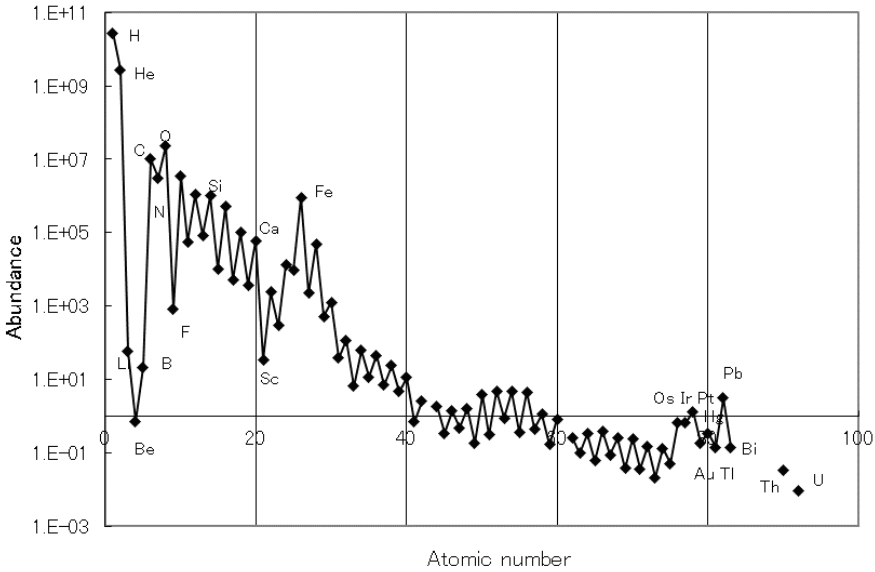

Fig. 3-1 – The Oddo-Harkins plot for the abundance of elements in the universe

The Oddo-Harkins plot is said to hold that elements with an even atomic number are more common than elements with an odd number.

In addition, it is said that it is because the elements with odd proton numbers have one unpaired proton, and are likely to capture another to balance the spin of the unpaired proton.

In general, the abundance of elements decreases with increasing atomic number. But there are some exceptions. The contents of Li, Be, and B are low and those of oxygen and iron are high.

By the way, this author had been thinking about the reason why Zr has a small thermal neutron absorption cross-section. He thought simply that Zr

has too many neutrons in the nucleus and cannot absorb neutrons any more. This speculation soon proved to be false, but at that time, the concept of the "**neutron multiple number**" was defined. [2]

The "neutron excess" had been defined as the difference between the number of neutrons and the number of protons. [3] But, the neutron multiple number is a quotient when the difference between the atomic weight and the atomic number is divided by the atomic number. It means an average number of neutrons per proton in the nucleus.

$$NMN = \frac{(M-Z)}{Z} \qquad (3\text{-}1)$$

MNM : Neutron multiple number
M : Atomic weight
Z : Atomic number

This author plotted the neutron multiple number of all elements on the TC-YM diagram without intension. Fig. 3-2 shows the result.

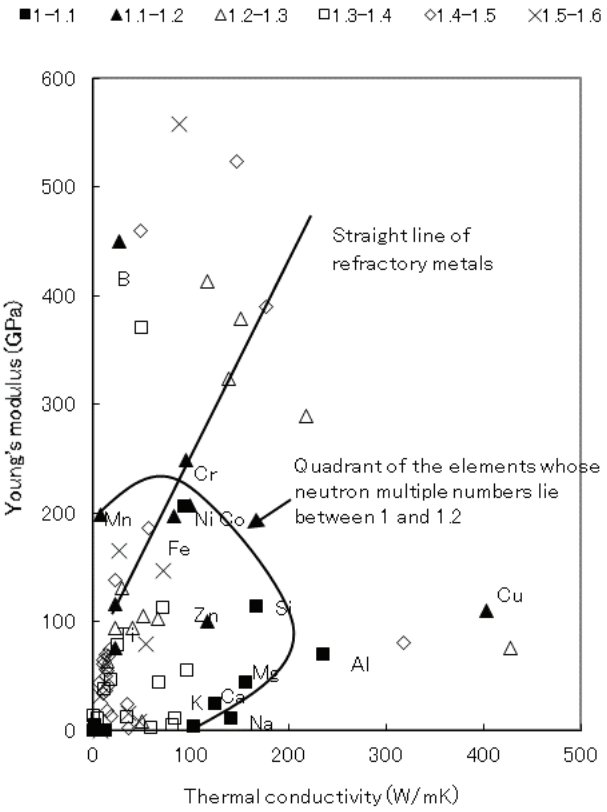

Fig. 3-2 – Distribution of the neutron multiple number of elements on the TC-YM diagram

The figures in the legend show the range of the neutron multiple number of elements. It spreads from 1 to 1.6.

Surprisingly, the neutron multiple numbers of elements show a pattern on the diagram. The elements with the smallest neutron multiple numbers (1-1.2) – Mn, Cr, Fe, Ni, Co, Si, Al, Zn, Mg, Ca, Na, and K – form a

quadrant on the diagram. Elements of large neutron multiple numbers are distributed inside or outside the quadrant. It is quite a new pattern and absolutely different from any other patterns obtained so far. **It is surprising that a character of the nucleus such as the neutron multiple number is related to physical properties of materials such as Young's modulus and thermal conductivity.**

This may be the only example of the material properties in which the characters of the nucleus have emerged.

Fig. 3-2 reminded this author of another figure. He had plotted the abundance of elements in the universe on the TC-YM diagram without intension.

Fig. 3-3 is just the TC-YM diagram which shows the distribution of the abundance of elements in the universe.

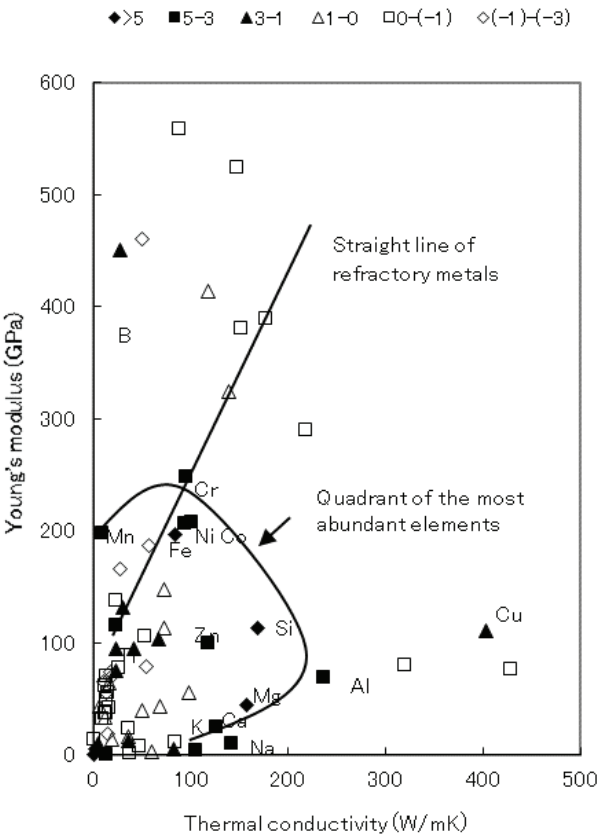

Fig. 3-3 – Distribution of the abundance of elements on the TC-YM diagram

The figures in the legend are the logarithms of the abundance of elements. Surprisingly, it is the same pattern as that of the neutron multiple numbers of elements.

Therefore, a good correlation between them was expected. Fig. 3-4 shows the correlation between the abundance of elements in the universe and the neutron multiple numbers of elements.

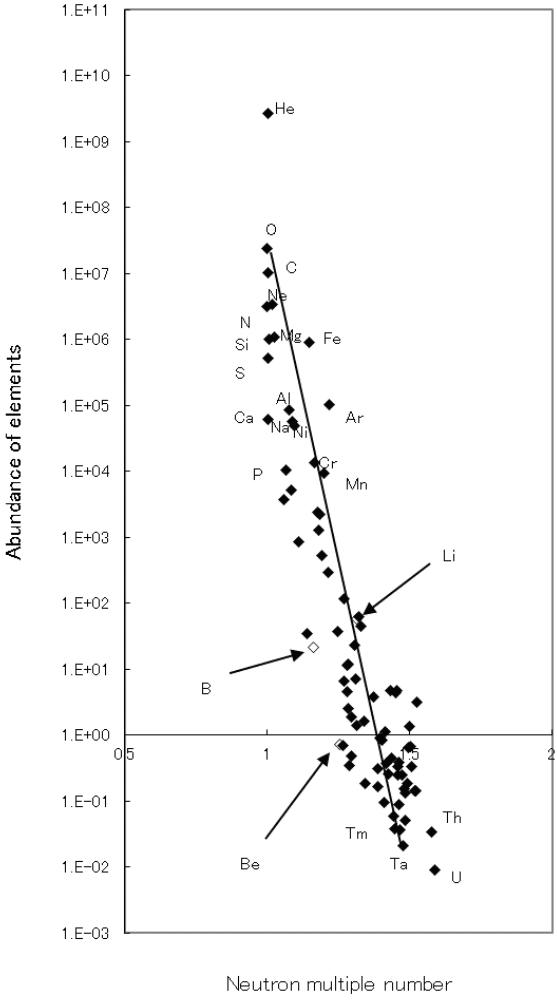

Fig. 3-4 – Correlation between the abundance of elements in the universe and the neutron multiple number of elements

Good correlation is seen. Is this not a surprise, either?

The “neutron excess” is defined as the difference between the number of neutrons and the number of protons. [3] But this “neutron multiple number” seems not to have been quoted so far, and Fig. 3-4 seems not to have been shown before.

In general, as the neutron multiple number increases, the abundance of the element decreases.

The elements are said to be created in the universe by many sorts of processes. [4]

Fig. 3-4 shows that the probability of the creating reaction of each element is dependent on how many neutrons are needed for its protons. The element which needs more neutrons for its protons is more difficult to be created.

Fig. 3-1 is the Oddo-Harkins plot with respect to the abundance of elements. How about the relationship between the neutron multiple number and the atomic number, then?

Fig. 3-5 shows the variation of the inverse neutron multiple number as a parameter of the atomic number.

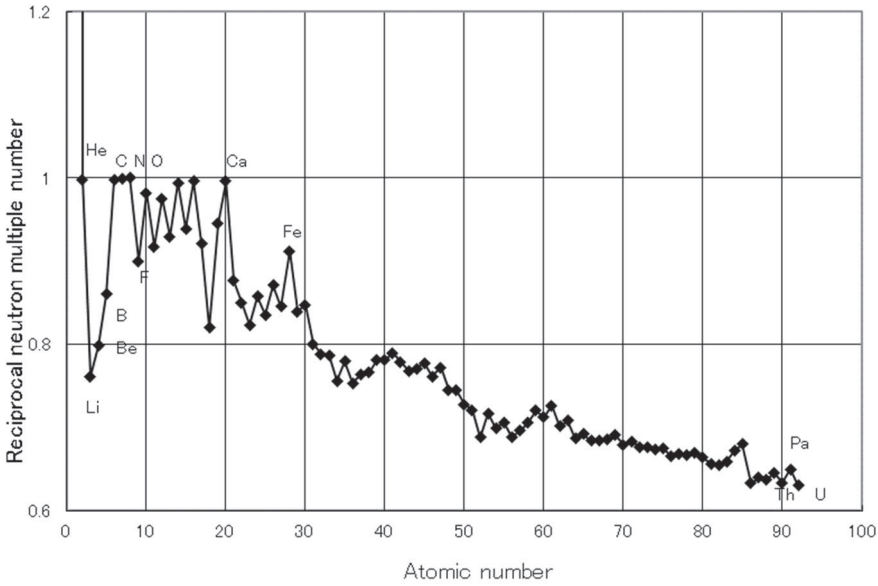

Fig. 3-5 – Reciprocal neutron multiple number as a parameter of the atomic number

The abundance is inversely proportional to the neutron multiple number. The inverse neutron multiple number varies also in a zigzag.

With increasing atomic number, the reciprocal neutron multiple number decreases.

It can be considered that, with increasing atomic number, the nucleus needs more neutrons per proton to shield the positive charges of protons and stabilize the nucleus. As a result, the frequency of atom formation decreases with increasing atomic number. In the elements with few protons such as Li, Be and B, they need many neutrons compared to their few protons. One more neutron increases the neutron multiple number greatly at the elements with few protons. This is the reason why their abundance is small in spite

of their small atomic numbers. For instance, Be is synthesized from 2 Helium atoms, but Be with 8 mass number (the neutron multiple number is 1) is unstable, and decomposes into He again. [5] Be is stable for the first time when it gets 5 neutrons, as is observed practically. Then, the neutron multiple number becomes 1.25 and the abundance decreases greatly according to the correlation between the abundance and the neutron multiple number shown in Fig. 3-4. Consequently, Be is located in the lower part of the correlation line and a little off the correlation line, as shown in Fig. 3-4.

In contrast to this, Li is located just on the lower part of the correlation line. B is located a little off the lower part of the correlation line, and is adjacent to Sc. As a whole, they are not isolated in Fig. 3-4, while they are exceptions in the Oddo-Harkins plot in Fig. 3-1.

It has been reported that the elements were created by various processes according to the atomic number. [4, 5, 6] But, they do not refer to the abundance of elements. The abundance of elements in the universe is controlled by the neutron multiple number of elements.

Fig. 3-6 shows the relationship between the abundance and the neutron multiple number at the elements with odd atomic numbers and those with even atomic numbers, respectively.

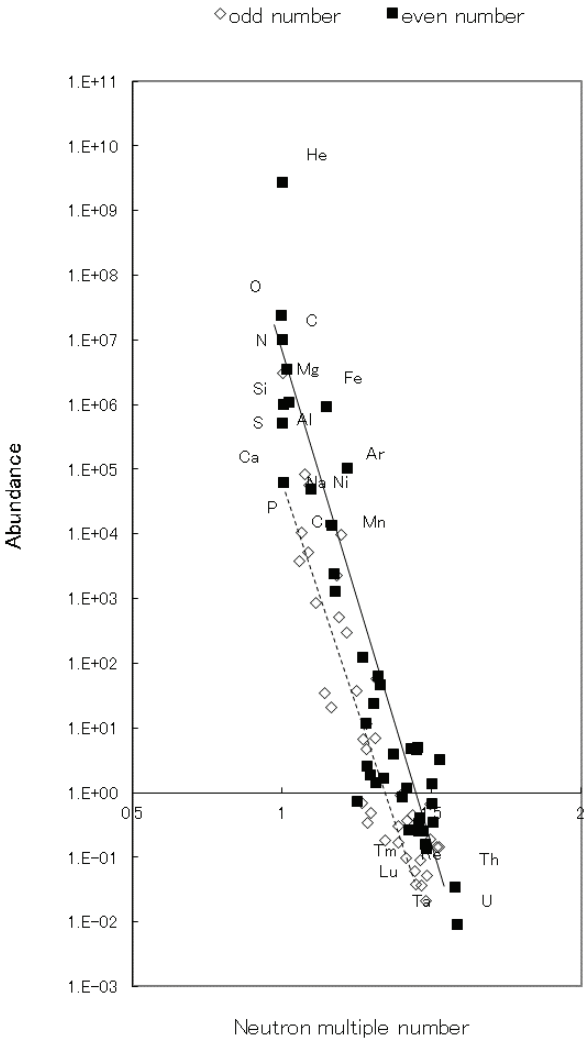

Fig. 3-6 – Correlation between the neutron multiple number and the abundance at the elements of odd atomic numbers and those of even atomic numbers, respectively

It is recognized that there are two correlation lines. Each correlation shows better correlation than in Fig. 3-4.

The elements of the most abundant and the smallest neutron multiple numbers are those with even atomic numbers. And throughout the whole range of the neutron multiple number, the elements with even atomic numbers are more abundant than those with odd atomic numbers.

The point is that at the same neutron multiple numbers, the elements with even atomic numbers are more abundant than those with odd atomic numbers.

This author plotted the abundance of elements on the TC-YM diagram to test the usefulness of this diagram. Unexpectedly, a tendency was found on the diagram. But the pattern was different from those of other properties. Therefore, this author left it for a while. A little later, he devised the "neutron multiple number" in order to explain the reason for the small neutron absorption cross-section of Zr.

Unexpectedly, he found that it showed the same pattern as the abundance. As a result, it was found that there was a correlation between the abundance and the neutron multiple number. The elements – Li, Be, and B – are very scarce on the Oddo-Harkins plot. But it can be explained by their large neutron multiple number. The abundance of elements is dependent on the neutron multiple number.

References

[1] M. Oda, Big cosmological dictionary, Maruzen, Tokyo, 1987, pp. 142-146.

[2] Y. Mae, Neutron multiple number as a factor ruling both the abundance and some materials properties of elements, J. Mater. Sci. Res. Vol. 6, No. 3, 2017, pp. 37-42.

[3] L. H. Aller, The abundance of the element, Interscience Publishing, New York, NY, 1961, pp. 2-3.

[4] W. Aoki, Cosmological history of materials, Shin-nihon Shuppan, Tokyo, 2004, pp. 40-127.

[5] K. Kyougoku, Structure of the universe and elementary particles, Ascii Media Works, Tokyo, 2011, pp. 112-113.

[6] N. Takigawa, Nuclear physics, Askura Bookstore, Tokyo, 2013, pp. 8-10.

4. MELTING POINTS OF ELEMENTS

The melting temperatures of elements are a very important factor. How are the melting temperatures of elements determined?

Every metallic element melts at each melting temperature, but nobody knows how each melting temperature is decided. The melting point of iron is 1808K (1535℃). This temperature was essentially unachievable during ancient times. Instead, iron was produced by heating a piece of bloom in a charcoal furnace near 1473K (1200℃), which was attainable for ancient people. [1] But, if the melting point of iron were higher than 1808K (1535K), this heating temperature would be higher than 1473K (1200℃); consequently, iron making would be impossible. The melting point of 1808K (1535℃) of iron, therefore, should have substantial meaning.

Fig. 4-1 shows variation of the melting temperature of elements at each periodic number with increasing group number.

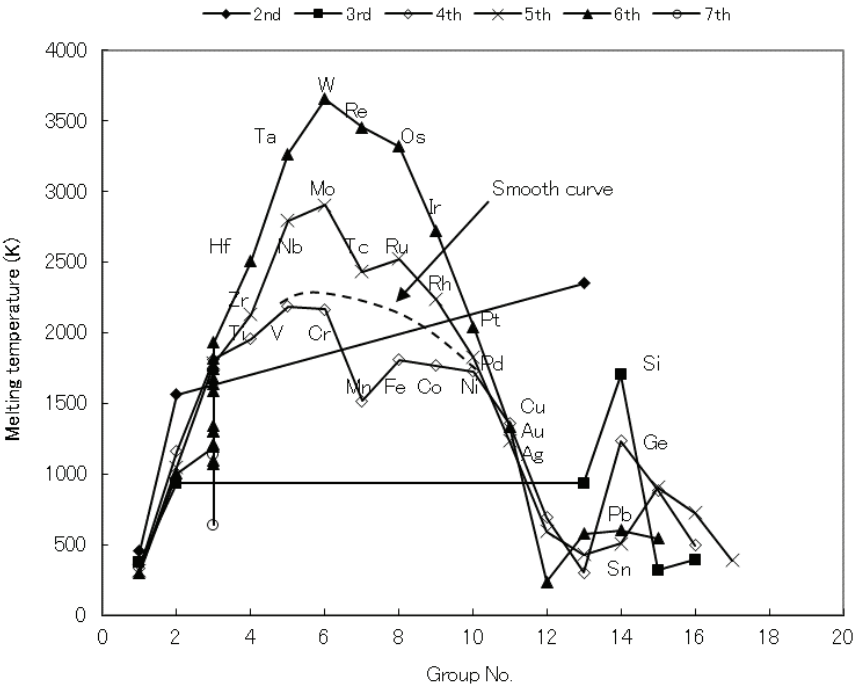

Fig. 4-1 – Melting temperatures of elements as a parameter of group number of the periodic table

Mountain-like distributions are seen with the peak at group 6. But after group 7, melting temperatures fall abruptly, especially at the 4th period elements, such as Mn, Fe, and Co. Essentially, it should follow such a trend as that shown by a dotted line.

But the real melting temperatures of Cr, Mn, Fe, and Co are lower than the dotted line as if the top of the mountain were cut off on purpose. The low melting temperatures of these metals, especially of Fe may be a sort of anthropic principle. [2] The anthropic principle is that nature is formed to

be convenient for the existence of mankind. [3]

The elements after Group 12 have low melting temperatures. But Si and Ge have high melting temperatures though the elements of the same group – Sn and Pb – have low melting temperatures.

4.1 Definition of Gulf Elements

Fig. 4-2 shows the distribution of all elements on the TC-YM diagram.

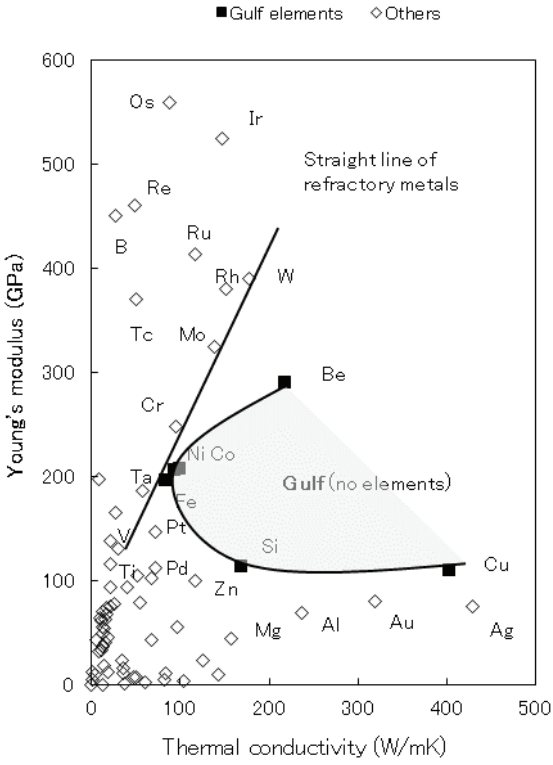

Fig. 4-2 – Positions of the gulf elements – Be, Ni, Co, Fe, Si and Cu – on the TC-YM diagram

The elements – W, Mo, Cr, Ta, and V – form *the straight line of refractory metals* of bcc structure. The elements – Be, Ni, Co, Fe, Si, and Cu – are located at the edge of the distribution of elements toward the open space of the diagram. They form a gulf shape, therefore, they will be referred to as the "*gulf elements*" hereafter. It will be shown that they commonly have unique properties.

4.2 Melting Temperatures of elements

The distribution of melting temperatures on the TC-YM diagram is shown in Fig. 4-3.

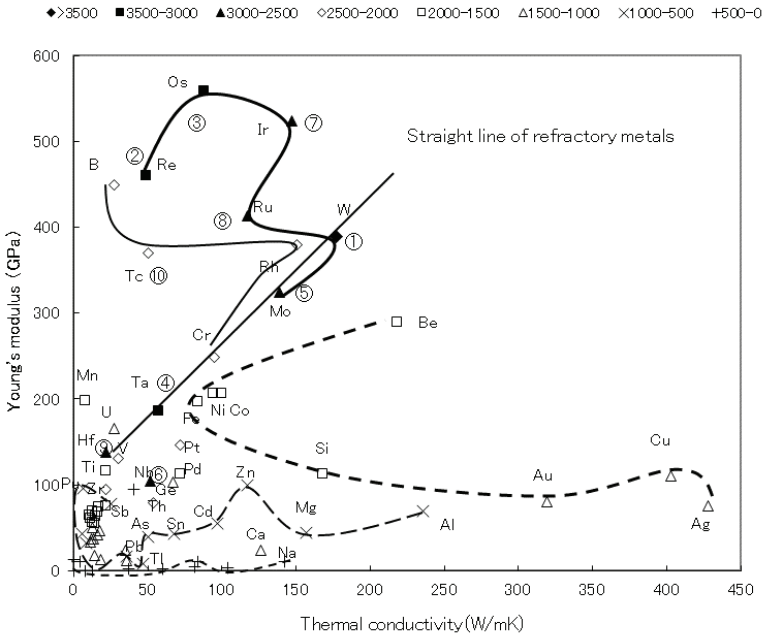

Fig. 4-3 – Distribution of the melting temperatures (K) of elements on the TC-YM diagram

The figures in the legend show the range of melting temperature in Kelvin. The circled numbers in the figure show the ranking of elements in the melting temperature.

In general, the melting temperature decreases with decreasing Young's modulus. But considerable exceptions are recognized.

W, the element with the highest melting temperature, is located at the top of the straight line of refractory metals. The elements on this line – W, Mo, Cr, Ta, and V – have high melting temperatures. Therefore, even the elements on the lower part of the straight line of refractory metals and nearby elements – Ta, Hf, Pt, V, Ti, Nb, Th, and Zr – show high melting temperatures. It can be considered that the specific value of the gradient of the straight line of refractory metals (the ratio of Young's modulus to thermal conductivity) maintains the melting temperatures of elements.

The elements with the Young's moduli around 100 MPa – Ga, Zn, Pu, Ge, Cu, Si, Pd, Ti, and Zr – which were described in Fig. 1.1, are distributed in a wide range of thermal conductivity. They belong to various groups and adopt various melting temperatures. This is the reason that the elements of the same Young's modulus show various melting temperatures.

But the most remarkable thing is that the gulf elements – Cu, Si, Fe, Ni, Co, and Be – have similar and medium melting temperatures, as well as the nearby elements – Au, Ag, Pd, and Ge. Though they are located separately on the periodic table and have different crystal structures, they show similar and medium melting temperatures. This is the reason why the melting temperature of Fe is lower than the value expected on the periodic table.

As mentioned above, iron was produced by heating a piece of bloom in a charcoal furnace near 1473K (1200℃), which was attainable for ancient people. [1] But, if the melting point of iron were higher than 1808K (1535K), this heating temperature would be higher than 1473K (1200℃); consequently, iron making would be impossible. The melting point of 1808K (1535℃) of iron, therefore, should have substantial meaning.

The elements – Si and Ge – showed high melting temperatures – higher than neighboring elements on the periodic table as shown in Fig. 4-1. This is because Si is included in the gulf elements, and Ge is located near Nb and is connected to the elements on the straight line of refractory metals. Other elements in Group 14 – Sn and Pb – are located near the bottom of the diagram; therefore, they show low melting temperatures.

Consequently, Si has a medium melting temperature similar to Fe. This may be another anthropic principle.

Cu is also included in the gulf elements. Cu shows superior ductility and conductivity. Al is also located near the gulf elements.

It should be noted that the most important elements for modern life such as Fe, Si, Cu, and Al are gulf elements.

W (tungsten) shows the highest melting temperature among the elements, but it doesn't have the highest Young's modulus among the elements. W has the largest thermal conductivity among the elements with high Young's moduli. It means that the thermal conductivity, i.e., the electron structure of atoms, also plays a role in the melting temperature.

The gulf elements show the same tendency also in other properties. Fig. 4-4 shows the distribution of atomic radii of elements on the TC-YM diagram. The figures in the legend show the range of atomic radius in 10^{-10} m.

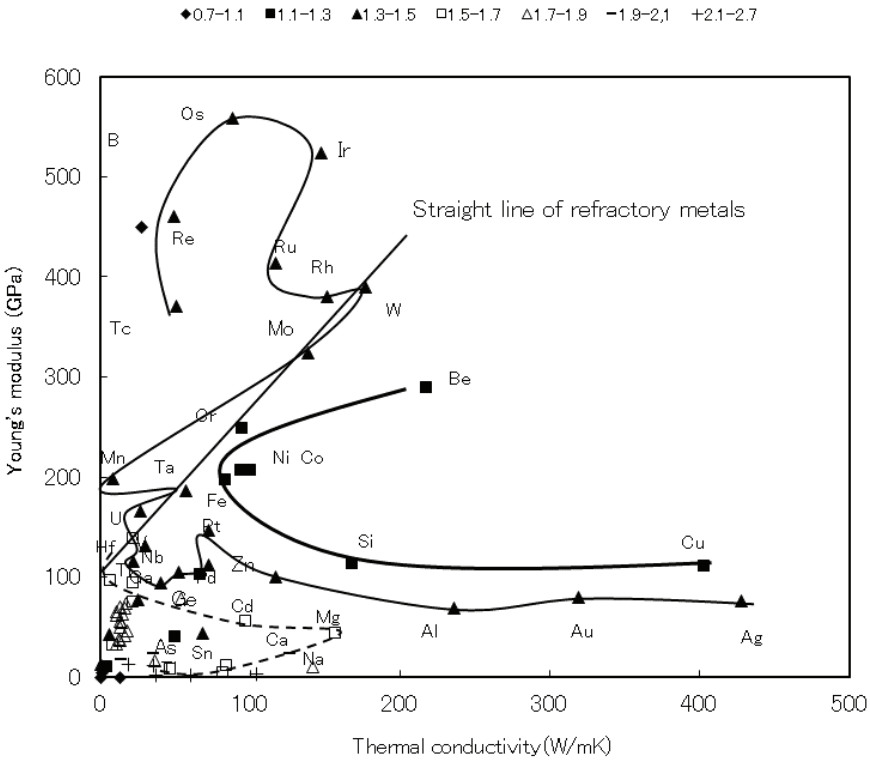

Fig. 4-4 – Distribution of the atomic radii of elements on the TC-YM diagram

The gulf elements show a similar tendency here also. But this time, they show the top values. **The gulf elements including nearby Cr show the smallest atomic radii among the metallic elements. The atomic radii of other elements increase in the form of an enlarging concentric circle on**

the TC-YM diagram. This is an excellent function of the TC-YM diagram.

Fig. 4-5 shows the distribution of atomic radii of elements on the periodic table. In general, the atomic radius decreases with increasing atomic number. It is considered as a result of the increasing nuclear charge attracting the electrons in the outermost shell. But from this figure, it cannot be recognized that the atomic radii of elements are ruled by the combination of Young's modulus and thermal conductivity.

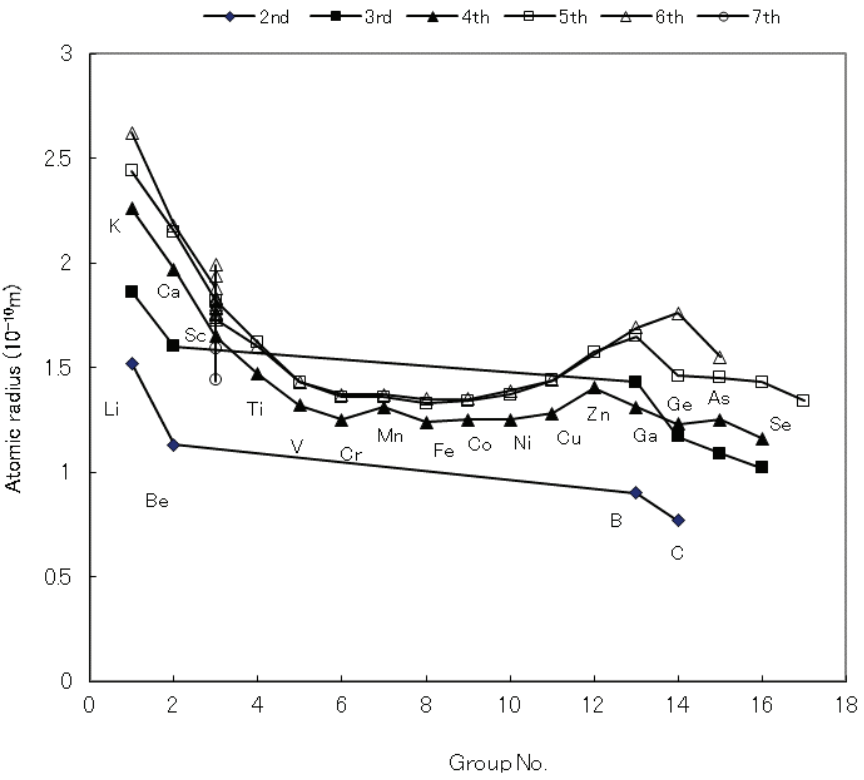

Fig. 4-5 – Distribution of atomic radii of elements on the periodic table

The **heat capacity** (specific heat) shows a similar tendency to the atomic radius on the TC-YM diagram. According to the **Dulong-Petit law**, the specific heat near room temperature is almost 3R (24.95 J/mol) regardless of whether the materials are metals or insulators. [4] Fig. 4-6 shows the distribution of the heat capacity of elements on the TC-YM diagram. In practice, the heat capacity of elements is variable around 3R (24.95 J/mol K) for each element. Elements among the gulf elements – Si and Be – adopt the minimum values. Other gulf elements – Cu, Co, and Cr – also adopt small values of heat capacity. The values of heat capacity increase with an enlarging circle centering on the gulf elements. This pattern in which the gulf elements adopt the minimum values is similar to that of the atomic radius. Therefore, a linear relationship between the atomic radius and the heat capacity of elements is generated. With decreasing atomic radius, the heat capacity decreases. The heat capacity depends upon the volume of the atom simply. But this is an appearance. Both the atomic radius and the heat capacity are controlled by Young's modulus (binding force between atoms) and thermal conductivity (electron mobility) in similar ways. As a consequence, they both show the tendencies on the TC-YM diagram and their dependence on each other.

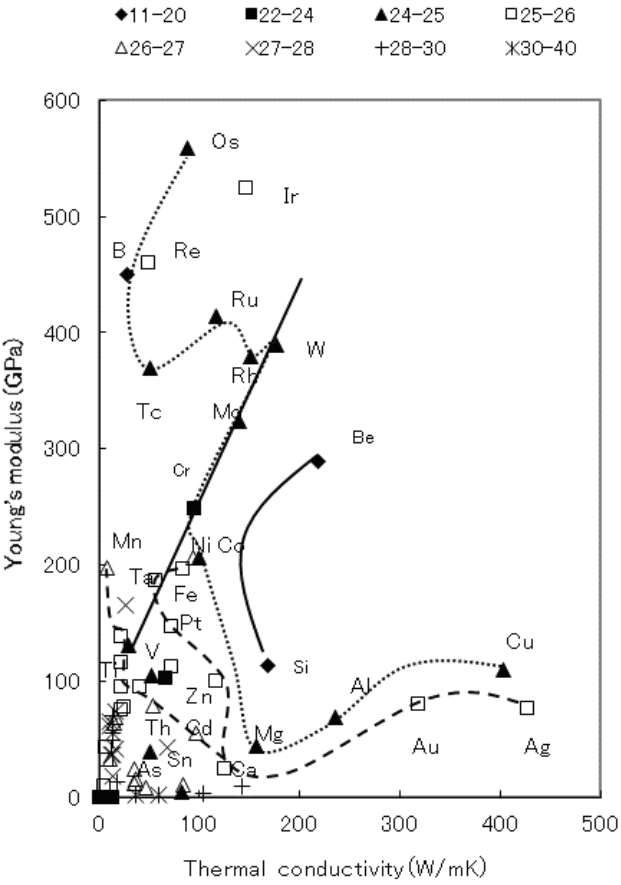

Fig. 4-6 – Distribution of the heat capacity of elements on the TC-YM diagram

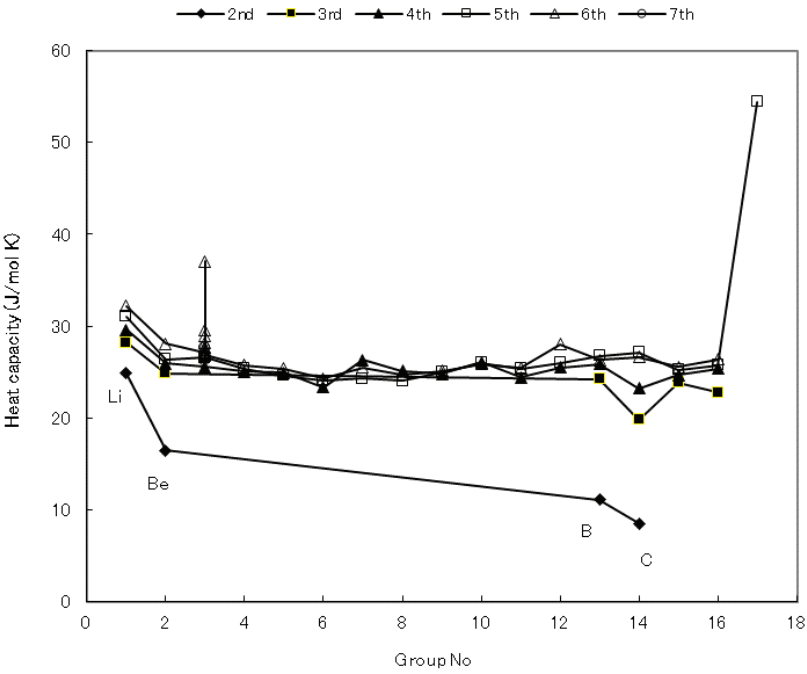

Fig. 4-7 – Distribution of the heat capacity of elements on the periodic table

Fig. 4-7 shows the distribution of the heat capacity of elements on the periodic table. Values of the heat capacity of elements vary subtly, but tendency cannot be recognized.

Finally, there is a mystery as to why W shows the highest melting temperature. Os, the element of the highest Young's modulus, shows only the third highest melting temperature. W, having a lower Young's modulus shows the highest melting temperature. W is located at the top of the straight line of refractory metals. W has rather large thermal conductivity. It

suggests that the thermal conductivity, i.e., electron mobility, contributes to the melting temperature of W.

Thermal expansion, boiling point, heat of fusion, and heat of evaporation show similar patterns to that of melting temperature. Fig. 4-8 shows the distribution of the thermal expansion coefficients of elements.

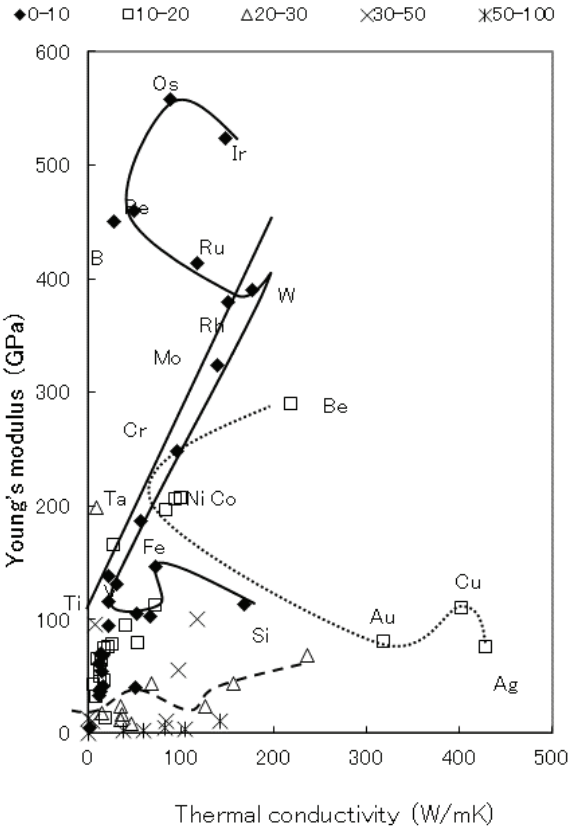

Fig. 4-8 – Distribution of the thermal expansion coefficients (10^{-6}/K) of elements

The straight line of refractory metals maintains the thermal expansion coefficients of elements, which are small even at the elements of low Young's modulus.

In this figure also, the relaxation of properties can be seen at the gulf elements, as seen in the melting points of elements.

Fig. 4-9 shows the distribution of the thermal expansion coefficient of elements on the periodic table. The values of thermal expansion coefficients vary randomly, and no tendency can be recognized.

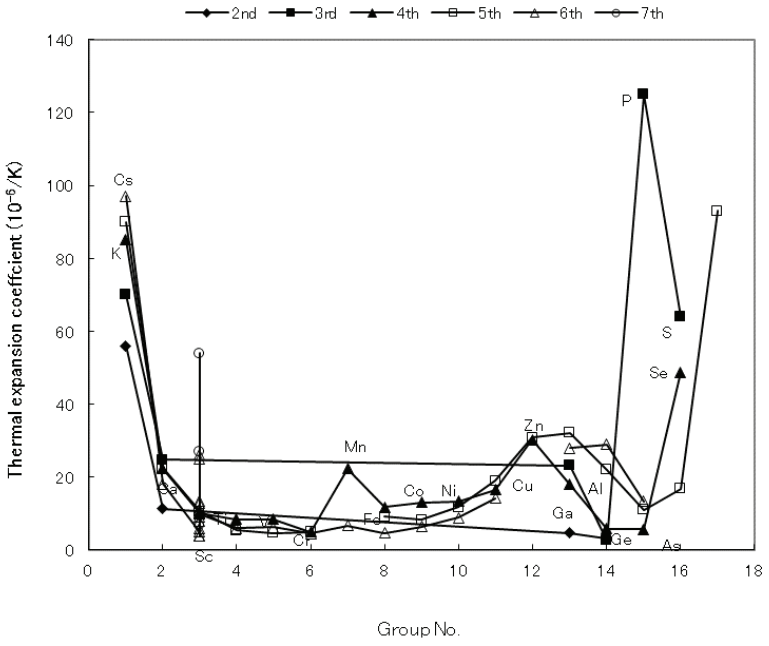

Fig. 4-9 – Distribution of the thermal expansion coefficient of elements on the periodic table

Nobody can tell why one element melts at its melting temperature. Some tendency can be known on the periodic table. But the reason why the melting temperatures of the elements – Cr, Mn, Fe, Co, and Ni – seem to be suppressed on the periodic table has not been known. For the first time, its reason was shown on the TC-YM diagram. The gulf elements – Be, Fe, Ni, Co, Si. and Cu – show similar behaviors in most properties. They commonly show medium melting temperatures. It brings large benefit to mankind.

References

[1] R. F. Hummel, Understanding materials science, Springer, New York, NY, 1998, p. 125.

[2] Y. Mae, Anthropic principle observed in the material properties of Fe, J. Mater. Sci. Res. Vol. 6, No. 3, 2017, pp. 11-19.

[3] A. Crossman, The anthropic principle explained. Retrieved from http://www.allancrossman.com/ap/amthropic.html, 2008.

[4] U. Mizutani, Introduction to the electron theory of metals, Cambridge University Press, 2001, p. 40.

5. ELECTRON CHARGE-DISCHARGE CHARACTERISTICS OF ATOMS

There are several quantities which describe the electron charge-discharge characteristics of atoms. Specifically, they are the electrode potential, electronegativity, ionization energy, and electron affinity. They are subtly different to each other in the definitions and tendencies. On the other hand, there is a quantity called Fermi energy, which means the maximum energy of the electron in the conduction band of the metallic elements.

Here, using the TC-YM diagram, several electron charge-discharge characteristics of atoms and the Fermi energy of elements will be discussed.

5.1 Electron charge-discharge characteristics of atoms

The periodicity of the ionization energy has been frequently referred to as the good example of the periodicity of the atomic structure. Fig. 5-1 shows the variation of the ionization energy of the solid elements as a parameter of group number.

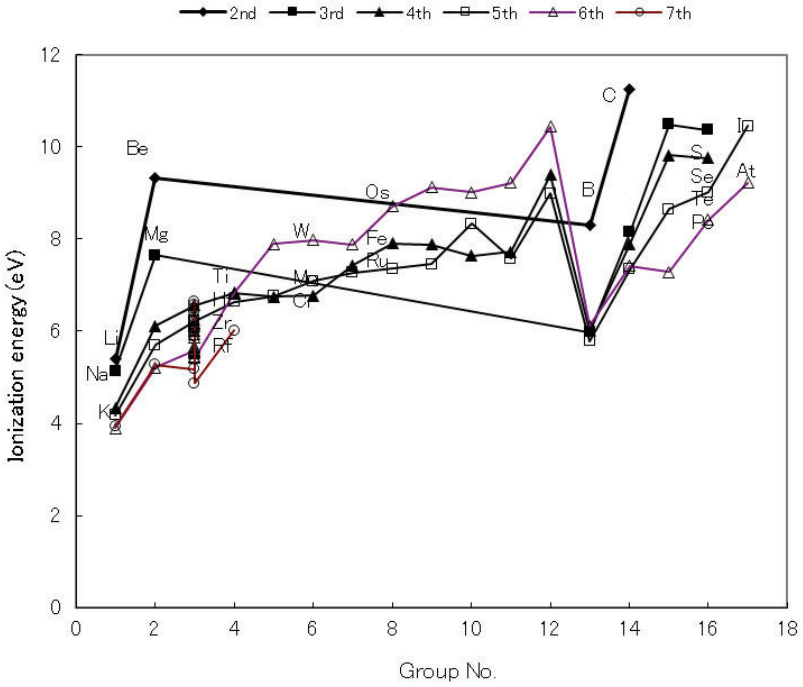

Fig. 5-1 – Ionization energies of elements as a parameter of group number

The alkali metals show small ionization energies. The ionization energy increases as the group number increases. This has been considered to be the evidence that verifies the validity of the periodic table. But, the situation of the increase is not simple, as shown in Fig. 5-1. The ionization energy drops abruptly at group 13, and increases again gradually with increasing group number. The characteristics of the ionization energies of the elements cannot be expressed well by the periodic table. There must be some reasons for it.

To clarify the electron charge-discharge characteristics of atoms, the

electrode potential, electronegativity, ionization energy, and electron affinity were studied using the YC-YM diagram.

(1) Electrode potential

The electrode potential refers to the ease with which the electrons are discharged from the metallic elements in the aqueous solution. [1, 2] The higher the electrode potential, the harder is the discharge of electrons from the metallic element.

The values of the standard electrode potential of elements are plotted on the TC-YM diagram and shown in Fig. 5-2. The figures in the legend show the range of the electrode potential in units of volt.

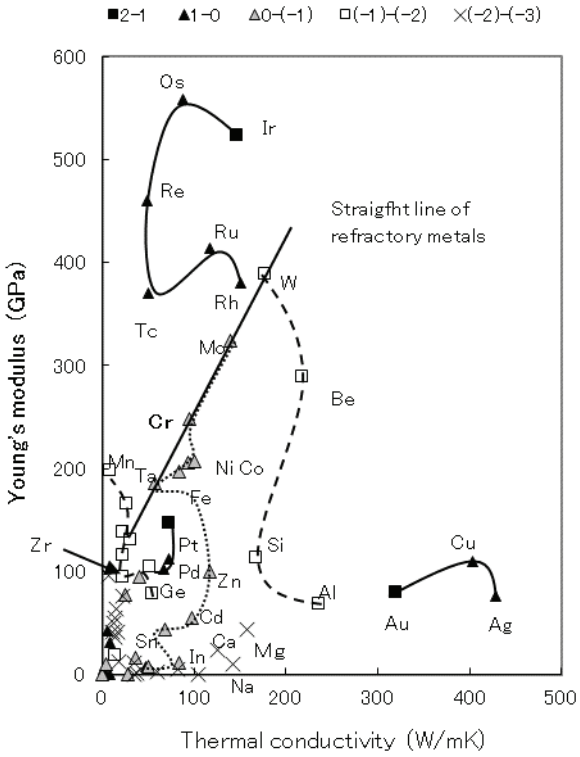

Fig. 5-2 – Electrode potential of elements on the TC-YM diagram

In contrast to the case of the periodic table, the electrode potential of elements shows a clear pattern.

There are three peaks of the electrode potentials of elements. The first is the element group of the largest thermal conductivity – Au, Cu, and Ag. The second is the element group of the highest Young's modulus – Rh, Ru, Tc, Re, Os, and Ir. The third is the element group of the medium thermal conductivity and medium Young's modulus – Ge, Pd, and Pt. The elements

– Ir, Au, and Pt – are the poles of the electrode potential on the TC-YM diagram, respectively.

Another remarkable point is that the elements which possess thermal conductivity around 100 W/mK show large electrode potentials. The elements on both their sides show small electrode potentials.

The total pattern is different from the patterns obtained so far in other properties.

(2) Electronegativity

The electronegativity shows how easily the electrons are attracted to the atoms in the chemical compounds. [3, 4]

The values of the electronegativity of elements are plotted on the TC-YM diagram and shown in Fig. 5-3.

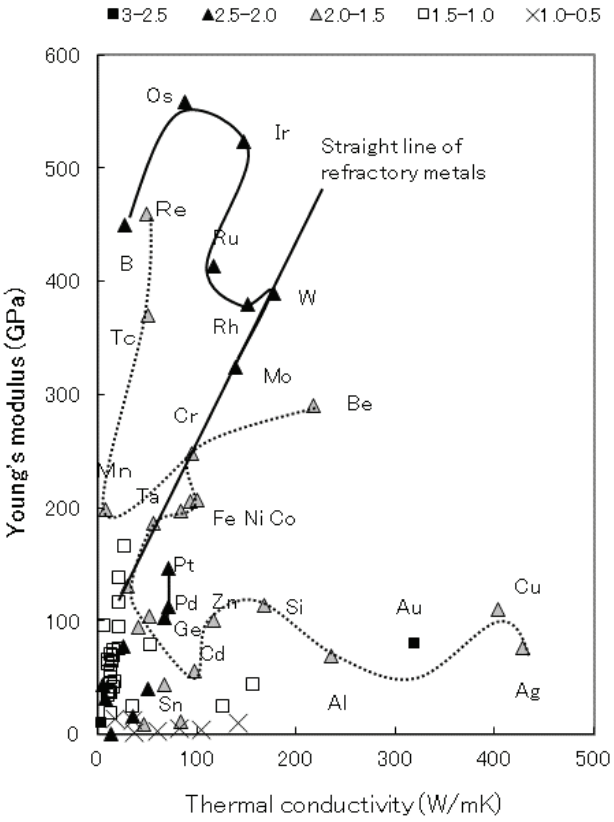

Fig. 5-3 – Electronegativities of elements on the TC-YM diagram

The general trend which was observed in electrode potential is obscure in the case of electronegativity. The range of elements with medium electrode potentials around 100 W/mK is expanded in the case of electronegativity.

Only the elements of larger Young's moduli show large electronegativities. In contrast to the electrode potential, only Au shows a large electronegativity in the high thermal conductivity range. The elements – Pt,

Pd, and Ge – show large electronegativities. Other elements show medium or small electronegativities.

(3) Ionization energy

The ionization energy means the energy which is needed when an electron is removed from an atom in the gaseous condition.

Fig. 5-4 shows the distribution of ionization energies of elements on the TC-YM diagram. The figures in the legend show the range of ionization energy in units of eV.

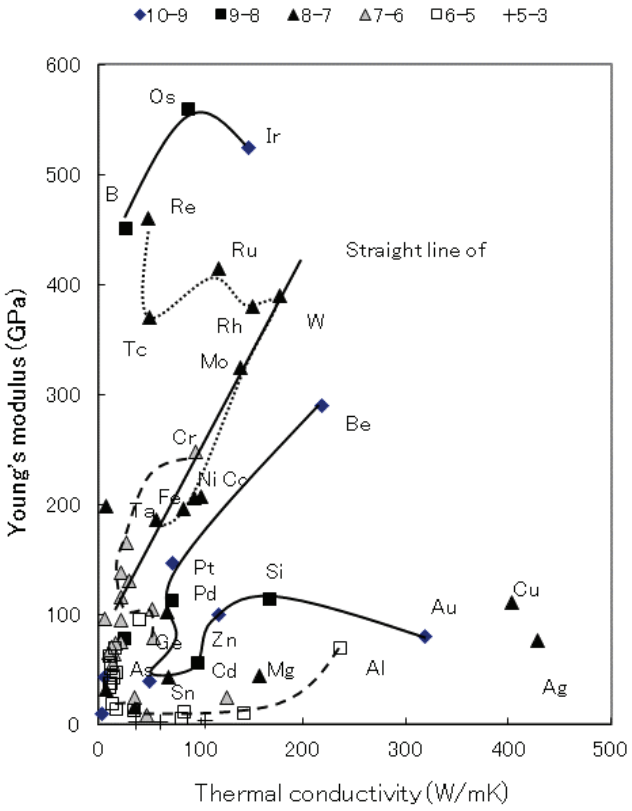

Fig. 5-4 – Ionization energy of elements on the TC-YM diagram

The area of the elements with large values is expanded inward.

The elements of the highest Young's moduli – Ir, Os, and B – show large ionization energy. But the most remarkable thing is that the gulf elements – Be, Fe, Ni, Co, Si, and Cu – show large ionization energies, and as the elements move far from them, the ionization energy decreases. This is the same pattern as in the atomic radius. As is referred to often, the ionization

energy increases with decreasing atomic radius. The elements which showed an abrupt drop of the ionization energy in Fig. 5-1– Tl, Ga, Al, and In – are included smoothly in the element group of low Young's modulus and small ionization energy, and show no anomaly. This is also an advantage of the TC-YM diagram.

(4) Electron affinity

The electron affinity means the energy which is needed when an electron is added to an atom in the gaseous condition.

Fig. 5-5 shows the distribution of the electron affinities of elements on the TC-YM diagram. The pattern is basically identical to that of the electrode potential.

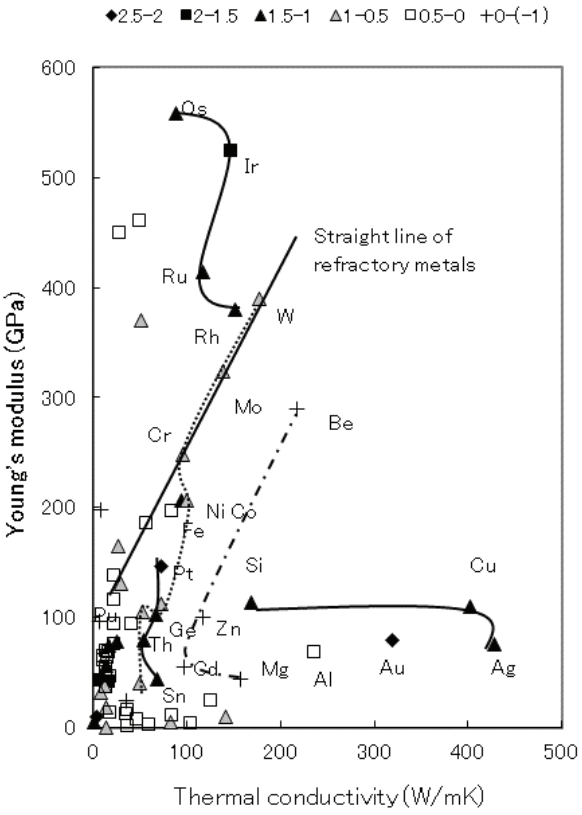

Fig. 5-5 – Electron affinity of elements on the TC-YM diagram

The elements of the largest Young's moduli – Os, Ir, Ru, and Rh – show large electron affinities. The elements around Au also show large electron affinities. Moreover, the elements around Pt also show large electron affinities. The other elements elsewhere show small electron affinities.

The remarkable thing is that the hcp-structured elements – Mg, Cd, Zn, and Be – show negative electron affinities, forming a deep valley. The elements

– Mg, Cd, Zn, and Be – are the elements which showed the largest ionization energies in Figure 5.4.

The elements – Ir, Au, and Pt – show the poles clearly in the electron affinity, identically in the electrode potential, electronegativity, and ionization potential.

5.2 Correlation with the periodic table

The electron charge-discharge characteristics have been discussed in terms of the periodicity of the elements. Fig. 5-6 shows the electrode potentials of elements on the periodic table.

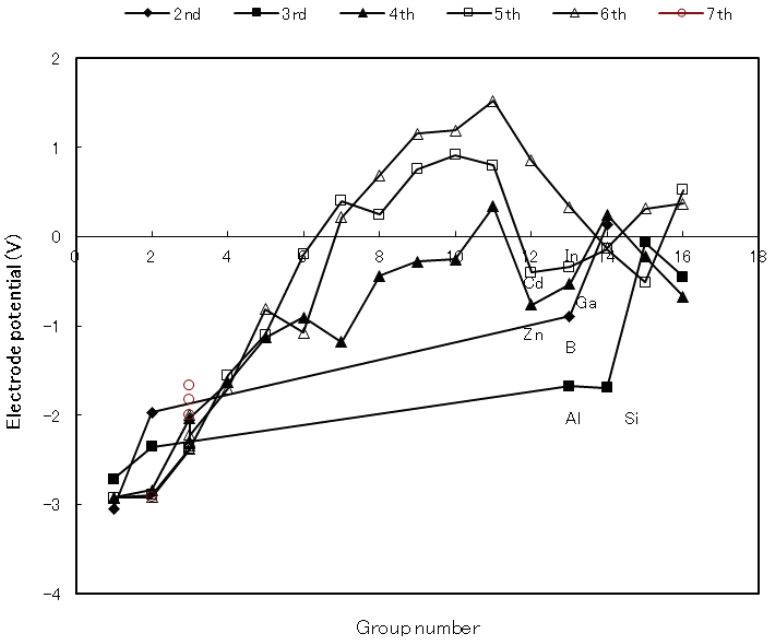

Fig. 5-6 – Electrode potentials of elements on the periodic table

With the increasing group number, the electrode potential increases. It drops at the elements of groups 12 and 13 – Zn, Ga, Cd, and In – abruptly. But in Fig. 5-2, Zn, Ga, Cd, and In are included smoothly in the elements of medium electrode potentials with the thermal conductivity around 100 W/mK. Furthermore, it is difficult to read the tendency of the electrode potentials of elements from the displays on the periodic table as shown in Fig. 5-6. In contrast to this, some tendencies can be read from the displays on the TC-YM diagram as shown in Fig. 5-2. It is proved that the displays of the electrode potentials of elements on the TC-YM diagram are much better. The electronegativity, ionization energy and electron affinity also show slightly different behaviors from each other on the TC-YM diagram. These can be clearly read from the diagrams. This is a great advantage of the TC-YM diagram.

5.3 Correlation with the atomic radius

The outer shell electrons are attracted by the protons in the nucleus. Therefore, with decreasing atomic diameter, the electron-discharge characteristics such as electronegativity and ionization energy increase. [5, 6] The ionization energy shown in Fig. 5-4 shows a similar pattern to that of the atomic radius of elements shown in Fig. 4-4. The elements with the smallest atomic radii form a gulf-shape in the center of the diagram, and those of the largest ionization energies form a gulf-shape in the center of the diagram.

Fig. 5-7 shows the relationship between the ionization energy and the atomic radius of elements. The ionization energy shows the strongest atomic radius dependence among these characteristics.

(In fact, Fig. 5-7 is the Darken-Gurry plot discussed in Chapter 13).

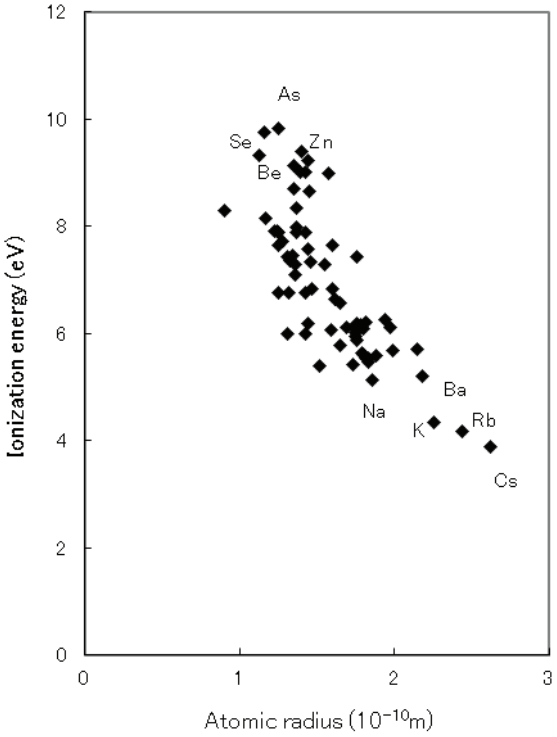

Fig. 5-7 – Relationship between the ionization energy and the atomic radius of elements

5.4 Correlation with the Fermi energy

From the above-mentioned, it was commonly found that there are three peaks in the electrode potential, electronegativity, ionization energy, and electron affinity on the TC-YM diagram. They are in the region of largest Young's modulus near Ir, in the region of the largest thermal conductivity

near Au, and in the center near Pt, respectively. The elements in those regions show the largest electrode potential, electronegativity, ionization energy, and electron affinity, respectively.

These phenomena may relate to the properties of the electrons in the outer shell of the atom. In general, the Fermi energy expresses the energy of these electrons. [7, 8]

The Fermi energy is given in the form of

$$E_F = 0.3646 \times \left(\frac{e/a}{\Omega}\right)^{2/3} \text{eV}, \qquad (5\text{-}1)$$

qwhere Ω is the volume per atom in units of nm^3 and e/a is the number of valence electrons per atom. [9] In this way, the Fermi energy is not a base quantity but a derived quantity. The volume of atom Ω is derived from the crystal structure and lattice constant.

Therefore, the values of the Fermi energy of elements do not show a simple pattern on the TC-YM diagram like the base quantities.

Fig. 5-8 shows the distribution of the Fermi energy of elements on the TC-YM diagram. The values of the Fermi energy of elements were adopted from the literature. [9]

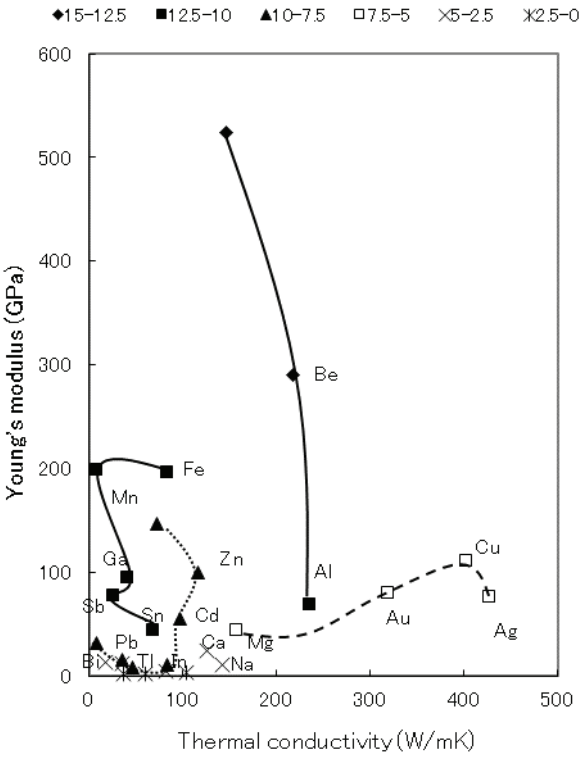

Fig. 5-8 – Fermi energies of elements on the TC-YM diagram

There can be seen an obscure trend. For the elements of low Young's modulus, with increasing thermal conductivity, the Fermi energy gradually increases. Consequently, Cu at the right-most end shows a medium Fermi energy. For the elements of high Young's modulus, with increasing Young's modulus and thermal conductivity, the Fermi energy increases. Be (beryllium) located in the high conductivity and high modulus region shows the largest Fermi energy.

Comparing Fig. 5-8 with Figures 5-2, 5-3, 5-4 and 5-5, it is difficult to speculate on correlations between them. Nevertheless, the correlations between them were examined here.

Fig. 5-9 shows the relationship between Fermi energy and electrode potential at the elements in which the values of the Fermi energy are available.

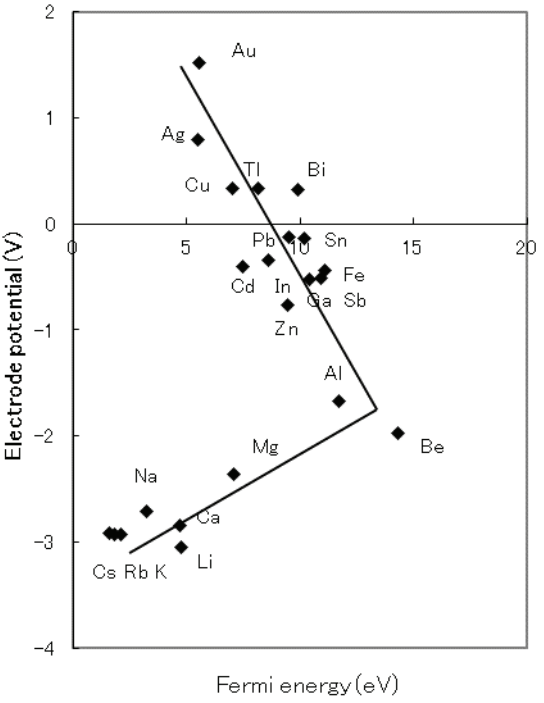

Fig. 5-9 – Relationship between the Fermi energy and electrode potential for the selected elements

Surprisingly, the correlation was recognized. But it doesn't have a simple linearity. With increasing Fermi energy, the electrode potential increases from the smallest Fermi energy and the lowest electrode potential at Cs, Rb, and K up to the elements Al and Be. After that, the electrode potential increases up to Ag, Au, and Cu with decreasing Fermi energy.

The relationship between the electrode potential and the Fermi energy is compared to the water in two buckets. [10]

Two buckets of different size and height are filled with water. The water levels at this time correspond to the Fermi energies of two metals. Next, the two buckets are connected with a pipe. The water flows from the high-level bucket to the low-level bucket and the same new water level is generated. In the same way, when two different metals are connected together, electrons in the metal with higher Fermi energy flow into the metal with lower Fermi energy to reach the same energy level. As a consequence, the metal which lost electrons is charged positive and the metal which obtained electrons is charged negative, and an electric potential difference is generated. This is called the **contact potential difference**. The metal which has extra electrons and is charged negative is the cathode, and the metal which has scarce electrons and is charged positive is the anode. In the conductive solvent, the anode metal is corroded. This is called **galvanic corrosion**. This type of corrosion is often experienced in aluminum parts in contact with brass parts.

If this hypothesis is valid, the metals with larger Fermi energy must have lower electrode potential. Fig. 5-9 shows this tendency in the high range of electrode potential from Au to Be. But the elements in the lower range of

electrode potential than Be show the inverse tendency. The above theory of contact potential difference is not always valid. This author indicated this point in the previous book. [11] At that time, the reasons were not known.

But now it can be explained as follows: The exceptional elements are Li, K, Rb, Cs, Ba, Sr, Ca, Na, and Mg. They are all elements of very low Young's modulus. The electrode potentials of elements shown in Fig. 5-2 show that these elements have the lowest potentials smoothly connected to each other in accordance with the trend on the TC-YM diagram. And the Fermi energies shown in Fig. 5-8 show that these elements have the smallest Fermi energies smoothly connected to each other in accordance with the trend on the diagram. As a result, the inverse trend shown in Fig. 5-9 occurs. Both the electrode potential and the Fermi energy are controlled by both the Young's modulus (binding force between atoms) and the thermal conductivity (electron mobility) of elements.

Correlation of electronegativity, ionization energy, and electron affinity with Fermi energy, is vaguer than the electrode potential.

5.5 Summary

The electron charge-discharge characteristics of elements, including electrode potential, electronegativity, ionization energy, and electron affinity, show three peaks on the TC-YM diagram. The first is the region of the highest Young's modulus near Ir. The second is the region of the highest thermal conductivity near Au. The third is the region around Pt near the center of the diagram. The elements – Ir, Au, and Pt – behave as the poles of these characteristics on the TC-YM diagram.

The electrode potential, electronegativity, ionization energy, and electron affinity show clear patterns on the TC-YM diagram, respectively.

In contrast to this, the correlation of these quantities to the periodic table shows no systematic tendencies.

The correlation of these quantities to the atomic radius shows vague tendencies.

The Fermi energy shows the largest values at Be and Ni, which are located in the medium thermal conductivity region on the TC-YM diagram.

Some correlations of the Fermi energy to these quantities were recognized. In the smaller range of the quantities, with increasing Fermi energy, the quantity increases. In contrast, in the larger range of the quantities, with increasing Fermi energy, the quantity decreases. This tendency is clearest in the electrode potential, and becomes obscurer in the order of electronegativity, ionization energy, and electron affinity. But even in the electrode potential, the correlation with the Fermi energy is not valid at the elements of very low Young's modulus. This is because these elements follow the trend on the TC-YM diagram more primarily than the Fermi energy.

References

1. R. E. Hummel, Understanding Materials Science, Springer, New York, USA, 1998, pp. 156-157.
2. D. R. Askeland, The Science and Engineering of Materials, 3rd ed., PWS, Boston, USA, 1989, pp. 726-727.

3. R. E. Hummel, Understanding Materials Science, Springer-Verlag, New York, USA, 1998, pp. 27-28.

4. D. R. Askeland, The Science and Engineering of Materials, 3rd ed., PWS, Boston, USA, 1989, pp. 24-25.

5. K. Saitou, Master the periodic table, Soft-bank Creative, Tokyo, 2012, p. 72.

6. G. E. Humiston and J. E. Brady, General Chemistry, Tokyo-Kagaku-Dojin, Tokyo, 1991, p. 144.

7. R. E. Hummel, Understanding Materials Science, Springer-Verlag, New York, USA, 1998, pp. 186-187.

8. D. R. Askeland, The Science and Engineering of Materials, 3rd ed., PWS, Boston, USA, 1989, pp. 600-602.

9. U. Mizutani, Introduction to the electron theory of metals, Cambridge Uni. Press, Cambridge, UK, 2001, pp. 26-27.

10. C. Newey and G. Weaver, Materials Principles and Practice, Butterworth Heinemann, 1990, p. 200.

11. Y. Mae, Stories on copper and aluminum, Nihon-Kikaku-Kyoukai, 2000, pp. 96-98.

6. LANTHANIDES

The lanthanides are the elements in the 3rd group and the 6th period of the periodic table.

In the 6th period, the orbits of 4s, 4p, 4d, 5s, and 5p are filled with electrons, and the 6s orbit begins to be filled at Cs. The 6s orbit is filled at Ba, and the 5d orbit begins to be filled at La. After La, the more inner orbit 4f begins to be filled. The 4f orbit is filled in the order of Ce, Pr, Nd, Pm, Sm, Eu, Gd, Tb, Dy, Ho, Er, Tm Yb, and Lu. The 4f orbit is fully filled at $_{71}$Lu.

The 5d orbit has two electrons at $_{72}$Hf, and Hf becomes the element of group 4.

The elements from La to Lu are referred to as the lanthanides, and shown outside the periodic table. They are said to have similar chemical properties, because they have the same three electrons ($5d^1 6s^2$) in the outer orbit. But, looking into the details, there are some differences in their properties.

Eu and Yb are introduced in the chemical dictionary, though the reasons are not stated, as the elements exhibiting peculiar properties compared with the other lanthanides. [1]

6.1 Explanations of the anomalies of Eu and Yb so far

(1) Crystal structure

Fig. 6-1 shows the crystal structures of the lanthanides with the atomic number.

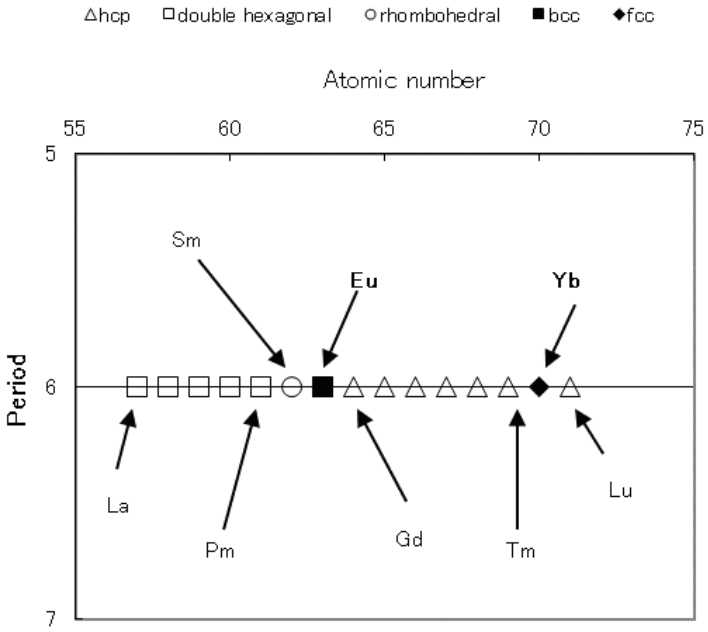

Fig. 6-1 – Crystal structures of the lanthanides with the atomic number

Most adopt hexagonal structures. Elements from La to Pm adopt the double hexagonal-closed-packed structure (ABAC structure). At Sm, the structure changes to a rhombohedral structure (cubic with three edges of different length). Eu has a bcc (body-centered-cubic) structure. Elements from Gd to Tm have the hcp (hexagonal-closed-packed) structures (AB structure). Yb

suddenly adopts an fcc (face centered-cubic) structure, which reverts to hcp for Lu. In short, the crystal structures of Sm, Eu and Yb change abruptly and without clear reason. These anomalies have been reported previously, but no explanation has been provided.

(2) Atomic radius

Eu and Yb also exhibit unexpected characteristics in their atomic radii. Fig. 6-2 shows the variation of the atomic radius of the lanthanides as a parameter of the atomic number.

The atomic radius tends to decrease with increasing atomic number, which is known as the lanthanide contraction. However, Eu and Yb show an abrupt increase in the atomic radius. It is noted that Eu and Yb exhibited divalent characteristics while other lanthanides exhibited trivalent characteristics, and that this was relevant to the increased atomic radii of Eu and Yb. [2] The reasons for their divalent characteristics were not discussed.

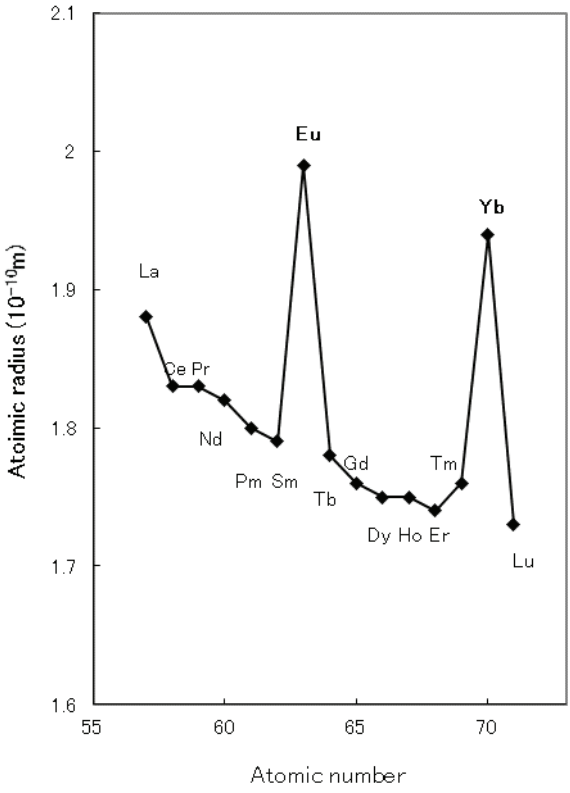

Fig. 6-2 – Atomic radii of the lanthanides with the atomic number

This figure has been referred to often. Their comments are as follows: Though there are disconnections at Eu and Yb, a stable decrease of the atomic radius is seen with increasing atomic number. This is called the "lanthanide contraction".

They say also that Eu and Yb have only two electrons on the 5d and 6s orbits, and have the electron configurations of $4f^7$ and $4f^{14}$, which lead to the largest

exchange energy for stabilization. Consequently, Eu and Yb have two electrons in the binding band, and their atomic radii become larger than other lanthanides which have 3 electrons there. [3]

(3) Melting temperature

Fig. 6-3 shows the variation of the melting temperature of the lanthanides as a parameter of the atomic number.

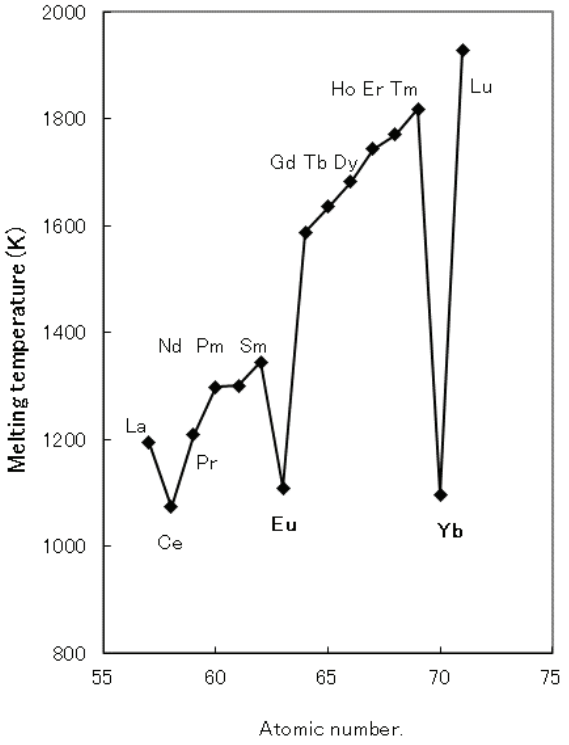

Fig. 6-3 – Melting temperature of the lanthanides with the atomic number

The melting temperature tends to increase with increasing atomic number, but abruptly decreases for Eu and Yb. It was noted again that divalent characteristics of Eu and Yb emerged in their melting temperature. [2]

Other properties like the thermal expansion coefficient, boiling point, heat of fusion, and heat capacity exhibit similar trends. Such anomalies for Eu and Yb among the lanthanides have long been recognized and have been somewhat accounted for by valence electrons. [2] However, the anomalies in the crystal structures for Eu and Yb cannot be accounted for by valence electrons. Therefore, a more comprehensive explanation is required.

6.2 Representation of Eu and Yb on the TC-YM diagram

In order to clarify the reasons for the anomalies for Eu and Yb, their properties were plotted on the TC-YM diagram.

(1) Crystal structure

Fig. 6-4 shows the distribution of crystal structures for elements of low Young's modulus and low thermal conductivity. [4]

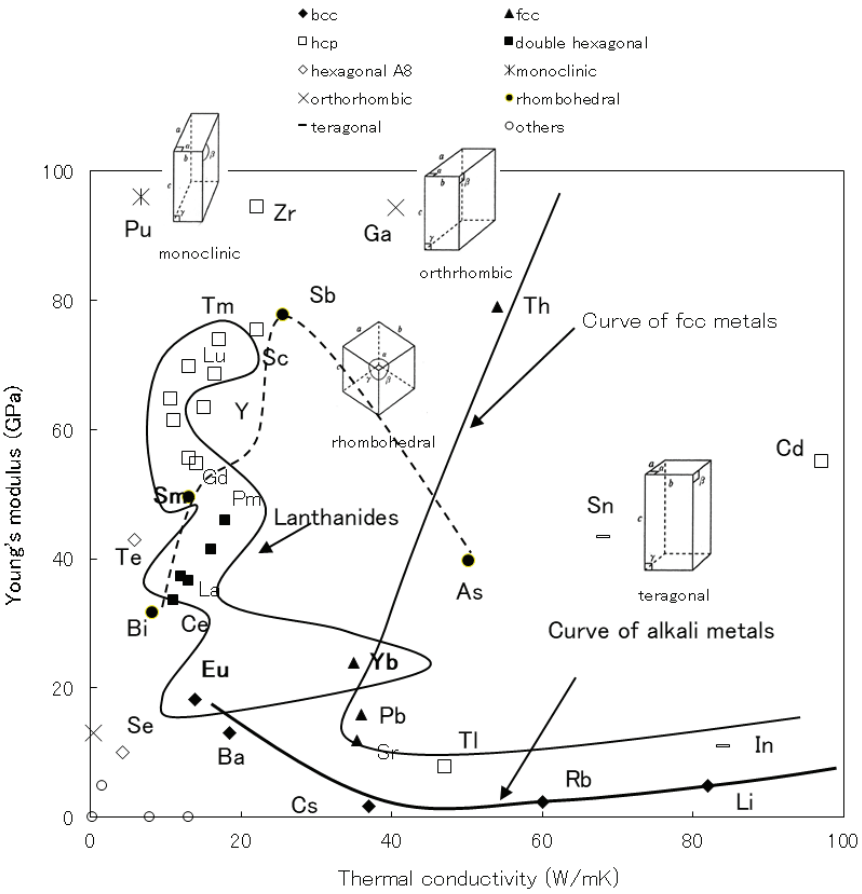

Fig. 6-4 – Distribution of crystal structures for elements with low Young's modulus and low thermal conductivity

The lanthanides are distributed across a wide Young's modulus range at low thermal conductivity. The lower Young's modulus elements include La, Ce, Pr, Nd, and Pm, which adopt double hexagonal (ABAC) structures. The higher Young's modulus elements include Gd, Tb, Dy, Ho, Er, Tm, and Lu,

which adopt hcp (ABAB) structures.

Sm is a transient element and lies between these groups, adopting a rhombohedral structure.

Eu and Yb do not follow this trend, and are instead at much lower Young's modulus.

Eu lies at lower Young's modulus and lower thermal conductivity, and on the extension of the curve of alkali metals. The curve of alkali metals contains Na, K, Li, Rb, and Cs, trending from high to low thermal conductivity. The alkaline earth metal Ba lies on the extension of the curve of alkali metals. Eu lies on this extension line after Ba. This is why Eu adopts a bcc structure, and does not follow the trend of the other lanthanides. This is also why Ba adopts a bcc structure, and does not follow the trend of the alkaline earth metals.

Yb is located at low Young's modulus but slightly higher thermal conductivity than Eu. It is located near Pb, which lies on the curve of fcc metals. The curve of fcc metals proceeds from Ag (right-most side) through Cu, Au, Al, Ca, Pb, Th, Pd, Pt, Ni and Rh, and ends at Ir, as shown in Fig. 2-2. Yb and Sr are located near Pb and the curve of fcc metals. This is why Yb adopts an fcc structure and does not follow the trend of the lanthanides. This is also why Sr adopts an fcc structure and does not follow the trend of the alkaline earth metals.

(2) Atomic radius

Fig. 6-5 shows the distribution of the atomic radii of elements of low

Young's modulus and low thermal conductivity.

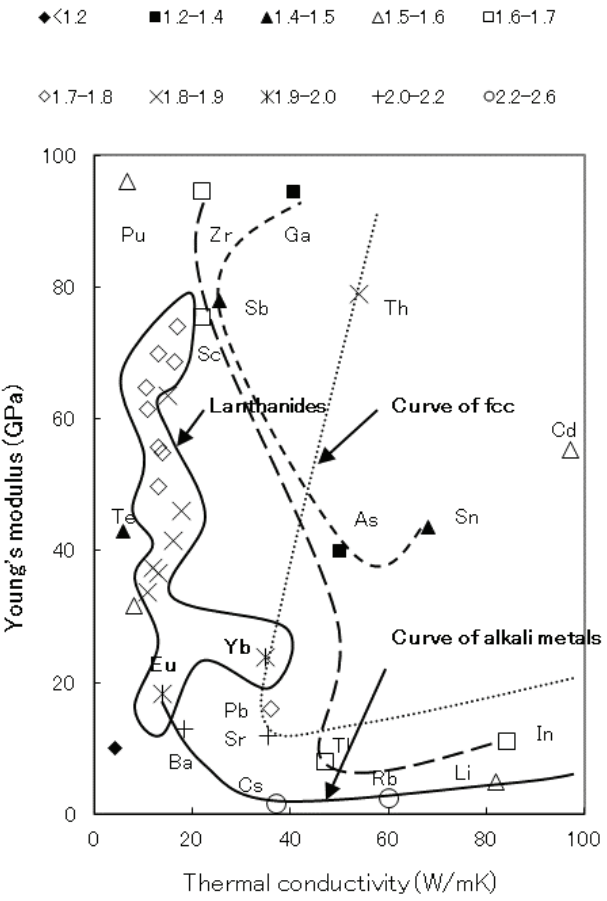

Fig. 6-5 – Distribution of the atomic radii of elements with low Young's modulus and low thermal conductivity

The figures in the legend show the range of atomic radii in units of 1×10^{-10} m. The elements – Ga, Sb, As and Sn – are located in an arch near the center

of the diagram and have the smallest atomic radii. The elements – Zr, Sc, Tl and In – form an outer concentric circle and have the next smallest atomic radii. The atomic radius increases with decreasing Young's modulus and decreasing thermal conductivity. The lanthanides are located outside of these more central elements, so have much larger atomic radii. For the lanthanides, atomic radius increases with decreasing Young's modulus. This means that Eu and Yb have large atomic radii. Eu connects to Ba, and Yb connects to Pb and Sr.

This is why the atomic radii of Eu and Yb abruptly increase with increasing atomic number.

(3) Melting temperature

Fig. 6-6 shows the distribution of melting temperatures (K) of elements with low Young's modulus and low thermal conductivity.

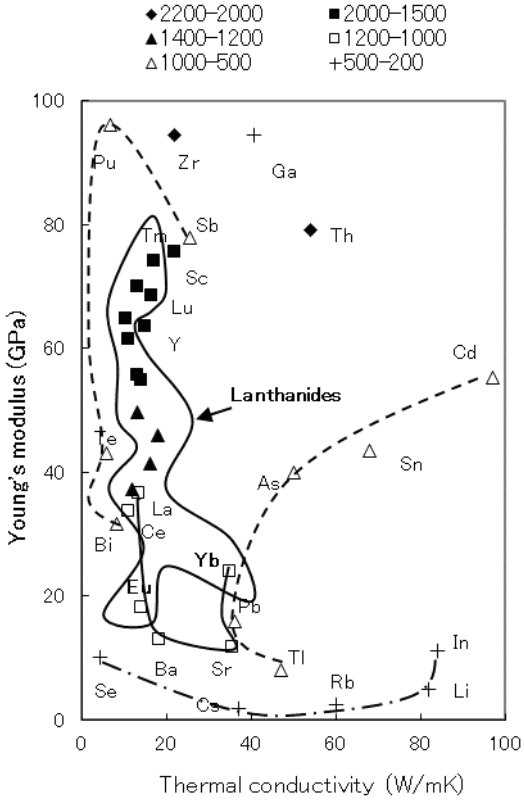

Fig. 6-6 – Distribution of melting temperatures (K) of elements with low Young's modulus and low thermal conductivity

Elements with the highest melting temperatures are distributed from Zr at the top of the diagram to the upper region of the lanthanides, according to the tendency that elements of high melting temperature follow the straight line of refractory metals. The melting temperatures of the lanthanides decrease with decreasing Young's modulus. Eu and Yb occupy the lowest positions of the lanthanides and have the lowest melting temperatures. Eu

connects smoothly to Ba, which has a similar melting temperature. Yb connects smoothly to Sr, which has a similar melting temperature. This is why the melting temperatures of Eu and Yb abruptly decrease with increasing atomic number.

(4) Valence

It is reported that Eu and Yb exhibit divalent characteristics while other lanthanides exhibit trivalent characteristics. [2] This was regarded as the cause of their large atomic radii. But their large atomic radii and divalence are equally the results of their low Young's moduli.

This can be explained from their locations on the diagram. Eu is located close to Ba lying on the same curve of alkali metals on the diagram. Therefore, Eu shows a similar behavior as Ba in valence. Ba is an alkaline earth metal and a divalent element. Therefore, Eu adopts divalence.

Yb is located close to Sr lying on the same curve of fcc metals. Sr is also an alkaline earth metal, and a divalent element. Therefore, Yb shows a similar behavior as Sr in valence. As a result, both Eu and Yb show divalence, while other lanthanides show trivalence.

6.3 Discussion

Anomalies in the crystal structures, atomic radii, melting temperatures, and valences of Eu and Yb are observed with increasing atomic number. Similar anomalies are observed to a greater or lesser degree in the thermal expansion, boiling point, heat of fusion, and vapor pressure.

The properties of Eu and Yb are strongly related to their positions in the

lower Young's modulus region of the diagram.

Why are Eu and Yb located there?

They likely play a role in bridging the lanthanides to other element groups. Such bridging and smooth connections seem to be necessary. This bridging effect can be seen elsewhere. Nb is a member of the refractory metals, but lies off the straight line of refractory metals, and is located near Ge, as shown in Fig. 2-2. Nb and Ge share a non-closed-packed structure. Nb plays a role in bridging the refractory metals group to the diamond structure group containing Ge and Si. It seems that an element group must smoothly connect to another element group, with regard to the Young's modulus and thermal conductivity. Eu and Yb *a priori* occupy positions at low Young's modulus, and connect to the alkali metals and fcc metals, respectively. As a result, Eu adopts a bcc structure and Yb an fcc structure.

The difference in the crystal structure between Eu and Yb is brought about by their differing thermal conductivities. Thermal conductivity is also an index to determine the properties of elements.

What mechanism results in their low Young's moduli? Fig. 6-7 shows the electronic configurations of the lanthanides [5], in which electrons progressively fill the 4f orbital, and the electron occupancy of the 5d orbital varies between zero to one.

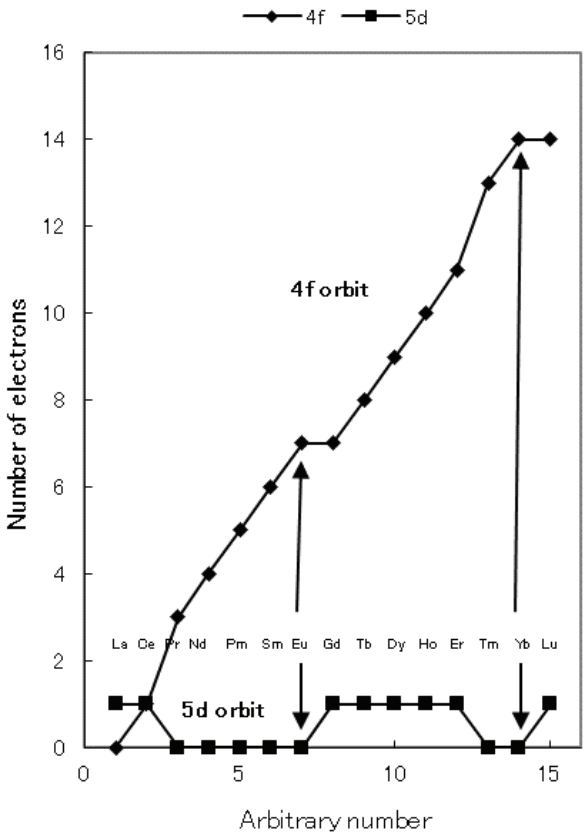

Fig. 6-7 – Electronic configurations of the lanthanides

Eu and Yb are the last elements where the 5d orbital is empty, but this does not explain their abrupt decrease in Young's modulus. The microscopic structure of the electron orbitals must be considered.

Some mechanisms may weaken the binding potential in Eu and Yb and consequently lower their Young's moduli.

6.4 Summary

Element groups smoothly connect to other element groups, in terms of Young's modulus and thermal conductivity. To satisfy this condition, Eu and Yb have low Young's moduli to connect with the alkali metal and fcc metal groups, respectively. This results in the specific crystal structures, large atomic radii, and low melting temperatures of Eu and Yb, which differ from the other lanthanides in these properties. Some mechanism in the electronic orbitals in Eu and Yb effectively lowers their Young's moduli.

In this way, Eu and Yb come to occupy the low Young's modulus region in the TC-YM diagram, and connect to the adjacent other element groups such as the alkali metals and the fcc metals. As a result, they behave like members of the adjacent element groups. This is the reason why Eu and Yb show the anomalies in the physical properties among the lanthanides.

References

[1] Tokyo-Kagaku-Doujin, Big Chemical Dictionary, Tokyo-Kagaku-Doujin, Tokyo, 1989, p. 190.

[2] E. C. Subbarao and W. E. Wallace, Science and technology of rare earth materials, Academic Press, New York, 1980, pp. 53-54.

[3] N. Imanaka, T, Masui and S. Tamura, Atomic structures and periodicity, Kagaku-Dojin, Tokyo, 2004, p. 71.

[4] Y. Mae, Schematic interpretation of anomalies in the physical properties of Eu and Yb among the lanthanides, Int. J. Mater. Sci. Appl. Vol. 6, No. 4, 2017, pp. 165-170.

[5] Japan Institute of Metals, Metals data book, 3rd ed., Maruzen, Tokyo, 1993, p. 5.

7. ACTINIDES

The actinides are the fifteen elements from atomic number 89 to 103. The elements – $_{89}$Ac, $_{90}$Th, $_{91}$Pa, $_{92}$U, $_{93}$Np and $_{94}$Pu – occur in nature, but the elements after atomic number 95 are the artificial elements. The actinides have electrons on the *f-orbit* similarly to the lanthanides. [1] It is often said that the lanthanides and the actinides show similar characteristics due to the electrons on the *f-orbit* . [1] But in fact, in comparison with the lanthanides, the actinides exhibit an unusually large range of physical properties. The element $_{89}$Ac and the actinide elements after $_{95}$Am behave similarly to the lanthanides. On the other hand, $_{90}$Th, $_{91}$Pa and $_{92}$U are much more similar to transition metals in their chemical properties. The elements $_{93}$Np and $_{94}$Pu show intermediate properties between the lanthanides and the transition metals. [2] It is also said that the elements after $_{95}$Am show very similar chemical characteristics to the lanthanides.

In summary, the first actinide element $_{89}$Ac is similar to the lanthanides, the next actinide elements – $_{90}$Th, $_{91}$Pa, and $_{92}$U – are similar to transition metals, $_{93}$Np and $_{94}$Pu are intermediate, and finally the elements after $_{95}$Am are similar again to the lanthanides.

In addition, it is noted that the oxidation number of Pa is +5, and its chemical properties are similar to Nb and Ta in group 5. [3, 4]

Furthermore, it is noted that $_{102}$No can adopt the oxidation number of +2 and +3, and has similar chemical properties to Yb. [5]

From these facts, it seems that the actinides form a cycle in the characters. But the mechanism is not known. The fundamental properties of the actinides are in the spotlight after the Fukushima-Daiichi accident. [6]

7.1 Representation of the properties of the actinides on the periodic table

The data of the properties are scarce in the actinides. The crystal structure, melting point, atomic radius and electronegativity were selected, because they are known in all actinides.

(1) Crystal structures on the periodic table

Fig. 7-1 shows the distribution of the crystal structures of the actinides with the atomic number, compared with those of the lanthanides.

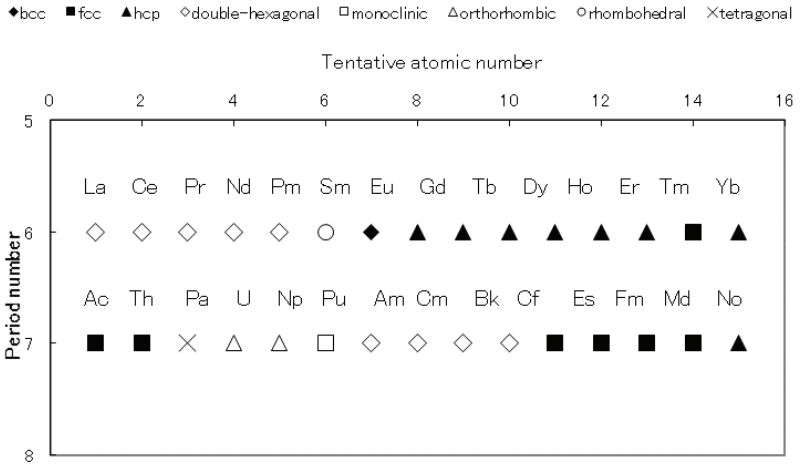

Fig. 7-1. – Distribution of the crystal structures of the lanthanides and actinides on the periodic table

The abscissa shows the arbitrary atomic number beginning from La and Ac, respectively. It has often been said that each actinide is similar to each lanthanide in the same column. But it is clear that the tendency of the crystal structures of the actinides is much different from that of the lanthanides. The mechanism for the crystal structures of the lanthanides has already been described in Chapter 6. From Fig. 7-1, it is noted that there are no orderings in the crystal structures of the actinides. But that is not the case.

(2) Atomic radius

Fig. 7-2 shows the variation of the atomic radius of the actinides with the atomic number compared with the lanthanides.

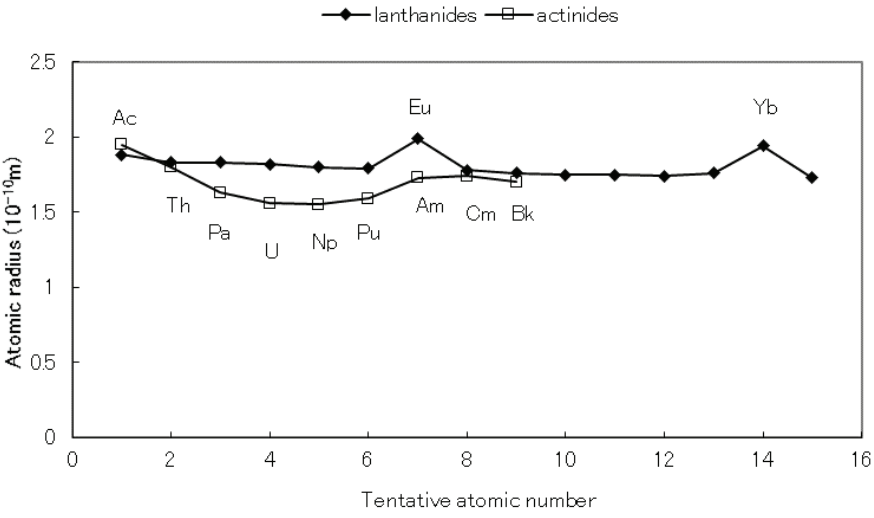

Fig. 7-2 – Variation of the atomic radii of the lanthanides and actinides with the atomic number

The tendency of the actinides in the atomic radius is different from that of the lanthanides. In the lanthanides, the atomic radius decreases slightly with the atomic number except for Eu and Yb. The reason for the anomalies of Eu and Yb was described in Chapter 6. In the actinides, the atomic radius decreases considerably after Ac, and takes the minimum at U and Np, and then increases again, reaching the plateau after Am.

(3) Melting point

Fig. 7-3 shows the variation of the melting temperatures of the actinides with the atomic number compared with the lanthanides.

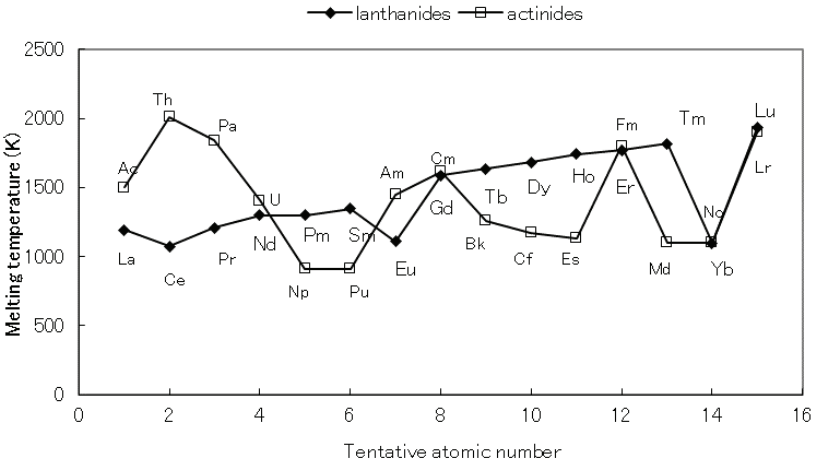

Fig. 7-3 – Variation of the melting temperatures of the lanthanides and actinides with the atomic number

The melting temperature of the lanthanides monotonically increases with the atomic number except for Eu and Yb. The reason for the anomalies of Eu and Yb was described in Chapter 6. In the actinides, it reaches the

maximum at Th, and then decreases gradually, and finally takes the minimum at Np and Pu. After that, it continues to fluctuate.

(4) Electronegativity

Electronegativity is the only chemical property available in the actinides. Electronegativity means a tendency of an atom to attract electrons towards itself. Fig. 7-4 shows the variation of electronegativity of the actinides with the atomic number compared with the lanthanides.

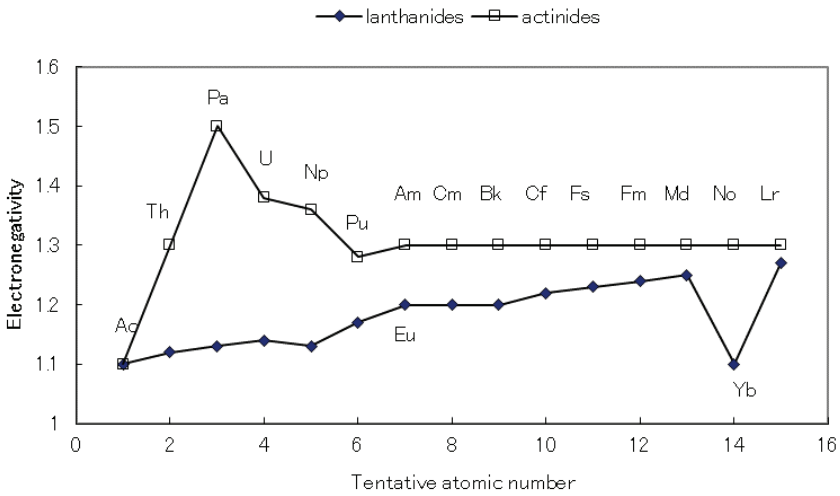

Fig. 7-4 – Variation of electronegativity of the lanthanides and actinides with the atomic number

The tendency of electronegativity of the actinides is quite different from that of the lanthanides. In the lanthanides, electronegativity increases gradually with the atomic number except for Yb. In the actinides, it increases rapidly,

takes the maximum at Pa and decreases gradually and reaches the plateau after Am. As a whole, electronegativities of the actinides are larger than those of the lanthanides.

7.2 Representation of the properties of the actinides on the TC-YM diagram

As mentioned above, the properties of the actinides are quite different from those of the lanthanides. The mechanism which causes these differences will be studied here using the TC-YM diagram. In order to draw a TC-YM diagram, data on the thermal conductivity and the Young's modulus of each element are necessary.

The only elements where both data are available are Th, U and Pu. There are no direct data for the other actinides. Therefore, missing data must be speculated somehow.

It is reported that the shear modulus of **Ac** is similar to that of Pb. [7] The Young's modulus of Ac, therefore, was assumed here to be the same as Pb.

Similarly, the Young's moduli of **Pa** and **Np** were assumed to be the same as Ti and Mn, respectively. [7, 8]

Additionally, it is reported that the elements **Bk, Cf, and Es** have the bulk moduli of 20 GPa, 50 GPa and 15 GPa, respectively. [9, 10]

Fig. 7-5 shows the correlation between the Young's modulus and the bulk modulus for most elements.

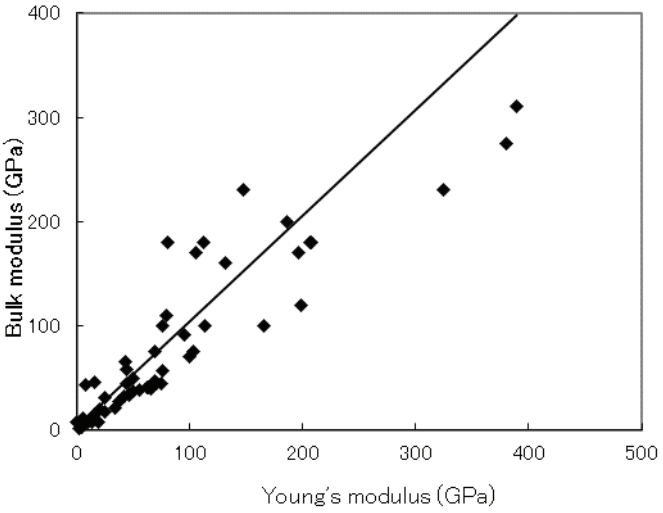

Fig. 7-5 – Correlation between the Young's modulus and the bulk modulus of the elements

From Fig. 7-5, the Young's modulus was assumed to be equal to the bulk modulus. But, since the data on the thermal conductivity of Cf and Es are missing, only Bk could be plotted. Consequently, the elements Ac, Th, Pa, U, Np, Pu and Bk could be displayed on the diagram, as shown in Figure 7.6.

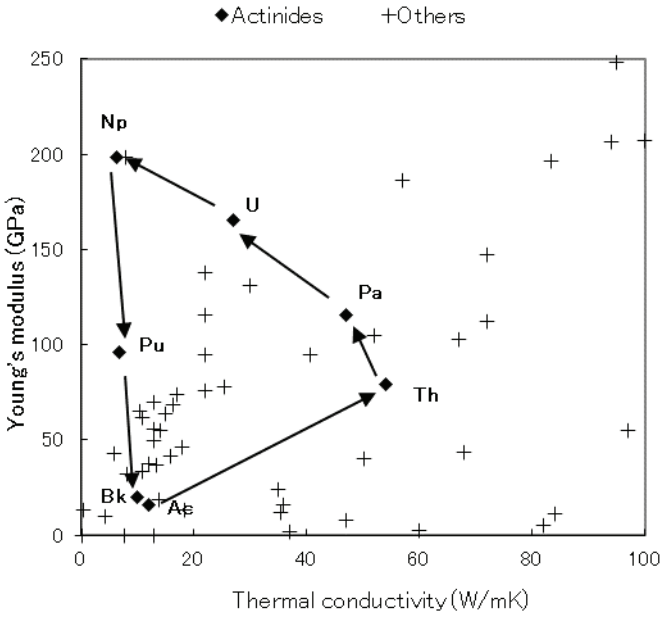

Fig. 7-6 – Moving direction of the elements from Ac through Th, Pa, U, Np, Pu to Bk on the TC-YM diagram

Surprisingly, the elements Ac, Th, U , Np, Pu and Bk among the actinides form a large triangle on the TC-YM diagram.

(1) Crystal structures of the actinides on the TC-YM diagram

The distribution of the crystal structures of all elements is shown in Fig. 2-2. Fig. 7-7 shows the distribution of the crystal structures of the actinides with other elements.

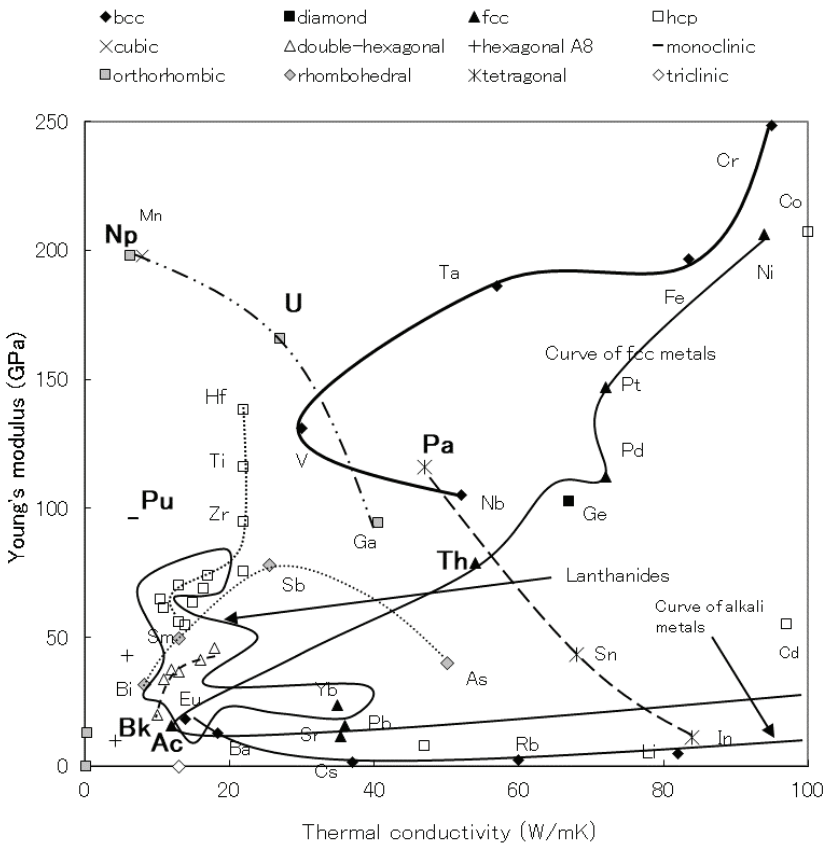

Fig. 7-7 – Distribution of the crystal structures of the actinides on the TC-YM diagram

Here, a small region of the diagram was shown, because the values of the thermal conductivity and the Young's modulus of the actinides are limited within the region of small thermal conductivity and small Young's modulus.

Ac has an fcc structure. Ac is located on the left side of Pb which has an fcc structure and lies on the curve of fcc metals. It can be considered, therefore,

that the curve of fcc metals should be extended to the position of Ac.

A large movement is observed from Ac to Th. The thermal conductivity and Young's modulus increase considerably from Ac to Th. Th is located on the curve of fcc metals. Therefore it has the same fcc structure as Ac.

From Th to Pa, the Young's modulus increases and the thermal conductivity decreases moderately. Pa forms a curve with Sn and In, and adopts the same **tetragonal** structures as Sn and In.

From Pa to U, the Young's modulus increases and the thermal conductivity decreases further. From U to Np, the Young's modulus increases further and the thermal conductivity decreases severely. Np and U form a curve with Ga, and adopt the same **orthorhombic** structures as Ga.

From Np to Pu, the Young's modulus decreases abruptly with the same thermal conductivity as Np. Pu adopts a **monoclinic** structure at room temperature. Pu is located relatively in the isolated position on the diagram. Therefore, it tends to adopt a rare crystal structure. But the elements U and Pu, including Hf, Ti and Zr, show a common aspect that they adopt bcc structures at high temperatures after allotropic transformation. [11]

From Pu to Bk jumping over Am and Cm which have no data of the Young's modulus, the Young's modulus decreases further with the same thermal conductivity as Pu. Bk adopts a **double-hexagonal structure**. It connects to the nearby lanthanide elements which have the same double-hexagonal structures.

In the periodic table, the actinides are shown in the margin. It seems that

they have no neighbors. But on the TC-YM diagram, it is clear that they each have neighbors and are affected by them.

In summary, **the early actinides form a triangle on the diagram, and each element adopts the crystal structure similar to the nearby elements on the TC-YM diagram.**

In contrast, the lanthanides are located within a very narrow area, forming a vertical row. Therefore, they mostly show only two crystal structures: hcp and double-hexagonal.

(2) Atomic radii on the TC-YM diagram

The distribution of the atomic radii of all elements is shown in Fig. 4-4. The gulf elements, which form a gulf-shape in the center of the diagram, Be, Cr, Fe, Ni, Co Si and Cu, show the smallest atomic radii among the metallic elements. With decreasing conductivity and Young's modulus, the atomic radius of the elements increases. Fig. 7-8 shows the distribution of the atomic radii of the actinides with other elements in the low conductivity and low modulus range of the diagram.

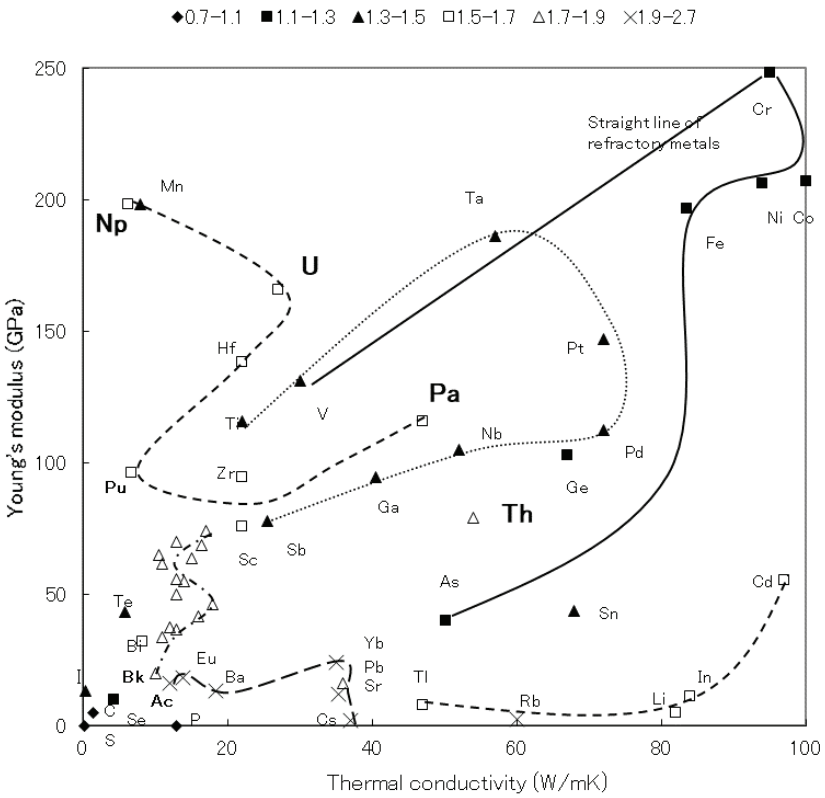

Fig. 7-8 – Distribution of the atomic radii of the actinides on the TC-YM diagram

The figures in the legend show the range of the atomic radius in units of 10^{-10} m. The elements with small atomic radii are located in the high conductivity and high modulus range. The elements with the largest atomic radii are located at the periphery along the abscissa and the ordinate. In general, with increasing thermal conductivity, and with increasing Young's modulus, the atomic radius decreases.

Ac belongs to the element group with the largest atomic radii.

From Ac to **Th**, the atomic radius slightly decreases, affected by the neighboring elements with small atomic radii such as Nb and Ga.

From Th to **Pa**, the atomic radius decreases further, affected by the surrounding elements with small atomic radii such as Nb, Ga, V and Ta.

Furthermore, **U, Np and Pu** have similar radii to Pa, because they are all commonly surrounded by the elements, Sb, Ga, Nb, Ge, Pd, Pt, Ta, V, Ti and Mn.

From Pu to **Bk**, the Young's modulus decreases rapidly, and the atomic radius increases again to the level of the nearby lanthanides.

The variation of the atomic radius with the atomic number shown in Fig. 7.2 can be explained schematically on the TC-YM diagram.

(3) Melting points on the TC-YM diagram

The distribution of the melting temperatures of all elements is shown in Fig. 4-3. As a whole, with decreasing Young's modulus and thermal conductivity, the melting temperature of elements decreases. Fig. 7-9 shows the distribution of melting temperatures (K) of the actinides with other elements in the low thermal conductivity and low Young's modulus range of the diagram.

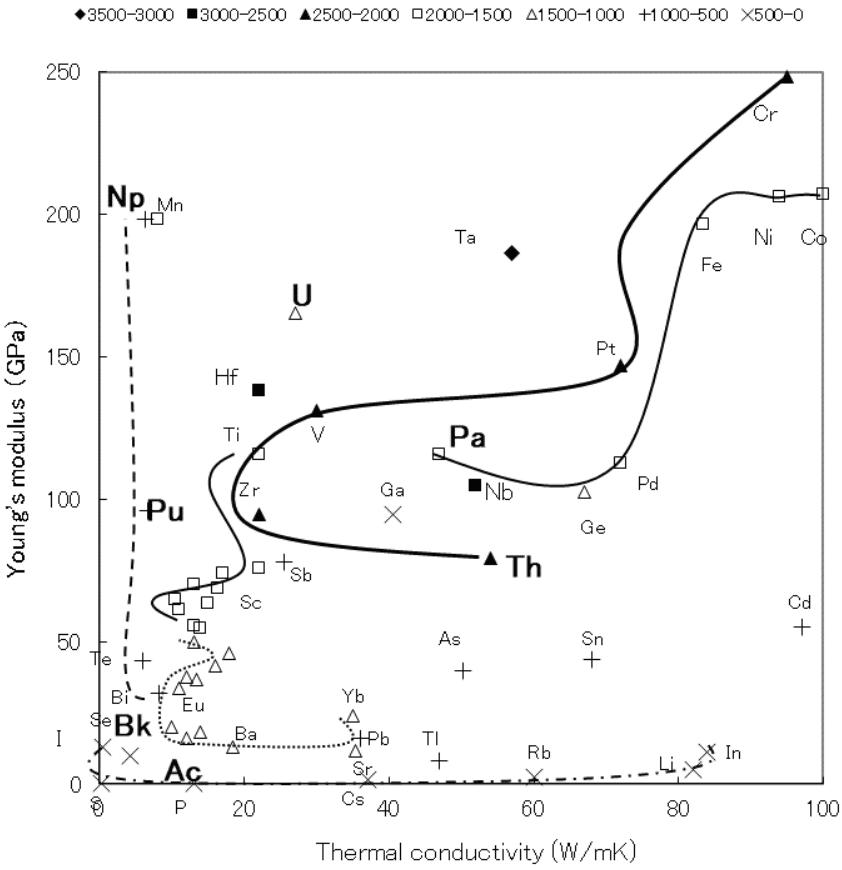

Fig. 7-9 – Distribution of the melting temperatures (K) of the actinides on the TC-YM diagram

Not only in the total range of the TC-YM diagram, but also in the low thermal conductivity and low Young's modulus range, with decreasing conductivity and modulus, the melting temperature decreases. The elements with high melting temperatures are located in the high conductivity and high modulus range. The elements with low melting temperatures are located in

the periphery along the abscissa and the ordinate.

Ac belongs to the element group with a medium melting temperature between 1000 and 1500K.

Th adopts a higher melting temperature, affected by the high melting temperature elements in the neighborhood.

After Th, with decreasing conductivity, the melting temperature decreases considerably.

Pa adopts an intermediate melting temperature similarly to Pd, Fe, Ni, and Co.

U adopts a lower melting temperature than Pa, though the adjacent elements are Hf and Ta which have high melting temperatures. It is probably because U is strongly affected by Np.

The elements on the periphery along the ordinate – **Np** and **Pu** – show melting temperatures as low as Te and Bi.

The element **Bk**, with thermal conductivity a little larger than Np, Pu and Te and Bi returns to the element group with medium melting temperature.

The variation of the melting temperature with the atomic number shown in Figure 7.3 can be explained schematically on the TC-YM diagram.

(4) Electronegativity on the TC-YM diagram

The distribution of the electronegativity of all elements is shown in Fig. 5-3. The gulf elements – Cu, Si, Fe, Ni, Co, Cr and Be – show the large values

of electronegativity. Most of the elements are distributed in the enlarging concentric circle with decreasing electronegativity.

Fig. 7-10 shows electronegativity of the actinides with other elements in the low conductivity and low modulus range.

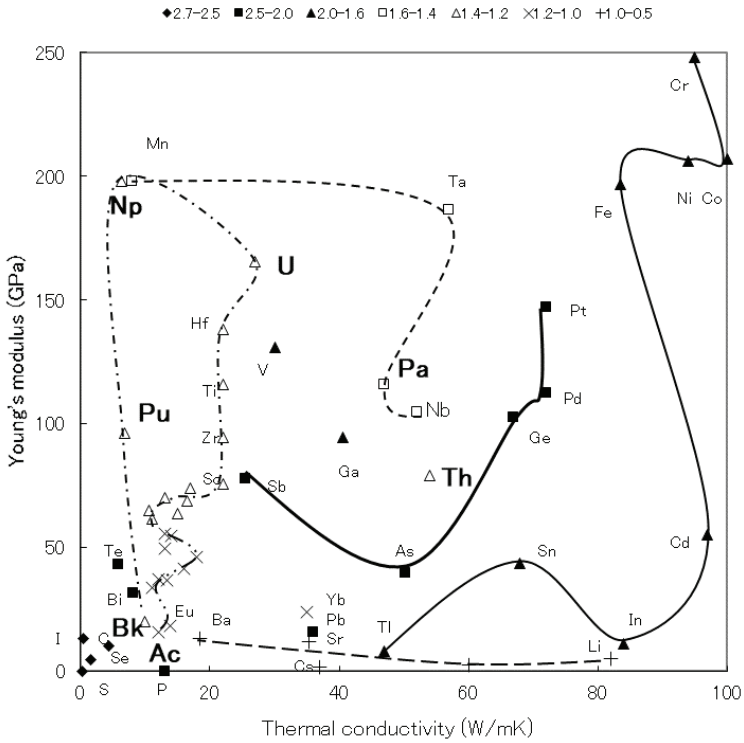

Fig. 7-10 – Distribution of the electronegativity of the actinides on the TC-YM diagram

In contrast to the atomic radius, the elements with high conductivity and high modulus show large values in electronegativity. The elements at the peripheries along the abscissa and the ordinate show small electronegativity.

Especially, the elements at the periphery along the abscissa show the smallest electronegativity and connect to the lower elements of the lanthanides with the next smallest electronegativity.

Ac has a small electronegativity similar to Eu and the lower elements of the lanthanides in the neighborhood.

Th has larger electronegativity, but lower than that of the elements – Ga, As, Ge, and Nb – surrounding it. Th should have higher electronegativity between 2.0 and 1.6, judging from its position.

Pa has large electronegativity similar to Nb and Ta in the neighborhood. This coincides with the previous statement that Pa has similar chemical properties to Nb and Ta. [3, 4]

The elements **– U, Np, Pu and Bk –** have small electronegativity similar to the elements – Hf, Ti, Zr, and Sc – and the elements in the upper parts of the lanthanides in the neighborhood.

The variation of electronegativity of the actinides with the atomic number shown in Fig. 7-4 can be explained except for the element Th which should have still larger electronegativity.

7.3 Speculation of the properties of other actinides

The data on the Young's modulus of Ac, Pa, and Np are missing. They were assumed here to be the same as Pb, Ti and Mn, respectively. [7, 8] Consequently, they showed reasonable behaviors on the TC-YM diagram.

In contrast to the lanthanides, the elements of the early actinides – Ac, Th,

Pa, U, Np and Pu – move widely on the TC-YM diagram. Their properties change widely according to their positions on the diagram.

As mentioned in the introduction, reference [2] says that, in comparison with the lanthanides, the early actinides exhibit an unusually large range of physical properties, while the element $_{89}$Ac and the late actinide elements after $_{95}$Am behave similarly to the lanthanides.

Above all, the elements – **$_{90}$Th, $_{91}$Pa and $_{92}$U** – are much more similar to transition metals in their chemical properties.

The elements – **$_{93}$Np and $_{94}$Pu** – show the intermediate properties.

These phenomena fit exactly the positions of these elements on the TC-YM diagram.

How about the other actinides?

It is reported that the thermal conductivity of Am is 10 W/mK and it has a lower bulk modulus than Th, Pa, U, Np and Pu. [9] The bulk modulus of Cf is 50 GPa, which is similar to lanthanide metals [10], and that of Es is as low as 15 GPa. [10]

Let’s speculate on the locations of these elements on the TC-YM diagram.

Fig. 7-11 shows the speculated possible locations of Am, Cf and Es.

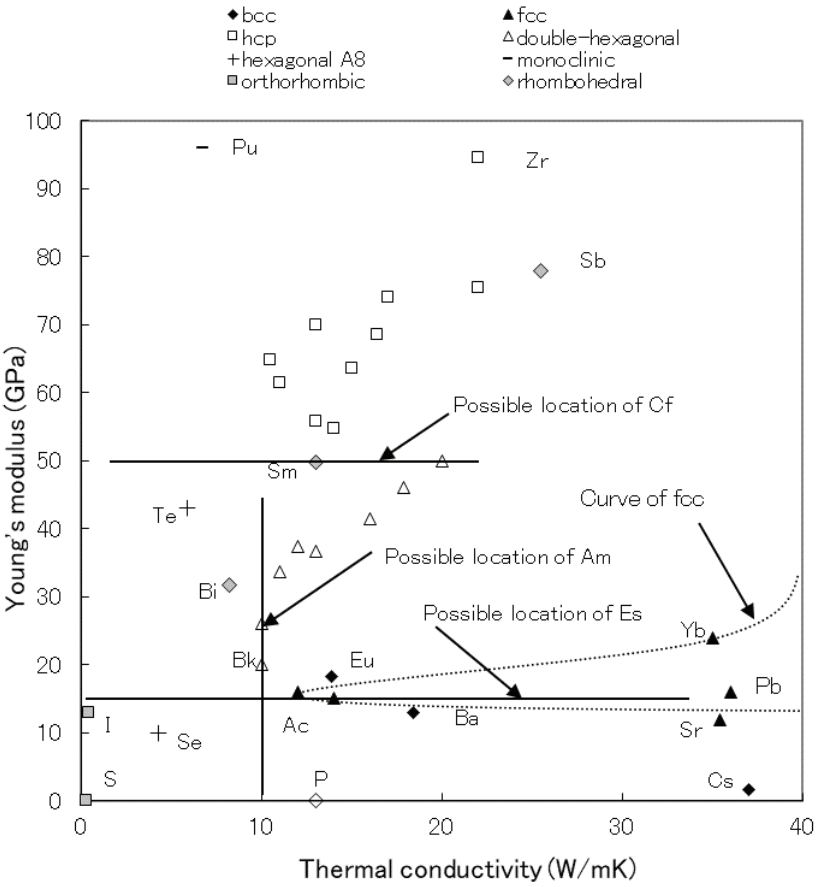

Fig. 7-11 – Possible locations of Am, Cf and Es on the diagram

Am must lie on the line of the thermal conductivity 10 W/mK. Am has a double-hexagonal structure. Therefore, it must be located near Bk and at the lower part of the lanthanides.

Cf must lie on the line of the Young's modulus 50 GPa. Cf has a double-

hexagonal structure. Therefore, it must lie near the upper part of the lanthanides with double-hexagonal structures. It must be just on the right side of Sm.

Es must lie on the line of the Young's modulus 15 GPa. Es has an fcc structure. The curve of fcc metals runs through nearby. Therefore, Es must be located near Ac.

Additionally, other properties of Am, Cf and Es are well consistent with those of the elements in the neighborhood, respectively. The orderings in the crystal structure on the TC-YM diagram were confirmed to be valid in the actinides, even in the late actinides after Pu.

Cm has no data on both the conductivity and the modulus. It is reported to be a hard and dense metal with a relatively high melting point of 1613K and a **double-hexagonal** crystal structure. It must be located near the top of the lanthanides with a double-hexagonal structure.

The elements **Fm, Md, and No** after Es have **fcc** structures. They must lie near Ac, Es, and Yb.

The last element of the actinides **– Lr** – has an hcp structure and a high melting temperature as high as 1900K. It must be located near the top of the lanthanides with hcp structures. It is surprising that the rules of the TC-YM diagram are valid in the actinides which were made artificially. The will of Nature governs even the artificial elements.

Next, where do such large varieties in the properties of the actinides come from?

Fig. 7-12 shows the electron configurations of the actinides. [12]

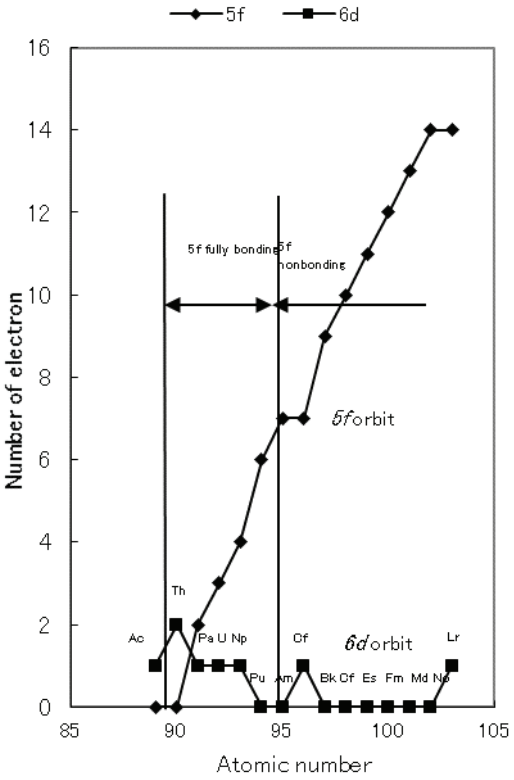

Fig. 7-12 – Electron configurations of the actinides

Fig. 7-12 shows that the *6d* and *7s* electronic shells are filled in Ac and Th, and the *5f* shell is being filled with a further increase in the atomic number.

Can the electron configuration explain the large variety of the thermal conductivity and Young's modulus of Th, Pa, U, Np, and Pu?

It is reported that the "5*f* fully bonding model" is valid in the early actinides such as Th, Pa, U, Np and Pu, and in contrast, the "5*f* nonbonding model" is valid in the late actinides such as Am, Cm, and Bk. [13] Namely, in the early actinides, the 5*f* electrons act in the bonding between atoms, and generate some binding forces, and increase the thermal conductivity and Young's modulus. Consequently, the elements – Th, Pa, U, Np and Pu – adopt the thermal conductivity and Young's modulus equivalent to the transition metals. As a result, the elements – Th, Pa, U, Np and Pu – show crystal structures, atomic radii, melting points, electronegativities and probably other properties characteristic for their locations on the TC-YM diagram.

In contrast to this, in the late actinides after Pu, the 5*f* electrons do not act in the bonding between atoms, and do not generate the binding force between atoms. It leads to the low Young's moduli and low thermal conductivities of the late actinides. As a result, the elements – Ac – and the late actinides – Am, Cm, Bk, Cf, Es, Fm, Md, No, and Lr – show crystal structures, atomic radii, melting points, electronegativities and probably other properties similar to those of the lanthanides.

References

[1] H. Sakurai, New Knowledge about the 111 Elements, Koudan-sha, Tokyo, 1997, p. 362.

[2] Yu. D. Tretyakov, Chemistry of transition elements 3, Academy, Moscow, 2007.

[3] Dictionary for knowing elements, M. Murakami, Narumi-sha, 2004, p. 277.

[4] Knowing all of the elements, K. Yamamoto, Natume-sha, 2011, pp. 246-247.

[5] Knowing all of the metals, K. Yamamoto, Natume-sha, 2011, p. 269.

[6] H. Yamana, Actinide Research for the Legacy of Damaged Nuclear Facilities, Actinides 2017, Sendai, 2017, p. 28.

[7] F. Seitz and D. Turnbull, Solid state physics: advances in research and applications, Academic Press, New York, 1964, pp. 289-291.

[8] S. Davos, C. Dufur, U. Benedict and M. Pages, Bulk modulus and P-V relationship up to 52 GPa of neptunium metal at room temperature, J. Magnetism and Magnet Mater. 63-64, 1987, pp. 661-663.

[9] U. Benedict, Study of actinide metals and actinide compound under high pressure, J. Less Comm. Met. 100, 1984, p. 153.

[10] R. G. Haire, Properties of the Transplutonium Metals (Am-Fm), Metals Handbook, vol. 2, 10th ed., ASM Int., Ohio, 1990.

[11] Japan Inst. Met., Metals manual, Maruzen, Tokyo, 1960, pp. 1163-1164.

[12] Japan Inst. Met., Metals data book, Maruzen, Tokyo, 1993. p. 5.

[13] P. E. A. Turchi, P. Soederlind, and A. I. Landa, From electronic structure to thermodynamics of actinide-based alloys, JOM 66(3), 2014, pp. 375-388.

8. ZR FOR NUCLEAR REACTOR

Zircaloy has been used widely as a cladding material of the nuclear fuels in water reactors due to a small thermal neutron absorption cross-section, good corrosion resistance to high temperature water and good mechanical properties. These excellent properties of Zircaloy seem to be self-evident, but some mysteries are hidden behind them.

Formerly, this author showed that the corrosion resistance of Zircaloy was provided by the precipitates in the alloy matrix through the mechanism of anodic protection. [1]

On the other hand, the low thermal neutron absorption cross-section of Zr is accepted as an axiom, but some mysteries are hidden behind it also.

8.1 Thermal neutron absorption characteristics of Zr

(1) Thermal neutron absorption cross-section of elements

The data of the thermal neutron absorption cross-section were taken from the old data of the JAERI (Japan Atomic Energy Research Institute) report in 1962. [2] Hereafter, the thermal neutron absorption cross-section is referred to simply as the “absorption cross-section”.

Fig. 8-1 shows the distribution of the absorption cross-section of elements on the TC-YM diagram. The figures in the legend show the range of the

absorption cross-section of elements in the logarithmic scale of barn.

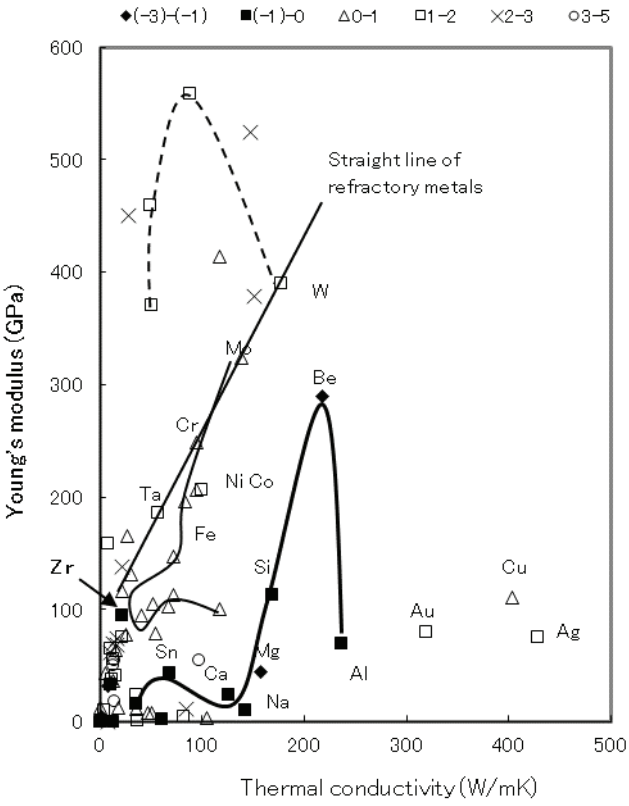

Fig. 8-1 – Absorption cross-section of elements on the TC-YM diagram

Surprisingly, the characteristics of the nucleus have emerged in the properties of the elements again following the neutron multiple number in Chapter 3.

Fig. 8-1 shows that the elements of the small absorption cross-section are located at the low Young's modulus range and from small thermal

conductivity up to medium range. This is quite a new pattern. It is different from any other patterns obtained so far. In the medium thermal conductivity range, an element such as Be has a small absorption cross-section in spite of its high Young's modulus.

Fig. 8-2 shows the area of small thermal conductivity and small Young's modulus in Fig. 8.1.

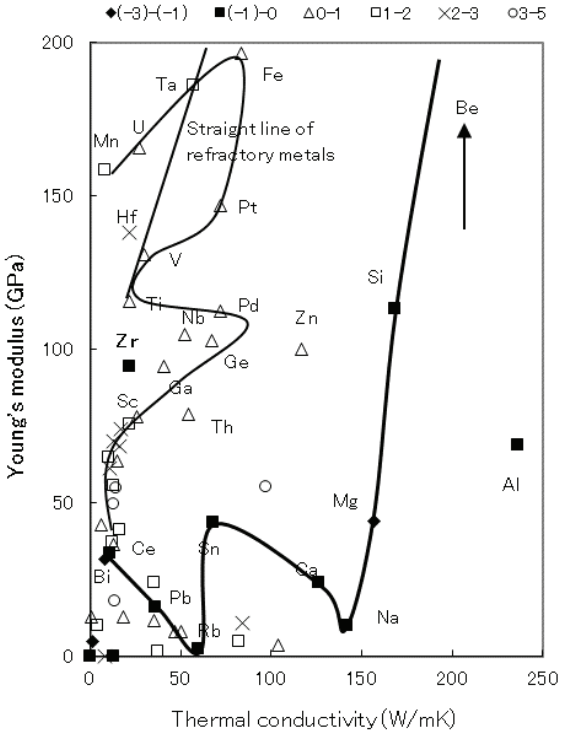

Fig. 8-2 – Absorption cross-section of elements with low Young's modulus and low thermal conductivity shown on the diagram

The elements of small absorption cross-section lie on a curve connecting Bi, Ce, Pb, Sn, Ca, Na, Mg, Si, Be and Al. They are all low melting temperature elements except for Be and Si. Therefore, they are not suitable for the fuel cladding in the water reactor.

Zr is located far from these elements, and surprisingly it shows a small absorption cross-section. As shown in Fig. 8-2, Zr is perfectly surrounded by the elements of large absorption cross-section. In this point of view, Zr is an exception in the distribution of elements on the TC-YM diagram.

Fig. 8-3 shows the distribution of the absorption cross-section of elements on the periodic table.

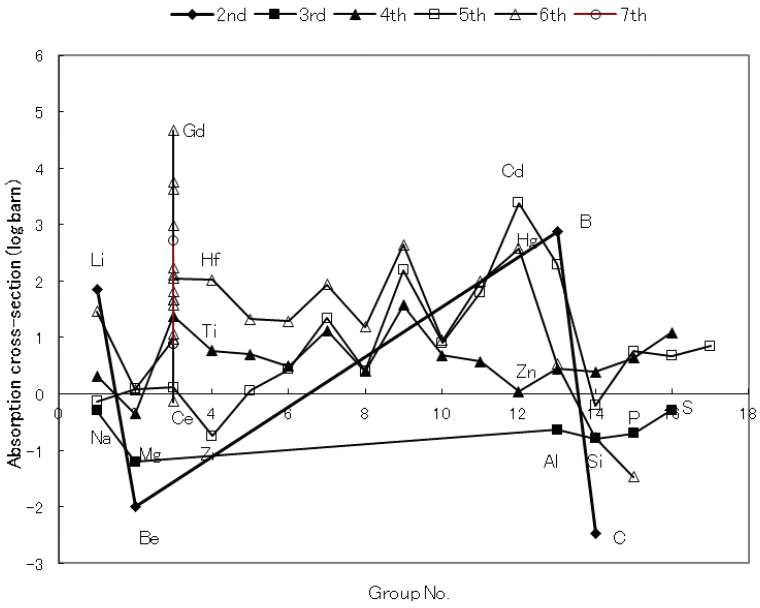

Fig. 8-3 – Absorption cross-section of elements displayed on the periodic table

All the elements in the 3rd period are elements of small absorption cross-section. The transition elements show a large absorption cross-section except for Zr. Zr is the only element of small absorption cross-section among the transition metals.

(2) The effect of the neutron multiple number on the absorption cross-section of elements

At first, this author speculated that the elements which have relatively many neutrons per proton in each nucleus are not apt to absorb neutrons. This author defined the “neutron multiple number” as the quotient when the number of neutrons is divided by the number of protons in the nucleus, as discussed in Chapter 3. [3] Fig. 8-4 shows the neutron multiple number of elements on the diagram.

The neutron multiple number varies from nearly 1 to nearly 1.6 for solid elements. The figures in the legend show the range of the neutron multiple number.

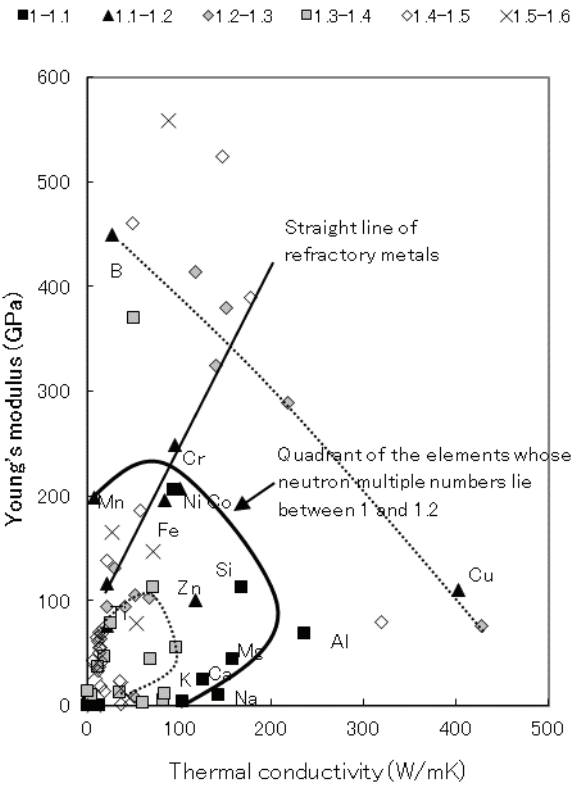

Fig. 8-4 – Neutron multiple numbers of elements on the diagram

Surprisingly, the neutron multiple number of elements also draws a pattern on the diagram. The elements of the smallest neutron multiple numbers form a quadrant on the diagram. The elements outside the quadrant and inside the quadrant show the next smallest multiple numbers.

This correlates to the abundance of elements in the universe, as mentioned in Chapter 3, but it doesn't seem to correlate to the absorption cross-section

shown in Fig. 8-1.

This author thought at first that the elements of small absorption cross-section were saturated with neutrons, and had large neutron multiple numbers. If so, the elements of small absorption cross-section should be located outside or inside the quadrant on the diagram. But in fact, among the elements of small absorption cross-section, Bi, Ce, Pb and Sn are located inside the quadrant, Be is outside the quadrant, and Ca, Na, Mg, Si and Al are included in the quadrant. Therefore, the correlation between the neutron multiple number and the absorption cross-section could not be expected.

Nevertheless, it was done for confirmation. Results are shown in Fig. 8-5.

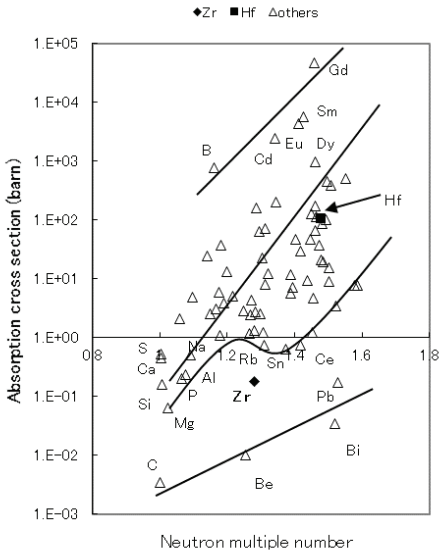

Fig. 8-5 – Correlation between the absorption cross-section and the neutron multiple number of elements

Though the correlation between both factors is complicated, there seem to be slight correlations. There are three groups of elements. The first is the group of large absorption cross-section including B, Cd, Eu, Dy., Sm, and Gd. The second is that of overwhelmingly many elements of medium absorption cross-section. The third is that of small absorption cross-section including C, Be, Bi and Pb. In each group of elements, it is recognized that with increasing neutron multiple number, the absorption cross-section increases.

As shown by a blue line, among the elements of the second group, the elements – S, Ca, Si, Mg, P, Al, Zr, Na, Rb, Sn, and Ce – are located at the lower edge of the second group.

Especially, Zr is located at a much lower location than other elements.

This fact shows that Zr is an exception among the elements of low absorption cross-section.

Zr is not a soft metal like other elements of small absorption cross-section.

Figure 8.6 shows the distribution of the melting temperature of elements on the diagram in the same area as in Fig. 8-2. The figures in the legend show the temperature range of the melting temperature in K. Zr is a high melting temperature element like Th, V, and Pt in the neighborhood.

Consequently, it is proved that Zr is the only element applicable for the cladding material of nuclear fuel in the light-water reactor.

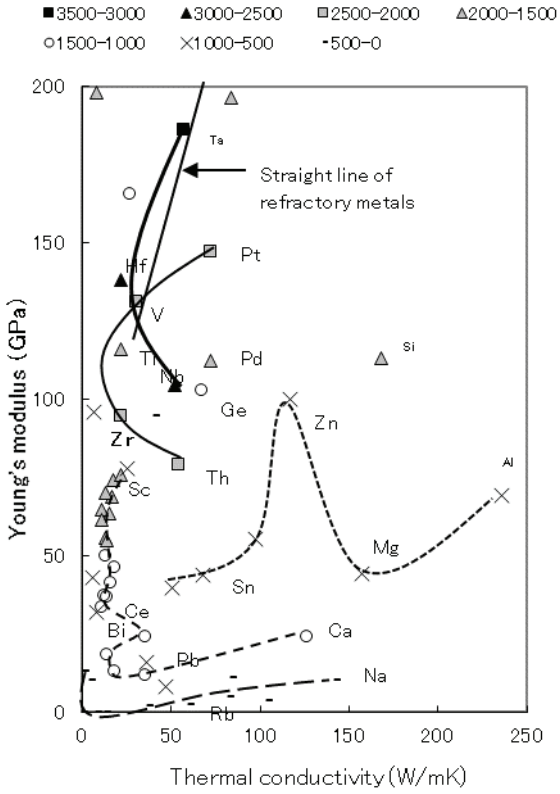

Fig. 8.6 – Melting temperatures of elements in the low thermal conductivity and low Young's modulus region on the diagram

The low Young's modulus is a necessary condition for the elements of small absorption cross-section.

As a second condition, the neutron multiple number must be small.

Zr is an exception at both conditions. Zr is a hard metal with high melting temperature, and its neutron multiple number is medium. Nevertheless, Zr

has a small absorption cross-section. [4] This author had heard once that, in English, there is a word “Nature”, which is spelled with a capital letter. The small absorption cross-section of Zr may be given by Nature. This may be a kind of anthropic principle.

8.2 Corrosion resistance of Zr to hot water

Zircaloy is an alloy developed for the cladding material of nuclear fuel in the water reactor. Its nominal chemical composition is Zr-1.3 mass% Sn-0.1 mass% Fe-0.1 mass% Cr. It is said that Sn is added for solution hardening and Fe and Cr are added for corrosion resistance. Formerly, this author clarified that the substance of corrosion resistance of Zircaloy is the anodic protection provided by the precipitates of $Zr(FeCr)_2$ in the Zr matrix [1].

Fig. 8-7 shows the relationship between the Fe/Cr content, the solution treatment temperature, and the weight gain in the corrosion test in 633K water for 15 days.

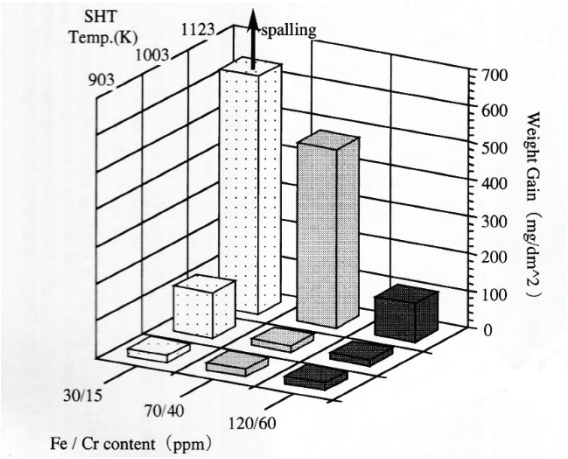

Fig. 8-7 – Relationship between the Fe/Cr content, the solution treatment

temperature, and the weight gain in the corrosion test in 633K water for 15 days

The specimens that were solution treated at 1123K, containing 30/15 ppm Fe/Cr and 70/40 ppm Fe/Cr, respectively, show no precipitates in the Zr matrix, and show inferior corrosion resistance. In contrast to this, the other specimens show precipitates to a greater or lesser extent in the Zr matrix and show good corrosion resistance. This is due to the fact that the precipitate serves an effective cathodic site during the anodic oxidation of the Zr matrix and enhances the formation of passivation film on the surface of the matrix metal.

It is also a fortunate coincidence that the solubilities of Fe and Cr are small in Zr and their electrode potentials are higher than that of Zr.

The precipitates of $Zr(FeCr)_2$ are nobler than the Zr matrix and enhance the formation of tough oxide film on the Zr matrix. For that purpose, Fe and Cr must be nobler than Zr and their solubility in Zr must be small.

Why are Fe and Cr nobler than Zr and their solubilities in Zr small?

(1) Standard electrode potentials of elements

The corrosion resistance of Zircaloy to hot water relates to the difference in the electrode potential between the matrix metal and the precipitates.

Fig. 8-8 shows the distribution of the standard electrode potentials of elements on the diagram.

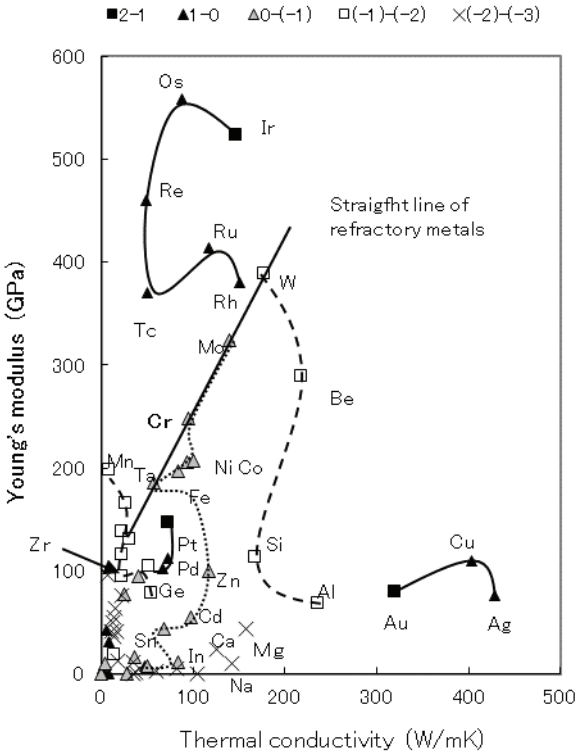

Fig. 8-8 – Electrode potentials of elements on the TC-YM diagram

The figures in the legend show the range of the standard electrode potential of elements in volts.

The less noble elements of the smallest electrode potentials start from Mn, descend to the bottom of the diagram, creep along the abscissa, and finally rise from Mg to W. Zr is included in this element group of low electrode potential.

The elements of medium electrode potentials lie on the vertical line at the constant and medium thermal conductivity around 100 W.mK, and are surrounded by the elements of the smallest electrode potentials. Fortunately, Fe and Cr are included in this element group of medium electrode potentials.

The elements of the largest electrode potentials are those of the largest Young's moduli or those of the largest thermal conductivities.

(2) Solubility of elements in Zr

As will be discussed in Chapter 13, elements with the same crystal structures as the matrix metal and those in the neighborhood of the matrix metal on the TC-YM diagram have a large solubility in the matrix metal. [5]

Fig. 8-9 shows the distribution of solubility of elements in the β-phase of Zr on the diagram. The maximum solubilities of elements in the β-phase of Zr at high temperatures were adopted as the solubility in the β-phase.

The figures in the legend show the solubility range in mol%.

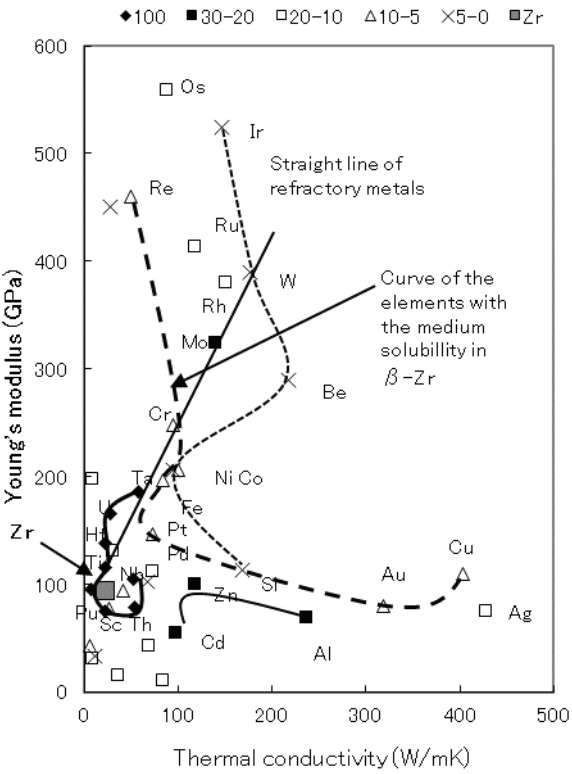

Fig. 8-9 – Solubility of elements in the β-phase of Zr on the TC-YM diagram

The elements with the bcc structure and near Zr have unlimited solubility.

The elements showing a medium amount of solubility lie on a line starting from Cu and ending at Re. Fe and Cr are included in this line.

The farther elements from this line – Si, Ni, Be, and Ir – show the smallest solubility.

Fig. 8-10 shows the distribution of the solubility of elements in the α-phase of Zr on the diagram. The maximum solubility of elements in the α-phase of Zr at high temperature was adopted as the solubility in the α-phase of Zr.

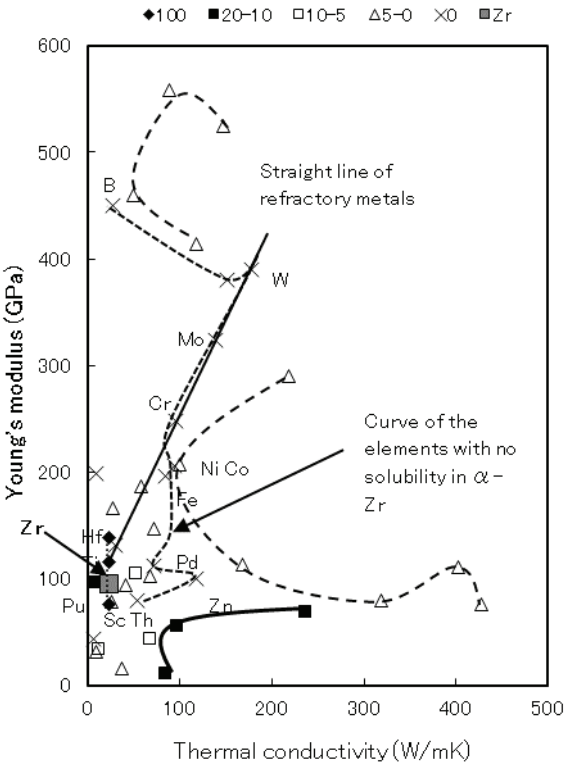

Fig. 8-10 – Solubility of elements in the α-phase of Zr on the TC-YM diagram

The elements with an hcp structure and near Zr show unlimited solubility. The elements of higher thermal conductivity and higher Young's modulus than Zr show low solubility in α-Zr.

The most remarkable fact is that the elements with the thermal conductivity at about 100 W/mK such as Th, Zn, Pd, Fe, Ni, Cr, Mo, W, Rh, and B show no solubility in α-Zr. Fe and Cr are included in this group. This is an anomaly, because the farther elements such as Ag, Cu, Au, Si, Ni, Co, and Be show small solubility. The tendency is reversed.

The fact that Fe and Cr possess no solubility means that Fe and Cr precipitate in the Zr matrix even in the small content. This is very useful for anodic protection. The fact that the elements with the thermal conductivity at about 100 W/mK including Fe and Cr show no solubility in α-Zr can be said also to be a kind of will of Nature.

For anodic protection, it is necessary that the alloying elements are nobler than the matrix metal and precipitate at a small amount of addition. The elements nobler than Zr are Cr, Ta, Fe, Ni, Mo and Sn, as shown in Figure 8.8. Among them, the elements of no solubility in α-Zr are Cr, Fe, Ni and Mo. But they are soluble in the β-phase of Zr. Therefore, they are solution treated in the β-phase and precipitate finely in α-Zr.

It is fortunate that the present alloying elements in Zircaloy – Fe and Cr – are included in the element group of high electrode potential and no solubility in the α-phase of Zr.

Moreover, Fe is an inevitable impurity in Zr. Zr is smelted by the Kroll process. Fe is included in Zr during smelting. Fe comes into Zr from the iron vessel for distillation.

It is fortunate that Fe is a useful element in Zr.

(3) Can the anodic protection theory explain the past corrosion data of Zr alloys?

This author studied the corrosion resistance of Zr alloys as a graduation thesis in 1966.

he binary alloys containing 2 and 4 mol% of Cu, Ni, Ti, Nb, Pb, V, Mo and Si are melted. The reactor grade Zr sponge was used. After forging and rolling, sheets of 0.5 mm thickness were subjected to the corrosion test in the steam of 673K under 30 atmospheric pressure. The corrosion test was carried out for 76 days.

The specimens of 2 and 4 mol% Si fractured during hot forging, and therefore they were abandoned.

The specimens, except for Zr-Si alloys, were subjected to the corrosion test. The break-away occurred early after the 20-day corrosion test in the specimens of Zr-Ti and Zr-V alloys.

The break-away occurred after 51 days in 1.27 mass% Cu alloy, and after 67 days in 2.03 mass% Nb alloy and 7.60 mass% Pb alloy, respectively.

Fig. 8-11 shows the variation of the corrosion increment versus corrosion time at each Zr alloy.

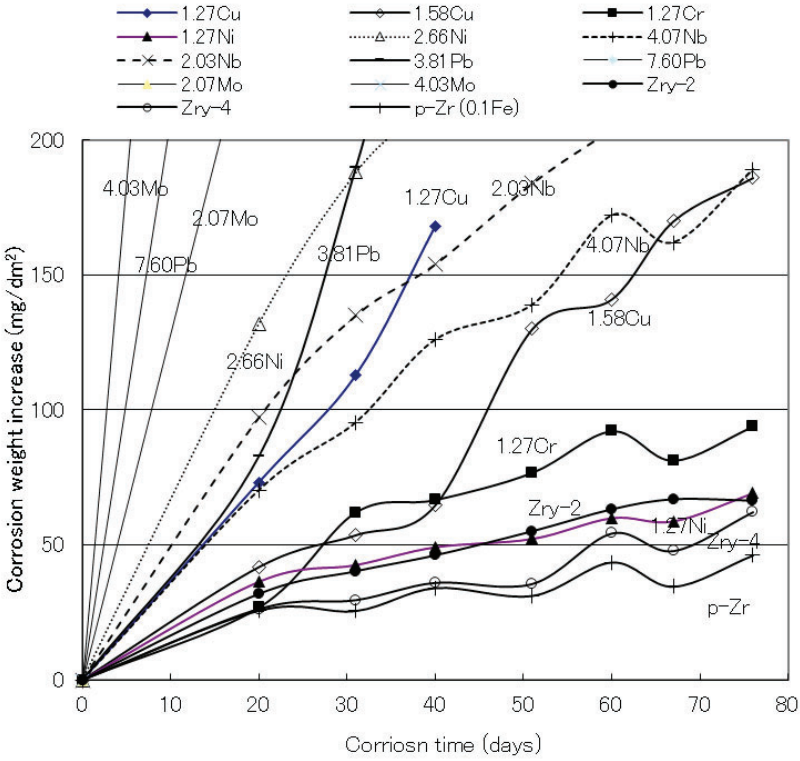

Fig. 8-11 – Variation of the corrosion increment versus the corrosion time in each Zr alloy (673K, 30 atmospheric pressure, steam)

The pure Zr (p-Zr in the figure) showed the best corrosion resistance. Zry-2 and -4 showed the next best corrosion resistance. Zr-1.27 mass% Ni alloy showed also the next best corrosion.

The reactor-grade commercially pure Zr contained approximately 0.1 mass% Fe originally. Zr is smelted in the Kroll process. In the Kroll process, the material is distilled in the steel vessel. As a result, Fe is included in the

material at about 0.1 mass%.

Therefore, it shows good corrosion resistance, as shown above.

Zry-2 and -4 contain Fe also. Therefore, they also show good corrosion resistance. The other alloys also should have shown good corrosion resistance because of their original Fe content. But in those days, the effects of Fe in such a small content were not known.

Zr-1.27 mass% Cr alloy also showed the next best corrosion resistance.

The other alloys such as Zr-Cu, Zr-Nb, Zr-Pb, and Zr-Mo alloys did not show good corrosion resistance.

Can these facts be explained by the above-mentioned anodic protection theory?

Fig. 8-12 shows the relationship between the electrode potential of each alloying element and the corrosion rate of each alloy at the addition of 2 mol%. The corrosion rate at the 2 mol% addition of each alloy system was obtained by the interpolation between two alloying contents.

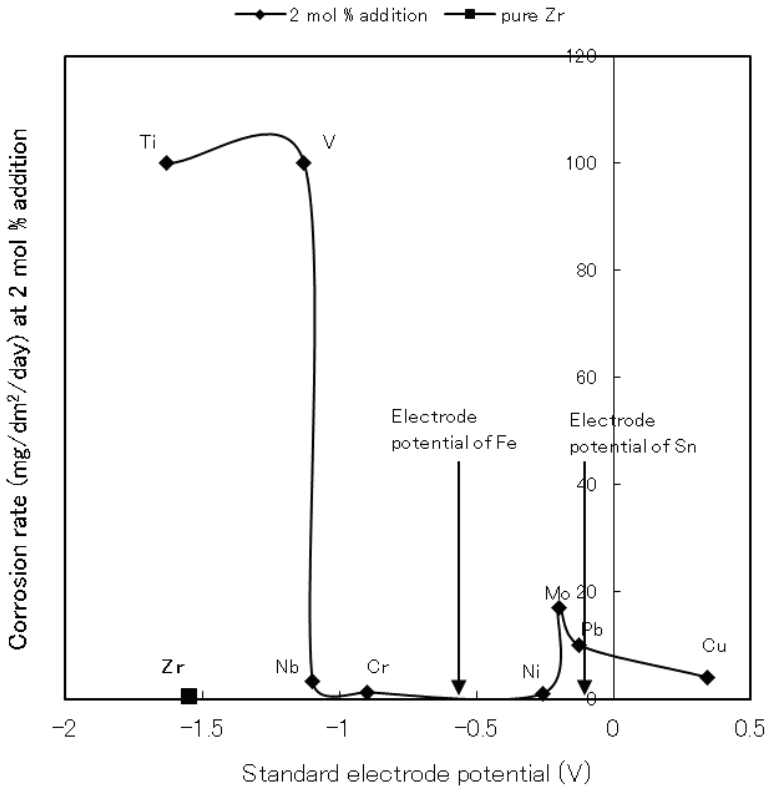

Fig. 8-12 – Corrosion rate versus the standard electrode potential for various alloying elements

The corrosion rates of Zr-Ti and Zr-V alloys which broke away after twenty days were assumed to be 100 mg/dm^2/day tentatively.

Ti and V, which have low standard electrode potentials equivalent to Zr, degrade the corrosion resistance badly.

Nb, Cr, and Ni, which have high standard electrode potentials similar to Fe, maintain the good corrosion resistance of Zr.

Mo, Pb, and Cu, which have much higher electrode potentials, degrade the corrosion resistance slightly. Sn, which is the major alloying element in Zircaloy, is included in this region. As confirmed in this test also, Sn degrades slightly the corrosion resistance of pure Zr containing 0.1 mol% Fe.

It is proved that the elements – Nb, Cr, Fe, and Ni – maintain the good corrosion resistance of Zr, and the anodic protection theory of these elements is confirmed.

Figure 8.12 shows that the elements between V and Mo in the electrode potential are not harmful to the good corrosion resistance of reactor-grade pure Zr containing 0.1 mass% Fe.

What are the other elements whose electrode potential lies between V and Mo except for Cr, Fe and Ni?

Fig. 8-13 shows the neutron absorption cross-sections of elements whose electrode potentials lie between V and Pb.

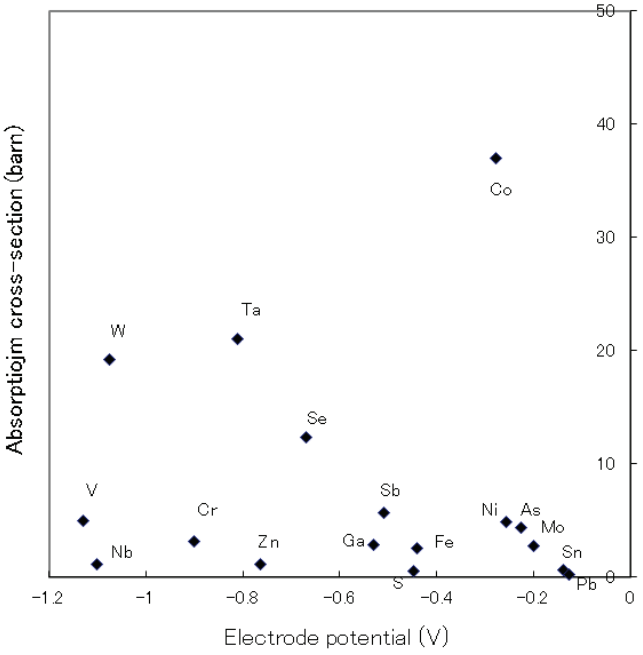

Fig. 8-13 – Neutron absorption cross-sections of elements whose electrode potentials lie between V and Pb

The elements – Nb, Zn, Ga, Sb, S, As, and Pb – except for Sn, Fe, Ni, and Cr, which are already contained in Zircaloy, show small neutron absorption cross-sections.

Nb forms eutectoid with Zr. It is soluble in Zr slightly. Zn doesn't alloy with Zr due to its high vapor pressure. Ga is soluble in β-Zr up to 9 mol%, and precipitates as Zr_2 Ga at room temperature. Sb is soluble in β-Zr up to 9 mol%, and precipitates as Zr_2Sb at room temperature. Both S and As are inadequate for alloying with Zr.

In conclusion, Nb, Ga, and Sb are left as the candidates.

8.3 Summary

The thermal neutron absorption cross-section of Zr is exceptionally small against the trend on the TC-YM diagram and against the correlation with the neutron multiple number. The will of Nature can be felt.

The elements – Fe, Cr, and Ni – with a small absorption cross-section are distributed in the range of higher electrode potential than Zr and low solubility in Zr on the TC-YM diagram. Consequently, they are dispersed in the Zr matrix and protect the Zr matrix from corrosion by hot water in the reactor in terms of the anodic protection.

References

1. T. Isobe, T, Murai, and Y. Mae, Anodic protection provided by precipitates in aqueous corrosion of Zircaloy, Zirconium in the nuclear industry, 11th Symposium, ASTM, 1999, pp. 203-216.
2. Japan Atomic Energy Research Institute, Data sheet, JAERI 6010, 1962.
3. Y. Mae, Neutron multiple number as a factor ruling both the abundance and some material properties of elements, J. Mater. Sci. Res. Vol. 6, No. 3, 2017, pp. 37-42.
4. Y. Mae, Peculiarity of Zr in the neutron absorption cross-section and corrosion resistance in water, Int. J. Mater. Sci. Appl. Vol. 6, No. 5, 2017, pp. 235-240.
5. Y. Mae, What the Darken-Gurry plot means about the solubility of elements in metals, Metall. Mater. Trans. A vol. 47, Dec. 2016, pp. 6498-6506.

9. HARDENABILITY OF STEELS

When steel is rapidly cooled from the γ-phase, martensite forms and the steel is hardened. Hardenability refers to the ease with which martensite forms. [1, 2] Plain-carbon steels have low hardenability, because they need rapid cooling such as water quenching. Alloyed steels have high hardenability, because martensite forms even by slow cooling such as air cooling. Alloying elements were added in order to improve hardenability of steels, and the effects of various alloying elements on the hardenability of steels are known experimentally. But the reasons for these effects are not well understood.

As mentioned above, this author has developed the TC-YM diagram, taking thermal conductivity on the abscissa and Young's modulus on the ordinate and plotting each element on it. Using this diagram, the mechanisms of the effects of the alloying elements on the hardenability of steels will be discussed here.

9.1 Effects of alloying elements on the upper critical cooling rates of steel

There are several methods to evaluate the effect of alloying elements on the hardenability of steel; the upper critical cooling rate was selected because of the abundant available data.

Fig. 9-1 is the original figure showing the upper critical cooling rates of various alloyed steels published by the research institute of the Japanese Navy in April, 1937. [3] The building of the battleship “Yamato” was begun in November of the same year. It is speculated that this research was conducted to confirm the effects of the alloying elements on the hardenability of steels. It says in the foreword that the special steels have been used as important components for weapons and others, and their importance has increased greatly in defense and industry. It says also that accurate research results about the hardenability of steels are very few due to the difficulties of the experiments.

The upper critical cooling rate is the lowest cooling rate at which all grains transform into martensite.

Fig. 9-1 is the original figure that shows the variation of the upper critical cooling rate as a parameter of the alloy content (mass%). The abscissa denotes the upper critical cooling rate (℃/s), and the ordinate denotes the alloying contents in mol%. [3]

The specimens were steel balls with the diameter smaller than 3 mm. The specimens were heated by the resistance heating coils nearby. And then, they were cooled by the gas stream of nitrogen or hydrogen. The temperature change of the specimen during cooling was measured by the thermocouple jointed directly to the specimen. The current was amplified by the Einthoven-galvanometer and recorded.

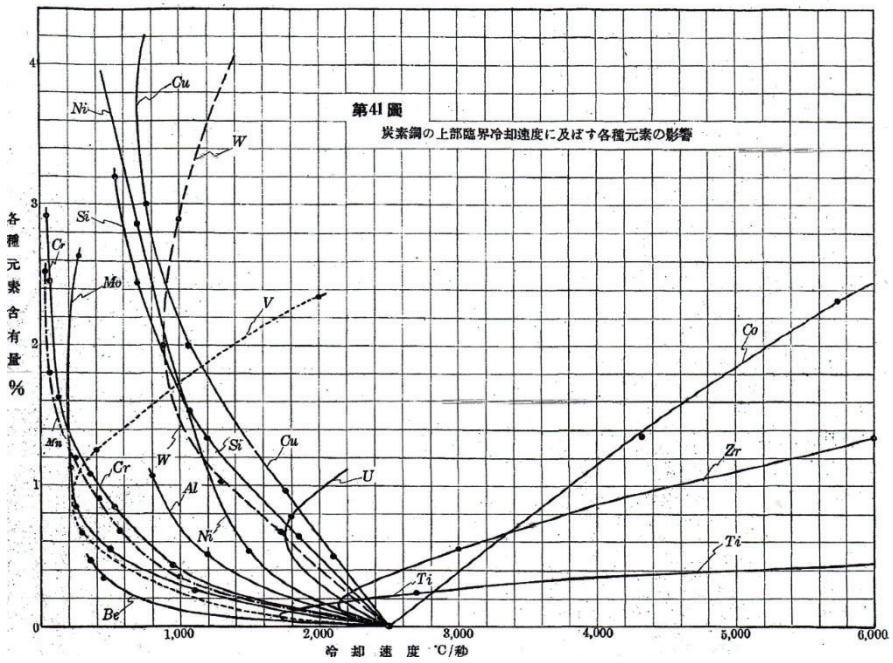

Fig. 9-1 – The original figure that shows the variation of the upper critical cooling rate (°C/s, abscissa) as a parameter of the alloying content (mass%, ordinate) (S. Tawara [3])

According to Fig. 9-1, V has the largest effect in reducing the upper critical cooling rate. This author has heard that Henry Ford had succeeded in the T-Ford by applying vanadium steels to it. This figure confirms this story.

Fig. 9-2 shows the changes in the upper critical cooling rate of 0.3 mass% C steel induced by various alloying elements as a function of alloy content in mol% (converted from original data expressed in mass% [3]).

The measured critical cooling rate of unalloyed 0.3 mass% C steel is 2500°C/s. The original figure [3] is very old, but is popular and still often cited in Japan [4-7], including very recently. [8]

Although this plot gives cooling rates that are too high compared with those measured by other experiments, it is nevertheless recognized that the tendencies are correct. [5]

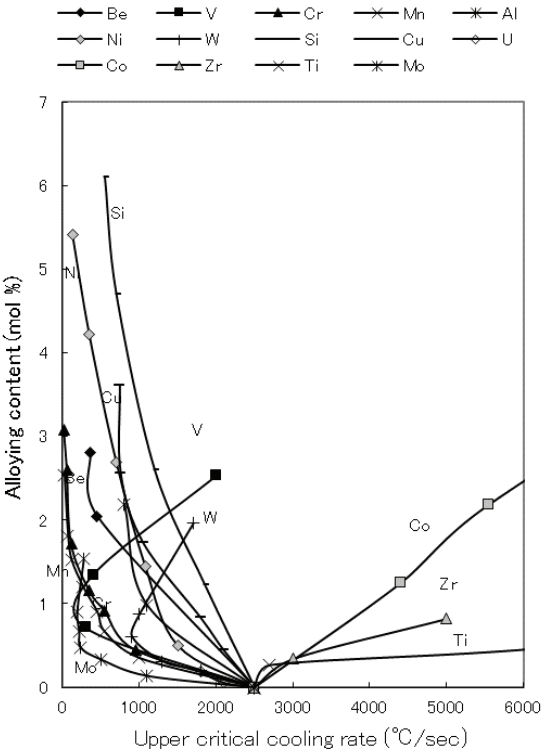

Fig. 9-2 – Changes of the upper critical cooling rate of 0.3 mass% C steel by various alloying elements as a function of the alloy content (mol%)

Most alloying elements reduce the upper critical cooling rate at small additions; the effect then saturates and, in some cases, reverses at large additions. For Zr and Ti, the upper critical cooling rates decrease at very small additions and then increase rapidly, while Co exhibits a continuous increase in the upper critical cooling rate with increasing alloy content.

Fig. 9-3 shows an expanded portion of Figure 9.2 for alloy contents below 1 mol%.

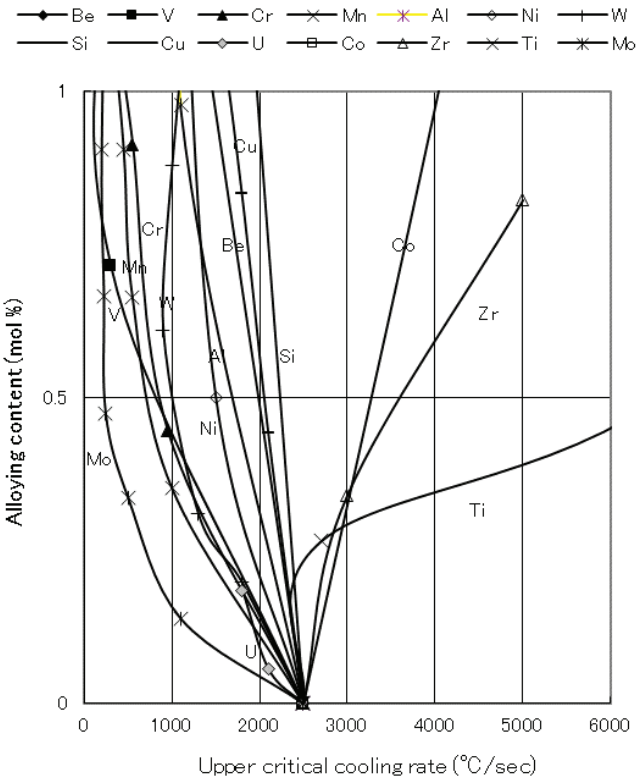

Fig. 9-3 – Expanded area of Fig. 9.2 for alloy contents below 1 mol%

In this concentration range, the upper critical cooling rates show good linearity for most elements. The critical cooling rates at 0.5 mol% and 1 mol% alloy content were therefore adopted as indexes of the effect of alloying elements on the hardenability of steel.

9.2 Display of the upper critical cooling rates on the TC-YM diagram

The values of the upper critical cooling rates of various alloying elements measured at 0.5 mol% alloy content are plotted on the TC-YM diagram shown in Fig. 9-4.

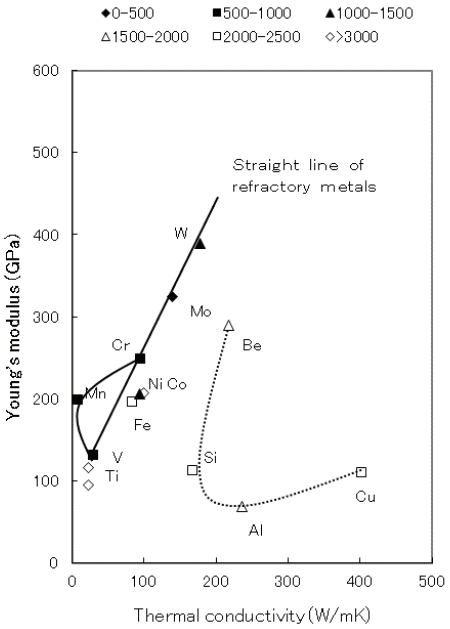

Fig. 9-4 – Distributions of the upper critical cooling rates (°C/s) of alloyed steels measured at 0.5 mol% alloying content on the TC-YM diagram

The numbers in the legend indicate the ranges of the upper critical cooling rates in units of °C/s: for example, the legend "500–1000" indicates that the upper critical cooling rates of the specified elements fall in the range from 500 to 1000°C/s. The upper critical cooling rate of steel itself is 2500°C/s.

Surprisingly, the upper critical cooling rates show a tendency on the TC-YM diagram. Elements with smaller upper critical cooling rate values improve hardenability; those with larger values degrade hardenability. The upper critical cooling rates are distributed regularly on the TC-YM diagram.

The elements lying on and near the straight line of refractory metals – W, Mo, Cr, Mn, and V – show large hardenability; elements with high thermal conductivity, such as Si, Al, and Cu, show medium hardenability; elements with low Young's modulus and low thermal conductivity – Ti, Zr, and Co – show negative hardenability.

The upper critical cooling rates measured at 1 mol% alloy contents show similar trends.

9.3. Diffusion coefficients of alloying elements in Fe

At first, this author did not think that there was a relationship between the upper critical cooling rate and the diffusion coefficient.

The distribution of diffusion coefficients of alloying elements in Fe on the TC-YM diagram had been independently studied. Diffusion coefficients in Fe are categorized for four phase regions: ferromagnetic α-Fe, paramagnetic α-Fe, γ-Fe, and δ-Fe. There are discontinuities at A_3 and A_4. However, within each phase, the order of magnitude of the diffusion coefficient values for a

specific element does not change across a wide temperature range.

The diffusion coefficient can therefore be represented by the value for a single temperature in each of the ferromagnetic α, paramagnetic α, and γ regions. Diffusion data were adopted from the Japan Institute of Metals. [9]

Fig. 9-5 shows the distribution of diffusion coefficients of alloy elements at 1073K (800°C) in paramagnetic α-Fe on a TC-YM diagram. “E-16” in the legend indicates, for example, that the particular elements have diffusion coefficients of a magnitude of 10^{-16} m^2/s.

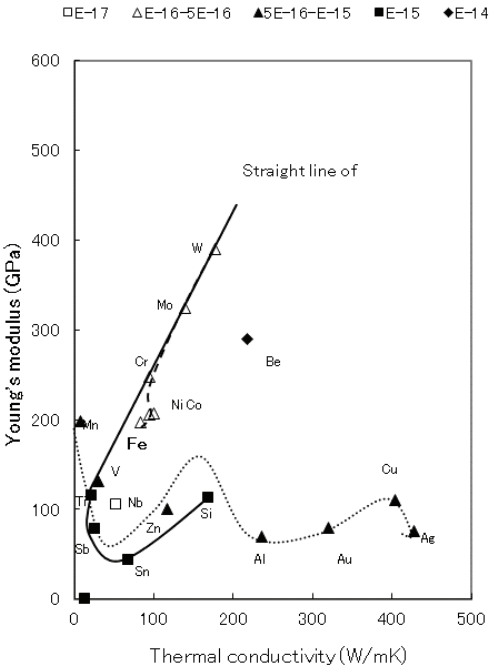

Fig. 9-5 – Distribution of the diffusion coefficients (m^2/s) of alloying elements in paramagnetic α-Fe at 1073K (800°C) on the TC-YM diagram

Fe has a small diffusion coefficient. The elements – Ni and Co – located near Fe, and the elements – Cr, Mo, and W – on the upper part of the straight line of refractory metals, have similar values to Fe. Elements around the lower part of the straight line of refractory metals, such as Mn, V, and Zn, and those of high thermal conductivity, such as Al, Au, Cu, and Ag, show slightly larger values. The elements on the lower side of the diagram – Ti, Sb, Sn, and Si – have larger values.

Fig. 9-6 shows the distribution of diffusion coefficients of elements at 1273K (1000°C) in γ-Fe on a TC-YM diagram.

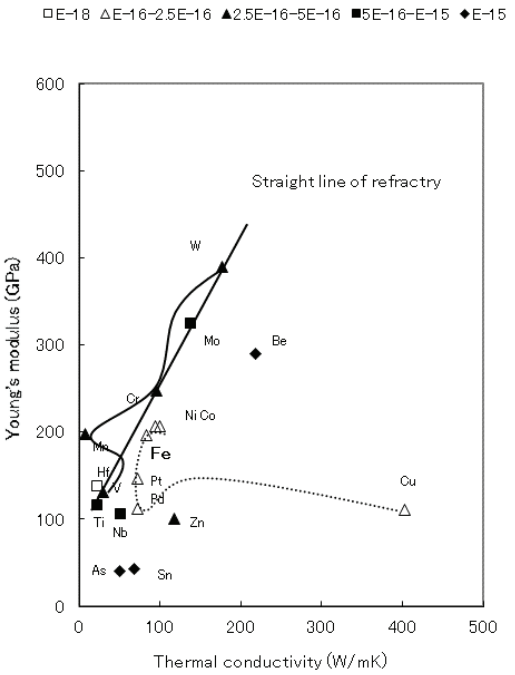

Fig. 9-6 – Distribution of diffusion coefficients (m^2/s) of alloying elements in γ-Fe at 1273K (1000°C) on the TC-YM diagram

The trend differs from that in α-Fe. Fe has the smallest diffusion coefficient, except for Hf; elements near Fe, such as Ni, Co, Pt, and Pd, and the elements with high thermal conductivity, such as Cu, show small and similar values to Fe; elements on and near the straight line of the refractory metals – W, Mo, Cr, Mn, V, Ti, Nb, and Zn – show large values. It is recognized that the diffusion coefficients of elements in Fe distribute regularly on TC-YM diagrams and that the patterns differ for α-Fe and γ-Fe.

9.4 Correlation between upper critical cooling rate and diffusion coefficient

Comparing Figs. 9-4 and 5, it is difficult to find any similarities. In particular, W, Mo, and Cr show different trends. Comparing Figs. 9-4 and 6, however, it is possible to recognize some similarities: W, Mo, Cr, Mn, and V show similar trends. This author was therefore inspired to speculate on a correlation between Fig. 9-4 and Fig. 9-6, i.e., between the upper critical cooling rate at 0.5 mol% alloying addition and the diffusion coefficient of the alloying element in γ-Fe at 1273K (1000°C).

For reference, correlation between the upper critical cooling rates measured at 0.5 mol% alloy content and the diffusion coefficients in paramagnetic α-Fe at 1073K (800°C) is shown in Fig. 9-7.

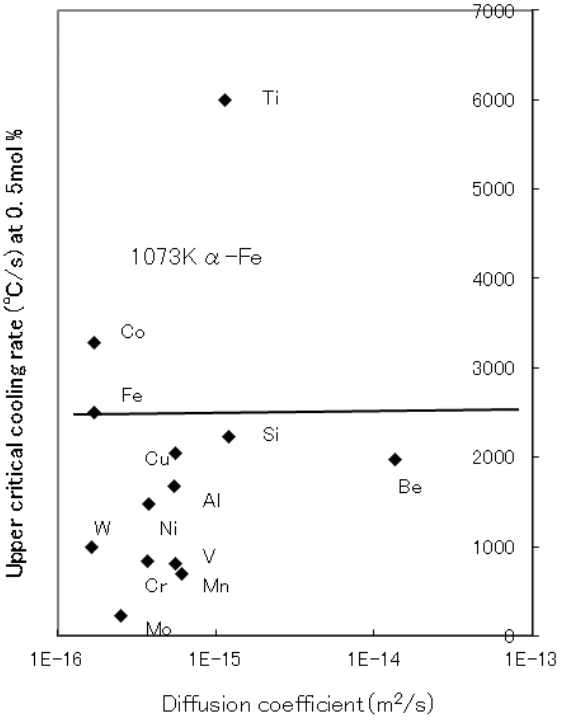

Fig. 9-7 – Correlation between the upper critical cooling rates measured at 0.5 mol% alloying content and the respective diffusion coefficients in paramagnetic α-Fe at 1073K (800°C)

Fig. 9-8 shows the correlation between the upper critical cooling rates measured at 0.5 mol% alloying content and the respective diffusion coefficients in paramagnetic α-Fe at the boundary temperature between the α-phase and the β-phase 1184K (911°C).

The elements are randomly distributed in both figures: the upper critical

cooling rates have no correlation with the diffusion coefficients in paramagnetic α-Fe.

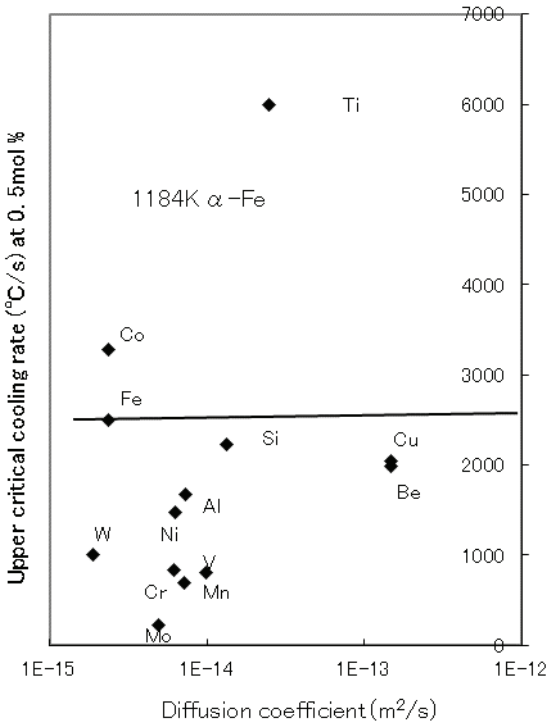

Fig. 9-8 – Correlation between the upper critical cooling rates measured at 0.5 mol% alloying content and the respective diffusion coefficients in paramagnetic α-Fe at 1184K (911°C)

In contrast, a clear correlation is recognized between the upper critical cooling rates measured at 0.5 mol% alloying content and the diffusion coefficients in γ-Fe.

Fig. 9-9 shows the correlation between the upper critical cooling rates measured at 0.5 mol% alloy content and the respective diffusion coefficients in γ-Fe at 1184K (911°C).

Fig. 9-10 shows the correlation between the upper critical cooling rates measured at 0.5 mol% alloy content and the respective diffusion coefficients in γ-Fe at 1273K (1000°C).

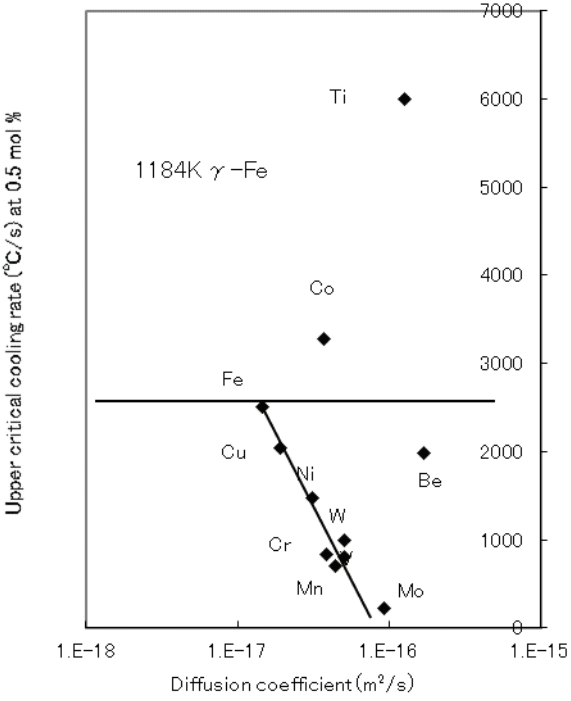

Fig. 9-9 – Correlation between the upper critical cooling rates measured at 0.5 mol% alloy content and the respective diffusion coefficients in γ-Fe at 1184K (911°C)

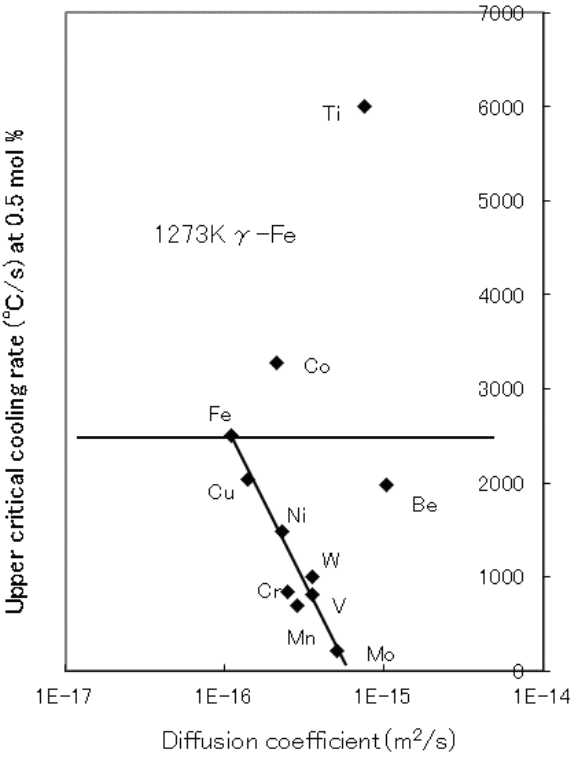

Fig. 9-10 – Correlation between the upper critical cooling rates measured at 0.5 mol% alloy content and the respective diffusion coefficients in γ-Fe at 1273K (1000°C)

The elements show the same tendency in both figures.

Surprisingly, the elements – Fe, Cu, Ni, W, Cr, V, Mn, and Mo – lie on a straight line. The upper critical cooling rate decreases linearly with the increasing diffusion coefficient of these elements, although Co and Ti show

the opposite tendency. Very similar results were also obtained at 1 mol% concentration of the alloy elements.

9.5. Correlation between the multiplying factor and the diffusion coefficient

As an alternative to using the upper critical cooling rate to evaluate the hardenability of steel, the multiplying factor can also be used. The ideal critical diameter D_I, from which full martensite is obtained at quenching, is expressed by the following equation for alloyed steel:

$$D_I = D_I^{\bullet} \times F_{Mn} \times F_{Si} \times F_{Cr} \times F_{Mo} \times \ldots \quad (9\text{-}1)$$

where $D_I^{\bullet}$ is the ideal critical diameter of the unalloyed steel, which is determined by the carbon content and austenite grain size. F_X is the multiplying factor of the alloying element X, represented by:

$$F_X = 1 + \alpha_X C_X \quad (9\text{-}2)$$

where α_X is a constant for element X and C_X is the alloy content of element X.

The multiplying factor can also be thought of as an index for the hardenability of steel. Multiplying factors for several elements are given by Hollomon and Jaffe [10, 11] as linear functions of alloy content. Fig. 9-11 shows the values of these multiplying factors for various alloying elements as a function of alloy content, converted from mass% to mol%.

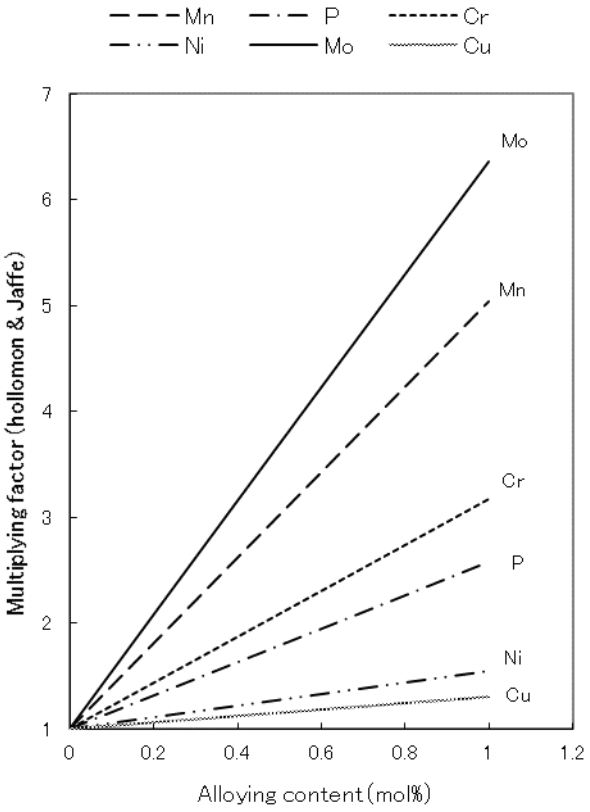

Fig. 9-11 – Multiplying factors for various elements as a function of their alloy content (mol%)

The values of the multiplying factor at 0.5 mol% alloy content were adopted here to represent the effect of that element on the hardenability of steel. Using the same methodology as for the upper critical cooling rate, correlation between the multiplying factor and the diffusion coefficient at 1273K (1000°C) was tested. The results are shown in Fig. 9-12.

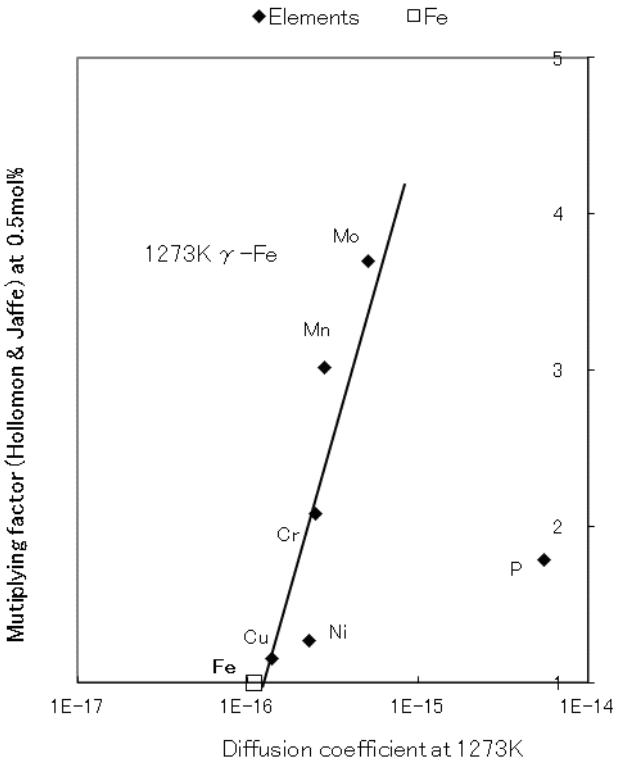

Fig. 9-12 – Correlation between the multiplying factor at 0.5 mol% alloy content and the diffusion coefficient of the respective alloy element in γ-Fe at 1273K (1000°C)

Although there are fewer data points, the elements – Cu, Ni, Cr, Mn, and Mo – show good correlation. Similar to the effect observed for the upper critical cooling rate, the hardenability of steel, as expressed by the multiplying factor, increases with the increasing diffusion coefficient of the alloy element.

9.6 Comparison with existing theories

Figs. 9-7 and 8 show no correlation between the upper critical cooling rates and the diffusion coefficients of alloy elements in α-Fe; Figs. 9-9 and 10, however, do show such correlation in γ-Fe. Fig. 9-12 also demonstrates a correlation between the multiplying factor and the diffusion coefficient of the respective alloying element in γ-Fe.

In general, martensite is formed from austenite. Rapid cooling is needed to avoid the "nose" of ferrite or pearlite formation on the continuous cooling transformation (CCT) diagram and to reach the martensite start (*M*s) temperature. The concept of hardenability refers to the ease with which martensite forms. [1, 2] The lower the cooling rate permitted, the better is the hardenability. The minimum cooling rate necessary to achieve a completely martensitic structure is called the upper critical cooling rate. In general, hardenability is ruled by the type and content of alloying elements in the γ-phase, the amount and distribution of undissolved carbon compound particles, the austenitizing temperature, and the austenite grain size. [12, 13]

(1) Effects of factors other than alloying elements

The austenitizing temperature changes the austenite grain size. With increasing grain size, the area of austenite grain boundary that provides a nucleation site for ferrite and pearlite decreases; the hardenability consequently increases. [13-15] Undissolved carbon compound particles lower the content of alloying elements in austenite and provide nucleation sites for transformation, consequently decreasing the hardenability. [16]

(2) Effects of alloying elements

Elements such as C, Cr, Mn, Ni, Mo, and B are added to improve hardenability. It is generally recognized that alloying elements improve hardenability in the series V, Mo, Mn, and Cr. In contrast, Ni and Si must be added in considerable amounts to improve hardenability, W has little effect, and Co shows the opposite tendency and degrades hardenability. [5] Figs. 9-1, 2, 3, and 9-11 confirm these effects. To date, however, the reasons for these effects are largely unknown. It is believed that Mo and W slow the rate of diffusion of carbon in the γ lattice and that Cr and Ni impede the γ→α rearrangement. [17] These phenomena suggest that these alloying elements play a role in increasing the hardenability of steel, but the mechanism is not clear.

In a paper of 1937, Tawara said that Be, Mn, Cr, Al, Si, Ni and so on decrease the upper critical cooling rate, because these elements prevent the diffusion of carbon. This author was surprised to know that this effect of carbon had already been asserted so long ago. This effect of carbon is still believed now, and is discussed in the introductory book of metallurgy. [18]

But as far as this author knows, there have been no studies which have confirmed the suppressed diffusion of carbon by the alloying elements.

In this study, the values of the upper critical cooling rates at 0.5 mol% and 1 mol% alloying content were adopted and plotted on diagrams of Young's modulus and thermal conductivity. It is assumed that other factors that affect hardenability (such as austenite grain size and the amount of undissolved carbon compound particles) remained essentially constant. The diffusion

coefficients of alloying elements in Fe were also plotted on a TC-YM diagram. Diagrams of the upper critical cooling rates and the diffusion coefficients in γ-Fe at 1273K (1000°C) showed a similar pattern, so a correlation between these properties was speculated. Good correlation was found between the upper critical cooling rate and the diffusion coefficient in the γ-phase, as shown in Figs. 9-9 and 10. Good correlation was also found between the multiplying factor and the diffusion coefficient in the γ-phase. The orders of magnitude of the diffusion coefficient values of the alloying elements studied here do not change in the temperature range of the γ-region: values determined at 1273K (1000°C) are therefore valid throughout the γ-phase.

The mechanism of the effect of alloying elements on the hardenability of steel can be considered as follows: if diffusion of alloying elements in the γ-phase is active, then, on cooling according to the CCT diagram, this increases the entropy and thermodynamically stabilizes the γ-phase, which impedes transformation to the α-phase at higher temperatures and retains the γ-phase down to lower temperatures, thereby enabling the γ-phase to reach the *M*s temperature even at low cooling rates. Martensite is then usually understood to form by a diffusionless process. [19, 20] The orders of magnitude of the diffusion coefficients of the elements discussed are speculated to be valid in this metastable γ-phase. No correlation was found between the upper critical cooling rate and the diffusion coefficient in α-Fe because the α-phase is excluded from this process.

Naturally, some exceptions are observed. Ti shows a very large upper critical cooling rate. Ti is a strong carbide former. It has the smallest

standard free energy for carbide formation among the alloying elements considered [21] and therefore reduces the solute contents of C and N in the γ-phase and degrades the hardenability. [7] Co also shows a large upper critical cooling rate, which has been reported previously. [5, 7] The reasons for this remain unknown. Be has a small upper critical cooling rate, but deviates from the correlation line: too large a difference in diffusion coefficient from that of Fe does not further improve hardenability. Some scatter in the correlations is considered to be due to differences in the austenite grain size, the amount and form of carbide, and the carbon content in solution induced by the presence of different alloying elements.

Fig. 9-13 shows the upper critical cooling rates of plain steel and alloyed steel schematically.

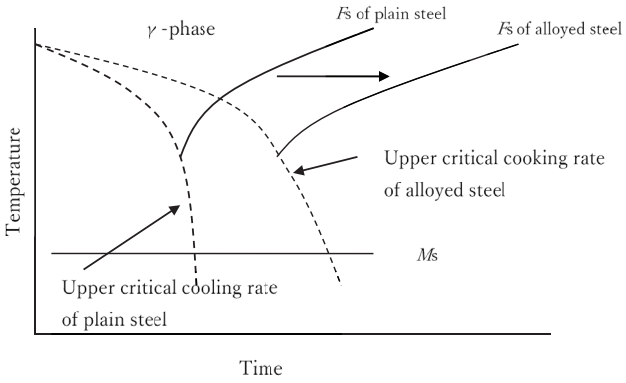

Fig. 9-13 – Schematics of the upper critical cooling rate of plain steel and alloyed steel

The alloying elements expand the region of the γ-phase by their rapid diffusion and give rise to the small upper critical cooling rate.

9.7 Summary

To improve the wear resistance of steels, carburizing and nitriding are applied to steels in which carbon and nitrogen diffuse into the steel. These are important techniques for machine parts.

In addition, it has been shown here that, increasing the diffusion coefficient of the alloying element contributes to the increase of hardenability. If this assumption is valid, modern civilization is built on diffusion, because many important components are made from hardened steel.

There has been a question; what is the greatest invention or discovery since the birth of mankind? This author would answer that it is the discovery of the quenching technique of steel.

Plots of thermal conductivity against Young's modulus (TC-YM diagrams) were used as a tool to illustrate the effects of alloying elements on the hardenability of steel and the diffusion coefficient of alloying elements in the γ-phase of steel. The following conclusions are drawn:

1. With the increasing diffusion coefficient of alloying elements in the γ-phase for elements such as Cu, Ni, Cr, Mn, W, V, and Mo, the upper critical cooling rate of the alloyed steel decreases and the multiplying factor increases, i.e., hardenability of the alloyed steel increases.

2. A large diffusion coefficient of the alloying element in the γ-phase increases the entropy of the phase, and, on cooling according to the CCT diagram, this thermodynamically stabilizes the γ-phase, thereby retarding transformation to the α-phase and retaining the γ-phase at a

lower temperature, finally enabling the γ-phase to reach the *M*s temperature, even at low cooling rates.

This author rewrote the Ref. 22 for this chapter.

References

1. D. R. Askeland, The Science and Engineering of Materials, PWS Publishing, Boston, 1994, p. 350.
2. R. E. Hummel, Understanding Materials Science, Springer, New York, 1998, p. 146.
3. S. Tawara, The effects of various alloying elements on the hardenability of steels (1st report), Tetsu-to-Hagane (Iron and Steel), The Iron and Steel Institute of Japan, 1937, pp. 27-61.
4. The Iron and Steel Institute of Japan, Handbook of Iron and Steel, 3rd ed. vol. 1, Maruzen, Tokyo, 1981, p. 415.
5. K. Monnma, Ferrous Materials, Jikkyo-publishing, Tokyo, 1981, p. 242.
6. I. Tamura, Ferrous Materials, Asakura Book-store, Tokyo, 1981, p. 66.
7. M. Tanino and S. Suzuki, Science on Steel, Uchida-Roukakluho, Tokyo, 2001, p. 105.
8. N. Masahasi, News Letter 25, Kansai Center for Industrial Materials Research Institute for Materials Research, Tohoku Univ., Osaka, 2013, p. 3.
9. Japan Institute of Metals, Metals Data Book, 4th ed., Maruzen, Tokyo, 2004, pp. 20-25.
10. K. Monnma, Ferrous Materials, Jikkyo-publishing, Tokyo, 1981, p. 250.
11. T. Kasuya, and N. Yurioka, Weld. J. 1993, vol. 72, pp. 263-268.
12. R. Tanaka, Dictionary of Metallic Materials, Asakura Book-store,

Tokyo, 1990,
p. 442.
13. H.K. D. H. Bhadeshia and R. Honeycombe, Steels, Microstructure and Properties, 3rd ed., Elsevier, Oxford, 2006, p.176.
14. The Iron and Steel Institute of Japan, Handbook of Iron and Steel, 5th ed. vol.3, Maruzen, Tokyo, 2014, p. 159.
15. G. E. Totten, Steel heat treatment of steels, 2nd ed., Taylor & Francis, NY, 2006, p. 195.
16. I. Tamura, Ferrous Materials, Asakura Book-store, Tokyo, 1981, p. 74.
17. G. E. Totten, Steel heat treatment, 2nd ed., Taylor & Francis, NY, 2006, p. 176.
18. S. Kohara, Introduction to the metallic materials, Askura-shoten, 1991, p. 269.
19. G. E. Totten, Steel heat treatment, 2nd ed., Taylor & Francis, NY, 2006, p. 177.
20. H. K. D. H. Bhadeshia, Journal De Physique V 1997, C5, p. 368.
21. Japan Institute of Metals, Metals Data Book, 3rd ed., Maruzen, Tokyo, 1993, p. 99.
22. Y. Mae, Correlation of the effects of alloying elements on the hardenability of steels to the diffusion coefficients of elements in Fe, Int. J. Mater. Sci. App. 2017, Vol. 6, pp. 200-06.

10. FAST DIFFUSION OF ELEMENTS IN METALS

Carburizing, nitriding and hardenability are important applications of diffusion to industry. Phenomena such as fast diffusion and slow diffusion are not important for industrial application, but they are physically interesting phenomena to clarify the behaviors of foreign atoms in metals.

The phenomenon of foreign elements diffusing faster than the self-diffusion of a matrix metal, often by a few orders of magnitude, is well known.

Fast diffusion was identified for the first time in the diffusion of Au in Pb by Roberts-Austen at the end of the 19th century. [1, 2]

The diffusion of alloying elements in steels has been examined to interpret their effects on the hardenability of steels in Chapter 9. Alloying elements with high diffusivity in austenite stabilize the austenite and retard the formation of martensite, consequently improving the hardenability. It has been clearly shown that, increasing the diffusion coefficient of the alloying element contributes to an increase of the hardenability. Thus, if this assumption is valid, modern civilization is built on diffusion, because many important components are made from hardened steel.

Normally, metallic elements diffuse in a matrix metal at a speed similar to the self-diffusion of the matrix metal, while interstitial elements, such as C and N, diffuse more rapidly in the matrix metals. However, in some metallic elements, foreign metallic elements also diffuse much faster than the self-

diffusion of the matrix elements. In this case, the diffusion coefficient of the foreign element is greater than the self-diffusion of the matrix metal, typically by more than three orders of magnitude. This effect is known as “fast diffusion”. [3] It has been reported that this phenomenon can be observed in many metallic elements, such as, multi-valence metals like Pb, Sn, Tl, and In; alkali metals like K and Na; lanthanides and actinides; and semiconducting elements like Ge and Si. [3] Many models have been proposed for the mechanism of fast diffusion, although interstitial diffusion is assumed by all models. [3]

However, the characteristics of metals that tend to act as matrix metals for fast diffusion and the characteristics of elements that tend to be diffuser elements have yet to be clarified.

In this chapter, the diffusion coefficients of elements in the various matrix metals are plotted as a parameter of atomic radius. Elements for which fast diffusion occurs are also plotted on the TC-YM diagram.

10.1 Matrix elements for which fast diffusion occurs

Fig. 10-1 shows the temperature dependence of the diffusion coefficients of various elements in Pb.

Diffusion coefficients were calculated by the following equation:

$$D = D_0 \, exp(-\frac{Q}{RT}) \qquad (10.1)$$

where D_0 is the frequency factor, R is the gas constant, Q is the activation energy, and T is the absolute temperature.

The values of D_0 and Q for each diffusion couple were adopted from Ref. 4.

The diffusion coefficient of each metal varies with temperature. However, the relative change of the diffusion coefficient for each element remains stable over a wide temperature range. The magnitude of the diffusion coefficients could, therefore, be compared with each other based on their values at a single temperature.

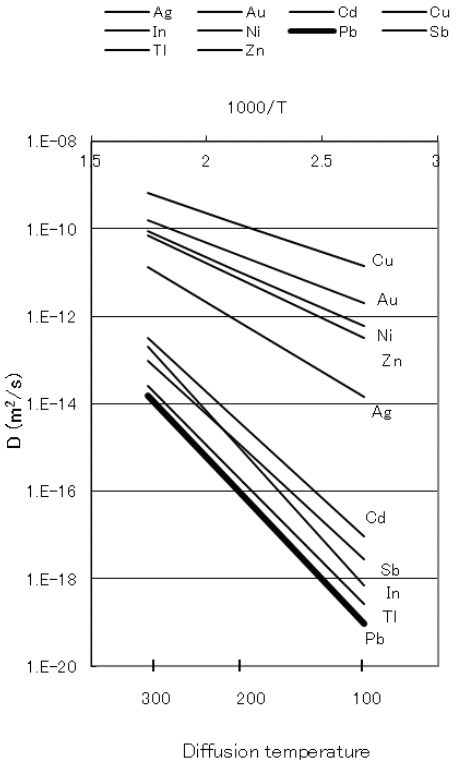

Fig. 10-1 – Temperature dependence of the diffusion coefficients of various elements in Pb

The elements – Cu, Au, Ni, Zn, and Ag – show extremely large diffusion coefficients across a wide temperature range. This kind of diffusion behavior is known as fast diffusion. Hereafter, a diffusion coefficient for a diffuser element more than three orders of magnitude (1000 times) greater than the self-diffusion of the matrix is referred to as fast diffusion.

Fig. 10-2 shows the relationship between the atomic radius of the alloying elements and diffusion coefficients at 473K in Pb. The horizontal bars in the figure enclose the range that is three orders of magnitude above and below the diffusion coefficients (*i.e.*, covering a total range of 6 orders of magnitude). These results are consistent with previous reports. [1]

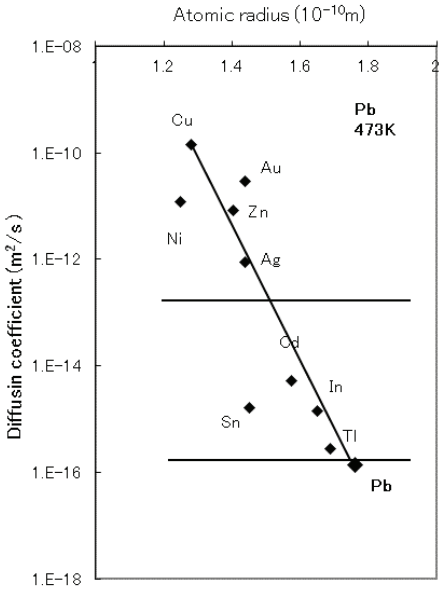

Fig. 10-2 – Atomic radii of the diffuser elements and their diffusion coefficients at 473K in Pb

Pb showed the smallest diffusion coefficient among the elements. The elements – Cu, Au, Ni, Zn, and Ag – show diffusion coefficients greater than that of the self-diffusion of Pb by more than three orders of magnitude. Thus, we denote this as fast diffusion of elements in Pb.

We note that the diffusion coefficients of elements often show a dependence on the atomic radii of the element. In general, the diffusion coefficient is inversely proportional to the atomic radius, that is, smaller atoms tend to diffuse more rapidly.

The reference diffusion data of most elements [4] indicate that fast diffusion is observed for many elements such as W, ferromagnetic α-Fe, Nb, α-Ti, α-Zr, γ-Ce, Sn, Pb, α-Tl, and In. These results correspond with literature reports. [5-8]

Fig. 10-3 shows the relationship between the diffusion coefficients of elements at 1073K in α-Ti and the atomic radii of the elements.

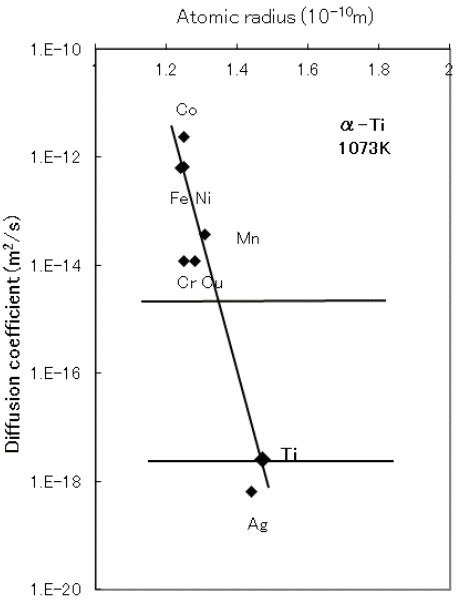

Fig. 10-3 – Atomic radii of the diffuser elements and their diffusion coefficients at 1073K in α-Ti

Except for Ag, Ti shows the smallest diffusion coefficient (self-diffusion) among elements. The elements – Co, Fe, Ni, Cr, and Cu – show much larger diffusion coefficients than that of Ti. The atomic radius dependence was also followed.

In addition, W, ferromagnetic α-Fe, and α-Zr also show fast diffusion.

Fig. 10-4 shows the relationship between the diffusion coefficients of the elements at 1023K in ferromagnetic α-Fe, versus the atomic radii of the elements.

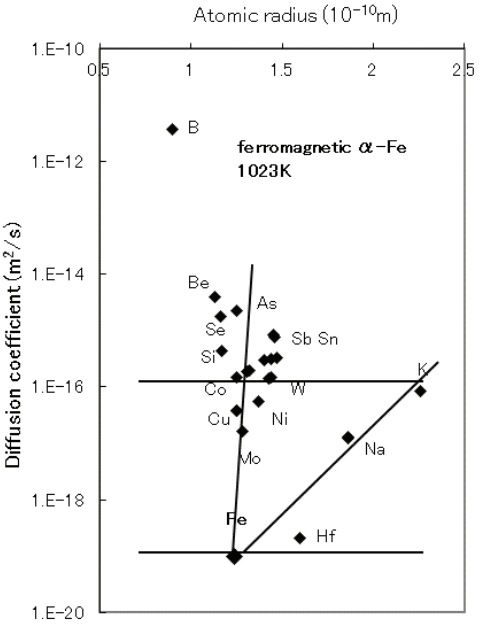

Fig. 10-4 – Atomic radii of the diffuser elements and their diffusion coefficients at 1023K in ferromagnetic α-Fe

Ferromagnetic α-Fe shows the smallest diffusion coefficient among the elements. All the elements diffuse faster than Fe in ferromagnetic α-Fe. We found no dependence of the diffusion coefficient on the atomic radius. Most of the elements lie on a vertical line. Only K, Na, and Hf show an inverse atomic radius dependence.

For reference, the relationship between the diffusion coefficients of the elements at 1073K in paramagnetic α-Fe and atomic radii of the elements are shown in Fig. 10-5.

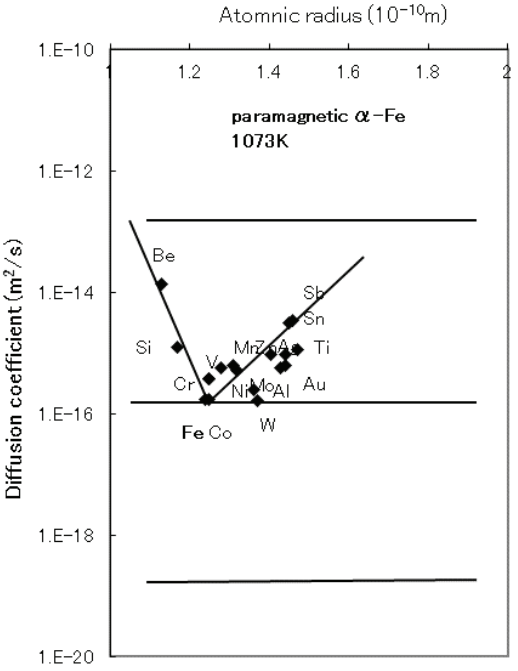

Fig. 10-5 – Atomic radii of the diffuser elements and their diffusion coefficients at 1073K in paramagnetic α-Fe

Many elements showed only a slightly larger diffusion coefficient than that of Fe and an inverse atomic radius dependence. Ferromagnetic α-Fe and paramagnetic α-Fe show very different behaviors, attributed to the existence and absence of magnetism, respectively. It is speculated that magnetism strongly promotes diffusion of the elements. [9]

Fig. 10-6 shows the relationship between the diffusion coefficients of elements at 1073K in α-Zr and the atomic radii of the elements.

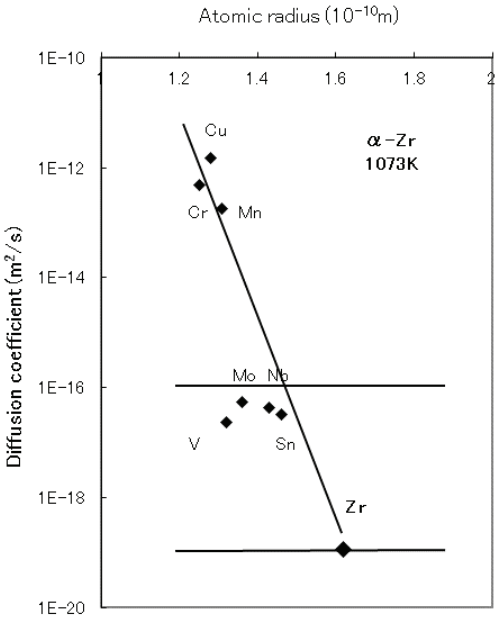

Fig. 10-6 – Atomic radii of the diffuser elements and their diffusion coefficients at 1073K in α-Zr.

α-Zr shows the smallest diffusion coefficient among the elements. The elements – Cu, Cr, and Mn – showed much larger diffusion coefficients than that of Zr and the atomic radius dependence was followed.

For reference, the relationship between the diffusion coefficients of the elements at 1273K in β-Zr versus the atomic radii of elements, is shown in Fig. 10-7.

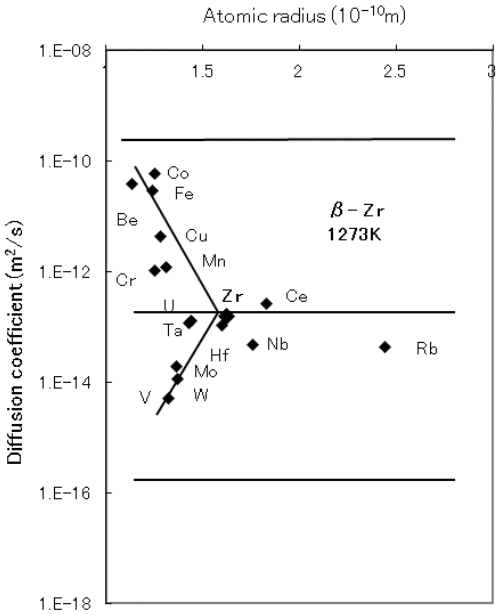

Fig. 10-7 – Atomic radii of the diffuser elements and their diffusion coefficients at 1273K in β-Zr.

Zr itself showed an intermediate diffusion coefficient. Neither fast diffusion nor an atomic radius dependence is shown in this case.

But a small atomic radius dependence is recognized in the diffusion range faster than Zr, and a small inverse atomic radius dependence is recognized in the diffusion range slower than Zr.

10.2 The matrix elements for which slow diffusion occurs

In contrast to elements that show fast diffusion of foreign elements, certain elements feature considerably suppressed diffusivity. This effect is denoted

as “slow diffusion,” and defined here as a diffusion coefficient of the diffuser elements more than three orders of magnitude smaller (*i.e.*, 1/1000) than the self-diffusion of the matrix element.

Elements for which slow diffusion occurs include Li, Ca, Mg, Al, and Be.

Fig. 10-8 shows the relationship between the diffusion coefficients of the elements at 423K in Li and the atomic radii of elements.

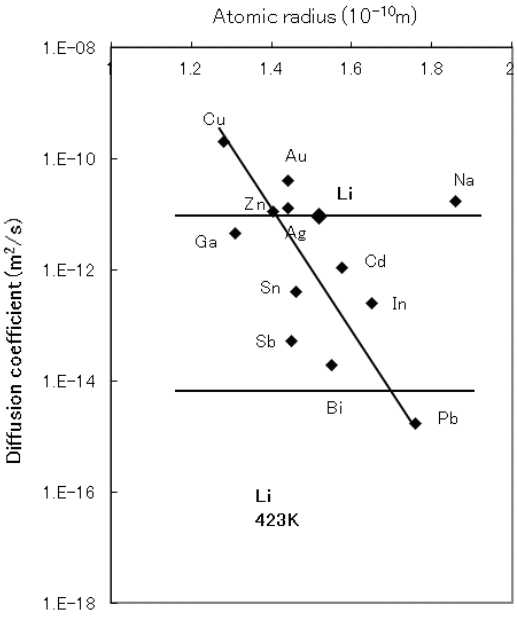

Fig. 10-8 – Atomic radii of the diffuser elements and their diffusion coefficients at 423 K in Li

The diffusion coefficient of Li is among the largest of these elements, and the elements – Pb, Bi, and Sb – show much smaller diffusion coefficients than that of Li. The atomic radius dependence was followed. Pb showed the largest atomic radius and the smallest diffusion coefficient, while Cu showed the smallest atomic radius and the largest diffusion coefficient.

Fig. 10-9 shows the relationship between the diffusion coefficients of the elements at 773K in Al versus the atomic radii of elements.

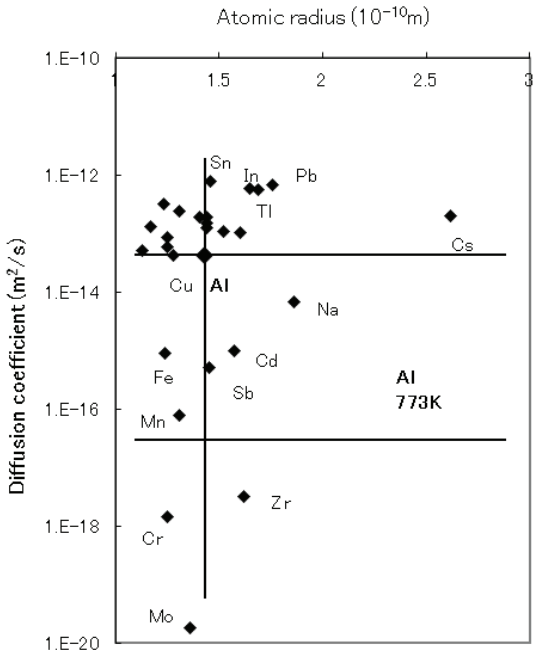

Fig. 10-9 – Atomic radii of the diffuser elements and their diffusion coefficients at 773K in Al

Al shows a relatively large diffusion coefficient and lies in a group with several other elements in the diagram. The elements – Mo, Cr, and Zr – showed much smaller diffusion coefficients than that of Al. An atomic radius dependence is not followed. The elements with similar atomic radii show quite different diffusion coefficients. Mo shows an equivalent atomic radius to that of Al and the smallest diffusion coefficient, while Sn shows an equivalent atomic radius to that of Al and the largest diffusion coefficient.

In addition, Mg and Be show slow diffusion.

Fig. 10-10 shows the relationship between the diffusion coefficients of the elements at 773K in Mg versus the atomic radii of the elements.

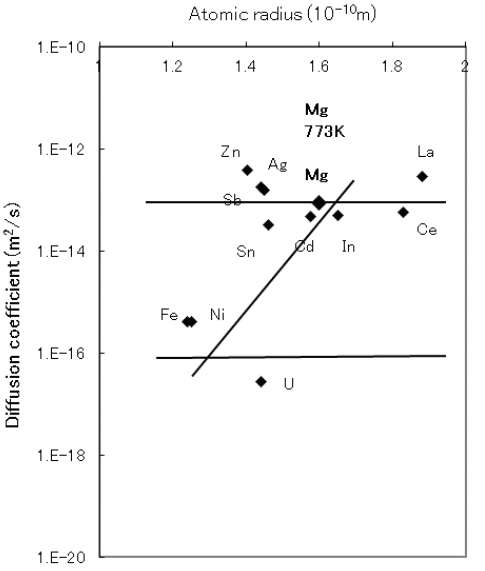

Fig. 10-10 – Atomic radii of the diffuser elements and their diffusion coefficients at 773K in Mg

Similar to Al, Mg shows a relatively large diffusion coefficient among the elements and lies in a group with the other elements in the diagram. The elements – U, Fe, and Ni – show much smaller diffusion coefficients than that of Mg and no atomic radius dependence was followed. U features an intermediate atomic radius and the smallest diffusion coefficient. Although Zn also shows an intermediate atomic radius, it features the largest diffusion coefficient.

Fig. 10-11 shows the relationship between the diffusion coefficients of elements at 1273K in Be versus their atomic radii.

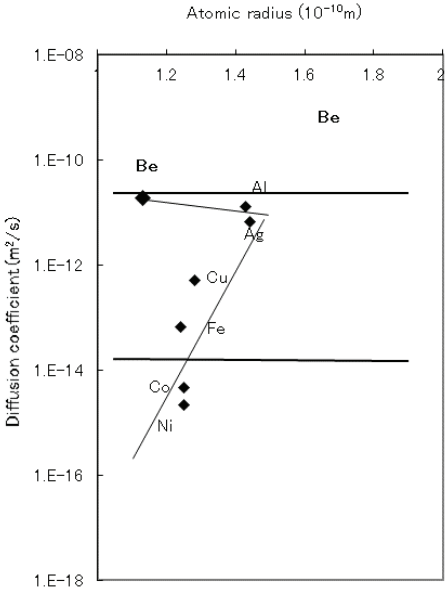

Fig. 10-11 – Atomic radii of the diffuser elements and their diffusion coefficients at 1273K in Be

Be shows the largest diffusion coefficient among the elements. The elements – Ni, Co and Fe – show much lower diffusion coefficients than that of Be. No atomic radius dependence was followed. Ni shows an equivalent atomic radius to that of Be and the smallest diffusion coefficient, while Al shows a larger atomic radius than that of Be and a diffusion coefficient equivalent to that of Be.

10.3 Elements for which normal diffusion occurs

Diffusion behavior is referred to as “normal diffusion,” when the diffusion coefficients of elements in a specific matrix metal are different from the self-diffusion of the matrix but within three orders of magnitude, smaller or larger than the self-diffusion.

Fig. 10-12 shows the relationship between the diffusion coefficients of elements at 1023K in Cu and the atomic radii of elements.

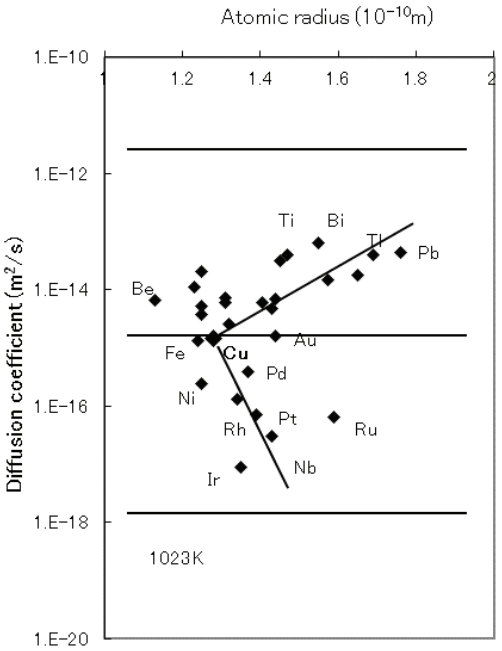

Fig. 10-12 – Atomic radii of the diffuser elements and their diffusion coefficients at 1023K in Cu

The elements are grouped together in the diagram. Cu is located near the center of the group of elements.

The elements – Ir, Nb, Pt, and Ru – show lower diffusion coefficients than that of Cu. The elements – Bi, Pb, Tl, and Ti – show larger diffusion coefficients than Cu, despite their larger atomic radii than that of Cu. An inverse atomic radius dependence is recognized in the elements with higher diffusion coefficients than that of Cu. A positive atomic radius dependence is recognized in the elements with lower diffusion coefficients than that of

Cu.

Fig. 10-13 shows the relationship between the diffusion coefficients of elements at 1273K in γ-Fe and the atomic radii of elements.

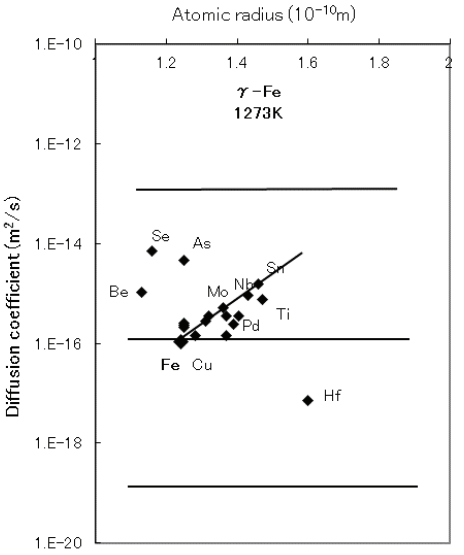

Fig. 10-13 – Atomic radii of the diffuser elements versus their diffusion coefficients at 1273K in γ-Fe

The elements formed a band in the diagram. Fe is located at the lower end of the band of elements. Except for Hf, Fe features the lowest diffusion coefficient among these elements, although Fe has the smallest atomic radius except for Se and Be. The elements – Sn, Nb, and Ti – show rather large diffusion coefficients although they have large atomic radii. As the atomic radius increases, the diffusion coefficient increases; hence, an

inverse atomic radius dependence is recognized.

Fig. 10-14 shows the relationship between the diffusion coefficients of elements at 623K in Zn and the atomic radii of the elements.

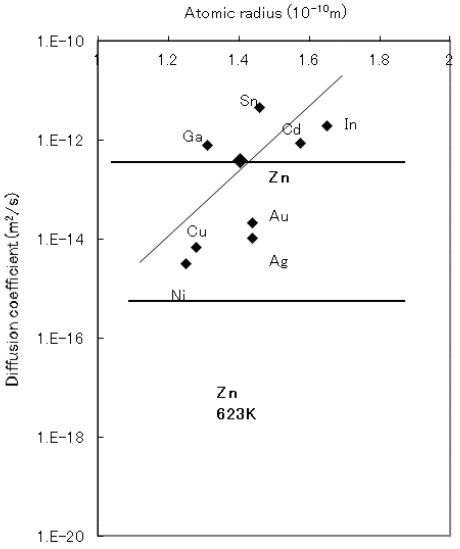

Fig. 10-14 – Atomic radii of the diffuser elements and their diffusion coefficients at 623K in Zn

The elements are arranged in a band in the diagram. Zn is located at the center of the band of elements. The elements – Sn, In, and Cd – show relatively large diffusion coefficients although they have large atomic radii.

The elements – Cu and Ni – show relatively small diffusion coefficients

although they have small atomic radii. As the atomic radii increase the diffusion coefficients also increase; hence, an inverse atomic radius dependence is recognized.

β-Ti shows a similar pattern to that of Cu. Fig. 10-15 shows the relationship between the diffusion coefficients of the elements at 1273K in β-Ti and the atomic radii of the elements.

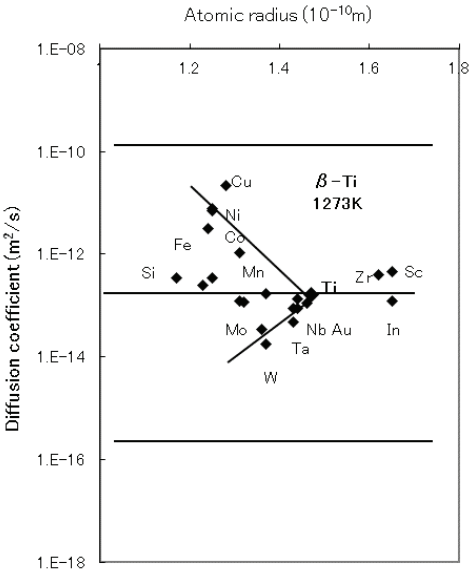

Fig. 10-15 – Atomic radii of the diffuser elements and their diffusion coefficients at 1273K in β-Ti

The elements form an agglomeration of the elements. Ti is located near the center of the group of elements. The elements – W, Mo, Nb, and Au – show smaller diffusion coefficients than that of Ti. The elements – Cu, Ni, Co,

and Fe – show larger diffusion coefficients than that of Ti. The elements with larger diffusion coefficients than β-Ti show a weak positive atomic radius dependence. The elements with smaller diffusion coefficients show a weak inverse atomic radius dependence.

10.4 Characteristics of the matrix metals for fast diffusion, slow diffusion, and normal diffusion

There are three kinds of diffusion behaviors in metallic elements, namely, fast diffusion, slow diffusion, and normal diffusion.

When this author read the reports on fast diffusion [1], he recognized the patterns of the matrix elements and the diffuser elements instantly, and anticipated that they would draw patterns on the TC-YM diagram.

To classify the matrix elements into element groups in which fast, slow, and normal diffusion occur, the matrix elements were plotted on a TC-YM diagram.

These results are shown in Fig. 10-16, and notable patterns can be discerned.

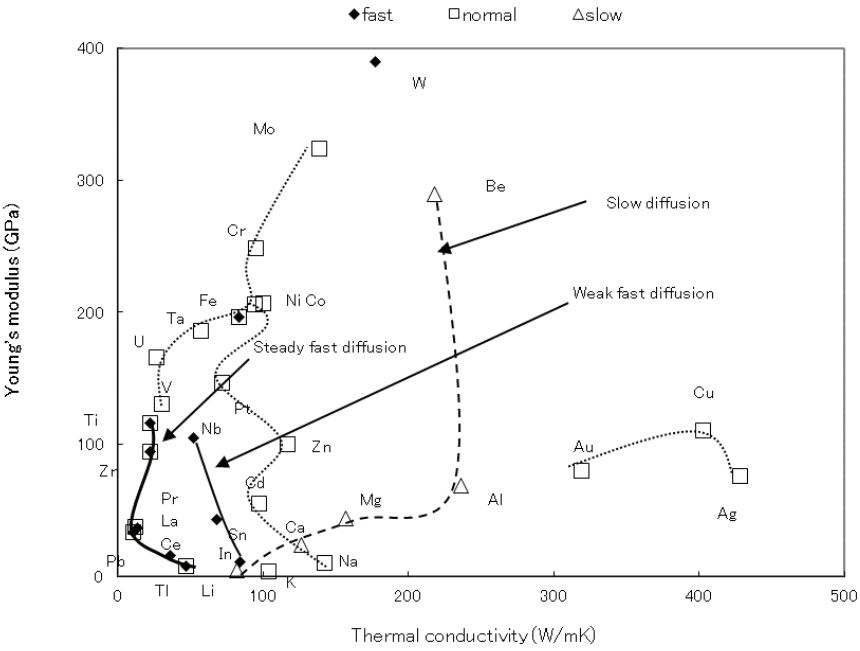

Fig. 10-16 – Distribution of the metallic elements that show fast, slow, and normal diffusion as a matrix metal, plotted on the TC-YM diagram

The plots of Tl, Ce, La Pr, Zr, Ti, and Fe are complicated due to their plural phases.

Table 10-1 shows the detail of these elements. Fast diffusion occurs in the low temperature phases.

Table 10-1 – Fast and normal diffusions in the elements showing plural phases

Element	Fast diffusion	Normal diffusion
Tl	α-Tl	β-Tl
Ce	γ-Ce	δ-Ce
La	β-La	
Pr		β-Pr
Zr	α-Zr	β-Zr
Ti	α-Ti	β-Ti
Fe	ferromagnetic α-Fe	paramagnetic α-Fe
		γ-Fe

First, the elements showing "steady" fast diffusion form a line from Fe *via* Ti, Zr, La, Ce, Pb to Tl. Furthermore, the elements showing "weak" fast diffusion, including Nb, Sn, and In, formed a straight line with a nearly constant thermal conductivity. Here, we use "steady" to indicate more than three elements showing fast diffusion behavior, and "weak" to indicate only one or two element(s) showing fast diffusion.

Next, it is noted that the matrix elements of slow diffusion form a particular curve starting from Li near the abscissa, and moving *via* Ca, Mg, Al, to Be.

Third, the matrix elements for normal diffusion elements lie between the line of fast diffusion and that of slow diffusion. The other elements showing normal diffusion, *i.e.*, Au, Cu, and Ag, are located at the right-most side.

According to literature reports [10], the elements – Li, Na, K, Ti, Y, Zr, Nb, La, Si, Ge, In, Sn, Tl, Pb, Ce, Pr, Nd, Gd, Er, U, and Pu – are good solvents

(matrix metals) for fast diffusion, and the elements – Fe, Co, Ni, Cu, Zn, Pd, Ag, Cd, Au, and Hg – are good solutes (diffuser elements). Although a few groupings of elements appear, based on their location in the periodic table, there are no notable tendencies.

Anthony has reported that for fast diffusion, solvent atoms tend to have large valences and solute atoms have small atomic radii and low valences. [1, 11] However, valence alone does not control the physical properties of the elements. The atomic radius dependence is valid for fast diffusion, but not for other diffusion behaviors. For instance, as shown in the next Fig. 10-17, in the elements – Ca, Cd, Zn, Fe (γ-Fe), and Cr, the inverse atomic radius dependence is observed. Therefore, valence and atomic radius are likely not the main factors controlling fast diffusion.

In contrast, Fig. 10-16 gives insight into the physical properties of both the solvent and solute atoms – for all cases of fast, slow, and normal diffusion.

The elements that behave as matrix metals and give rise to fast diffusion are those with low thermal conductivities and low Young's modulus values.

Fast diffusion in ferromagnetic α-Fe is neglected here, because magnetism appears to affect these results. Therefore, Ti is the element with the largest Young's modulus in the element group for fast diffusion.

The matrix metal elements contributing to slow diffusion are those of intermediate thermal conductivity with Young's modulus values ranging from low to high (as for Be).

Fig. 10-17 shows the distribution of the matrix elements, which feature an atomic radius dependence of the diffusion coefficients.

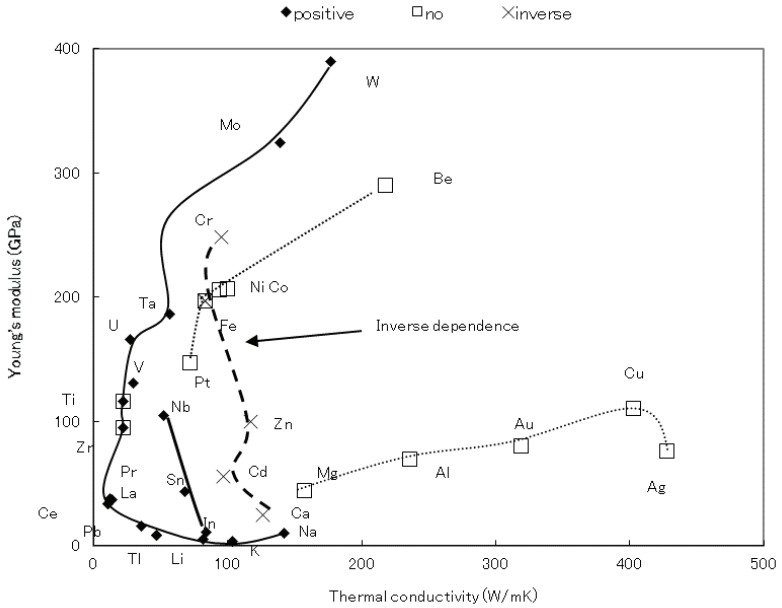

Fig. 10-17 – Distribution of metallic elements for which diffusion of foreign elements shows an atomic radius dependence

These results follow a similar pattern to that shown in Fig. 10-16. The matrix elements for which the diffusion coefficients show a positive atomic radius dependence, lie on a line from Na to W, which includes many elements of low thermal conductivity. Particularly, the elements – U, V, and Pb – lie on a straight line of constant thermal conductivity.

The matrix elements, which show an inverse atomic radius dependence, *i.e.*, Ca, Cd, Zn, Fe (γ-Fe), and Cr, lie on a line of similar thermal conductivity.

The matrix elements that show no dependence are located elsewhere and form two curves. The elements – Ta, Fe, Ni, Co, and Be – are located in the upper part of the diagram. The elements – Mg, Al, Au, Cu, and Ag – are located in the lower and right side of the diagram.

The positive-atomic radius dependence has been previously reported. [1, 5] However, in this study, we also identified an inverse atomic radius dependence.

Elements that show a positive atomic radius dependence as matrix metals lie on a line of low thermal conductivity, with both low and high Young's modulus values. These elements typically show fast diffusion.

Anomalous elements that show an inverse atomic radius dependence as matrix metals are those of intermediate thermal conductivity and low-to-intermediate Young's modulus value. These elements are those giving rise to normal diffusion.

To clarify the reasons for fast, slow, and normal diffusion behavior and the relationships with the atomic radius dependence, the diffusion coefficients of each element are plotted on the TC-YM diagram.

In this chapter, only fast diffusion behavior is discussed.

10.5 Distribution of diffusion coefficients of diffuser elements on the TC-YM diagram in the case of fast diffusion

In order to clarify the differences in the properties between the matrix metals and diffuser elements, the matrix element and diffuser elements were

plotted on the TC-YM diagram for each fast diffusion couple.

Fig. 10-18 shows the distribution of the diffusion coefficients of elements at 1023K in ferromagnetic α-Fe.

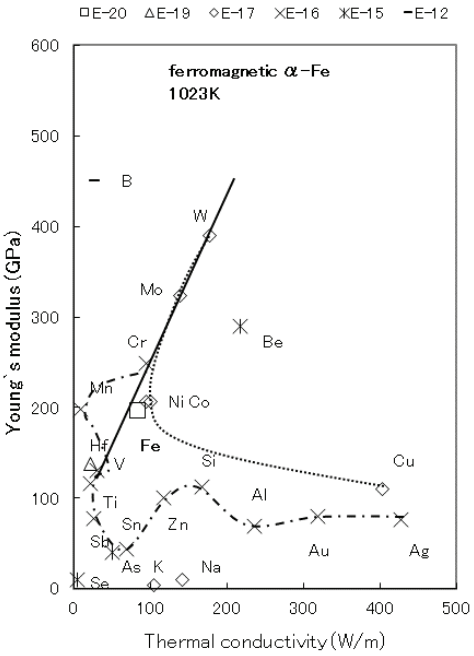

Fig. 10-18 – Distribution of the diffusion coefficients of elements at 1023K in ferromagnetic α-Fe on the TC-YM diagram

"E-20" in the legend indicates, for example, that the particular elements have diffusion coefficients with a magnitude of 10^{-20} m^2/s. The ferromagnetic α-Fe shows an extremely small self-diffusion coefficient. Elements with high Young's modulus values or high thermal conductivities, such as W, Mo, Ni, Co, and Cu show similar and intermediate diffusion

coefficients, drawing a curve on the diagram. The elements with smaller Young's modulus values and smaller thermal conductivities show similar and much larger diffusion coefficients than that of Fe. These elements are denoted as diffuser elements in fast diffusion in Fe.

It is difficult to speculate on the physical properties of diffuser elements contributing to fast diffusion, from Fig. 10.4; however, the TC-YM diagram suggests that their Young's moduli must be smaller than that of Fe, and/or their thermal conductivities must be smaller than that of Fe, to enable their fast diffusion in ferromagnetic α-Fe.

Note that the fast diffusion in ferromagnetic α-Fe may operate through a different mechanism from that of other elements, because of the effects of magnetism.

Fig. 10-19 shows the distribution of the diffusion coefficients of elements at 1773K in Nb.

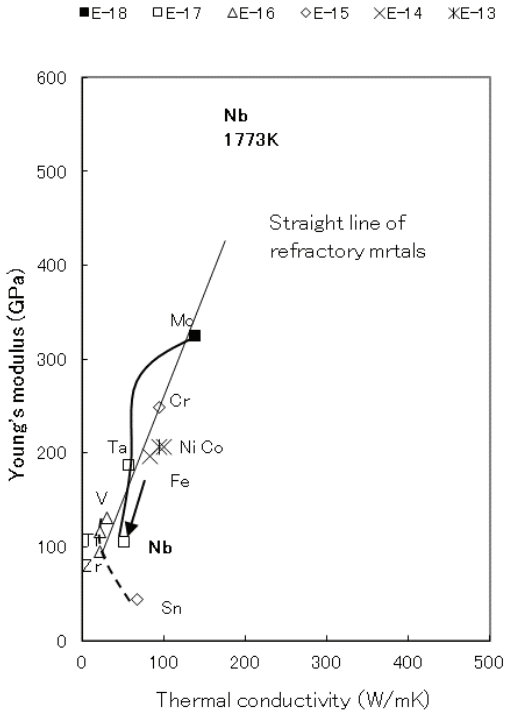

Fig. 10-19 – Distribution of the diffusion coefficients of elements at 1773K in Nb on the TC-YM diagram

The elements – Mo and Ta – on the straight line of refractory metals have similar diffusion coefficients to that of Nb. Conversely, the gulf elements – Fe, Ni, and Co, which are located off the straight line of the refractory metals – show large diffusion coefficients. However, the increase of their diffusion coefficients is small. Hence, fast diffusion in Nb is weak. This effect is denoted as “weak fast diffusion.”

The **arrow** in the figure shows the direction and distance from a diffuser

element to a matrix metal in the case of fast diffusion. The length and direction of the arrow will be an important factor to interpret fast diffusion.

In Ta and V, fast diffusion does not occur. Ta and V are near to Fe, Ni and Co on the diagram. Thus, a considerable difference in the thermal conductivity and Young's modulus seems to be necessary to enable fast diffusion.

Fig. 10-20 shows the distribution of the diffusion coefficients of elements at 1073K in α-Ti.

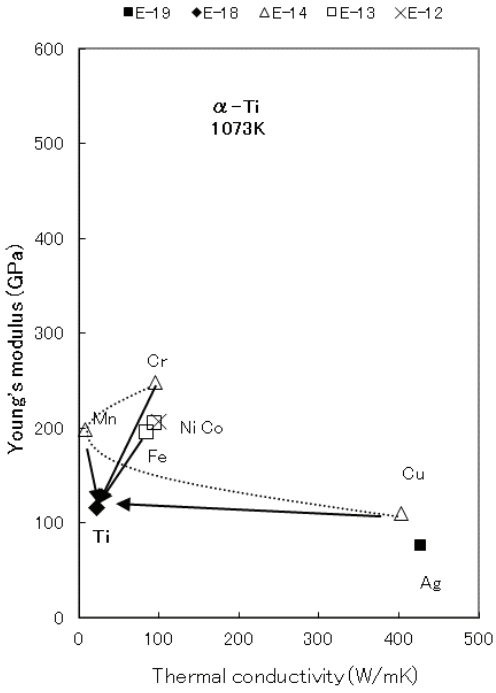

Fig. 10-20 – Distribution of the diffusion coefficients of elements at 1073K in α-Ti on the TC-YM diagram

The elements of higher Young's modulus than Ti, such as Fe, Co, Ni, Mn, and Cr, show extremely large diffusion coefficients. This effect is denoted as "steady fast diffusion." Ti has a smaller conductivity than that of Nb, and therefore, the gulf elements, Fe, Ni, and Co, diffuse faster in Ti than when they are in Nb. This large difference in thermal conductivity may be the driving force for fast diffusion.

In addition, Cu, shows a larger diffusion coefficient. In metals of low thermal conductivity, elements of high thermal conductivity such as Cu diffuse rapidly. **It is noted again that the large difference in thermal conductivity may be the source of the driving force for fast diffusion.** Ag does not diffuse rapidly, because its Young's modulus is lower than that of Cu. The arrows represent these situations well.

Fig. 10-21 shows the distribution of the diffusion coefficients of the elements at 1073K in α-Zr.

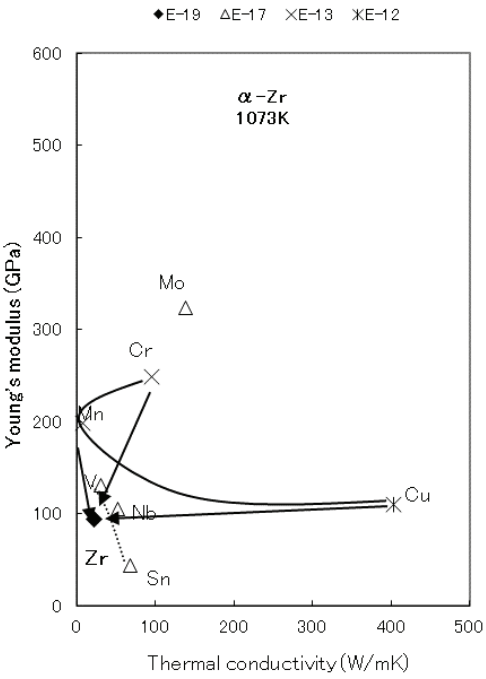

Fig. 10-21 – Distribution of the diffusion coefficients of elements at 1073K in α-Zr on the TC-YM diagram

Zr is located directly below Ti on the diagram, and therefore, shows a similar pattern to that of Ti. Mn, and the gulf elements – Cr and Cu – show extremely large diffusion coefficients. The elements – V, Nb, and Sn – in the same region near Zr, also show relatively large diffusion coefficients.

Fig. 10-22 shows the distribution of the diffusion coefficients of elements at 473K in Sn.

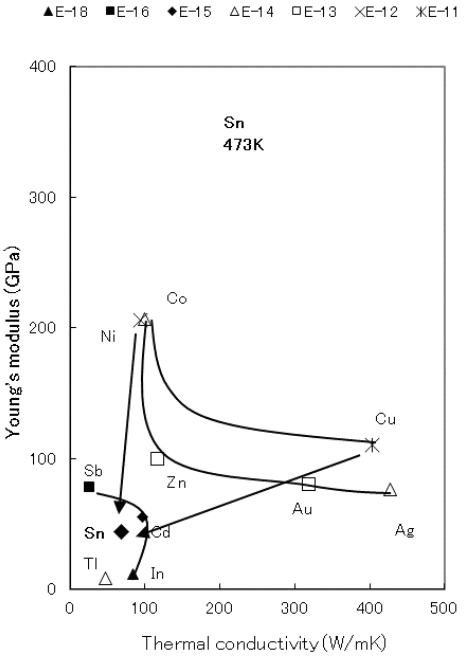

Fig. 10-22 – Distribution of the diffusion coefficients of elements at 473K in Sn on the TC-YM diagram

Sn is located at the position of low Young's modulus, and its thermal conductivity is as low as Nb. The gulf elements – Ni and Cu – show large diffusion coefficients; however, the values of their diffusion coefficients are not so large. Fast diffusion in Sn is weak, which may be attributed to Sn being located at the higher conductivity side and near the gulf elements such as Ni, Co, and Cu. The elements – Sb, Cd, and In – in the region of Sn show slower diffusion than that of Sn, unlike the case of Pb in Fig. 10-23. This is because fast diffusion is weak in Sn.

The elements which show fast diffusion in Sn – Ni and Cu – have long and downward arrows.

Fig. 10-23 shows the distribution of the diffusion coefficients of elements at 473K in Pb.

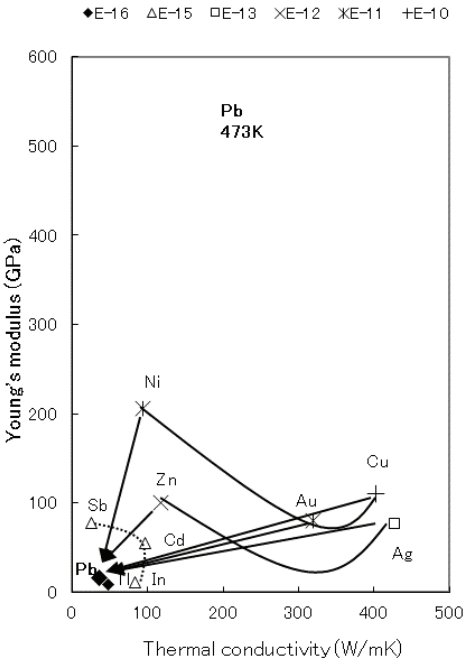

Fig. 10-23 – Distribution of the diffusion coefficients of elements at 473K in Pb on the TC-YM diagram

Cu, Au, Ni, Zn, and Ag show extremely large diffusion coefficients. Above all, the gulf elements, Cu and Ni, show the largest diffusion coefficients. Tl is nearest Pb. It shows the same diffusion coefficient as Pb. The elements – Sb, Cd, and In – closely surround Pb. These elements also show slightly

larger diffusion coefficients than that of Pb. Zn is located further from Pb and shows a larger diffusion coefficient. Finally, the gulf elements form in groups, at some distance from Pb, and show the largest diffusion coefficients. With the increasing distance from Pb on the diagram, the diffusion coefficients increase.

Pb is located at a position of smaller Young's modulus and smaller conductivity than those of Sn. Therefore, Pb shows a large difference from other elements in terms of its conductivity and Young's modulus. For this reason, there are many elements that show fast diffusion in a Pb matrix.

In addition, the diffusion coefficients of elements in Pb are distributed, forming concentric circles with an inner circle formed by the gulf elements on the TC-YM diagram. The atomic radii of elements are distributed in the same way as shown in Fig. 2-2. Therefore, the diffusion coefficients and atomic radii show a linear correlation, as shown in Fig. 10-2.

The elements which show fast diffusion – Ni, Au, Cu, Zn, and Ag – have long and downward arrows.

In this way, the TC-YM diagram is an effective tool for explaining the diffusion coefficients of these elements.

Both Fe and Co diffuse rapidly at 973K in γ-Ce. Both Au and Ag diffuse rapidly at 473K in α-Tl. Both Ag and Au diffuse rapidly at 373K in In, and Au diffuses rapidly at 973K in La. In this way, the elements – La, Ce, Tl, and In – are also metals in which steady fast diffusion occurs.

10.6 Proposal to the mechanism of fast diffusion

In summary, the elements in which steady fast diffusion occurs are W, Fe, Ti, Zr, Pr, Ce, Pb, and Tl. The elements in which weak fast diffusion occurs are Nb, Sn, and In.

These situations are shown in Fig. 10-16. The elements showing steady fast diffusion lie on the left sideline, while those showing weak fast diffusion lie on the right sideline.

The diffuser elements giving rise to fast diffusion include Fe, Ni, Co, Cr, Mn, Au, Ag, and Cu, *i.e.*, all the gulf elements and some elements near the gulf elements. The gulf elements are located in the region at the outside of the TC-YM diagram and have the smallest atomic radii among the elements. In addition, the gulf elements have the largest combination of thermal conductivity and Young's modulus.

Thus, large differences in the thermal conductivity and the Young's modulus between the matrix metals and the diffusing elements are the necessary conditions for fast diffusion.

Hence, fast diffusion phenomena occur for matrix metals with low electron mobility and small binding forces, and diffuser elements with high electron mobility and large binding forces between atoms. These characteristics summarize the occurrence of fast diffusion and explain how atoms with high electron mobility diffuse in a matrix consisting of atoms with low electron mobility. Many models have been proposed to account for the mechanism of fast diffusion. [3, 13] However, these theories must take electron mobility into consideration.

If atoms with different electron mobilities touch each other, a repulsive force will be generated. If one atom has a soft outer electron shell, the shell may be deformed by this repulsive force. The elements of the matrix metals that show fast diffusion behavior are such elements. For example, Pb has a low Young's modulus and a low thermal conductivity. A low Young's modulus indicates a soft outer electron shell, because the Young's modulus reflects the gradient of the binding forces between atoms. Conversely, diffuser elements are atoms with a rigid outer electron shell, which are typically elements on or near the curve of the gulf elements, and have a large thermal conductivity and/or large Young's modulus. If an element with a small atomic radius, high electron mobility, and rigid electron shell enters a lattice of atoms with a large atomic diameter, low electron mobility, and soft outer electron shell, the latter will become considerably deformed by the repulsive force. **Consequently, the matrix elements yield to provide paths for the invading atoms.**

Conversely, if the atoms of low electron mobility enter a lattice of atoms with high electron mobility, then the atoms with low electron mobility may be easily deformed and pass through the lattice rapidly. In fact, Pb, Tl, In, Cd, and Bi, diffuse faster in Cu, although their atomic radii are larger than that of Cu, as shown in Fig. 10-12.

In the same way, the elements – Sb, Sn, Ti, Ag, Zn, and Mn – diffuse faster in paramagnetic α-Fe than Fe, as shown in Fig. 10-5. The elements – Sn, Nb, Ti, Pd, and Mo – diffuse faster in γ-Fe, as shown in Fig. 10-13. The elements – In, Sn, and Cd – diffuse faster than Zn in Zn, as shown in Fig. 10-14. **This explains the inverse atomic radius dependence.**

In these cases, the diffuser elements are those that act as matrix metals for fast diffusion. A repulsive force operates between the atoms of the matrix metals and the foreign atoms, when there is a substantial difference in the thermal conductivity and Young's modulus. Notably, the **solubility** of foreign elements in a metal decreases as the difference in the thermal conductivity and Young's modulus increases on the TC-YM diagram. [12] When the difference in the thermal conductivity and Young's modulus, *i.e.*, the difference in the electron mobility and the binding force between atoms, is large, the repulsive force is enhanced, and the foreign atoms are excluded from the matrix. In fact, the elements that diffuse fast in Pb have only very small solubilities for foreign elements. In the literature [1, 5, 13], it has been recognized that the solubilities of Cu, Ag, and Au in Pb are low; however, the importance of the repulsive force between atoms has not been commented on.

In the liquid state, the elements – Cu, Fe, Ni, and Zn – form a **miscibility gap** with Pb, in which two liquid phases coexist, which are insoluble in one another, likely because of the repulsive force between them. These are elements, which show fast diffusion in Pb, as shown in Figure 10.2. Only Ag does not form a miscibility gap with Pb among the fast diffuser elements. Notably, fast diffusion of Ag is relatively small compared with other fast diffuser elements, as shown in Fig. 10-2.

For reference, the distribution of elements which form a miscibility gap with Pb in the molten state on the TC-YM diagram is shown in Fig. 10-24.

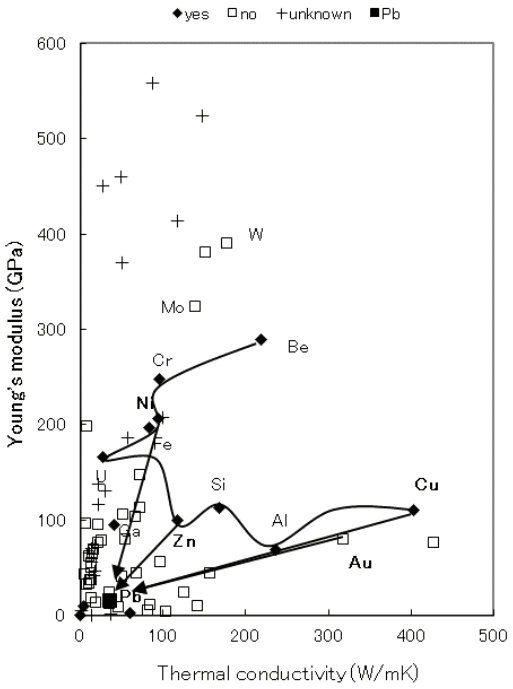

Fig. 10-24 – Distribution of elements which form a miscibility gap with Pb in the molten state shown on the TC-YM diagram

The word “yes” in the legend means the existence of a miscibility gap and “no” means no existence of a miscibility gap. The elements – Cu, Al, Si, Zn, Ga, U, Fe, Ni, Cr, and Be – form a miscibility gap with Pb. They are the gulf elements and those near the curve of the gulf elements. It is proved that the repulsive force is generated between these elements and Pb.

10.7 The effects of allotropic transformation on fast diffusion

As shown in Table 10.1, fast diffusion occurs in α-Tl, γ-Ce, β-La, α-Zr, α-Ti, and ferromagnetic α-Fe, but doesn't occur in β-Tl, δ-Ce, β-Pr, β-Pr, β-Zr, β-Zr, β-Ti, paramagnetic α-Fe, and γ-Fe. In short, fast diffusion occurs in the phase of lower temperature.

What is the reason for it?

Fig. 10-25 shows the temperature dependence of the diffusion coefficients of various elements in α-Ti and β-Ti.

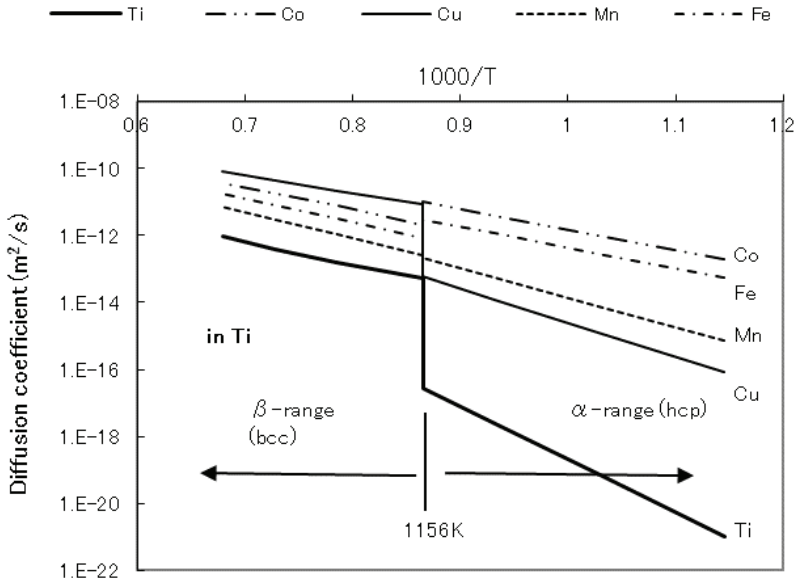

Fig. 10-25 – Temperature dependence of the diffusion coefficients of various elements in α-Ti and β-Ti

The diffusion coefficient of the self-diffusion of Ti is very small in the α-range of Ti. It increases abruptly at the allotropic temperature of 1156K.

Changes in the diffusion coefficient of various foreign elements at the allotropic temperature are small.

The elements – Co and Fe – diffuse fast in Ti in the range of α-Ti. This is fast diffusion of these elements in α-Ti. This is not because these elements diffuse anomalously fast in Ti, but because the self-diffusion of Ti is very slow in the α-range of Ti. Why do Ti atoms diffuse slowly in the Ti matrix? It can be suspected that the Ti atoms have a soft atomic shell because Ti has low thermal conductivity and low Young's modulus, and the friction between the adjacent atoms is large compared to the case of hard atoms. Consequently, Ti atoms diffuse slowly in the Ti matrix. On the other hand, the atoms of foreign elements deform the soft atomic shell of Ti by the repulsive force generated from the difference in the thermal conductivity and the Young's modulus, open the passageway and diffuse fast, shown in Fig. 10-20.

In the β-phase, the atoms of Ti change into hard atoms, and diffuse smoothly in the Ti matrix.

Fig. 10-26 shows the distribution of diffusion coefficients of elements at 1273K in β-Ti on the TC-YM diagram.

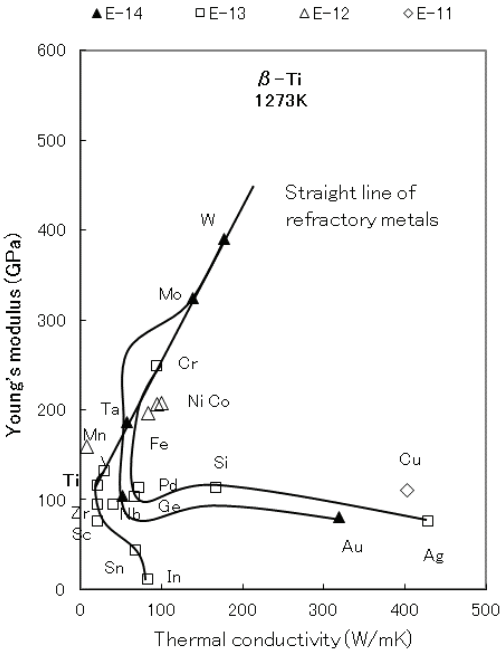

Fig. 10-26 – Distribution of diffusion coefficients of elements at 1273K in β-Ti on the TC-YM diagram

Fast diffusion of Fe Ni, Co, and Cu is suppressed, and a small slow diffusion, which will be explained in Chapter 11, is obverted at the elements – W, Mo, Ta, Nb, and Au. These are all because Ti atoms in the β-phase have hard atomic shells.

Fig. 10-27 shows the temperature dependence of the diffusion coefficients of various elements in α-Zr and β-Zr.

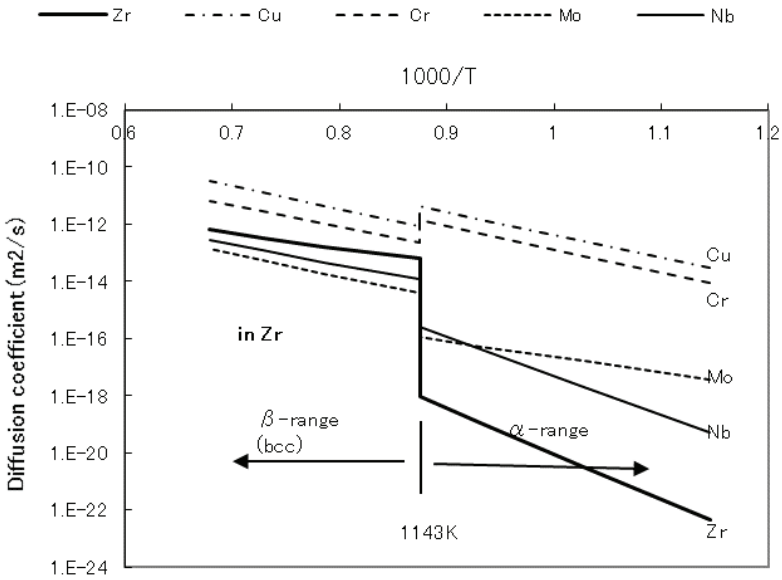

Fig. 10-27 – Temperature dependence of the diffusion coefficients of various elements in α-Zr and β-Zr

The situation is the same as in Ti. It can be suspected that Zr atoms in the α-range have soft atomic shells and diffuse very slowly in the Zr matrix. The elements – Cu and Cr – diffuse fast in the Zr matrix in the same manner as in Ti as shown in Fig. 10-21.

In the β-phase, the atoms of Zr change into hard atoms, and diffuse smoothly in the Zr matrix.

Fig. 10-28 shows the distribution of diffusion coefficients of elements at 1273K in β-Zr on the TC-YM diagram.

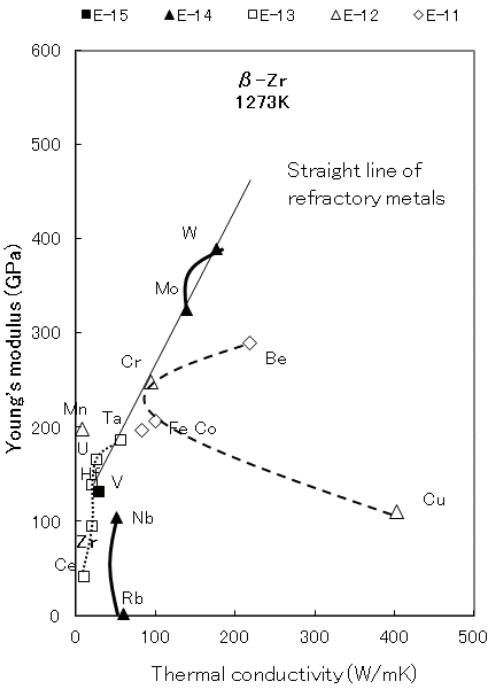

Fig. 10-28 – Distribution of diffusion coefficients of elements at 1273K in β-Zr on the TC-YM diagram

TFast diffusion of Fe Cr, Mn, and Cu is suppressed, and a small slow diffusion, which will be explained in Chapter 11, is obverted at the elements – W, Mo, V, Nb, and Rb. These are all because Zr atoms in the β-phase have hard atomic shells.

Fig. 10-29 shows the temperature dependence of the diffusion coefficients of various elements in γ-Ce and δ-Ce.

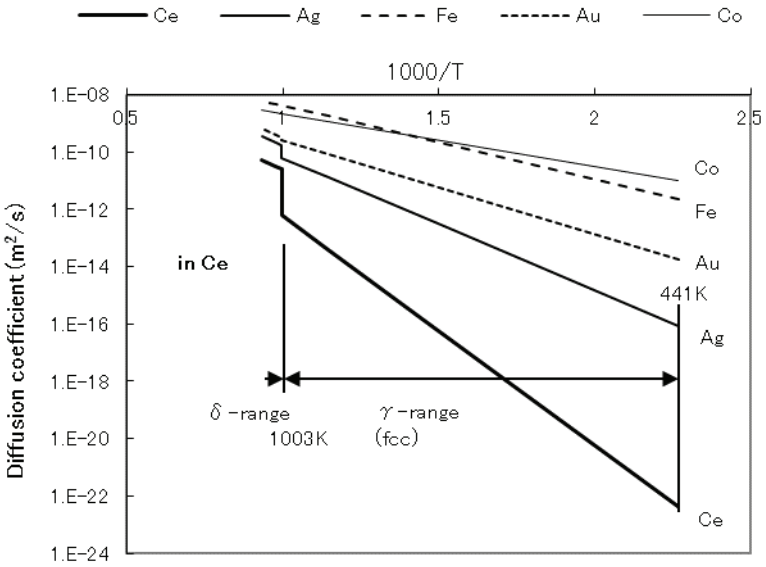

Fig. 10-29 – Temperature dependence of the diffusion coefficients of various elements in γ-Ce and δ-Ce

The situation is the same as in Ti and Zr, though the temperature range in which fast diffusion occurs is the range of the fcc structure. Ce atoms diffuse very slowly in the Ce matrix in the γ-range, and the elements – Co and Fe – diffuse fast. It can be speculated that Ce atoms have soft atomic shells in the γ-range.

In the δ-phase, the atoms of Ce change into hard atoms, and diffuse smoothly in the Ce matrix.

Fig. 10-30 shows the distribution of diffusion coefficients of elements at 973K in γ-Ce on the TC-YM diagram.

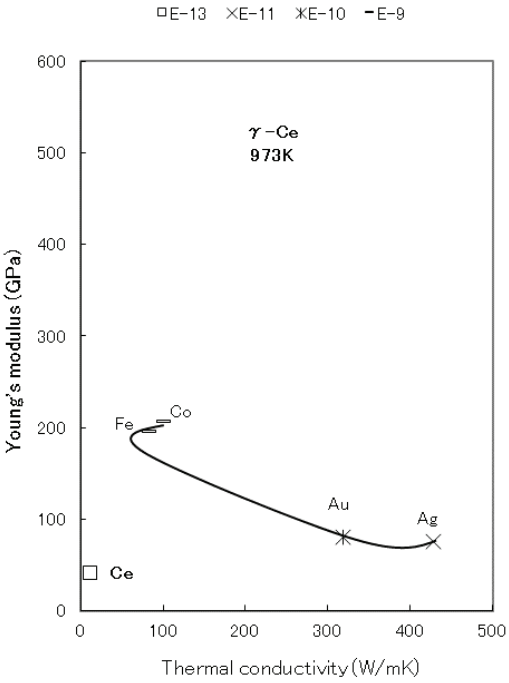

Fig. 10-30 – Distribution of diffusion coefficients of elements at 973K in γ-Ce on the TC-YM diagram

The elements – Co, Fe, Au, and Ag, which are far from Ce on the TC-YM diagram, show fast diffusion, because Ce itself diffuses very slowly in γ-Ce. It can be speculated that Ce atoms in the γ-phase have soft atomic shells.

Fig. 10-31 shows the distribution of diffusion coefficients of elements at 1023K in δ-Ce on the TC-YM diagram.

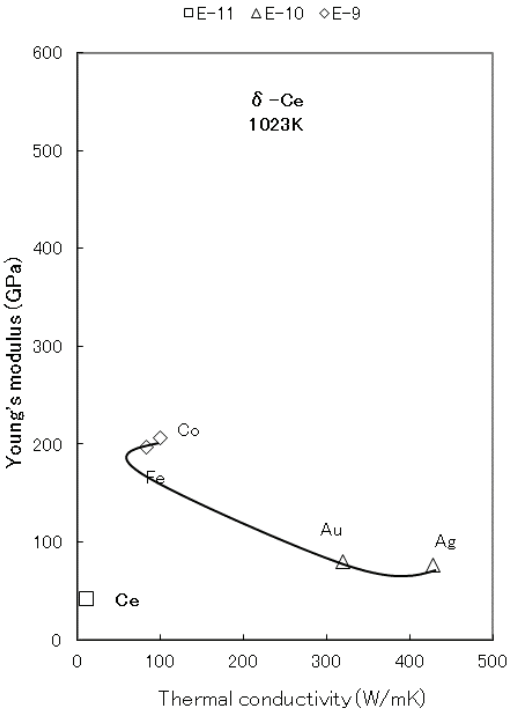

Fig. 10-31 – Distribution of diffusion coefficients of elements at 1023K in δ-Ce on the TC-YM diagram

The elements – Co, Fe, au, and Ag – diffuse fast, but Ce itself diffuses fast in the δ- range, and therefore, they diffuse slightly faster than Ce inδ-Ce.

Fig. 10-32 shows the temperature dependence of the diffusion coefficients of various elements in α-Tl and β-Tl.

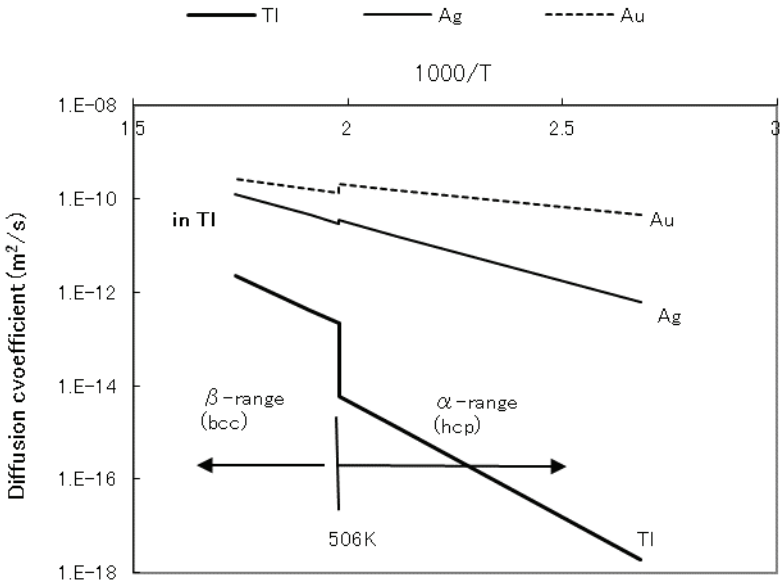

Fig. 10-32 – Temperature dependence of the diffusion coefficients of various elements in α-Tl and β-Tl

The situation is the same as in Ti, Zr, and Ce. Tl atoms diffuse slowly in the α-range due to the large friction between their soft atoms. They diffuse fast in the β-range because they transform to hard atomic shells. But they are still soft because Tl has low thermal conductivity and low Young's modulus, and therefore, Tl atoms diffuse more slowly than foreign atoms, compared to the cases of Ti, Zr, and Ce.

Fig. 10-33 shows the temperature dependence of the diffusion coefficients of various elements in ferromagnetic α-Fe, paramagnetic α-Fe, γ-Fe, and δ-Fe, respectively.

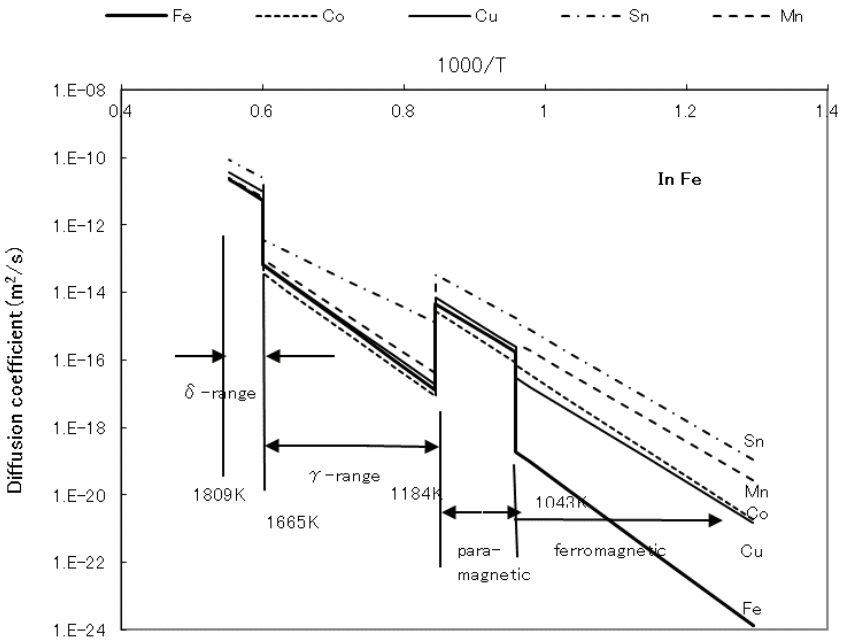

Fig. 10-33 – Temperature dependence of the diffusion coefficients of various elements in ferromagnetic α-Fe, paramagnetic α-Fe, γ-Fe, and δ-Fe, respectively

Fe atoms diffuse slowly in the ferromagnetic α-range. Why do they diffuse slowly in the ferromagnetic α-range? Fe should have hard atoms due to its high Young's modulus and high thermal conductivity. It can be speculated that magnetism gives rise to the affinity between iron atoms and slows down their mobility in the matrix, and therefore, they diffuse slowly in the matrix.

On the other hand, foreign atoms diffuse fast because they have no magnetism. As shown in Fig. 10-18, only iron atoms diffuse slowly.

In the paramagnetic α-range, Fe atoms diffuse as fast as foreign atoms, because they have no magnetism, as shown in Fig. 10-34.

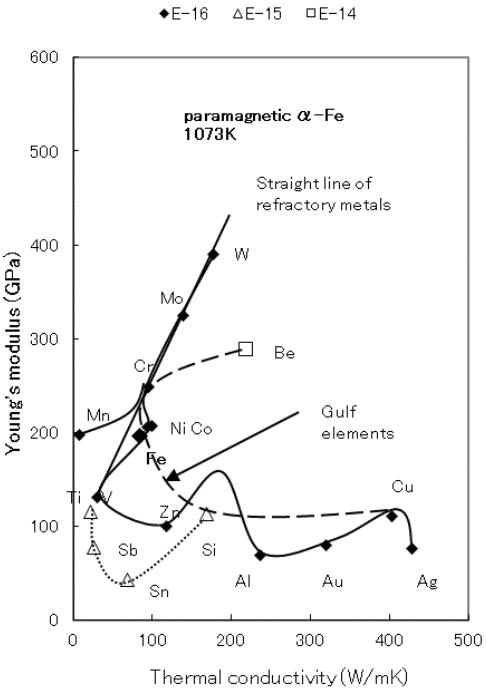

Fig. 10- 34 – Distribution of diffusion coefficients of elements at 1073K in paramagnetic α-Fe on the TC-YM diagram

Fig. 10-35 shows the distribution of diffusion coefficients of elements at 1273K in γ-Fe on the TC-YM diagram.

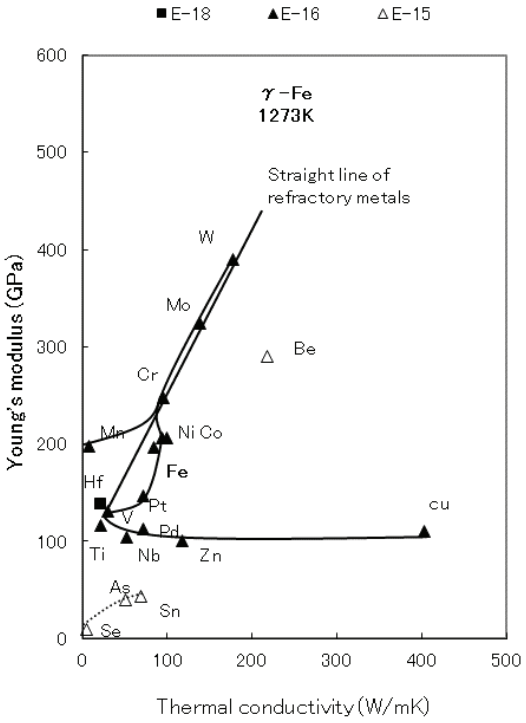

Fig. 10-35 – Distribution of diffusion coefficients of elements at 1273K in γ-Fe on the TC-YM diagram

Fe is located near the center of the diagram, and therefore, it has many elements in the neighborhood. Consequently, Fe has affinity with many elements. Thus, many elements diffuse in γ-Fe similarly to the self-diffusion of Fe. Only the elements far from Fe on the TC-YM diagram such as Be, Sn, As, Se diffuse slightly faster than Fe.

Fig. 10-36 shows the temperature dependence of the diffusion coefficients of various elements in Be.

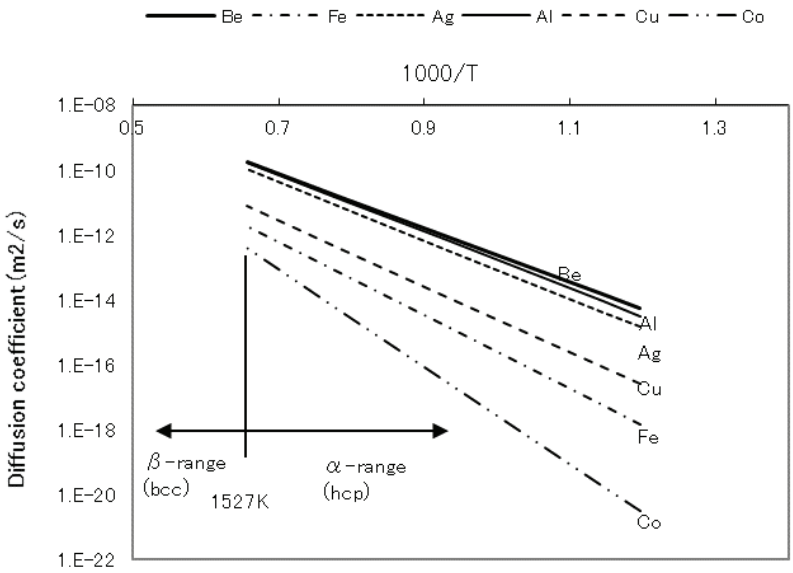

Fig. 10-36 – Temperature dependence of the diffusion coefficients of various elements in Be

As for Be, there are only diffusion data in the α-range. Remarkably, Be diffuses faster in Be than any other elements.

Fig. 10-37 shows the distribution of diffusion coefficients of elements at 1273K in α-Be on the TC-YM diagram.

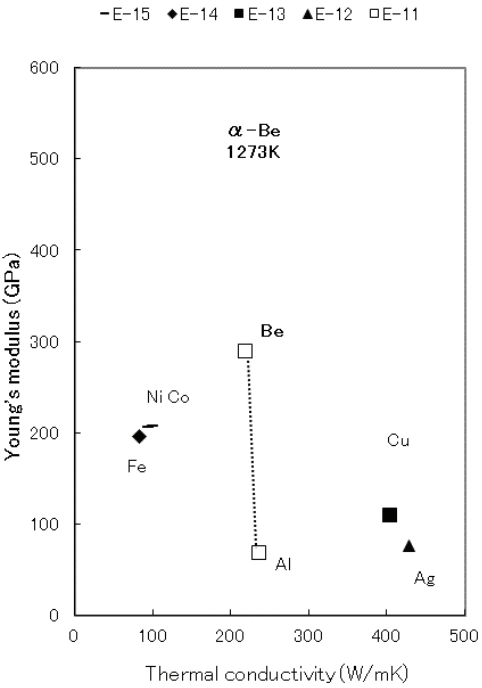

Fig. 10-37 – Distribution of diffusion coefficients of elements at 1273K in γ α-Be on the TC-YM diagram

Be is located at the center of the diagram. It has medium thermal conductivity and medium Young's modulus. Thus, it can be speculated that it has a hard atomic shell already in the α-range. This is the difference between Be and (Ti and Zr). The elements – Fe, Ni, Co, Cu, and Ag – are far from Be on the TC-YM diagram. Consequently, a repulsive force is generated and the atoms of these elements are repelled by the Be atoms of the matrix. Furthermore, the atoms of these elements are also hard because they have large thermal conductivity or high Young's modulus. The atoms

of these elements cannot pass between Be atoms by deforming themselves. As a result, the atoms are repelled by Be atoms, and their diffusions in Be are suppressed. It is referred to as “slow diffusion”, and will be explained in Chapter 11.

In conclusion, the elements in which fast diffusion of foreign metallic elements occurs in the phase of lower temperature are elements of low thermal conductivity and low Young’s modulus. The self -diffusion in these elements is suppressed by the friction between soft atoms. Foreign atoms deform the soft atomic shells of the matrix metal and open a passageway, and diffuse fast.

The atoms of these elements change to hard atoms in the phase at high temperature. Thus, in the phase of higher temperature, fast diffusion doesn’t occur.

The elements which undergo no allotropic transformation such as Nb, Pb, Sn, and In have soft atoms up to the melting temperature.

10.8 Summary

For specific combinations of matrix metals and diffuser elements, fast diffusion phenomena involve some diffuser elements diffusing faster than the self-diffusion of the matrix metals, typically showing a diffusion coefficient more than three orders of magnitude as large as that of self-diffusion.

Good matrix metals are mainly those elements with low thermal conductivity and low Young's modulus. A few examples include Ti, Zr, Nb, Sn, Ce, Pb, Tl, and In.

Good diffuser elements are mainly gulf elements, which have the largest combination of thermal conductivity and Young's modulus. A few examples include Fe, Ni, Co, Cr, and Cu.

For fast diffusion to occur there should be a large difference between the matrix metal and the diffuser elements in terms of electron mobility and the binding force between atoms.

If this difference is large, a repulsive force operates between the matrix atoms and the diffuser atoms; thus, matrix atoms which have a soft and large outer electron shell are deformed and provide passages for diffusion of the diffuser atoms, which have hard and small outer electron shells.

Conversely, when the matrix metal is an element with a hard and small outer electron shell, and the diffuser element is an element with a soft and large outer electron shell, the diffuser atom is deformed and passes through the matrix atoms rapidly. This causes the inverse atomic radius dependence where elements with a larger atomic radius diffuse faster than those with a smaller atomic radius.

The elements – Ti, Zr, Ce, and Tl – which have low thermal conductivity and low Young's modulus have soft atoms. They change to hard atoms by allotropic transformation. Consequently, they show fast diffusion of foreign elements in the phase of low temperature, but not in the phase of high temperature.

This author rewrote Ref. 14 for this chapter.

References

1. H. Nakajima, Materia, 1983, vol. 22, pp. 480-487.
2. W. C. Roberts-Austen, Proc. Roy. Sic., 1896, Vol. 59, pp. 281-285.
3. M. Koiwa, Materia, 1998, vol. 37, pp. 347-355.
4. Japan Institute of Metals, Metals Data Book, 4th ed., Maruzen, Tokyo, 2004,
pp. 20-25.
5. G. M. Hood, Phys. Rev. B. 1981, vol. 23, p. 4253.
6. M. Koiwa, Materia, 2006, vol. 45, pp. 341-346.
7. H. Nakajima and M. Koiwa, Materia, 1991, vol. 30, pp. 526-535.
8. Y. Yoshida, Materia, 1989, vol. 28, pp. 610-616.
9. Th. Heumann, Diffusion in Metallen, Springer, Berlin, 1992, pp. 157-159.
10. K. Kusunoki, K. Tsumuraya and S. Nishikawa, Trans. Jap. Inst. Met., 1981, vol. 22, No. 7, pp. 501-513.
11. T. R. Anthony, Vacancies and Interstitials in Metals, ed. by Seeger et al., North-Holland Publ., Amsterdam, 1970, p. 939.
12. Y. Mae, Metall. Mater. Trans. A. 2016, vol. 47, pp. 6498-6506.
13. Chr. Herzig, DIMETA-82 Diffusion in Metals and Alloys, Trans Tech publications, Switzerland, 1983, pp. 23-38.
14. Y. Mae, Metall. Mater. Trans. A, vol. 49A, April, 2018, pp. 1336-1347.

11. SLOW AND NORMAL DIFFUSIONS OF ELEMENTS IN METALS

In contrast to the elements that show fast diffusion of foreign elements, certain elements feature considerably suppressed diffusivity. This effect is referred to as “slow diffusion,” and defined here as a diffusion coefficient of the diffuser elements more than three orders of magnitude smaller (i.e., 1/1000) than the self-diffusion of the matrix element.

Elements for which slow diffusion occurs include Li, Ca, Mg, Al, and Be.

Another diffusion behavior is referred to as “normal diffusion,” when the diffusion coefficients of elements in a specific matrix metal are different from the self-diffusion of the matrix but within three orders of magnitude, smaller or larger than the self-diffusion.

In conclusion, the mechanisms of slow diffusion and normal diffusion are explained as follows:

The difference in thermal conductivity, i.e., in the electron mobility, generates a repulsive force between the matrix atoms and the diffuser atoms. When the repulsive force is large enough to deform the soft atoms of the matrix metal, the diffuser atoms pass through the lattice of the matrix metal and fast diffusion occurs.

When the difference in thermal conductivity is medium, and the resulting repulsive force is not large enough to deform the atoms of the matrix metal, the diffuser atoms undergo only the repulsive force, consequently, diffusion of the diffuser atoms is suppressed and slow diffusion occurs.

Normal diffusion consists of minor forms of fast diffusion and slow diffusion (small fast diffusion and small slow diffusion).

11.1 Distribution of diffusion coefficients of elements on the TC-YM diagram in the case of slow diffusion

The atomic radius dependences of the diffusion coefficients of elements in the case of slow diffusion have already been discussed in Section 10. 2. Therefore, their distribution on the TC-YM diagram will be discussed here.

Fig. 11-1 shows the distribution of the diffusion coefficients of elements at 423K (150°C) in Li on the TC-YM diagram.

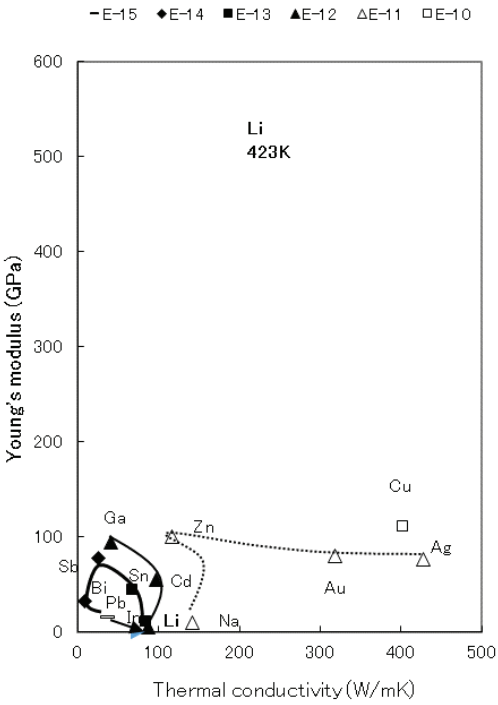

Fig. 11-1 – Distribution of the diffusion coefficients of elements at 423K (150°C) in Li on the TC-YM diagram

"E-15" in the legend indicates that, for example, the particular elements have diffusion coefficients with a magnitude of 10^{-15} m^2/s. Li shows a diffusion coefficient with a magnitude of 10^{-12} m^2/s.

Li is located at the position of medium thermal conductivity and very low Young's modulus. The elements that diffuse faster than Li are located on the right side of the diagram. The elements with equivalent diffusion coefficients to Li such as Cd and Ga are located near Li. The elements that

diffuse much slower than Li are located on the left side of Li. Pb that is included in the “slow diffusion” is located just on the left side of Li. The arrow shows the direction and distance from the diffuser element to the matrix element in the case of slow diffusion.

As a whole, the atoms of elements with larger thermal conductivity than Li deform the atoms of Li and pass through the lattice and diffuse fast.

In contrast, the atoms of elements with smaller thermal conductivity than Li cannot deform the atoms of Li, and undergo only repulsive force, and diffuse slowly.

Fig. 11-2 shows the distribution of the diffusion coefficients of elements at 773K (500°C) in Mg on the TC-YM diagram.

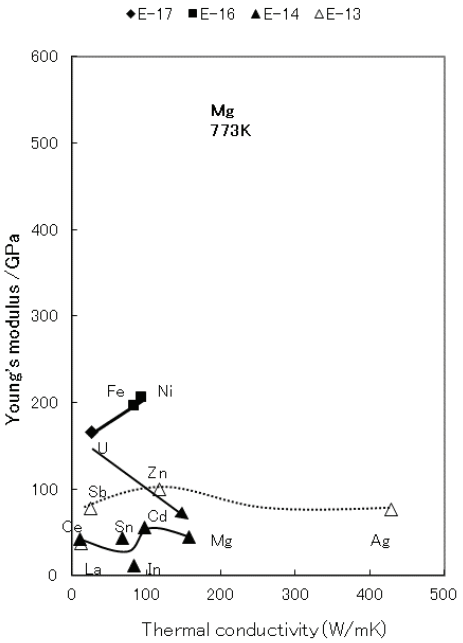

Fig. 11-2 – Distribution of the diffusion coefficients of elements at 773K (500°C) in Mg on the TC-YM diagram

Mg is located at the position of medium thermal conductivity and small Young's modulus. The elements on the left side of Mg diffuse at the same speed as the self-diffusion of Mg. The elements of slightly higher Young's modulus – Sb, Zn, and Ag – diffuse slightly faster than the self-diffusion of Mg. The elements of higher Young's modulus – U, Fe, and Ni – diffuse very slowly in Mg. U of much smaller thermal conductivity is categorized as slow diffusion.

As a whole, the repulsive force by the elements in the neighborhood is small, and therefore, they diffuse at similar speed. The elements with higher Young's modulus generate large repulsive force, but cannot deform Mg atoms. They undergo only the repulsive force and diffuse slowly.

Fig. 11-3 shows the distribution of the diffusion coefficients of elements at 773K (500°C) in Al on the TC-YM diagram.

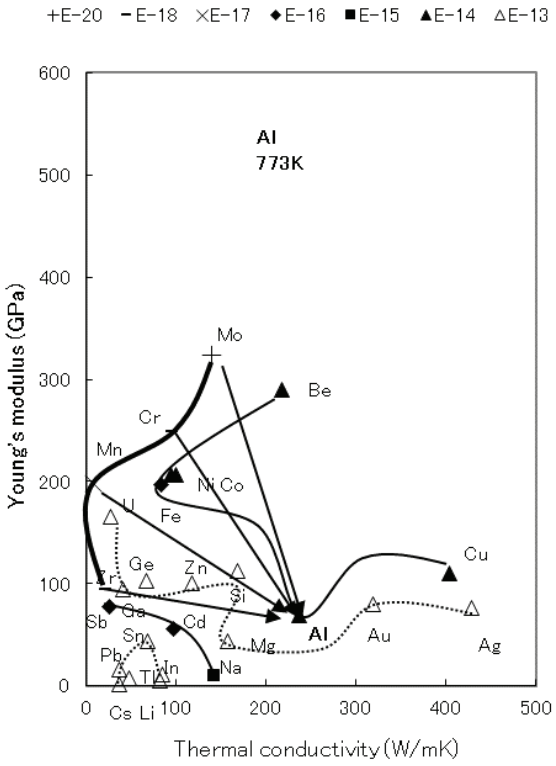

Fig. 11-3 – Distribution of the diffusion coefficients of elements at 773K (500°C) in Al on the TC-YM diagram

Al is located at medium thermal conductivity and medium Young's modulus. The gulf elements – Cu, Fe, Ni, Co, and Be – diffuse at the same speed as Al. The elements at the lower side of Al diffuse slightly faster than Al. The elements far from Al such as Zr, Mn, Cr, and Mo diffuse very slowly. They are categorized as slow diffusion.

Totally, the repulsive force generated by the elements in the neighborhood is small, therefore, they diffuse at similar speeds. The elements far away from Al generate large repulsive force, but cannot deform Al atoms. They undergo only the repulsive force and diffuse slowly.

Though not shown in the figures, Ca and α-Be also showed a similar tendency to Al as the matrix metals.

From the above, it is concluded that the matrix elements for slow diffusion are those of medium thermal conductivity, and the diffuser elements are those of smaller thermal conductivity.

11.2 Distribution of diffusion coefficients of elements on the TC-YM diagram in the case of normal diffusion

The atomic radius dependences of the diffusion coefficients of elements in the case of normal diffusion have already been discussed in Section 10. 3, and therefore, their distributions on the TC-YM diagram will be discussed here.

Fig. 11-4 shows the distribution of the diffusion coefficients of elements at 1023K (750°C) in Cu on the TC-YM diagram.

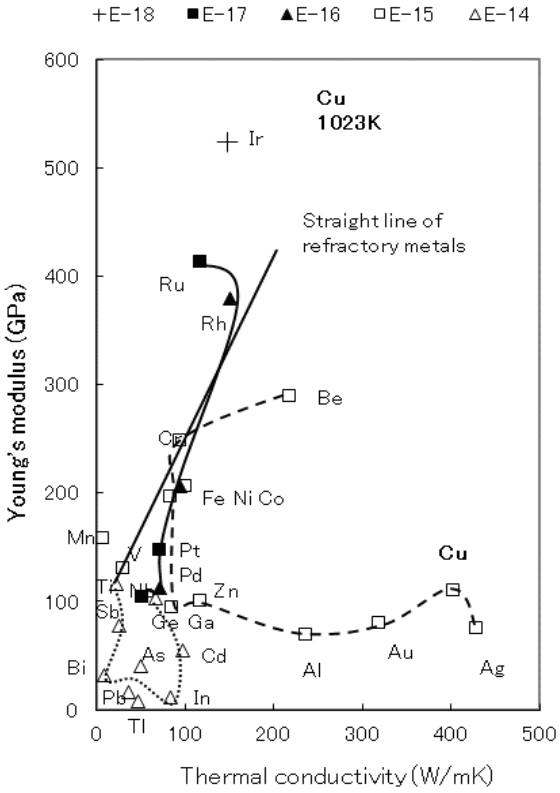

Fig. 11-4 – Distribution of the diffusion coefficients of elements at 1023K (750℃) in Cu on the TC-YM diagram

The self-diffusion of Cu adopts the medium value and the gulf elements including Cu show equivalent diffusion coefficients to Cu.

The elements near Cu – Ag, Au, Al, Zn, Ga, Fe, Co, Cr, and Be – diffuse equivalently to Cu.

The large difference in thermal conductivity between the elements of low

thermal conductivity – Ge, Cd, In, As, Tl, Pb, Bi, Sb, and Ti – and Cu generates a large repulsive force, and consequently, their atoms are deformed by Cu atoms and pass through the lattice of Cu. It gives rise to their small fast diffusion. In addition, they are located in the region of larger atomic diameter than Cu. Consequently, they show inverse atomic radius dependence which means that larger atoms diffuse faster than small atoms, as shown in Fig. 10-12.

The elements in the medium distance from Cu – Pd, Ni, and Rh– undergo repulsive force and diffuse slowly. The elements in the farthest distance from Cu – Nb, Pt, Ru, and Ir – undergo larger repulsive force and diffuse more slowly. But as a whole, the repulsive force is weak, and therefore, these elements show small slow diffusion. As a result, Cu shows normal diffusion.

Fig. 11-5 shows the distribution of the diffusion coefficients of elements at 1223K (950°C) in γ-Fe on the TC-YM diagram.

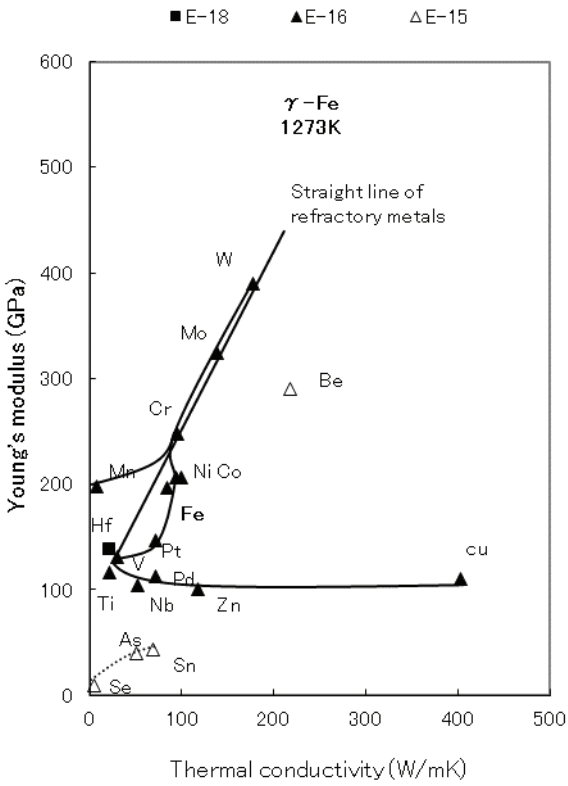

Fig. 11-5 – Distribution of the diffusion coefficients of elements at 1223K (950°C) in γ-Fe on the TC-YM diagram

As Fe is located at the center of the element group, the difference between Fe and other elements in thermal conductivity and Young's modulus is small, and the repulsive force is small. Consequently, most elements show very similar diffusion coefficients to that of the self-diffusion of γ-Fe. Only Be and the elements of very low Young's modulus and thermal conductivity – Se, As, and Sn – show slightly larger diffusion coefficients.

As a whole, the repulsive force is weak, and therefore, foreign elements diffuse moderately in γ-Fe.

Though not shown in the figures, the elements adjacent to Fe – Ni and Co – show very similar trends.

Fig. 11-6 shows the distribution of the diffusion coefficients of elements at 623K (350°C) in Zn on the TC-YM diagram.

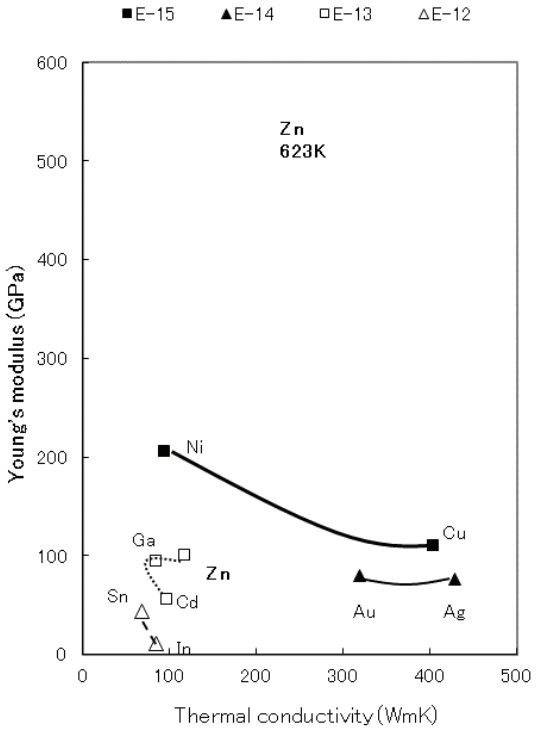

Fig. 11-6 – Distribution of the diffusion coefficients of elements at 623K (350°C) in Zn on the TC-YM diagram

The elements in the nearest neighborhood – Ga and Cd – show very similar diffusion coefficients to Zn. The elements with lower Young's modulus and thermal conductivity such as Sn and In diffuse faster than Zn, because a small repulsive force is generated and their atoms are deformed a little and pass through the lattice of Zn. The elements with higher Young's modulus and thermal conductivity – Au, Ag, Ni, and Cu – diffuse slowly, because the repulsive force is generated, but not large enough to deform atoms of both the matrix and the diffuser, and therefore, the diffuser atoms undergo only the repulsive force, and diffuse slower.

As a whole, the repulsive force is small, because Zn is located near the center of the diagram, and consequently, normal diffusion occurs in Zn.

Here, let's compare Zn in Fig. 11-6 with Pb in Fig. 10-23 and Sn in Fig. 10-22. The elements – Ni and Cu – which diffuse fast in Pb and Sn diffuse slowly in Zn. The difference between the matrix metal and (Ni and Cu) in thermal conductivity and Young's modulus decreases as the matrix metal changes from Pb via Sn to Zn. With the decreasing difference in thermal conductivity and Young's modulus, the repulsive force decreases and the hardness of the electron shell of the matrix elements increases. Consequently, fast diffusion of Ni and Cu occurs in Pb and Sn, and slow diffusion of Ni and Cu occurs in Zn.

Furthermore, Ni diffuses slowly in Mg with larger thermal conductivity as shown in Fig. 11-2. But in Al with much larger thermal conductivity, Ni and Cu diffuse at a similar speed to Al as shown in Fig. 11-3, because the differences between Al and (Cu, and Ni) in thermal conductivity and Young's modulus become small. This is a good sample of this theory.

Fig. 11-7 shows the distribution of the diffusion coefficients of elements at 1273K (1000°C) in β-Ti on the TC-YM diagram.

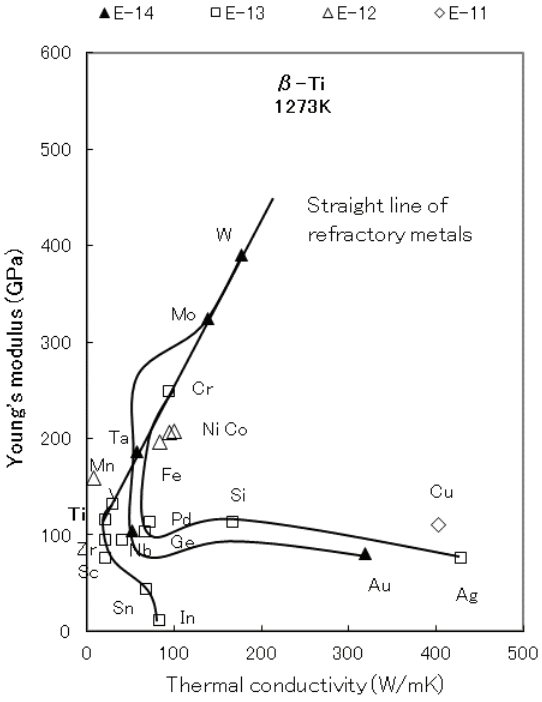

Fig. 11-7– Distribution of the diffusion coefficients of elements at 1273K (1000°C) in β-Ti on the TC-YM diagram

Ti is located at the position of very low thermal conductivity and medium Young's modulus. The elements with lower Young's modulus than Ti diffuse at a similar speed to β-Ti. The elements with higher Young's modulus diffuse faster, because the repulsive force is large and deforms the atoms of β-Ti and pass through the lattice of β-Ti.

The elements on the right side of Ti – Au, Nb, Ta, Mo, and W – generate repulsive force but not large enough to deform the atoms of β-Ti, and consequently, diffuse the slowest.

As a whole, the repulsive force is small and the atoms of β-Ti are hard, and therefore, normal diffusion occurs in β-Ti.

As shown in Fig. 10-16, normal diffusion occurs in the elements which are located at the place between the elements of fast diffusion and those of slow diffusion, and at the right-most side of the diagram.

11.3 Distribution of diffuser elements and matrix elements in fast and slow diffusion

As mentioned above, the type of diffusion of a single element in a single matrix metal is determined by the positions of both elements on the TC-YM diagram. As the differences in thermal conductivity, and/or in Young's modulus increase, the repulsive force between both elements increases.

(1) Fast diffusion

When the repulsive force is large enough to deform the matrix atoms, the passageways are opened and the diffuser atoms diffuse fast. This is fast diffusion.

In fast diffusion, a large difference in thermal conductivity is needed, and the matrix atoms must be soft. Therefore, the diffuser elements tend to be those of high thermal conductivity and/or high Young's modulus. Specifically, the diffuser elements tend to be Fe, Ni, Co, Cr, Mn, Cu, Ag, Au, and Zn.

On the other hand, the matrix elements tend to be elements of low thermal conductivity and low Young's modulus. Specifically, they are γ-Ce, In, La, Pb, Sn, Nb, α-Tl, α-Ti, α-Zr, and W.

Fig. 11-8 shows the distribution of diffuser elements and matrix metals in fast diffusion displayed on the TC-YM diagram.

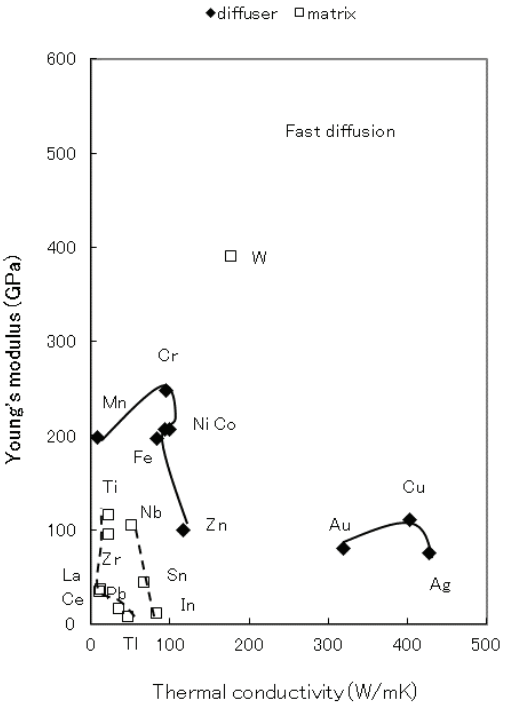

Fig. 11-8 – Distribution of diffuser elements and matrix metals in fast diffusion displayed on the TC-YM diagram

The matrix elements are located in the low Young's modulus and low thermal conductivity region in order to satisfy the condition of a large

difference in thermal conductivity and Young's modulus, and another condition that they must be soft atoms to be deformable.

The diffuser elements are located on the high thermal conductivity side and/or high Young's modulus side. Most of them are gulf elements. Gulf elements with a combination of high thermal conductivity and high Young's modulus include Cu, Fe, Ni, Co, and Cr. The other diffuser elements also are located near the gulf elements.

(2) Slow diffusion

When the repulsive force is not large enough to deform the atoms, or when the atoms are too hard to be deformed, the repulsive force cannot open passageways for the diffuser elements. Under these circumstances, the diffuser atoms undergo the repulsive force only. As a result, the diffusion of the diffuser elements is suppressed, leading to the slow diffusion of the diffuser elements.

Therefore, the conditions for slow diffusion are the medium difference in thermal conductivity and Young's modulus. Specifically, the matrix elements tend to be Be, Al, Mg, Ca, and Li. The diffuser elements tend to be Mo, Cr, Fe, Ni, Co, U, Zr, and Pb.

Fig. 11-9 shows the distribution of diffuser elements and matrix metals in slow diffusion shown on the TC-YM diagram.

The matrix elements are located at the position of medium thermal conductivity, so they have medium distances from everywhere in the

diagram. Specifically, they are Be, Al, Mg, Ca, and Li.

The diffuser elements are located at the position of low thermal conductivity. Specifically, they are Mo, Cr, Ni, Co, Fe, U, Zr, and Pb.

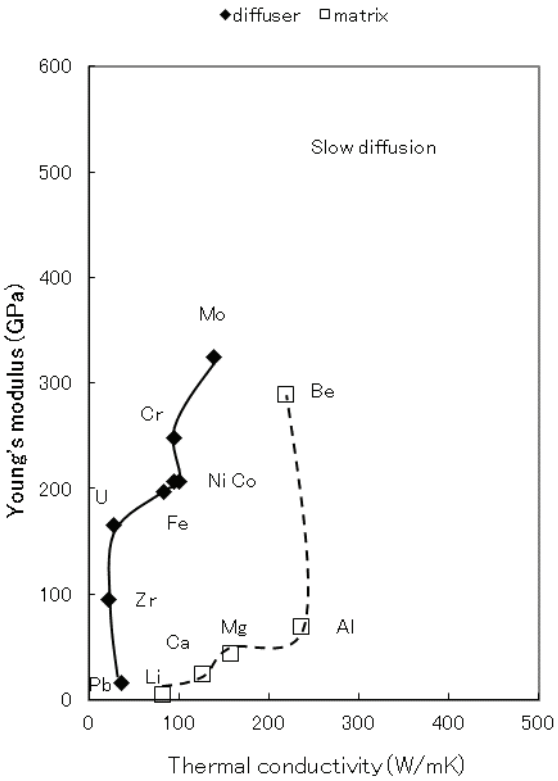

Fig. 11-9 – Distribution of diffuser elements and matrix metals in slow diffusion on the TC-YM diagram.

(3) Displays by arrows in fast and slow diffusion

Each combination of the diffuser element and the matrix element in fast diffusion and slow diffusion is shown in Tables 11-1 and 11-2, respectively.

Table 11-1 Combination of the matrix elements and diffuser elements in fast diffusion

Matrix element	Diffuser element
γ-Ce	Fe, Co
In	Au
La	Au
Nb	Ni
Pb	Cu, Au, Ni, Zn
Sn	Cu
α-Ti	Co, Fe, Ni, Mn, Cr, Cu
α-Tl	Au, Ag
W	Fe, Co
α-Zr	Cu, Cr, Mn

Table 11-2 Combination of the matrix elements and diffuser elements in slow diffusion

Matrix element	Diffuser element
Be	Co, Ni
Ca	U, Ni, Fe
Li	Pb
Mg	U
Al	Mo, Cr, Zr

Figs. 11-10 and 11-11 show the relationship between the diffuser element and the matrix element of each diffusion couple in which fast diffusion and slow diffusion occur, respectively, displayed on the TC-YM diagram.

The root of the arrow is the diffuser element, and the tip is the matrix metal. Each arrow can be considered to be a vector. In fast diffusion, arrows are long, and face to the left or downward except for the W-Fe and W-Co couples. In slow diffusion, arrows are medium, and face to the right and downward except for the Be-Co and Be-Ni couples.

It is noted that the arrows are long in fast diffusion and medium in slow diffusion, respectively.

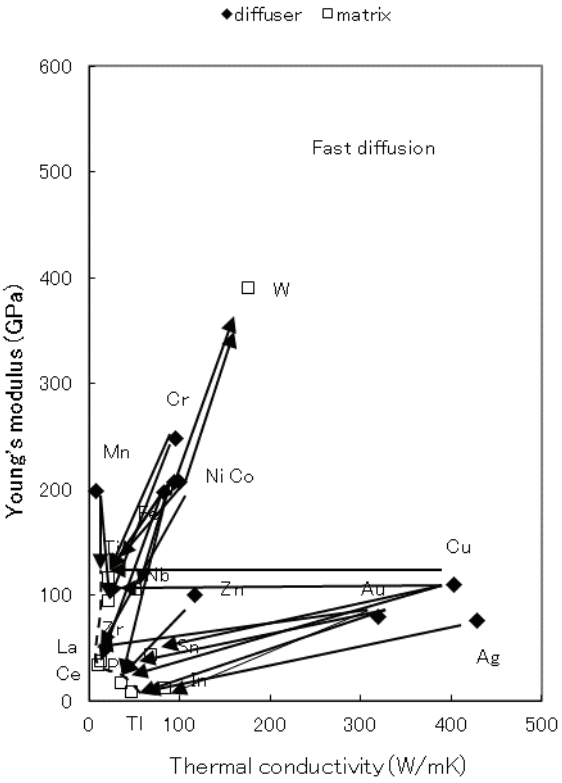

Fig. 11-10 – Relationship between the diffuser element and the matrix element of each diffusion couple in which fast diffusion occurs, displayed on the TC-YM diagram

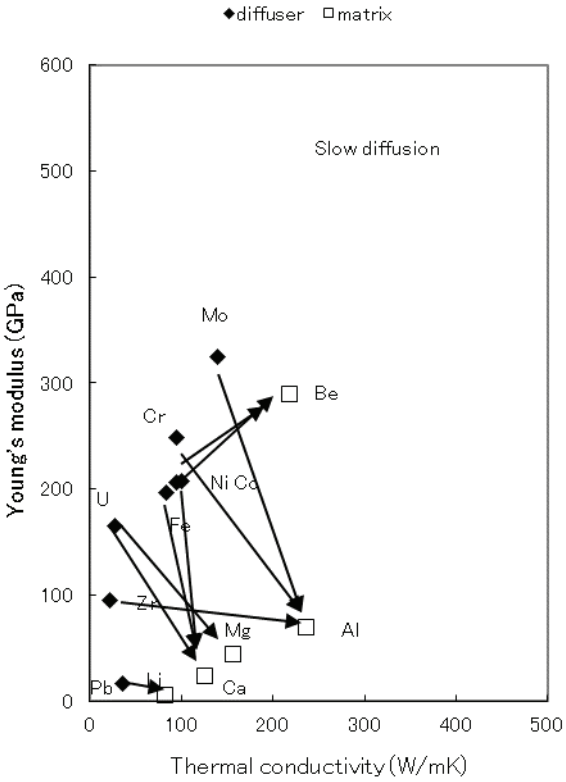

Fig. 11-11 – Relationship between the diffuser element and the matrix element of each diffusion couple in which slow diffusion occurs, displayed on the TC-YM diagram

Figs. 10-12, 13, and 14 show the schematics of the diffusion mechanism in fast, slow, and normal diffusion, respectively.

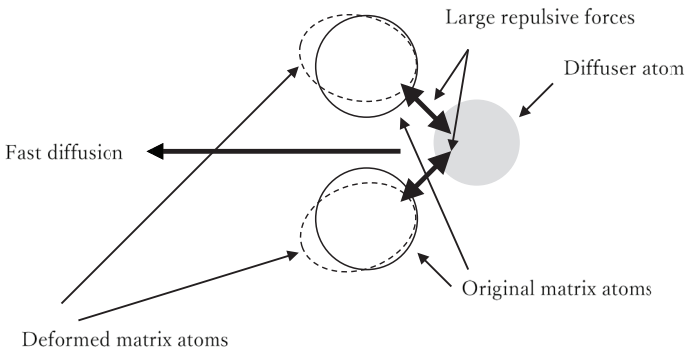

Fig. 11-12 – Schematics of the matrix atoms and diffuser atoms in fast diffusion

In fast diffusion, the repulsive force is large and the atoms of the matrix metal are soft. The repulsive force deforms the atoms of the matrix metals and opens the passageway for the diffuser atoms. Consequently, the diffuser atoms pass through the matrix atoms easily.

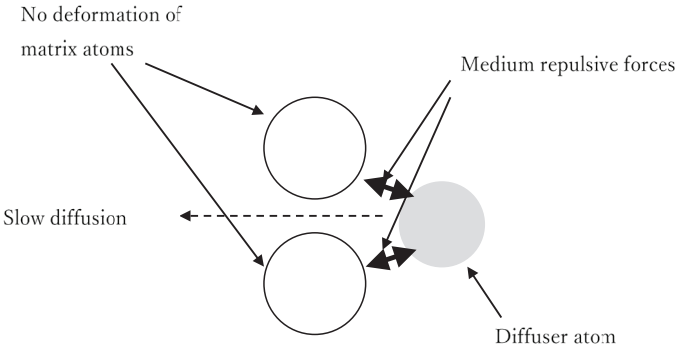

Fig. 11-13 – Schematics of matrix atoms and diffuser atoms in slow diffusion

In slow diffusion, the repulsive force is medium, and not large enough to deform the atoms of the matrix metal. The diffuser atoms undergo the repulsive force, and their movement is blocked. The diffuser atoms pass through the matrix metal very slowly.

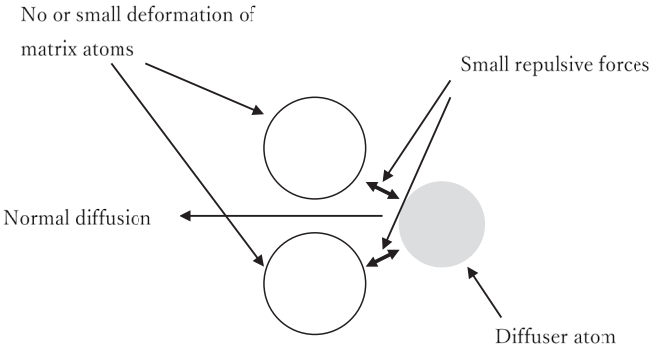

Fig. 11-14 – Schematics of matrix atoms and diffuser atoms in normal diffusion

In normal diffusion, the repulsive force is small. When the atoms of the matrix metal are deformed a little, small fast diffusion occurs. When the atoms of the matrix metal are not deformed, small slow diffusion occurs.

11.4 Atomic radius dependence of the diffusion coefficients of elements

As shown in Fig. 10-2, with decreasing atomic radius of the diffuser elements, the diffusion coefficient of diffuser elements in Pb increases. This is a positive atomic radius dependence of diffusion coefficients of the diffuser elements. These are observed in the elements of low thermal conductivity such as Pb, α-Ti, α-Zr, and Li. The reasons for them can be explained on the TC-YM diagram, as shown in Fig. 10-23. The elements with large thermal conductivity and Young's modulus diffuse fast in Pb. Those elements are located in the region of small atomic radius on the TC-

YM diagram. Therefore, the positive atomic radius dependence of diffusion coefficients of elements is a coincidence.

As shown in Fig. 10-13, with increasing atomic radius of diffuser elements, the diffusion coefficients in γ-Fe increase. This is an inverse atomic radius dependence.

As shown in Fig. 10-14, with the increasing atomic radius of diffuser elements, the diffusion coefficients in Zn increase. This is also an inverse atomic radius dependence. These are observed in the elements of medium thermal conductivity – Ca, Cd, Zn, paramagnetic α-Fe, γ-Fe, and Cr. The reasons for them can be explained on the TC-YM diagram, as shown in Figs. 11-5 and 11-6, respectively. In Zn, the elements with larger thermal conductivity than Zn – Ni, Cu, Au, and Ag – diffuse slowly due to the repulsive force. They are located in the region of small atomic radius. The elements with low thermal conductivity – Sn and In – diffuse fast due to the deformation of diffuser atoms. They are located in the region of large atomic radius. Consequently, an inverse atomic radius occurs.

In conclusion, the atomic radius dependence of diffusion coefficients is random. Diffusion coefficients of elements have no relationship with their atomic radii.

11.5 Summary

The changes of the distribution of diffusion coefficients of Ni and Cu in the matrix metal varying from Pb through Sn, Mg, Zn, and Al to Cu show the good example of both fast diffusion and slow diffusion.

Fig. 11-15 shows the change of the distribution of diffusion coefficients of elements in the matrix metal varying from Pb through Sn, Mg, Zn, and Al to Cu. The thermal conductivity and Young's modulus increase from Pb through Sn, Mg, Zn, and Al to Cu. In contrast to this, Ni and Cu have high Young's modulus or high thermal conductivity.

Ni and Cu show fast diffusion in the farthest elements such as Pb and Sn.

Ni and Cu show slow diffusion in the nearer elements such as Mg and Zn.

Ni and Cu show normal diffusion in the nearest elements such as Al and Cu.

The diffusion coefficients of diffuser elements are determined by the distance from the matrix metal and the hardness of the outer electron shell of the matrix metal.

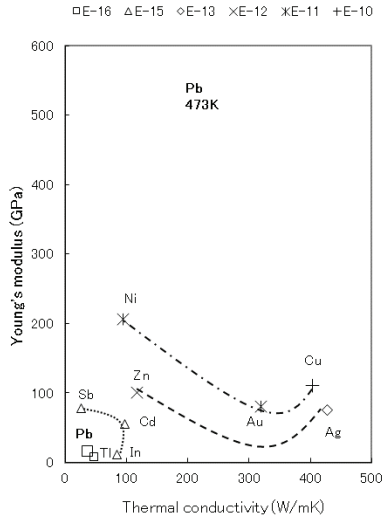

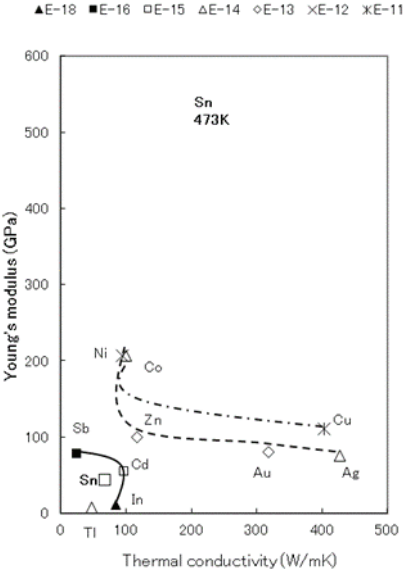

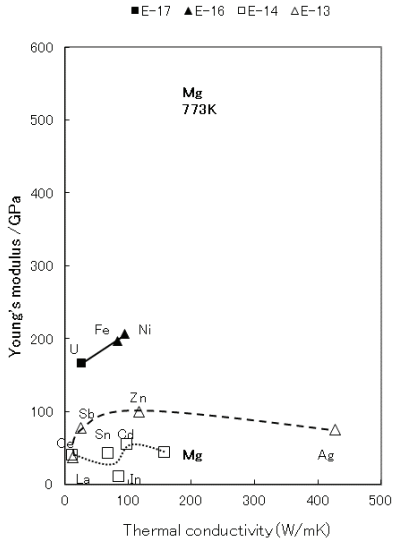

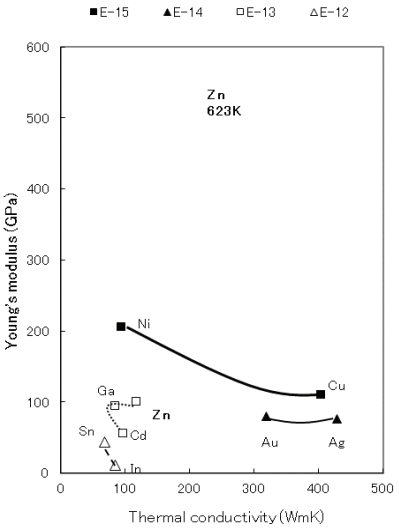

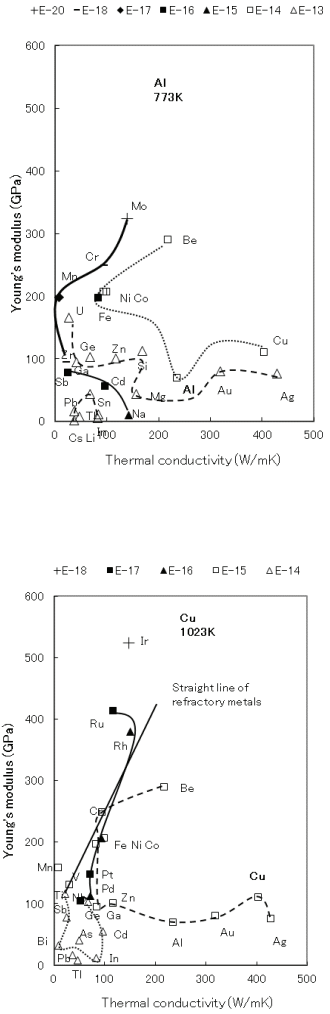

Fig. 11-15 – The change of the distribution of diffusion coefficients of elements, especially of Ni and Cu, in the matrix metal varying from Pb through Sn, Mg, Zn, and Al to Cu

(1) Fast diffusion

The difference in thermal conductivity and in Young's modulus generates the repulsive force between the diffuser element and the matrix elements. When the repulsive force is large, the hard atoms of the diffuser element deform the soft atoms of the matrix elements, open the passageways, and diffuse fast.

Therefore, in fast diffusion, the matrix metals tend to be the elements with low Young's modulus and low thermal conductivity, and the diffuser elements tend to be the gulf elements and near gulf elements possessing a combination of the largest thermal conductivity and largest Young's modulus. This coincides well with the data.

(2) Slow diffusion

When the difference in thermal conductivity or in Young's modulus is medium, the repulsive force is not large enough to deform the atoms of the matrix metal. Furthermore, as the atoms of the matrix metals are hard due to relatively high thermal conductivity and high Young's modulus, the diffuser atoms cannot deform the matrix metals, but only undergo the repulsive force. In this situation, the diffusion of the diffuser element is strongly suppressed. This is slow diffusion.

Consequently, in slow diffusion, the matrix elements tend to be the elements of medium thermal conductivity, and the diffuser elements tend to be the elements of low thermal conductivity. This also coincides well with the data.

(3) Normal diffusion

The repulsive force does not act between the elements near to each other on the TC-YM diagram. In this case, normal diffusion similar to self-diffusion occurs. Normal diffusion is small fast diffusion or small slow diffusion.

In this way, all the diffusion phenomena can be explained by the same logic. This author rewrote his paper [2] for this chapter.

References

1. M. Koiwa: Materia, 1998, Vol. 37, pp. 347-355.
2. Y. Mae, Characteristics of matrix metals in which fast diffusion of foreign metallic elements occurs, Met. Mater. Trans. A Vol. 49A, April 2018, pp. 1336-1347.

12. SOLUTION HARDENING OF METALS

It has long been thought that solution hardening is brought about by differences in atomic radii between solute atoms and matrix atoms. Nevertheless, this rule is not valid in many cases.

When the alloying elements are dissolved into metals, the metals are hardened. This is called the solution hardening of metals. The mechanism of solution hardening has long been studied. One hypothesis is that the degree of hardening is inverse-proportional to the solubility of the alloying elements in the matrix metals (Rosenhain, Solubility hypothesis). [1] An alternative explanation is that the degree of hardening is determined by the degree of lattice distortion caused by the difference of the atomic radius between the solute atoms and the matrix atoms (Incoherence hypothesis). [1-5]

Fig. 13-1 shows the distortion of lattices by the impurity atoms. [5]

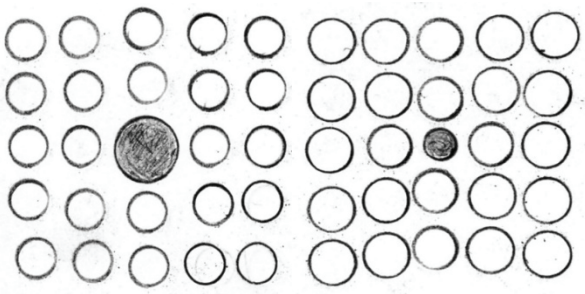

Fig. 12-1 – Lattice distortion by inserting a larger atom (left) and a smaller atom (right)

The latter is the current major rule. However, this rule is not valid in many cases.

In Chapters 11 and 12, the diffusion mechanism of the foreign elements was discussed. The diffusion mechanism may also have a relationship with solution hardening.

Therefore, the relationship between the solution hardening of metals by the alloying elements and the atomic radius, solubility, and diffusivity of the alloying elements is discussed here.

12.1 Correlation of solution hardening to atomic size, solubility of the alloying elements, and diffusivity of the alloying elements

The two existing hypotheses of the atomic size difference and the solubility of the alloying elements in the matrix metals as well as the diffusivity of the alloying elements were studied for most metals as below.

(1) Cu

Cu has been adopted frequently as an example for the explanation of solution hardening.

Fig. 12-2 shows typical data for the solution hardening of Cu by alloying elements. [6] The increment of the yield strength at 1 mol% alloying content was adopted as the index of solution hardening of each element.

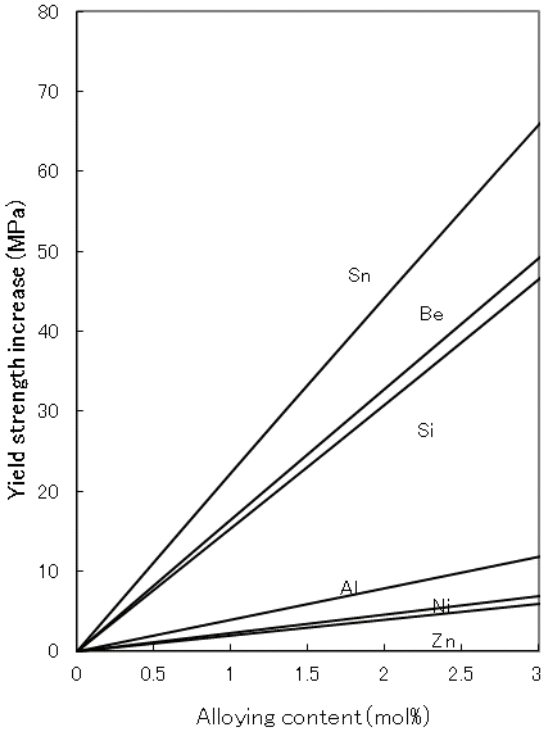

Fig. 12-2 – Yield strength increase of Cu as a parameter of the alloying content of elements

Fig. 12-3 shows the relationship between the yield strength increase (MPa/mol%) of Cu by alloying elements and the atomic radii of alloying elements.

A relatively good correlation can be seen. This may be the reason why Cu has been cited often to validate the atomic size incoherence hypothesis.

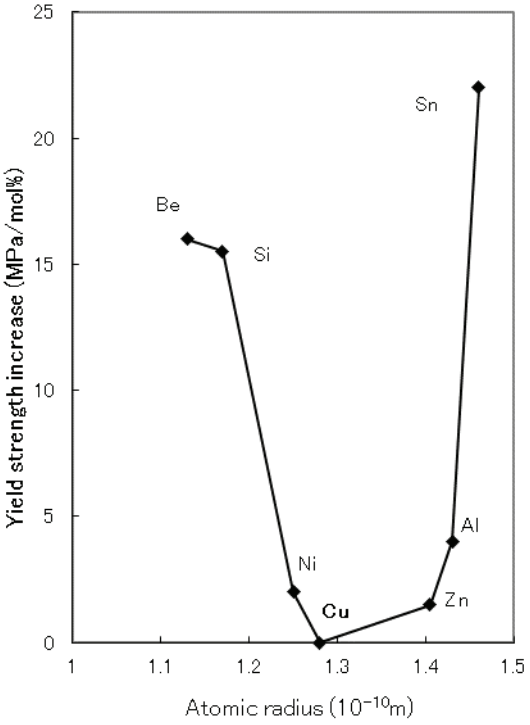

Fig. 12-3 – Relationship between the yield strength increase (MPa/mol%) of Cu by alloying elements and atomic radii of alloying elements

Fig. 12-4 shows the relationship between the yield strength increase (MPa/mol%) of Cu by alloying elements and the solubility of solute atoms. The solubility of elements varies with temperature; therefore, the maximum solubility at high temperature was adopted as the solubility. All of the elements – Sn, Be, Si, Al, Ni, and Zn – lie on a curve. It seems that the abandoned solubility hypothesis is valid still.

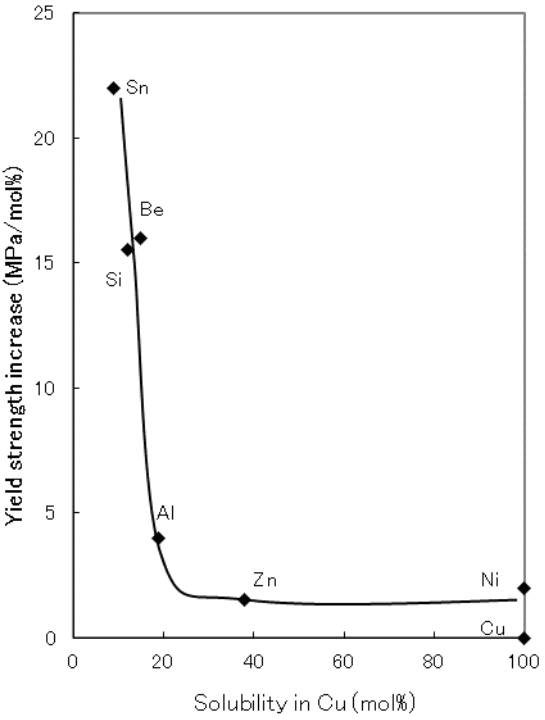

Fig. 12-4 – Relationship between the yield strength increase (MPa/mol%) of Cu by alloying elements and the solubility of alloying elements

Previously, this author coincidentally discovered the correlation between

the solution hardening of Fe by the alloying elements and the diffusion coefficients of the alloying elements in Fe, by comparing the distribution of the yield strength increase of Fe and that of the diffusion coefficients of the alloying elements in Fe, displayed on the TC-YM diagram.

Therefore, correlation with diffusion coefficients will be tested in every alloy system hereafter.

Fig. 12-5 shows the correlation of the yield strength of Cu to the diffusion coefficients of the alloying elements in Cu at 1273K.

Data points are very few. It is difficult to judge whether the correlation is valid.

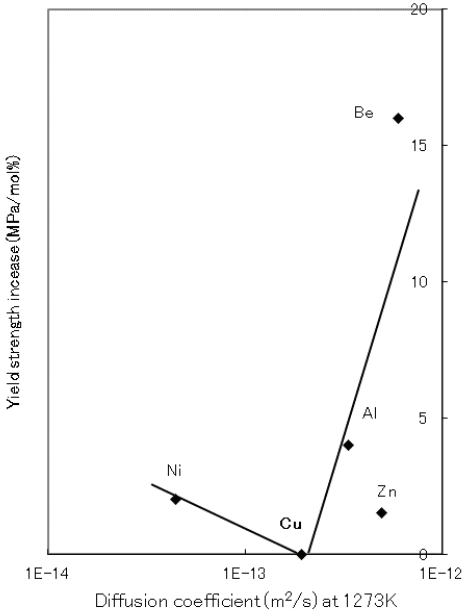

Fig. 12-5 – Yield strength increase of Cu as a parameter of the diffusion coefficients of alloying elements in Cu at 1273K

(2) Fe

Fig. 12-6 shows classical data for the solution hardening of ferrite steel by alloying elements. [7]

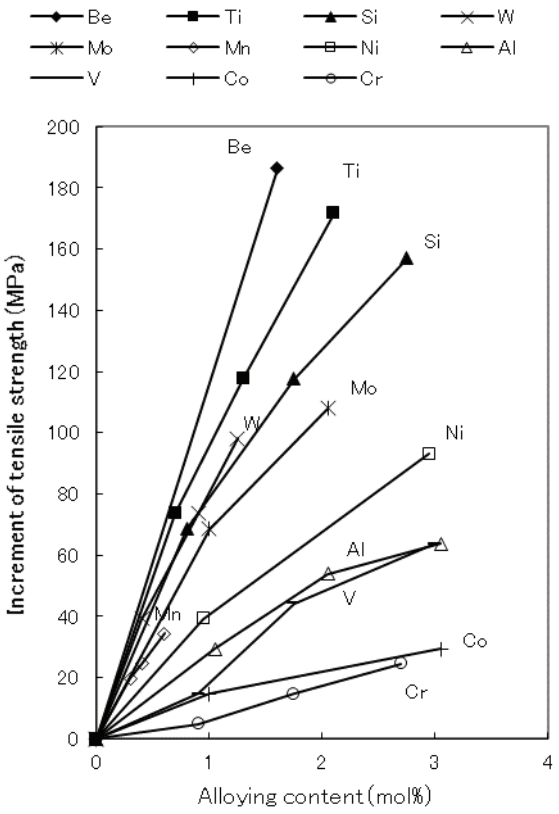

Fig. 12-6 – Tensile strength increase of α-Fe as a parameter of the alloying content of elements

The tensile strength increases from 225 MPa with increasing alloying

content. The carbon content must have been kept constant, but this was not specifically mentioned. The same relationship as that in Fig. 12-3 was pursued. The change in tensile strength at 1 mol% alloying content was adopted as the index of solution hardening of each alloying element.

Fig. 12-7 shows the relationship between the tensile strength increase of Fe by the alloying elements and the atomic radii of the alloying elements.

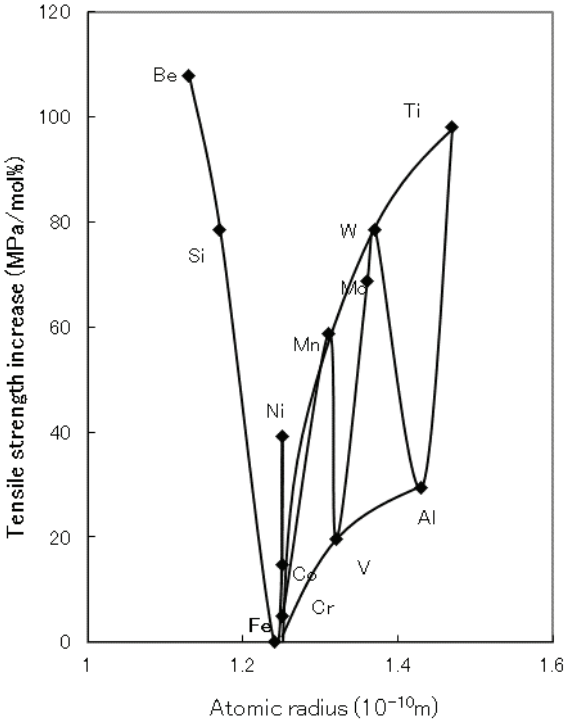

Fig. 12-7 – Relationship between the tensile strength increase (MPa/mol%) of Fe by alloying elements and the atomic radii of alloying elements

The scatter is large. The elements – Co, Ni, Mn, Mo, W, and Ti – lie on one curve, but the elements – Cr, V, and Al – lie on another curve.

Fig. 12-8 shows the relationship between the tensile strength increase (MPa/mol%) of Fe by alloying elements and the solubility of alloying elements in α-Fe.

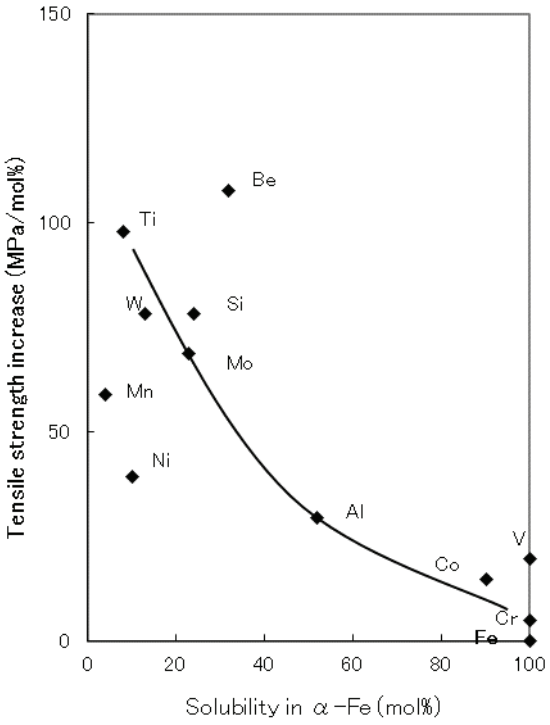

Fig. 12-8 – Relationship between the tensile strength increase (MPa/mol%) of Fe by the alloying elements and the solubility of alloying elements in α-Fe

The scatter is large. The elements – Ti, W, Si, Mo, Al, Co, and Cr – lie on

a curve, but the other elements – Be, Mn, Ni, and V – deviate from the curve.

Fig. 12-9 shows the relationship between the tensile strength increase (MPa/mol%) of Fe by alloying elements and the solubility of solute atoms in γ-Fe.

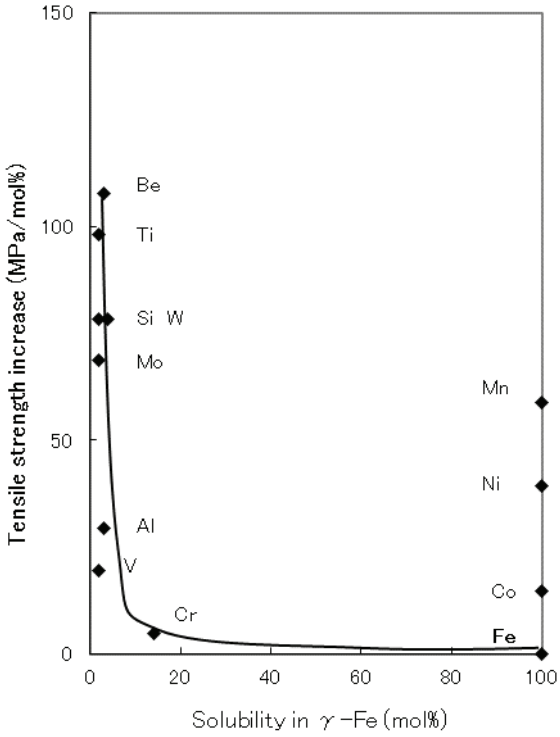

Fig. 12-9 – Relationship between the tensile strength increase (MPa/mol%) of Fe by alloying elements and the solubility of solute atoms in γ-Fe

The tensile strength increase decreases rapidly with the increasing solubility of alloying elements in γ-Fe. The elements of unlimited solubility – Co, Ni,

and Mn – also give rise to solution hardening. This is an exception of the solubility hypothesis.

Fig. 12-10 shows the relationship between the tensile strength increase and the diffusion coefficients of alloying elements in ferromagnetic α-Fe at 1023K.

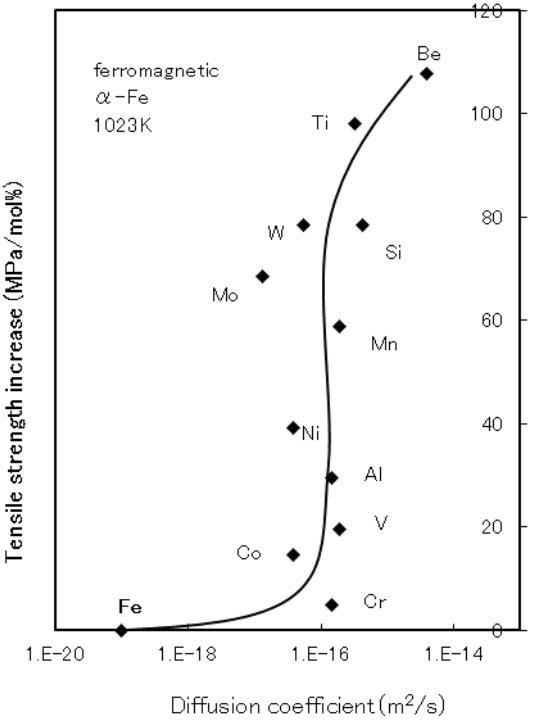

Fig. 12-10 – Correlation between the tensile strength increase (MPa/mol%) and the diffusion coefficient of alloying elements (m^2/s) in ferromagnetic α-Fe at 1023K

Except for Fe and Be, most of the elements adopt the similar values of the diffusion coefficient in ferromagnetic α-Fe. Therefore, the correlation curve

becomes steep.

Fig. 12-11 shows the relationship between the tensile strength increase and the diffusion coefficients of alloying elements in paramagnetic α-Fe at 1073K.

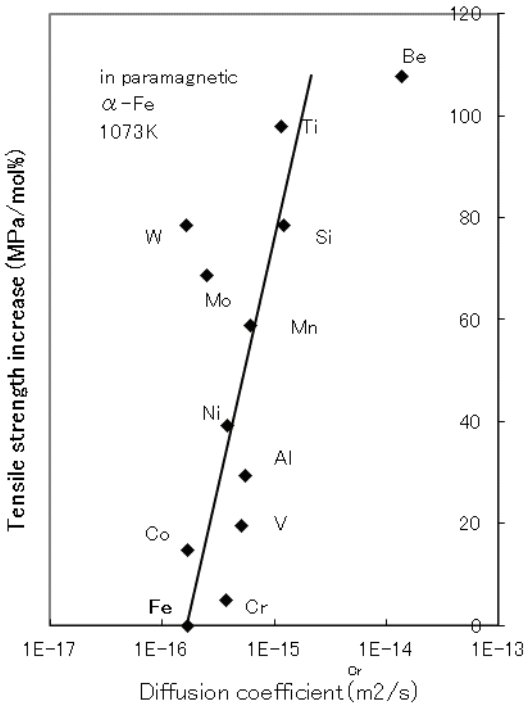

Fig. 12-11 – Correlation between the tensile strength increase (MPa/mol%) and the diffusion coefficient of alloying elements (m^2/s) in paramagnetic α-Fe at 1073K

Values of the diffusion coefficients are distributed in a wider range, and rather good correlation can be seen. The elements – V and Al – which

deviate greatly from the tendency in Fig. 12-7 are included in the correlation in this figure. As the diffusion coefficient increases, the effect of solution hardening increases.

Fig. 12-12 shows the correlation between the tensile strength increase (MPa/mol%) of Fe by alloying elements and the diffusion coefficients of alloying elements in γ-Fe at 1273K.

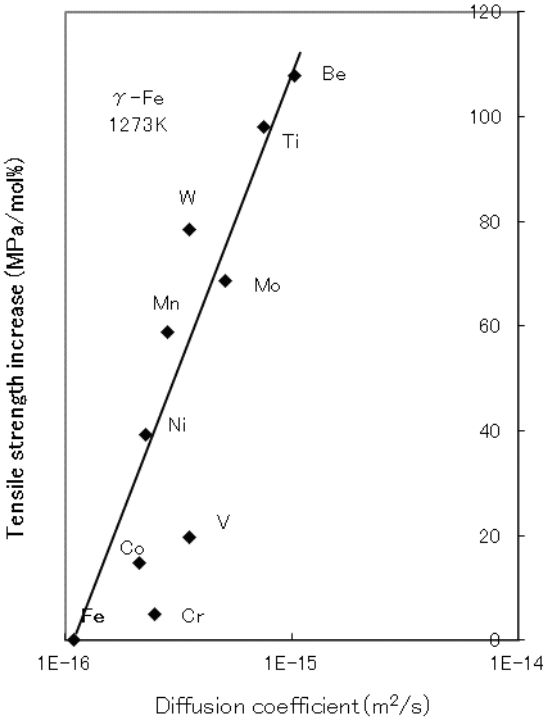

Fig. 12-12 – Correlation between the tensile strength increase (MPa/mol%) of α-Fe by alloying elements and the diffusion coefficient of alloying elements (m^2/s) in γ-Fe at 1273K

Rather good correlation is found. The tensile strength enhancement increases with the increasing diffusion coefficient of the alloying elements in γ-Fe. The elements – Fe, Cr, Ni, Mn, Mo, W, Ti, and Be – show good linearity except for Cr and V.

Fig. 12-13 shows the correlation between the tensile strength increase (MPa/mol%) of Fe by alloying elements and the diffusion coefficients of alloying elements in γ-Fe at 1473K.

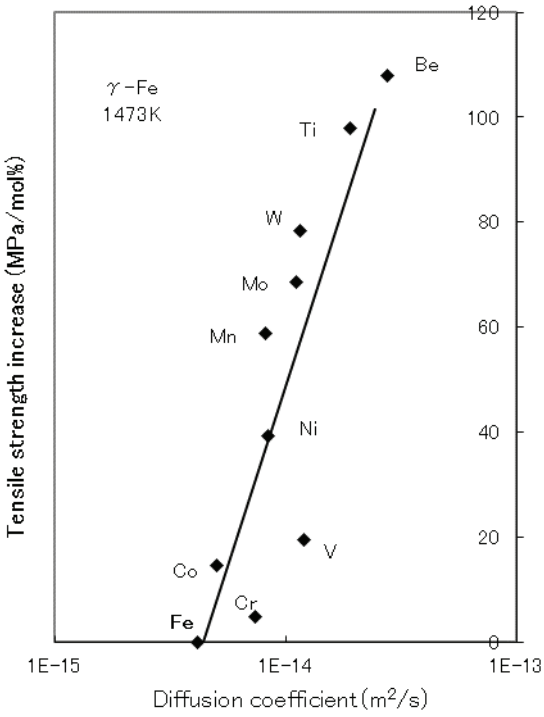

Fig. 12-13 – Correlation between the tensile strength increase (MPa/mol) of α-Fe by alloying elements and the diffusion coefficients of alloying elements in γ-Fe at 1473K

Rather good correlation is found in the high temperature range of the γ-phase also. Totally, the tensile strength enhancement shows good correlation with the diffusion coefficients in the paramagnetic α-region and γ-region. The tensile strength enhancement increases with the increasing diffusion coefficient of the alloying elements. The elements – Fe, Cr, Co, V, Al, Ni, Mn, Mo, W, Si, Ti, and Be – show good linearity.

It is noted, furthermore, that solution hardening is controlled by the same factors as those which act in the diffusion of elements at high temperatures.

(3) Pt

The Vickers hardness increases of Pt by the alloying elements are studied. [8]

Fig. 12-14 shows the relationship between the tensile strength increase of Pt and the atomic radii of alloying elements. Correlation cannot be found.

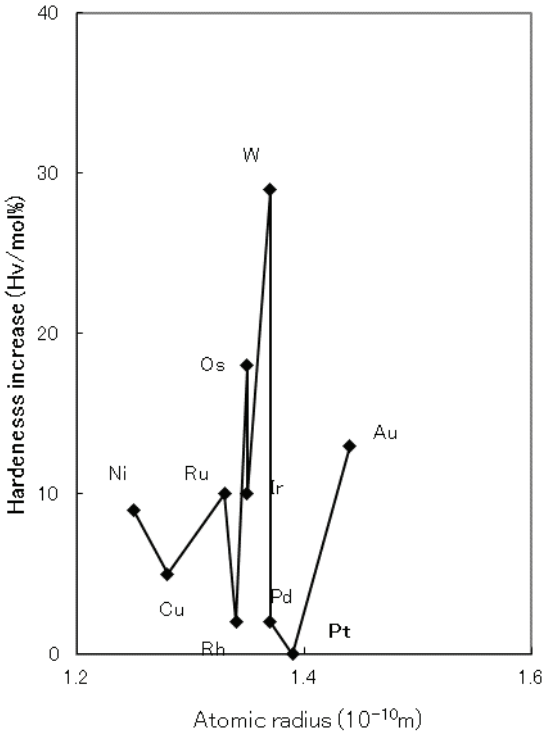

Fig. 12-14 – Hardness increase of Pt as a parameter of the atomic radius of alloying elements

Fig. 12-15 shows the relationship between the Vickers hardness increase (Hv/mol%) of Pt by alloying elements and the solubility of alloying elements.

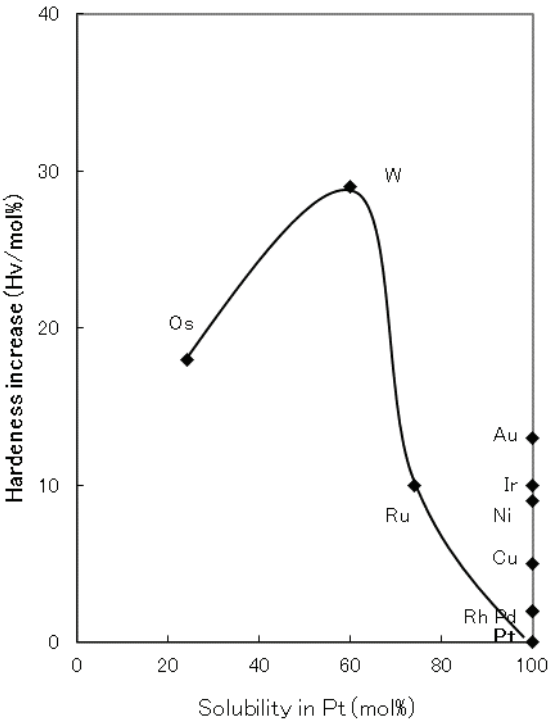

Fig. 12-15 – Relationship between the Vickers hardness increase (Hv/mol%) of Pt by alloying elements and the solubility of alloying elements

Pt is located in the center of the TC-YM diagram and near to many elements, therefore, Pt is very capable of dissolving many elements. Correlation cannot be seen.

Unfortunately, diffusion data of elements in Pt are missing.

(4) Ti

The Brinell hardness increase of Ti by the alloying elements is studied. [9]

Fig. 12-16 shows the relationship between the tensile strength increase (MPa/mol%) of Ti by alloying elements and the atomic radii of alloying elements.

Ti is located near the ordinate of the TC-YM diagram, therefore, its atomic radius is large. Correlation cannot be found.

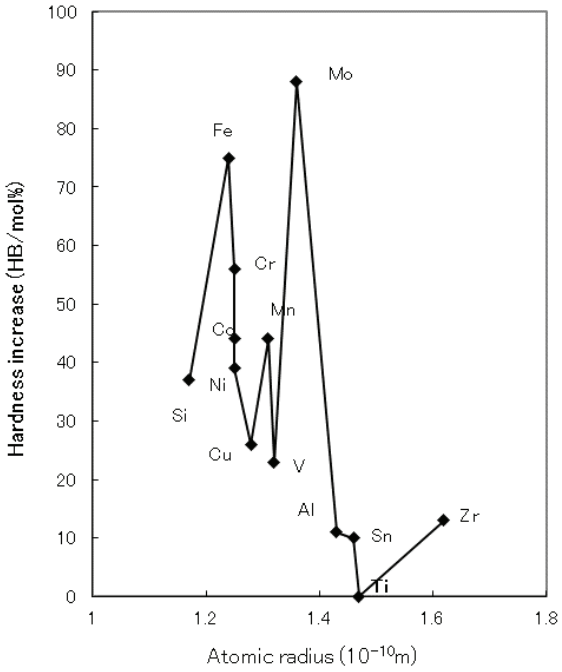

Fig. 12-16 – Relationship between the tensile strength increase (MPa/mol%) of Ti by alloying elements and the atomic radii of alloying elements

Fig. 12-17 shows the relationship between the Brinell hardness increase (H_B/mol%) of Ti by alloying elements and the solubility of alloying elements in α-Ti.

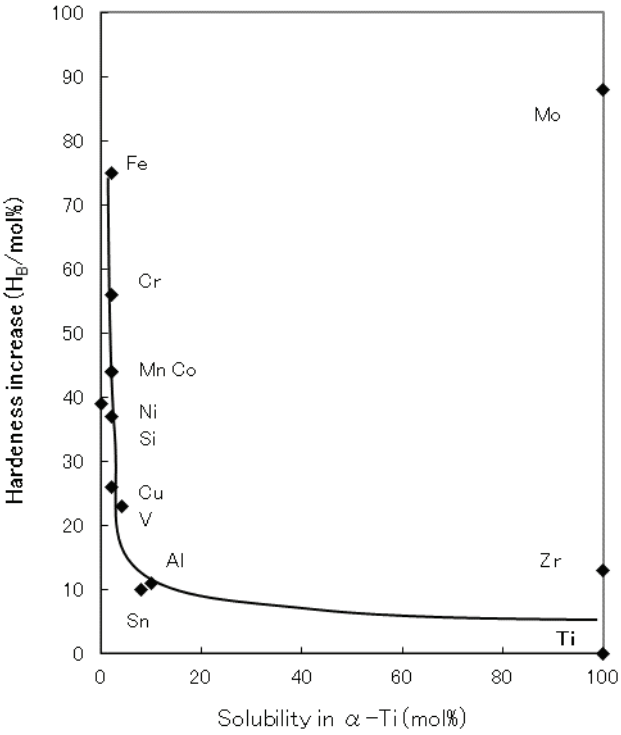

Fig. 12-17 – Relationship between the Brinell hardness increase (H_B/mol%) of Ti by alloying elements and the solubility of alloying elements in α-Ti

The solution hardening of Ti decreases rapidly with the increasing solubility of alloying elements in α-Ti. Most of the elements lie on a clear curve.

Fig. 12-18 shows the relationship between the Brinell hardness increase (H_B/mol%) of Ti by alloying elements and the solubility of alloying elements in β-Ti. Scatter is very large. Correlation cannot be found.

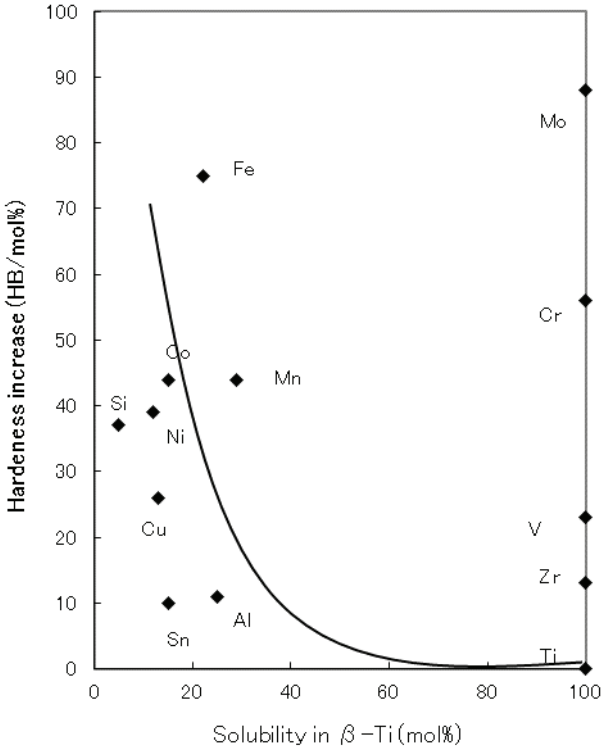

Fig. 12-18 – Relationship between the Brinell hardness increase (H_B/mol%) of Ti by alloying elements and the solubility of alloying elements in β-Ti

Fig. 12-19 shows the relationship between the hardness increase of Ti by the alloying elements and the diffusion coefficients of the alloying elements in α-Ti at 1073K. Only very obscure correlation is found.

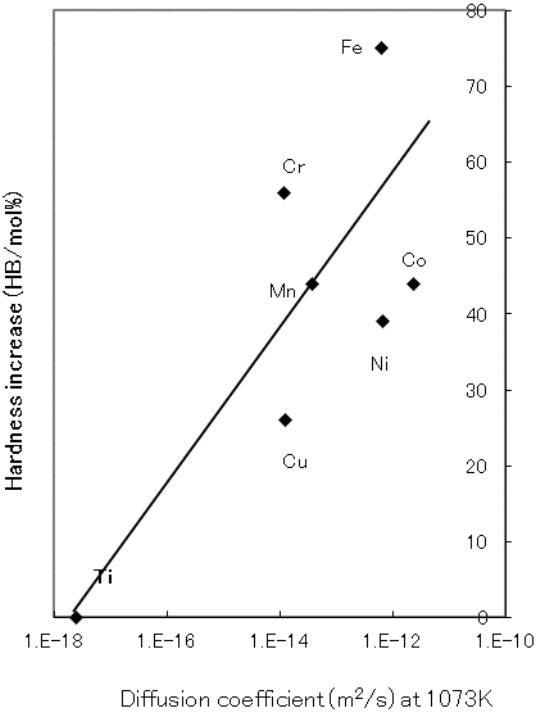

Fig. 12-19 – Hardness increase of Ti as a parameter of the diffusion coefficients of alloying elements in α-Ti at 1073K

Fig. 12-20 shows the relationship between the hardness increase of Ti by the alloying elements and the diffusion coefficients of the alloying elements in β-Ti at 1273K.

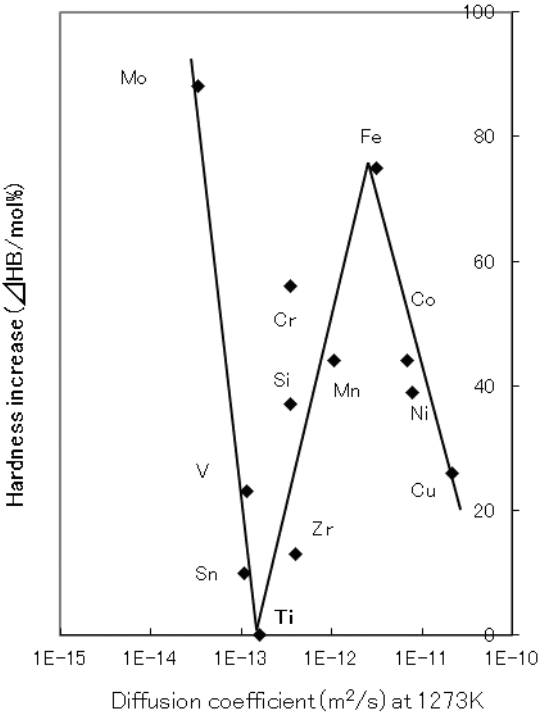

Fig. 12-20 – Hardness increase of Ti as a parameter of the diffusion coefficients of alloying elements in β-Ti at 1273K

A good correlation is seen. The elements – Sn, V, and Mo – show smaller diffusion coefficients than Ti. As for these elements, solution hardening increases with decreasing diffusion coefficient. As for other elements, solution hardening increases with increasing diffusion coefficient. After it reaches the peak at Fe, it decreases with increasing diffusion coefficient.

(6) Zr

Secondary to Fe, the element for which the largest amount of solution hardening data is available is Zr. [10] The change in the proof strength of Zr at 1 mol% alloying content was adopted as the index of solution hardening. The values were plotted as a parameter of atomic radius as shown in Fig. 12-21.

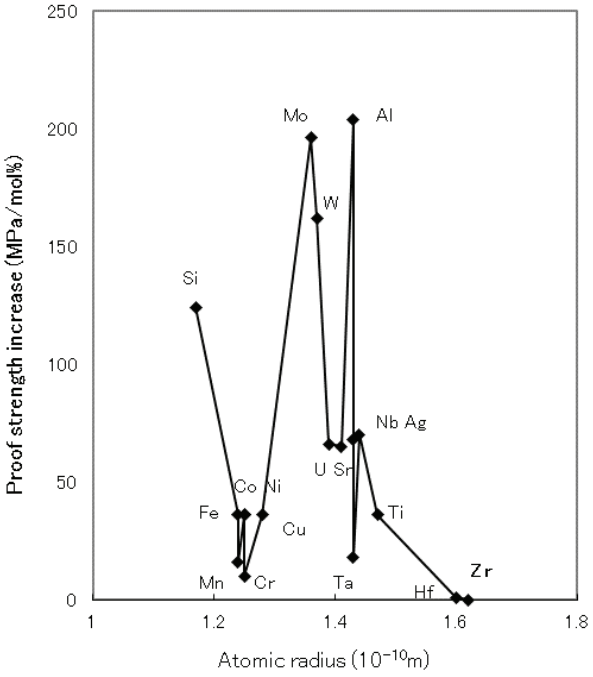

Fig. 12-21 – Relationship between the proof strength increase (MPa/mol%) of Zr by alloying elements and the atomic radii of alloying elements

Zr has the largest atomic radius among the elements studied here. In this case, the proof strength enhancement increases with decreasing atomic radius from that of Zr. The fluctuation is large. Two kinds of trends can be seen.

Fig. 12-22 shows the relationship between the proof strength increase (MPa/mol%) of Zr by alloying elements and the solubility of alloying elements in α-Zr.

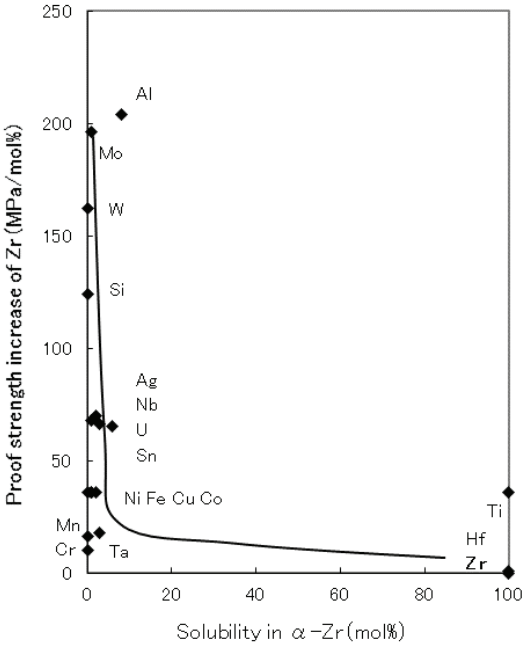

Fig. 12-22 – Relationship between the proof strength increase (MPa/mol%) of Zr by alloying elements and the solubility of alloying elements in α-Zr

Most of the elements show small solubility in α-Zr. Solution hardening

decreases rapidly with increasing solubility in α-Zr. Correlation cannot be found.

Fig. 12-23 shows the relationship between the proof strength increase (MPa/mol%) of Zr by alloying elements and the solubility of alloying elements in β-Zr.

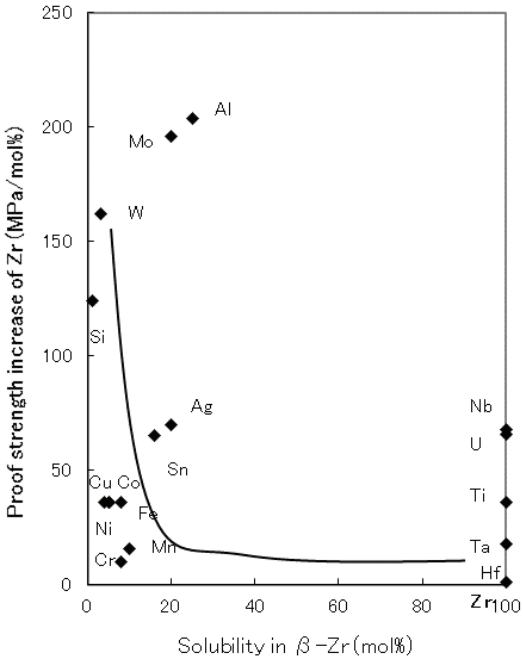

Fig. 12-23 – Relationship between the proof strength increase (MPa/mol%) of Zr by alloying elements and the solubility of alloying elements in β-Zr

In general, the solubility of alloying elements is larger in β-Zr than in α-Zr. But, correlation is very obscure.

Fig. 12-24 shows the relationship between the proof strength increase (MPa/mol%) of Zr by alloying elements and the diffusion coefficient of alloying elements in α-Zr at 1073K.

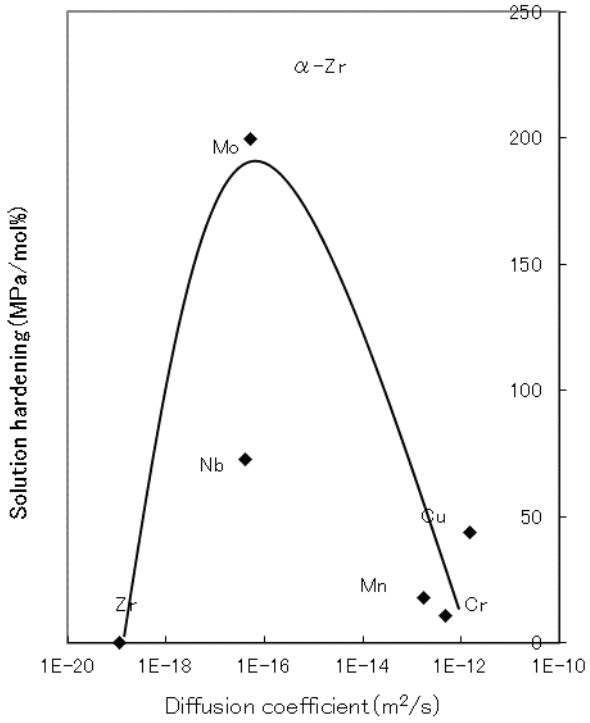

Fig. 12-24 – Relationship between the proof strength increase (MPa/mol%) of Zr by alloying elements and the diffusion coefficient of alloying elements in α-Zr at 1073K

With increasing diffusion coefficient, solution hardening increases at first, but after that, it decreases rapidly.

Fig. 13-25 shows the correlation between proof strength enhancement

(MPa/mol%) in Zr by alloying elements and the diffusion coefficient of alloying elements in β-Zr at 1273K.

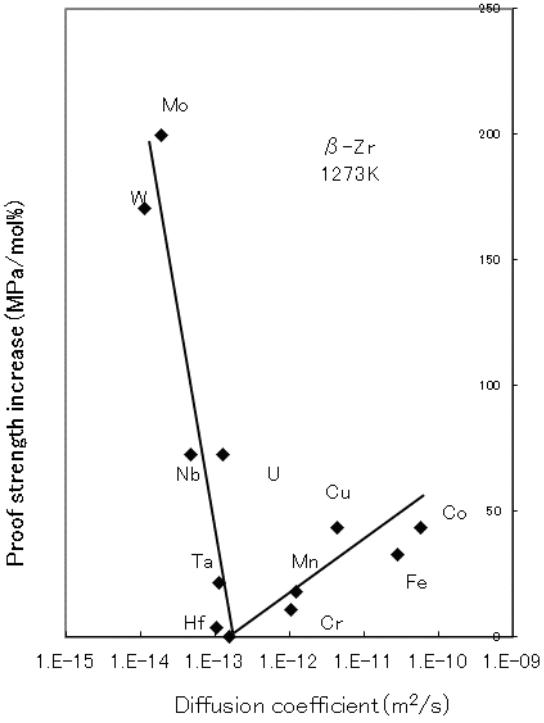

Fig. 12-25 – Correlation between the proof strength increase (MPa/mol%) of Zr by alloying elements and the diffusion coefficient of alloying elements in β-Zr at 1273K

Surprisingly, a beautiful correlation was obtained. Similar correlations were confirmed in β-Zr at 1173K and 1373K. The proof strength enhancement increases linearly with an increasing diffusion coefficient from that of Zr. With a decreasing diffusion coefficient from Zr, the proof strength enhancement increases linearly and sharply. Superbly, Zr is located just at the cross point of the two lines.

12.2 Discussion on the correlation between solution hardening and the diffusion coefficient

As mentioned above, the atomic size incoherence hypothesis is not valid in many matrix metals. Many elements deviate from the correlation line to a greater or lesser extent. In contrast, the solubility hypothesis is rather valid. These are existing hypotheses.

The third one, the correlation with the diffusion coefficient, is a new one which was found by this author. As shown so far, the diffusion coefficient shows the best fit to the solution hardening of various metals. The reasons for it will be studied as follows:

(1) Cu

The change in yield strength (MPa/mol%) of Cu in Fig. 12-2 was plotted on the TC-YM diagram as shown in Fig. 12-26.

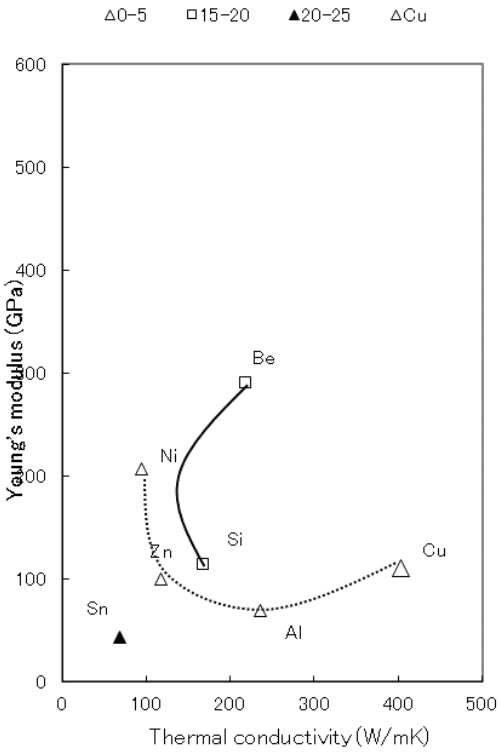

Fig. 12-26 – Yield strength increase (MPa/mol%) of Cu shown on the TC-YM diagram

The figures in the legend show the range of the yield strength increase (MPa/mol%).

The elements with an equivalent Young's modulus to Cu such as Al and Zn show a small strength increase. Ni also shows a small strength increase because it has the same crystal structure as Cu. The elements – Si and Be – show medium hardening, because they have larger Young's moduli than Cu.

The element Sn shows the largest strength increase because it is away from Cu on the diagram. This trend is the same as that in the solubility in Cu; therefore, the hardening correlates with the solubility of elements in Cu as shown in Fig. 12-4.

Fig. 12-27 shows the distribution of the DC ratio of diffuser elements in Cu at 1273K on the TC-YM diagram. **The DC ratio is defined as the diffusion coefficients of an alloying element divided by the diffusion coefficient of the self-diffusion of the matrix metal. They are represented in the logarithmic scale in the legend.**

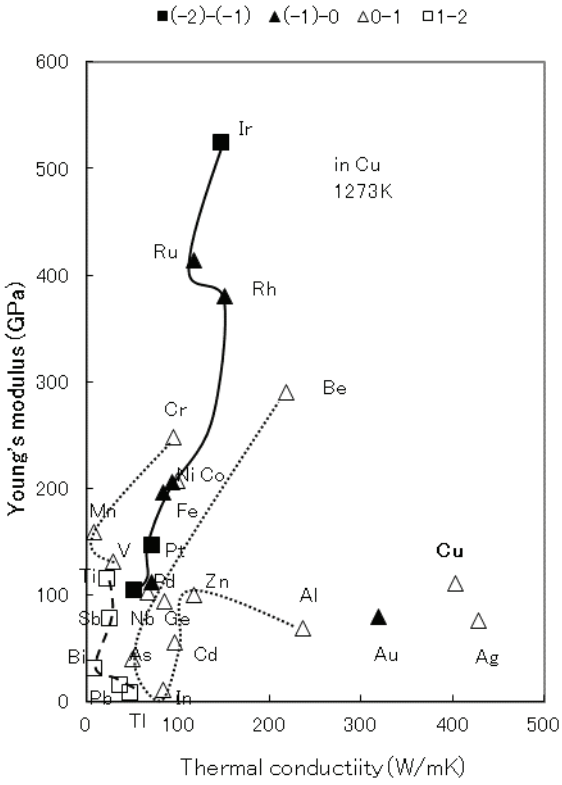

Fig. 12-27 – Distribution of the DC ratio of diffuser elements in Cu at 1273K on the TC-YM diagram. (cf. Fig. 11-4)

As explained in Chapters 10 and 11, the difference in thermal conductivity, i.e. in the electron mobility, generates the repulsive force. The elements near the matrix element on the TC-YM diagram diffuse moderately at a similar speed to that of the self-diffusion of the matrix metal due to the weak repulsive force. This is normal diffusion. In this figure, the elements – Ag, Al, Zn, Cd, In, As, Ge, Ga, and Be – are included in this group.

The elements in the medium distance from the matrix metal on the TC-YM diagram diffuse more slowly than the self-diffusion of the matrix metal, because the repulsive force is large, but not large enough to deform the matrix atoms or the diffuser atoms, consequently the diffuser atoms undergo the repulsive force only and their diffusions in the matrix metal are suppressed. This is slow diffusion. The elements – Nb, Pd, Fe, Ni, Rh, Rh, and Ir – are slow diffuser elements in Cu.

The elements in the farthest distance from the matrix metal on the TC-YM diagram diffuse faster than the self-diffusion of the matrix metal, because the repulsive force is large enough to deform the matrix atoms or the diffuser atoms, and opens the passageways for fast diffusion. This is fast diffusion. The elements – Tl, Pb, Bi, Sb, Ti, V, Mn, and Cr – are fast diffuser elements in Cu. In this group, the elements – Tl, Pb, Bi, Sb, and Ti – diffuse faster, because they have softer atoms due to their low Young's moduli. Conversely, the elements – V, Mn, and Cr – diffuse relatively slowly, because they have relatively hard atoms due to their high Young's modulus.

In summary, the variation of the DC ratios of alloying elements in Cu is relatively small; therefore the solution hardening of Cu is generally small. As shown in Fig. 12-5, the yield strength of Cu by the alloying elements – Ni, Al, and Zn – is small except for Be.

(2) Fe

The change in the tensile strength (MPa/mol%) of Fe in Fig. 12-6 was plotted on the TC-YM diagram as shown in Fig. 12-28.

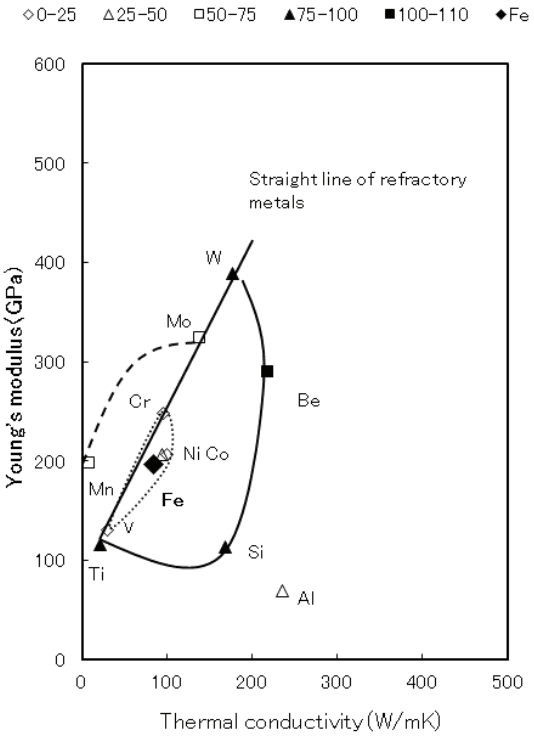

Fig. 12-28 – Tensile strength increase (MPa/mol%) of Fe shown on the TC-YM diagram

The numbers in the legend indicate the ranges of tensile strength increase. The values of tensile strength enhancement (MPa/mol%) are distributed regularly on the diagram. Elements on the right side of the straight line of refractory metals – Ti, Si, Be and W – show the largest strength enhancement. In contrast, Al is too far to strengthen Fe. The elements on the left side of the straight line of refractory metals – Mo, and Mn – show a medium change in strength. Elements near Fe – Cr, Ni, Co, and V – show

the smallest changes.

This pattern is different from that of the atomic radius as shown in Fig. 4-4. Therefore, the atomic size incoherent hypothesis is not valid as shown in Fig. 12-7. In contrast to this, the pattern of solubility shows such a tendency that, with moving far from the matrix metal, the solubility of the alloying elements decreases. Namely, with moving far from the matrix metals, the solubility of the alloying elements decreases, and solution strengthening by the alloying elements increases. Therefore, the solubility hypothesis is valid in Fe as shown in Figs. 12-8 and 12-9, though the scatter is rather large.

Figs. 12-29, 30, and 31 show the DC ratios of alloying elements in ferromagnetic α-Fe, paramagnetic α-Fe, and γ-Fe, respectively.

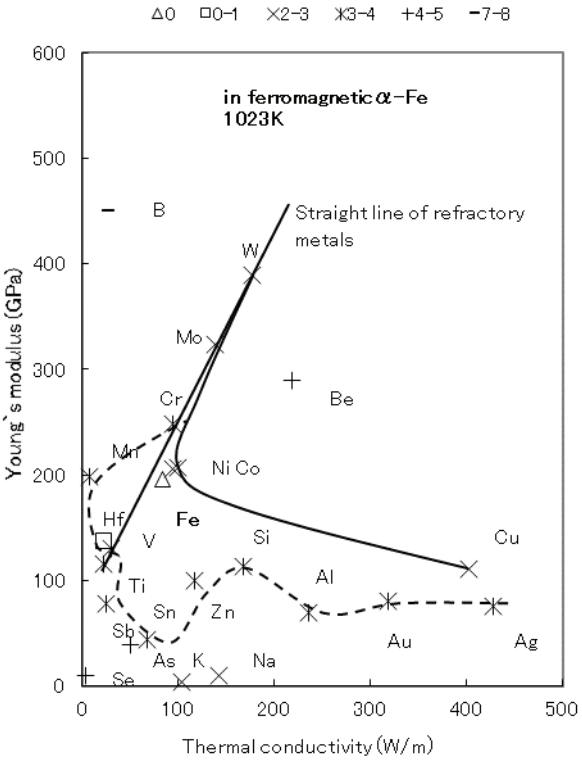

Fig. 12-29 – DC ratios of the diffuser elements in the ferromagnetic α-Fe at 1023K (cf. Fig. 10-18)

In ferromagnetic α-Fe, Fe atoms diffuse very slowly compared to the alloying elements. The elements on the straight line of refractory metals – Mo and W – and the elements near Fe – Ni and Co – diffuse faster than Fe. The other elements with lower thermal conductivity or lower Young's modulus diffuse much faster than Fe. There is no similarity to the solution hardening of Fe shown in Fig. 12-28.

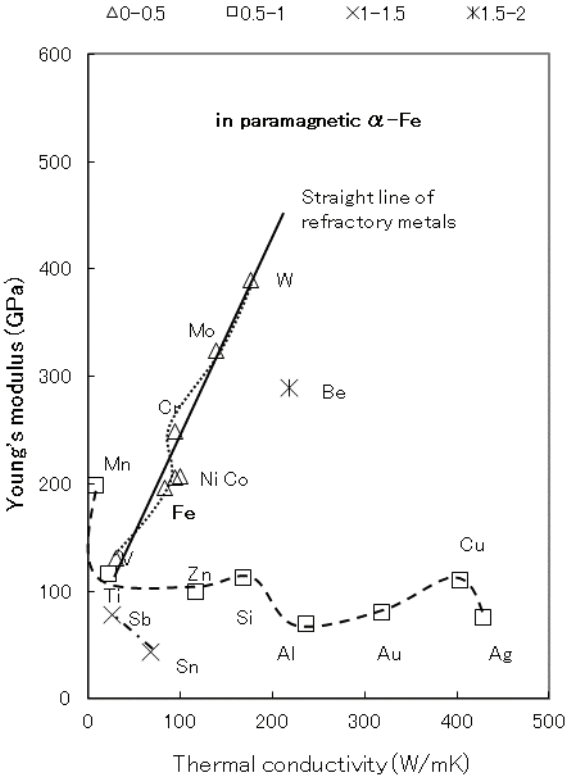

Fig. 12-30 – DC ratios of the diffuser elements in the paramagnetic α-Fe at 1073K (cf. Fig. 10-34)

In paramagnetic α-Fe, Fe atoms diffuse at a similar speed to that of the alloying elements. The elements on the straight line of the refractory metals – V, Cr, Mo, and W – and the elements near Fe – Ni and Co – diffuse at a similar speed to that of Fe. The other elements with low thermal conductivity or low Young's modulus diffuse faster than Fe. The elements with the lowest Young's modulus – Sb and Sn – diffuse much faster.

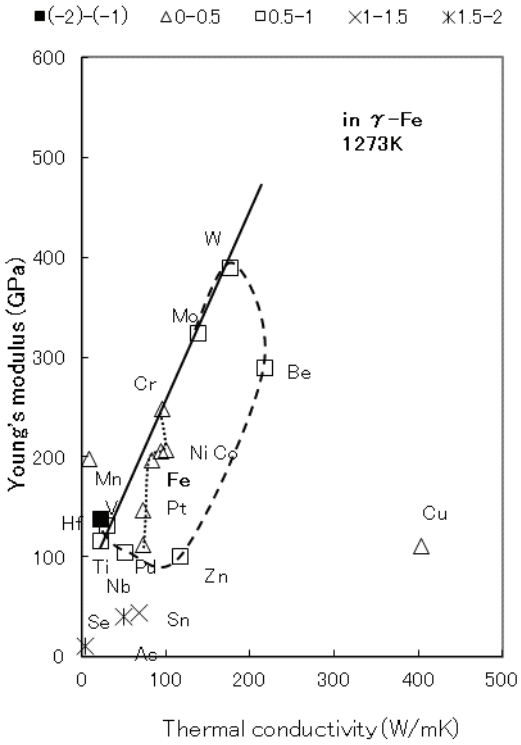

Fig. 12-31 – DC ratios of the diffuser elements in γ-Fe at 1273K (cf. Fig. 10-35)

In γ-Fe, Fe atoms diffuse most slowly among the elements except for Hf. The elements near Fe – Cr, Ni, Co, Pt, and Pt – diffuse at a similar speed to Fe. The elements surrounding them – Mo, W. Be, Zn, Nb, Ti, and V – diffuse a little faster than Fe. The elements with the lowest Young's modulus – Sn, Se, and As – diffuse much faster than Fe. This shows the similarity with the solution hardening of Fe in Fig. 12-28.

It can be concluded that the diffusion of elements in the highest temperature phase coincides well with the solution hardening of the matrix metal.

(3) Pt

The change in Vickers hardness (Hv/mol%) of Pt in Fig. 13-13 was plotted on the TC-YM diagram as shown in Fig. 12-32.

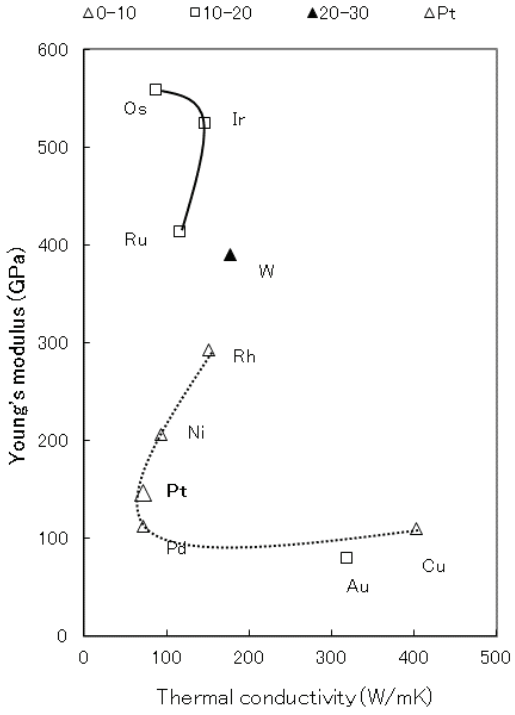

Fig. 12-32 – Vickers hardness increase of Pt (Hv/mol%) shown on the TC-YM diagram

The elements of the equivalent Young's modulus to Pt and those on the curve of the fcc metals and near Pt – Cu, Pd, Ni, and Rh – show small hardening.

The elements far from Pt in the upper side of the diagram – Ru, Ir and Os – show rather large hardening. This pattern is different from that of the atomic radius in Fig. 4-4; therefore, the atomic size incoherence hypothesis is not valid as shown in Fig. 12-14.

Pt is an element on the curve of fcc metals, therefore it dissolves many elements on the curve of fcc metals. The element W, which has larger Young's modulus and a bcc structure, shows a large hardness increase as shown in Fig. 13-32.

Unfortunately, diffusion data of alloying elements in Pt are missing.

(4) Ti

The change in Brinell hardness (H_B/mol%) of Ti in Fig. 12-14 was plotted on the TC-YM diagram as shown in Fig. 12-33.

,

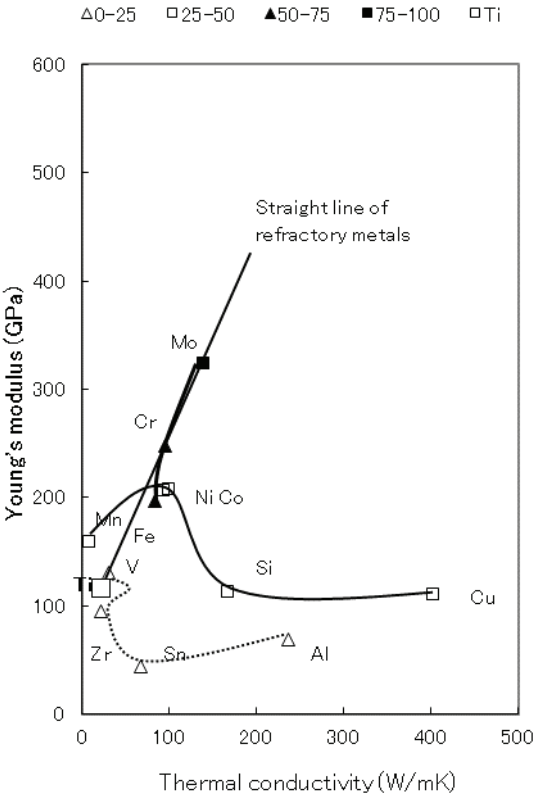

Fig. 12-33 – Brinell hardness increase of Ti (H_B/mol%) on the TC-YM diagram

Ti is located near V which is an element at the lowest end of the straight line of refractory metals. The elements near Ti – V, Zr, Sn, and Al – show small hardening.

The elements with higher Young's moduli – Mn, Ni, and Co – and those at a far distance – Si and Cu – show rather large hardening.

The elements of bcc structures at a far distance – Fe, Cr and Mo – show the largest hardening.

This pattern is different from that of the atomic radius, therefore, the atomic size incoherence hypothesis is not valid as shown in Fig. 12-16. But this pattern shows fundamentally the same tendency as that of the solubility of elements in metals, in that point that the characteristics change with moving far from the matrix metal. As a result, the solubility hypothesis is partly valid as shown in Figs. 12-17 and 18.

Figs. 12-34 and 12-35 show the DC ratios of alloying elements in α-Ti and β-Ti, respectively.

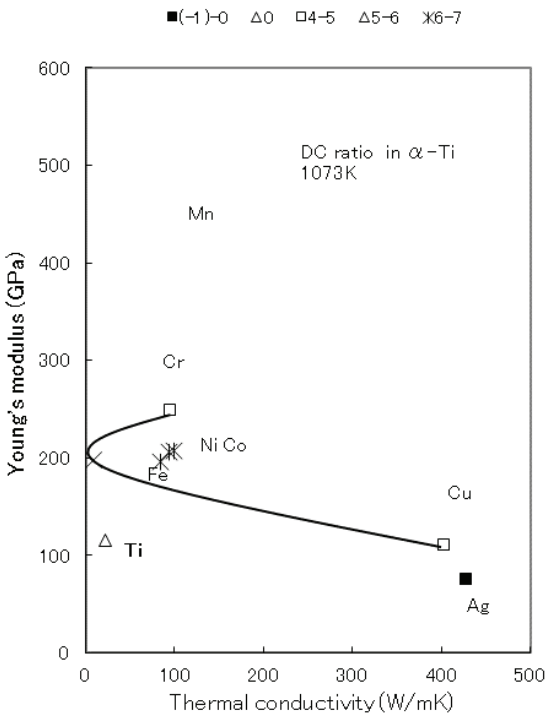

Fig. 12-34 – DC ratios of the diffuser elements in α-Ti at 1073K (cf. Fig. 10-20)

In α-Ti, the gulf elements – Cu, Fe, Ni, Co, and Cr – and the element near the gulf elements – Mn – diffuse very fast. The hard atoms of these elements deform the soft atoms of Ti in the α-phase and open the passageways for fast diffusion.

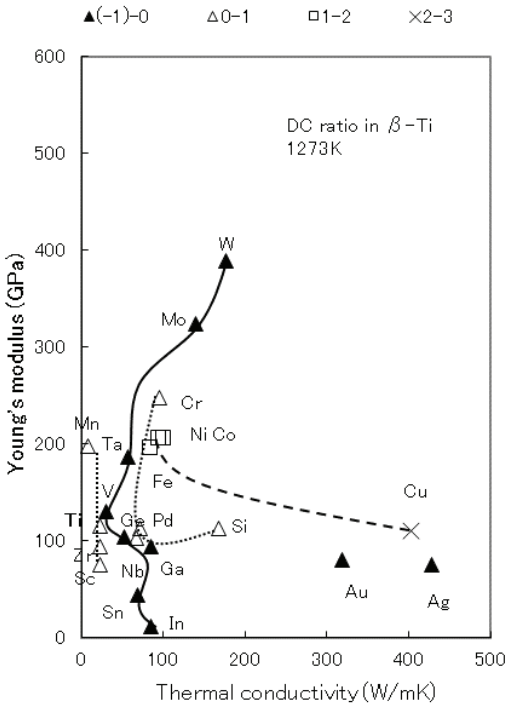

Fig. 12-35 – DC ratios of the diffuser elements in β-Ti at 1273K (cf. Fig. 10-26)

In β-Ti, the elements with similar thermal conductivity – Sc, Zr, and Mn – diffuse at a similar speed to Ti. Note that Mn diffuses much faster than Ti in α-Ti as shown in Fig. 12-35.

The elements with medium thermal conductivity – In, Sn, Ga, Nb, V, Ta, Mo, and W – diffuse slower in β-Ti than Ti itself. This is a slow diffusion. The difference in thermal conductivity, i.e., in the electron mobility is not large enough to deform the atoms of Ti, consequently they undergo the repulsive force only, and their diffusion in β-Ti is suppressed.

The elements near Ti – Sc, Zr, and Mn – diffuse at the same speed as Ti itself, because the difference in thermal conductivity is small. The elements near the gulf elements – Si, Ga, and Cr – also diffuse at the same speed as Ti itself.

The gulf elements with the largest combination of thermal conductivity and Young's modulus – Cu, Fe, Ni, and Co – diffuse faster than Ti itself. This is small fast diffusion. The difference in thermal conductivity is large enough to generate a large repulsive force and it deforms the atoms of Ti, and opens the passageways for fast diffusion.

Comparing with Fig. 12-33, it is shown that the elements with larger and smaller DC ratios than Ti show large solution hardening. It validates Fig. 12-20.

(5) Zr

The change in the proof strength of Zr in Fig. 13-21 was plotted on the TC-YM diagram as shown in Fig. 12-36.

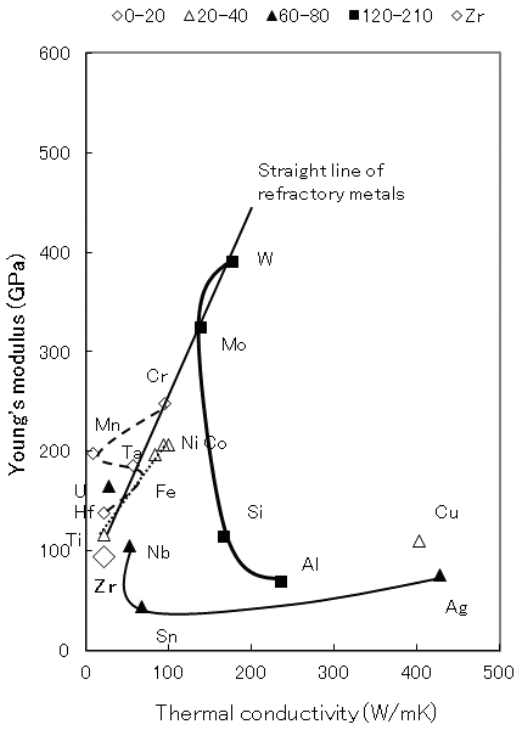

Fig. 12-36 – Proof strength increase of Zr by the alloying elements displayed on the TC-YM diagram

Zr is located just under Ti. The elements near Zr – Ti, Hf, Mn, Ta, Fe, Ni, and Co – show small hardening.

The elements just on the right side of Zr – Ag, Sn, Nb, and U – show larger hardening.

The elements with higher thermal conductivity – W, Mo, Si, and Al – show the largest hardening.

Fig. 12-37 and Fig. 13-38 show the DC ratios of alloying elements in α-Zr and β-Zr, respectively.

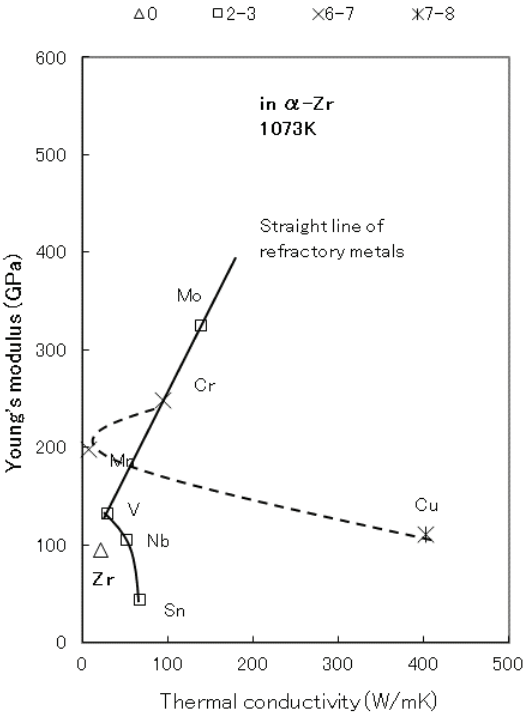

Fig. 12-37 – DC ratios of the diffuser elements in α-Zr at 1073K (cf. Fig. 10-21)

In α-Zr, the elements near and on the right side of Zr – Sn, Nb, and V – diffuse a little faster than Zr itself. The difference in thermal conductivity is small, consequently a small repulsive force is generated. It deforms the soft atoms of α-Zr, and opens the passageways a little. As a result, these elements diffuse a little faster than Zr itself.

The gulf elements – Cu and Cr, and Mn – diffuse much faster than Zr. This is fast diffusion in α-Zr. Quite similarly to Ti, the difference in thermal conductivity is large enough to generate the large repulsive force and it deforms the atoms of α-Zr, and opens the passageways for fast diffusion.

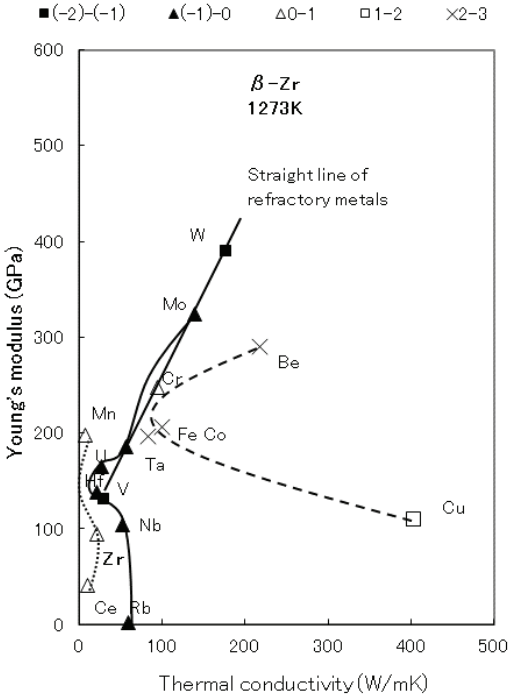

Fig. 12-38 – DC ratios of the diffuser elements in β-Zr at 1273K (cf. Fig. 10-28)

In β-Zr, elements of similar thermal conductivity to Zr – Ce and Mn – diffuse at a speed similar to Zr itself.

The elements with slightly larger thermal conductivity – Rb, Nb, V, Hf, Ta, Mo, and W – diffuse a little more slowly than Zr itself. The difference in thermal conductivity between these elements and Zr is medium, therefore, the repulsive force is not large enough to deform the atoms of β-Zr. Consequently, these atoms undergo only the repulsive force and are repelled by the atoms of Zr. As a result, the diffusion of these elements in Zr is suppressed.

The gulf elements – Cu, Fe, Co, Cr, and Be – diffuse faster than Zr. The difference in thermal conductivity and Young's modulus between these elements and Zr is large and a large repulsive force is generated. It deforms the atoms of β-Zr and opens the passageways for fast diffusion.

Ti and Zr have the same values of thermal conductivity and similar Young's modulus. Therefore, Ti and Zr show very similar behaviors of DC ratios on the TC-YM diagram. They both show very clear patterns on the diagram.

(6) Al

Data on the solution hardening of Al are very few. Therefore, they are not shown in a figure here. But there are abundant data of the diffusion coefficients of alloying elements in Al. They are shown in Fig. 12-39.

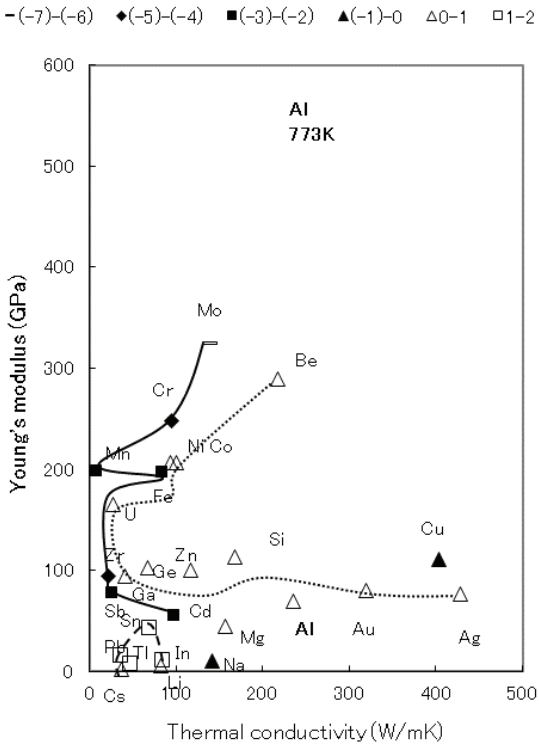

Fig. 12-39 – DC ratio of the diffuser elements in Al at 773K (cf. Fig. 11-3)

Al is located at the halfway point of thermal conductivity. Therefore, the elements in the vast area near Al – Ag, Au, Si, Mg, Zn, Ge, Ga, U, Ni, Co, and Be – diffuse at a similar speed to Al. They draw a half circle on the diagram.

The elements with lower thermal conductivity – Cd, Sb, Zr, Fe, Mn, Cr, and Mo – diffuse much slower than Al. They are surrounding the inner half circle.

The elements of the lowest thermal conductivity and Young's modulus – In, Sn, Pb, and Tl – diffuse faster than Al. This is small fast diffusion. The difference in thermal conductivity between these elements and Al is large, and a repulsive force is generated. The atoms of these elements are soft due to their low Young's modulus and thermal conductivity; therefore, the diffuser atoms are deformed by the repulsive force and pass through the lattice of the matrix atoms of Al.

The elements with small thermal conductivity and relatively large Young's modulus – Cd, Sb, Zr, Fe, Mn, Cr and Mo – show slow diffusion. They can give rise to the solution hardening of Al. But they are located far from Al; therefore, their solubilities in Al are very small. As a result, practically, they do not harden Al.

12.3 Summary

Solution hardening is determined by the relative locations of the matrix metals and the alloying elements on the TC-YM diagram.

Solution hardening by the alloying elements near the matrix metal on the TC-YM diagram is small. As the alloying elements move far from the matrix metal, solution hardening by the alloying elements increases.

This pattern is in an inverse relation to that of the solubility of elements in metals, and therefore the solubility hypothesis that the degree of hardening is inversely proportional to the solubility of the alloying elements in the matrix metals is valid.

In contrast, the atomic radii of elements are distributed in the enlarging concentric circle with increasing atomic radius on the TC-YM diagram, and therefore the pattern is different from that of solution hardening. As a result, the hypothesis that the degree of hardening is determined by the degree of lattice distortion caused by the difference of the atomic radius between solute atoms and matrix atoms is not always valid.

The pattern of diffusion coefficients of alloying elements is also similar to that of solution hardening, and therefore solution hardening and diffusion coefficients show good correlation.

The diffusion coefficients of elements are controlled by the repulsive force and the rigidity of atoms of matrix metals and diffuser elements.

The patterns of diffusion ratios show very clear tendencies on the TC-YM diagram.

It can be speculated that solution hardening is caused by the repulsive force between the atoms of alloying elements and matrix metals. This is the reason why solution hardening has a correlation with the diffusivity of alloying elements.

Fig. 12-40 shows the situation in which a solute atom exerts a repulsive force to the surrounding matrix atoms and distorts the lattice, regardless of the atomic size of the solute atom. Arrows in the figure represent the repulsive force.

Fig. 12-40 – Lattice distortion by the repulsive force acting between the matrix atoms and a solute atom

In this chapter, this author showed the diffusion behaviors of elements in terms of DC ratios instead of diffusion coefficients on the TC-YM diagram. DC ratios showed much clearer tendencies than diffusion coefficients. Diffusion is a fundamental property of elements as well as the crystal structure of elements. They both validate the TC-YM diagram basically.

References

1. Japan Institute of Metals, Metals Manual, Maruzen, Tokyo, 1960, pp. 315-317.
2. C. E. Racy and M. Gensamer, Trans. ASM Vol. 32, 1944, p. 586.
3. H. K. D. H. Bhadesia and R. W. K. Honeycombe, Steels, 3rd ed., BH, Amsterdam, 2006, pp. 27-28.
4. M. Tanino and S. Suzuki, Science of Steel, Uchida-rokakuho, 2006, pp. 119-123.
5. R. E. Hummel, Understanding Materials Science, Springer, 1998, p. 75.
6. D. R. Askeland, The Science and Engineering of Materials, 3rd ed., PWS,

Boston,1994, p. 242.

7. Japan Institute of Metals, Metals Manual, Maruzen, Tokyo, 1960, p. 316.
8. Japan Institute of Metals, Metals Data Book, Tokyo, 3rd ed., Maruzen, 1993, p194.
9. Japan Institute of Metals, Metals Data Book, Tokyo, 3rd ed., Maruzen, 1993, p190.
10. Japan Institute of Metals, Metals Data Book, Tokyo, 3rd ed., Maruzen, 1993, p193.

13. SOLUBILITY OF ELEMENTS IN METALS AND THE EFFECTS OF ALLOTROPIC TRANSFORMATIONS OF ELEMENTS ON IT

The solid elements adopt various crystal structures.

As shown in Fig. 1-6, the bcc-structured elements mostly lie on the straight line connecting V, Ta, Cr, Mo, and W, which can be called *the straight line of refractory metals*. Additionally, elements with fcc structures lie on a clear curve, which can be called *the curve of fcc metals*. Elements with hcp and other structures are distributed in between.

The detailed distribution of crystal structures around the lanthanides is shown in Fig. 6-4.

In this way, the crystal structures are distributed regularly on the TC-YM diagram. But, the crystal structures of elements are not constant. There are many elements which transform to other crystal structures at high temperatures (allotropic transformation). But the reason for the allotropic transformation is not known. Therefore, the orderings of the crystal structures of elements after the allotropic transformation are studied here.

13.1 Crystal structures of elements after the allotropic transformations

(1) Elements which adopt bcc structures after the allotropic transformation

Fig. 13-1 shows the elements of genuine bcc structures and those which adopt bcc structures after the allotropic transformation.

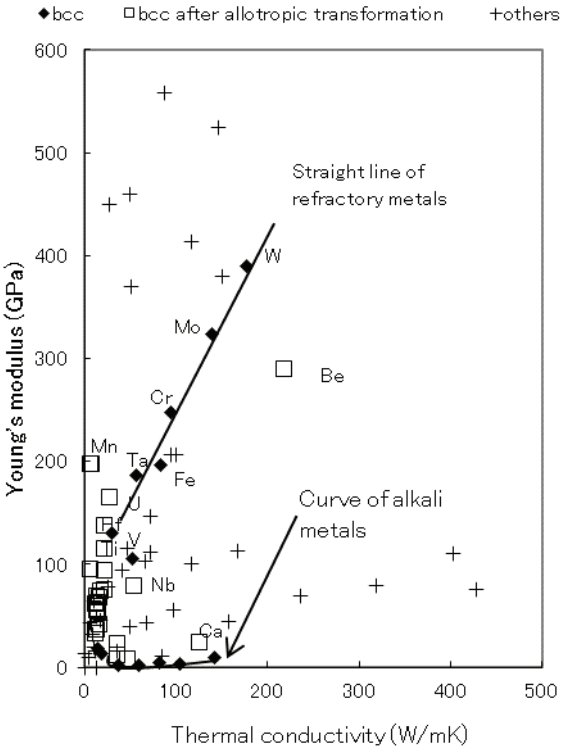

Fig. 13-1 – Elements of genuine bcc structures and those of bcc structures after the allotropic transformation shown on the TC-YM diagram

Ti, Zr and the lanthanides, etc., lie between the straight line of refractory metals and the curve of alkali metals. These elements have hcp structures because they fall within the hcp region. But most of them transform to bcc structures at high temperatures, because they are affected by the refractory metals and the bcc alkali metals. In general, elements with bcc structures can potentially lie anywhere from W (at the top of the straight line of refractory metals) to Na (at the right-most end of the curve of alkali metals). Elements with bcc structures do not exist elsewhere in the diagram.

It is found from Fig. 13-1 that the elements which adopt bcc structures after the allotropic transformations connect the refractory metal group with the alkali metal group.

In addition, it can be speculated that the bcc structure is a phase at high temperatures.

The alkali metals adopt bcc structures because the room temperature is already a high temperature for them. Ti, Zr and many lanthanides, etc., adopt bcc structures at high temperatures. The refractory metals adopt bcc structures because their bcc structures are stable even at room temperature. Owing to this theory, the reason why the refractory metals of high melting temperatures and the alkali metals of low melting temperatures possess the same bcc structures can be explained. In his youth, this author was taught that the bcc structure is a heat resistant structure, but could not understand why the alkali metals of very low melting temperatures adopt bcc structures. This can be understood for the first time by means of the TC-YM diagram.

The pattern of bcc metals is preserved also after the allotropic transformations.

(2) Elements which adopt fcc structures after the allotropic transformation

Fig. 13-2 shows the distribution of elements of genuine fcc structures and those of fcc structures after the allotropic transformation on the TC-YM diagram.

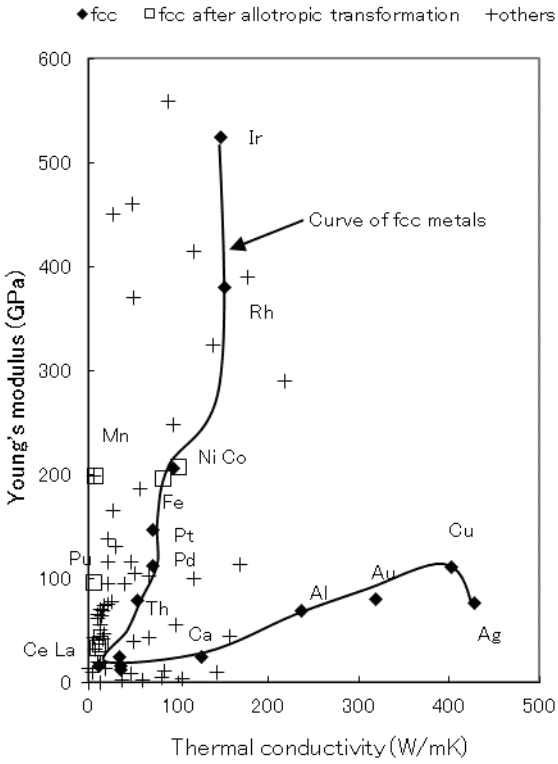

Fig. 13-2 – Elements of genuine fcc structures and those of fcc structures after the allotropic transformation shown on the TC-YM diagram

The elements of genuine fcc structures lie on the curve of fcc metals.

Fe and Co transform into fcc structures at high temperatures. Fe, Ni and Co lie in close proximity from left to right, near the straight line of refractory metals. Ni is a genuine fcc-structured element, so it lies on the curve of fcc metals. Fe lies slightly to the left of Ni, and nearer to the straight line of refractory metals. Consequently, Fe has a bcc structure at room temperature, and an fcc structure at high temperature, following the crystal structure of nearby Ni. Co lies slightly to the right of Ni, and in the hcp region, so it has an hcp structure at room temperature. However, it transforms to an fcc structure at high temperature, following the crystal structure of nearby Ni.

The order of Fe–Ni–Co on the diagram explains their crystal structures, while Fe–Co–Ni is their order in the periodic table.

Some elements with low thermal conductivity transform to fcc structures.

As shown in Fig. 13-2, elements which adopt fcc structures after the allotropic transformation are

Mn, Pu, La, and Ce. They commonly show very low thermal conductivity.

It is also remarkable that they transform to fcc structures at medium temperatures and transform further to bcc structures at higher temperatures.

The orderings of fcc structures are preserved also after the allotropic transformations.

(3) The elements which adopt multiple phases

There are some elements which transform to other phases more than twice. Mn transforms from cubic (A12) to cubic (A13), fcc, and bcc. Np and U do from orthorhombic to tetragonal, and bcc. Pu does from monoclinic to orthorhombic, fcc, and bcc. La and Ce do from double hexagonal to fcc and bcc. Sr does from fcc to hcp and bcc. They are shown in Fig. 13-3.

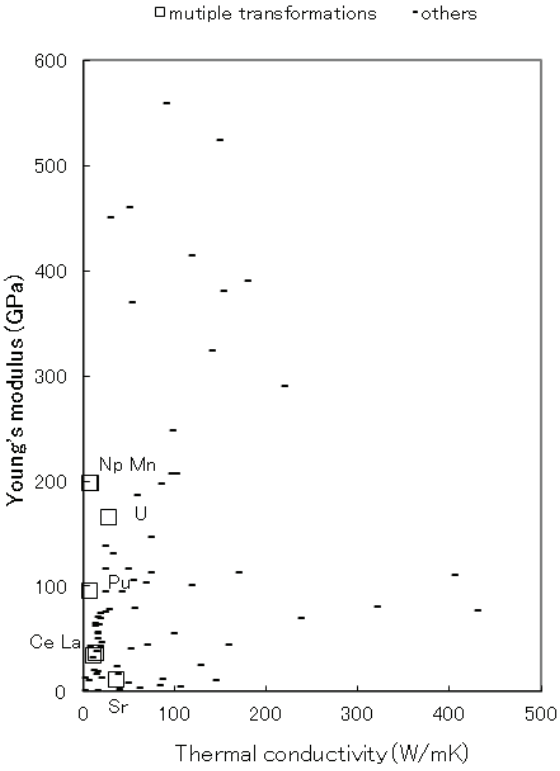

Fig. 13.3 – Elements of multiple transformations shown on the TC-YM diagram

They are all elements of low thermal conductivity. Np and Mn are very close to each other.

The elements which adopt fcc structures after the allotropic transformation – Mn, Pu, Ce, and La – are included in this element group of multiple transformations. Only U and Np do not adopt fcc structures in their multiple transformations.

13.2 Solubility of elements in metals considering allotropic transformations

From that mentioned above, it is found that the elements which transform to bcc structures play a role in bridging the refractory metal group to the alkali metal group. It is also found that the elements which transform to fcc structures are Fe and Co in the proximity of Ni and are Mn, Pu, La, and Ce which lie in the very low thermal conductivity region. The elements – Mn, Pu, La, and Ce – undergo multiple transformations, namely they transform further to bcc structures at higher temperatures.

How the crystal structures of elements after the allotropic transformation affect the solubility of elements in metals will be studied here.

The conditions for solubility in metals are known as the **Hume-Rothery rules** and are as follows: [1]

(1) Size factor: The difference in atomic radius must be less than 15 pct.

(2) Crystal structure: The elements must have the same structure as the base metal.

(3) Valence: The elements must have the same valence as the base metal.

(4) Electronegativity: The element must have electronegativity similar to the base metal.

As one of the derivatives of the Hume-Rothery rules, the Darken-Gurry plot has been used to explain the solubility in metals. [2, 3] In the Darken-Gurry plot, the size factor is taken as the abscissa and the electronegativity as the ordinate. It is understood that the Darken-Gurry plot takes into consideration the first and fourth items of the Hume-Rothery rules.

Fig. 13-4 shows the maximum solubility elements in γ-Fe, in the neighborhood of Fe on the Darken-Gurry plot.

The solubility of elements varies with temperature; therefore, the maximum solubility in the γ phase at high temperature was adopted as the solubility.

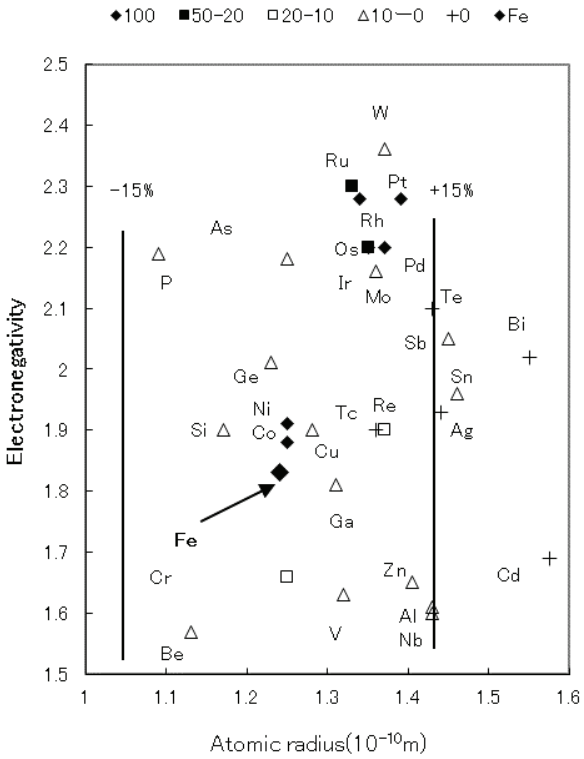

Fig. 13-4 – Solubility of elements in γ-Fe (mol pct) shown on the Darken-Gurry plot

The figures in the legend show the range of solubility in mol per cent. The vertical lines show the boundaries of ±15 pct difference in atomic radius. The elements – Ni and Co – near Fe show 100 pct solubility, but other elements near Fe show only small solubility. On the contrary, elements – Rh, Ir, Pt, and Pd – relatively far from Fe, show 100 pct solubility.

The same situations are seen in other metals. It cannot be said that the Darken-Gurry plot is effective in regard to the solubility of elements in

metals.

Fig. 13-5 shows the distribution of solubility of elements in γ-Fe shown on the TC-YM diagram.

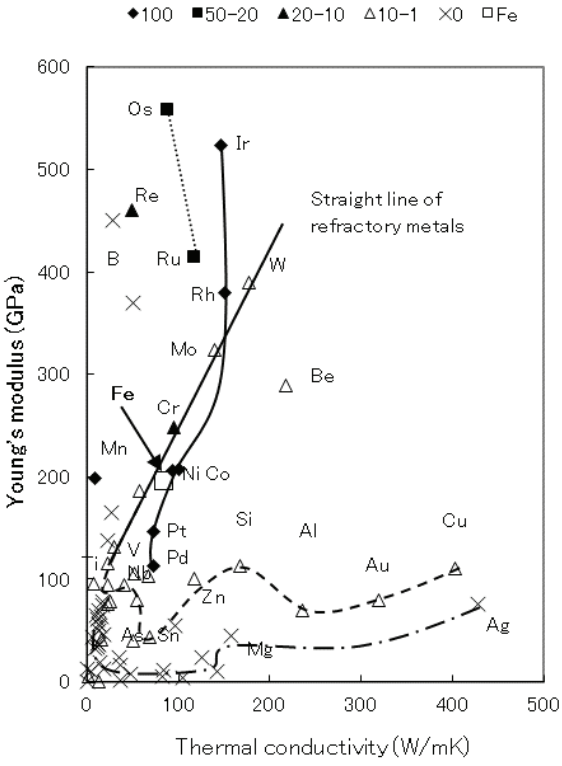

Fig. 13-5 – Solubility of elements in γ-Fe shown on the TC-YM diagram

The data of solubility are the same as in Figure 13.4. The figures in the legend show the range of solubility in mol pct. Iron is located near the center of the diagram. Most of the elements show a clear distribution. Elements of 100 pct solubility – Pd, Pt, Rh, and Ir – lie on the curve of fcc metals and

are relatively near Fe. They have the same fcc structure as γ-Fe. The other fcc elements of lower Young's modulus, Cu, Au, and Al, and those of other crystal structures and of similar Young's modulus – Si, Zn, As, Th, Ga, Zr, Pu, Ti, and V – show small solubility. In general, the solubility decreases with increasing distance from Fe.

The same situations are seen in other metals. It can be said that the solubility of elements in metals is distributed regularly on the TC-YM diagram. [4]

The following can be said about the factors affecting the solubility of elements in metals.

1. The crystal structure of elements must be the same as the matrix metals to have large solubility.

2. The elements must be near the matrix metal on the TC-YM diagram to have large solubility. It shows that the binding force of atoms represented by the Young's modulus and the configuration of electrons represented by the thermal conductivity must be similar.

These conditions will be examined below.

(1) Solubility of elements in metals of bcc structures

Fig. 13-6 shows the distribution of solubility of elements in α-Fe on the TC-YM diagram.

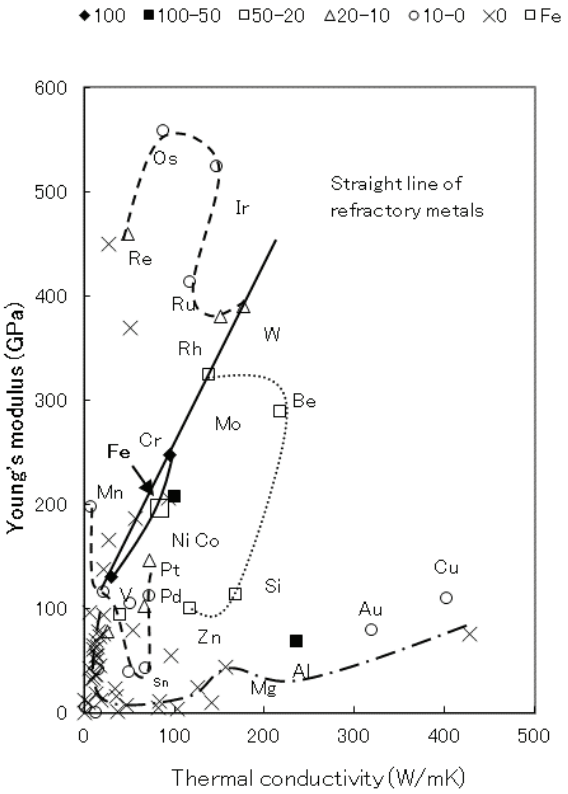

Fig. 13-6 – Solubility of elements in α-Fe shown on the TC-YM diagram

The solubility of elements varies with temperature; therefore, the maximum solubility in the α-phase was adopted as the solubility in α-Fe. The figures in the legend show the range of solubility in mol per cent.

The elements near Fe and on the straight line of refractory metals – Cr and V – show 100 pct solubility. The elements on the straight line of refractory metals have the same bcc structure as α-Fe. However, the elements – Mo

and W – far from Fe show small solubility, although they are located on the straight line of refractory metals. The elements – Mo, Be, Si, Zn, and Ga – surrounding the elements – Cr and V – of 100 pct solubility show the next largest solubility. The farther elements show small or no solubility. Especially, the elements of low Young's modulus show no solubility.

Among the elements of multiple transformations, only Mn shows solubility in α-Fe. This is probably because only Mn has an equivalent Young's modulus to Fe.

Fig. 13-7 shows the distribution of solubility of elements in Mo on the TC-YM diagram.

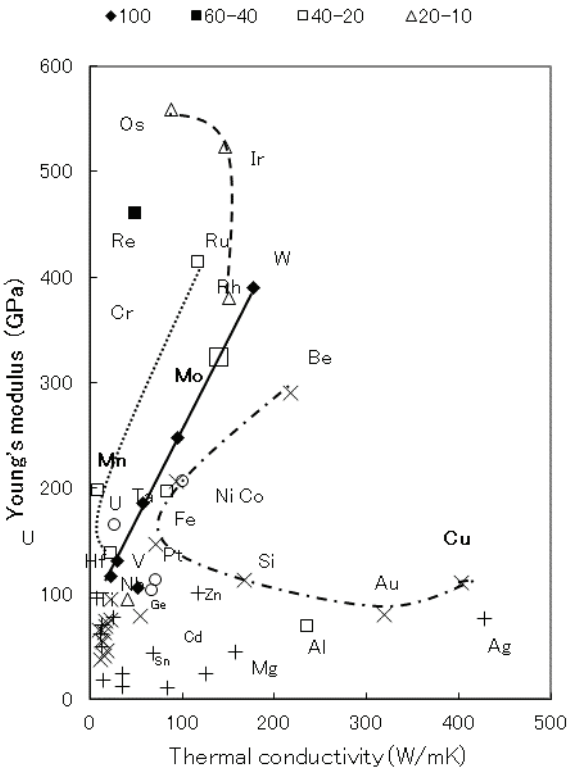

Fig. 13-7 – Solubility of elements in Mo shown on the TC-YM diagram

Mo is located at the upper part of the straight line of refractory metals. All of the elements on the straight line of refractory metals – W, Cr, Ta and V – show 100 pct solubility. Ti which transforms to bcc at high temperature and Nb of genuine bcc structure also show 100 pct solubility. The elements of multiple transformations – Mn and U – show medium solubility. The farther from Mo, the smaller is the solubility of elements.

Fig. 13-8 shows the distribution of solubility of elements in V on the TC-YM diagram.

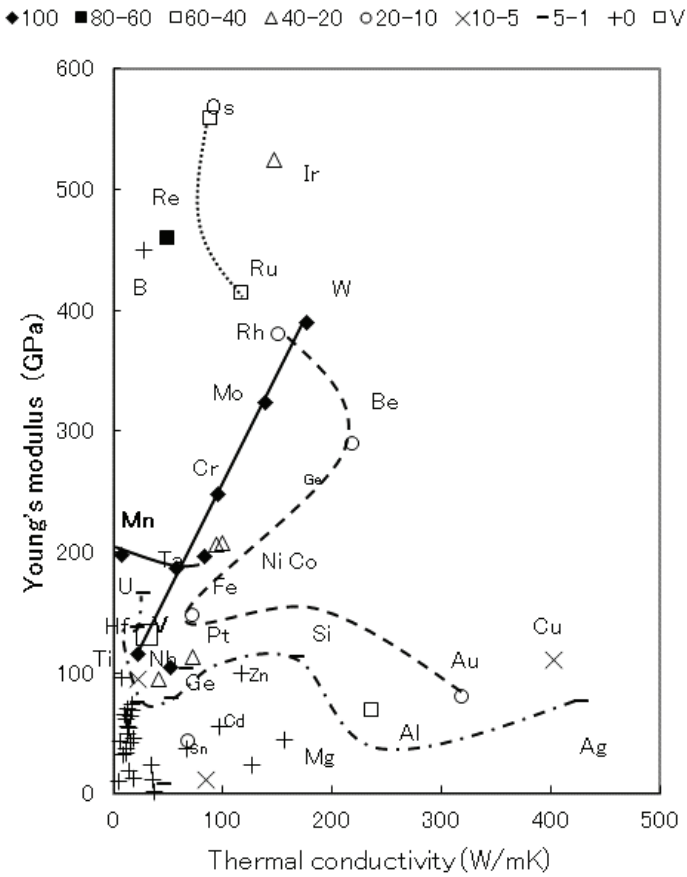

Fig. 13-8 – Solubility of elements in V shown on the TC-YM diagram

V is located at the lowest end of the straight line of refractory metals. All of the elements on the straight line of refractory metals – W, Mo, Cr, and Ta – show 100 pct solubility. Ti which transforms to bcc at high temperature and Nb of genuine bcc structure also show 100 pct solubility. The element of

multiple transformation Mn also shows 100 pct solubility, while U shows small solubility. The farther from V, the smaller is the solubility of elements.

Fig. 13-9 shows the distribution of solubility of elements in β-Ti on the TC-YM diagram.

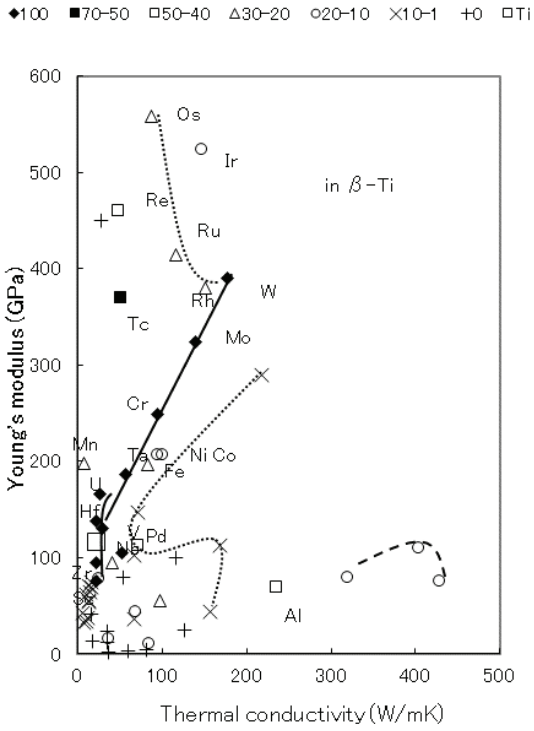

Fig. 13-9 – Solubility of elements in β-Ti shown on the TC-YM diagram

Ti is located on the extension line of the straight line of refractory metals and near V. Ti adopts a bcc structure at high temperature. All of the elements on the straight line of refractory metals – W, Mo, Cr, Ta, and V – show 100

pct solubility. Nb of genuine bcc structure also shows 100 pct solubility. The elements which adopt bcc structures at high temperatures – Hf, Zr, and Sc – also show 100 pct solubility.

The element of multiple transformation U also shows 100 pct solubility, while Mn shows medium solubility. It is because U is nearer to Ti than Mn.

(2) Solubility of elements in metals of fcc structures

The distribution of solubility of elements in γ-Fe on the TC-YM diagram is shown again in Fig. 13-10.

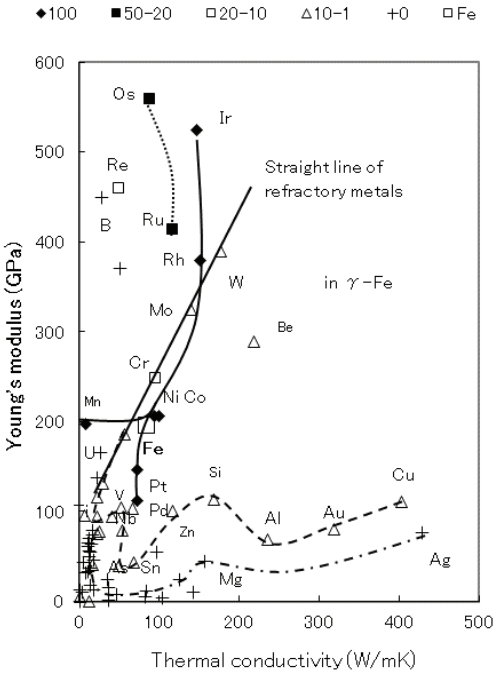

Fig. 13-10 – Solubility of elements in γ-Fe shown on the TC-YM diagram

Elements of 100 pct solubility lie on the curve of fcc metals and are relatively near Fe. They have the same fcc structure as γ-Fe. The other fcc elements of lower Young's modulus – Cu, Au, and Al – and those of other crystal structures and of similar Young's modulus – Si, Zn, Sn, As, Th, Ga, Zr, Pu, Ti, and V – show small solubility.

In this case, Mn shows 100 pct solubility, while U shows no solubility. It is proved that Mn behaves also as an fcc-structured element. U has no fcc structure in its multiple transformations, therefore, it shows no solubility in γ-Fe. The farther from Fe, the smaller is the solubility of elements.

Fig. 13-11 shows the distribution of solubility of elements in Ni on the TC-YM diagram.

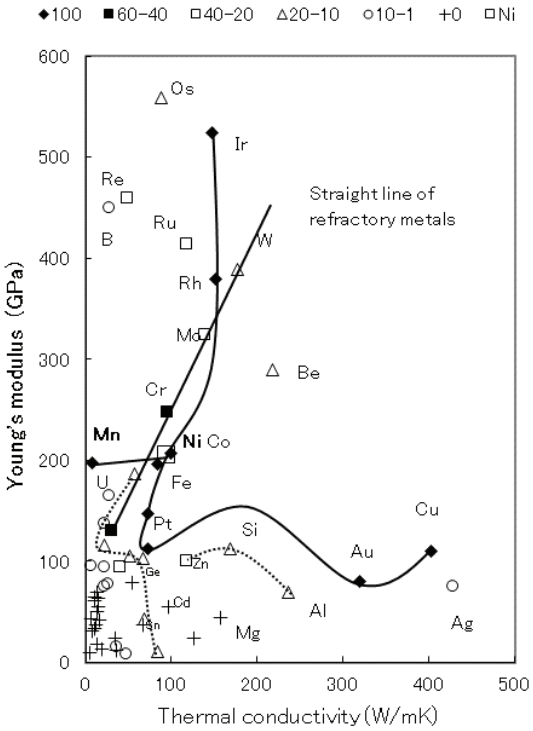

Fig. 13-11 – Solubility of elements in Ni shown on the TC-YM diagram

Most of the elements on the curve of fcc metals – Cu, Au, Pd, Pt, Rh, and Ir –, and the elements near Ni – Fe and Co – show 100 pct solubility.

In this case also, Mn shows 100 pct solubility, while U shows small solubility. It is proved again that Mn behaves as an fcc-structured element.

Some decades ago, a Japanese professor wrote in a journal that Ni is a good solvent, but no reason was stated. Now, it can be explained from the fact that Ni is located at the center of the diagram surrounded by many elements

and lies on the curve of fcc metals. Pt and Pd are also good solvents from the same reason.

Fig. 13-12 shows the distribution of solubility of elements in Cu on the TC-YM diagram.

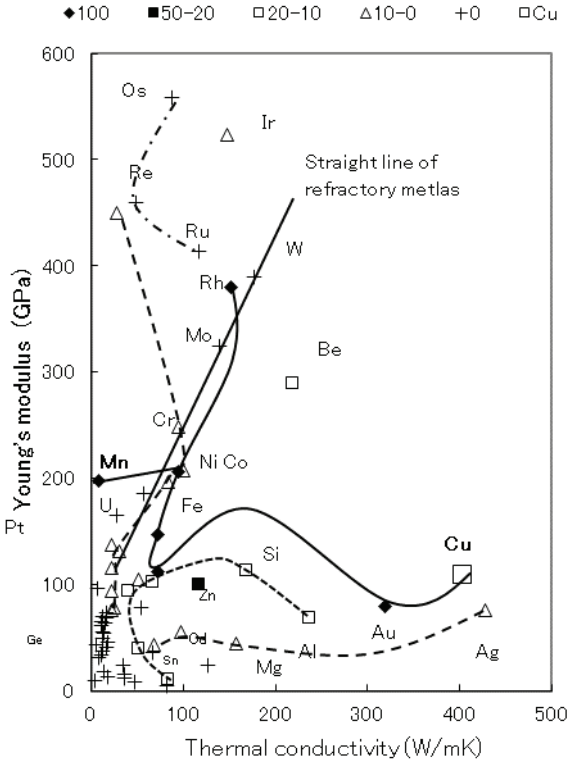

Fig. 13-12 – Solubility of elements in Cu shown on the TC-YM diagram

Cu is located nearly at the right-most end of the curve of fcc metals. Most of the elements on the curve of fcc metals – Au, Pd, Pt, Ni, and Rh – show 100 pct solubility. They have the same fcc structure as Cu. Among other fcc

elements, Al of smaller Young's modulus and smaller thermal conductivity shows small solubility, while the elements – Ca, Pb, and Th – of much smaller Young's modulus and thermal conductivity show no solubility. The element of the highest Young's modulus – Ir – on the curve of fcc metals shows small solubility. The farthest elements show no solubility.

The elements – Fe, Co, and Ir – do not show 100 pct solubility in contrast to the case of Ni. It is because Cu is farther from these elements than Ni on the TC-YM diagram.

In this case also, Mn shows 100 pct solubility, while U shows no solubility. It is proved again that Mn behaves as an fcc-structured element.

This author has been wondering for a long time why Cu shows unlimited solubility with Mn, in spite of that Cu shows very different thermal conductivity from Mn. It can be understood now.

Fig. 13-13 shows the distribution of solubility of elements in Al on the TC-YM diagram.

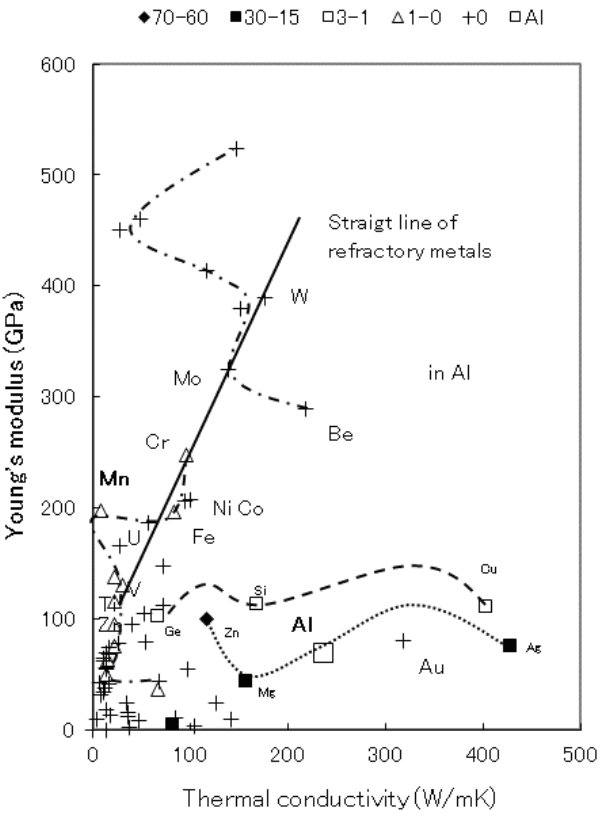

Fig. 13-13 – Solubility of elements in Al shown on the TC-YM diagram

Al is located nearly at the middle of the curve of fcc metals. Aluminum has no elements of 100 pct solubility. This is probably because Al has lower Young's modulus and smaller thermal conductivity than Cu. The elements near Al and with equivalent Young's modulus – Ag, Mg, and Zn – show relatively large solubility. Aluminum has an fcc structure, but it cannot dissolve most of the fcc elements, except Cu and Ag. This is also because Al has low Young's modulus and the resulting low alloying capacity.

Aluminum only dissolves the elements near Al and with the equivalent or slightly higher Young's modulus.

Nevertheless, in this case also, Mn shows some solubility, while U shows no solubility. It is proved again that Mn behaves as an fcc-structured element.

Fig. 13-14 shows the distribution of solubility of elements in Pb on the TC-YM diagram.

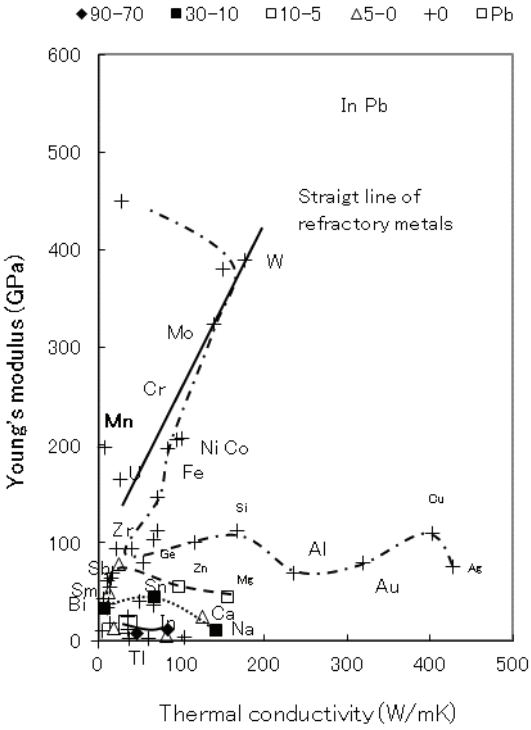

Fig. 13-14 – Solubility of elements in Pb shown on the TC-YM diagram

Pb is located at the corner near the origin of the diagram. It is a location of very low thermal conductivity and very low Young's modulus. Therefore, Pb has small capacity to dissolve other elements. Pb dissolves only the elements in the neighborhood. It dissolves neither Mn nor U, because they are both far from Pb.

(3) Solubility of elements in metals of other crystal structures

Fig. 13-15 shows the distribution of solubility of elements in α-Ti on the TC-YM diagram.

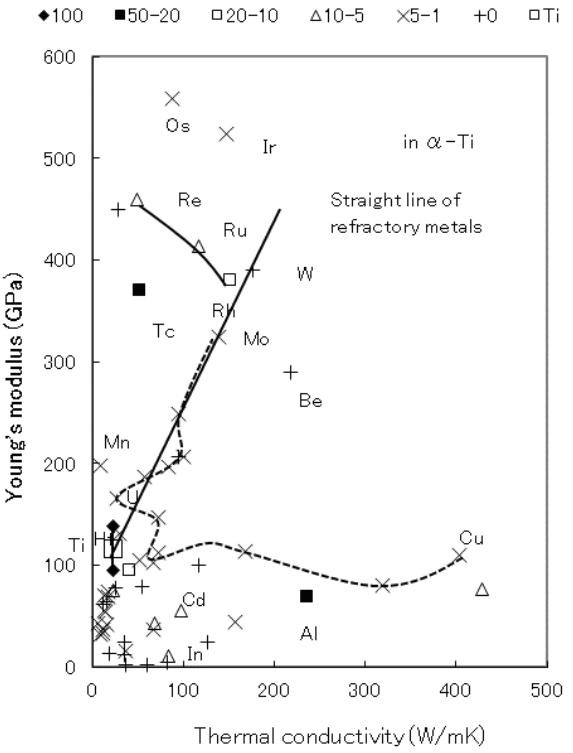

Fig. 13-15 – Solubility of elements in α-Ti shown on the TC-YM diagram

α-Ti adopts an hcp structure. The elements with the same hcp structure as α-Ti – Hf and Zr – show 100 pct solubility.

The elements with very high Young's modulus – Ru and Re – show considerable solubility in α-Ti in spite of their locations far from Ti, because they possess the same hcp structure.

The most remarkable thing is that Al shows considerable solubility in both α-Ti and β-Ti. Al is an fcc-structured element and undergoes no allotropic

transformation. The fact that Al has large solubility in both α-Ti (hcp structure) and β-Ti (bcc structure) is an exception of the solubility rule displayed on the TC-YM diagram. Al is surrounded by elements which show small solubility. This is a fortunate coincidence. Al is one of the most important strengthening elements for Ti alloys and is contained in most of the Ti alloys.

Mn and U show small solubility, because they have no hcp structures in their allotropic transformations.

Fig. 13-16 shows the distribution of solubility of elements in Mg on the TC-YM diagram.

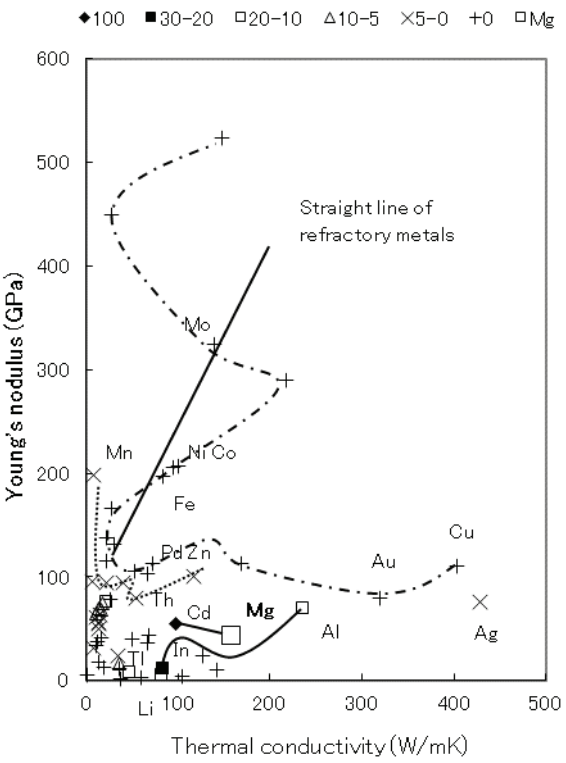

Fig. 13-16 – Solubility of elements in Mg shown on the TC-YM diagram

Mg is located at a position of lower thermal conductivity than Al, and therefore, it dissolves fewer elements than Al. Mg is a genuine hcp-structured element. Cd with the same hcp structure shows 100% solubility.

Al shows large solubility in Mg, because Mg is located near Al on the TC-YM diagram.

Fig. 13-17 shows the distribution of solubility of elements in Zn on the TC-YM diagram.

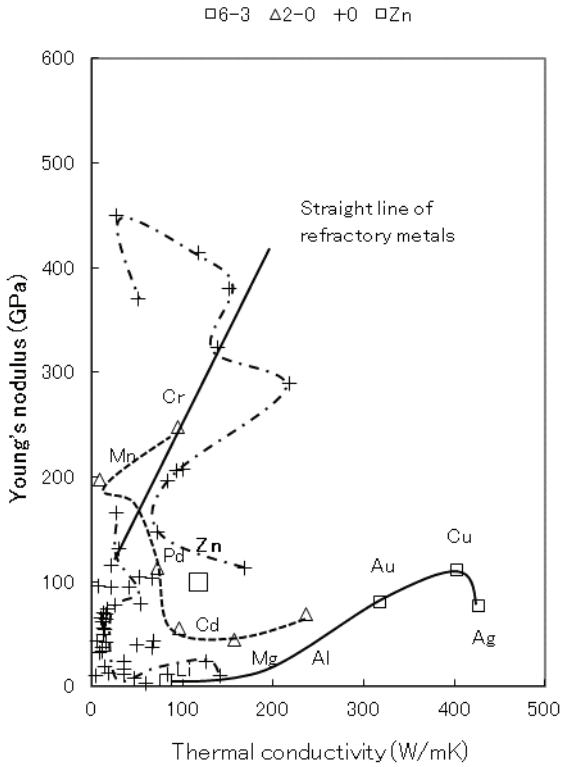

Fig. 13-17 – Solubility of elements in Zn shown on the TC-YM diagram

Zn shows an hcp structure, low thermal conductivity and low Young's modulus; therefore, Zn has small capacity to dissolve other elements. Only the elements in the neighborhood show some solubility. Nevertheless, Mn shows small solubility in Zn.

Fig. 13-18 shows the solubility of elements in Sn on the TC-YM diagram.

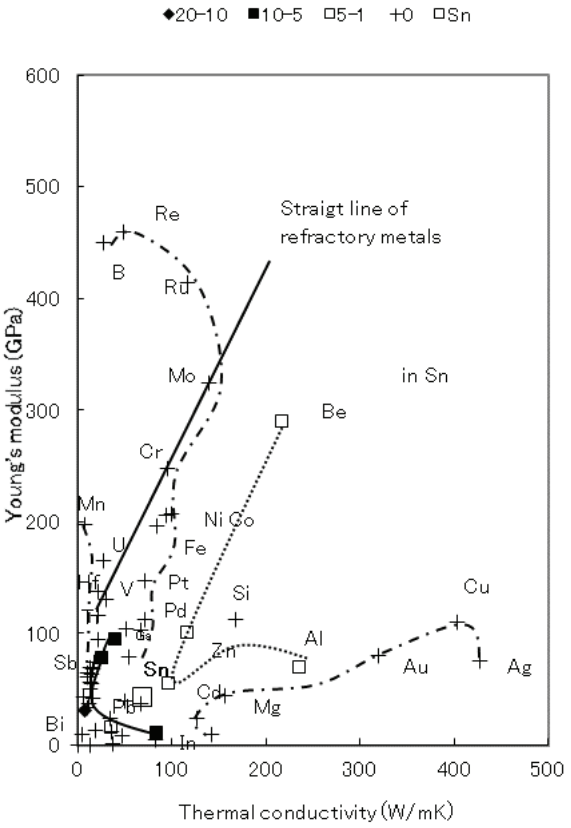

Fig. 13-18 – Solubility of elements in Sn shown on the TC-YM diagram

Sn is a complicated metal. Sn adopts a diamond structure at low temperatures (α-Sn, grey tin), and transforms to the body-centered tetragonal structure at 286K (13°C) (β-Sn, white tin). Therefore, Sn shows a tetragonal structure at room temperature. Indium also adopts a tetragonal

structure. Sn is a metal of low thermal conductivity and low Young's modulus. Therefore, it dissolves only the elements in the neighborhood.

Why does Sn adopt a diamond structure at low temperature? Ge of the diamond structure is located just above Sn on the diagram. Si, Ge and Sn form a line of the diamond structure on the diagram.

Sn belongs to group 14 of the periodic table. The elements of the same group – C, Si, and Ge – adopt diamond structures. Therefore, it can be said that Sn also adopts a diamond structure. But Pb, the last element of group 14, is a genuine fcc metal. The ordering of the periodic table fails. Pb adopts an fcc structure, because it lies on the curve of the fcc metals in the TC-YM diagram. The orderings of the crystal structures can be explained only by the TC-YM diagram.

Fig. 13-19 shows the solubility of elements in U on the TC-YM diagram.

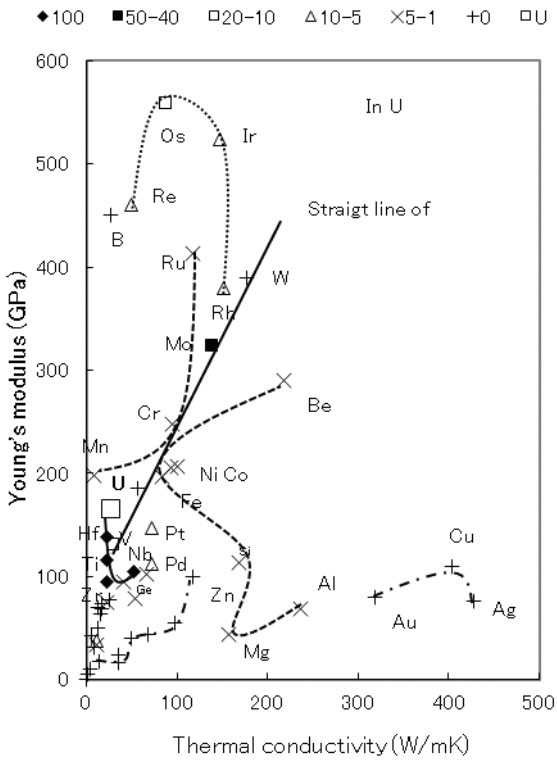

Fig. 13-19 – Solubility of elements in U shown on the TC-YM diagram

U is located at the lowest thermal conductivity and medium Young's modulus. Probably due to its position on the diagram, it undergoes multiple allotropic transformations, shortly, the α-phase (orthorhombic) is stable up to 933K (660°C), the β-phase (tetragonal) is stable from 933K (660°C) to 1033K (760°C), and the γ-phase (bcc) is stable from 1033K (760°C) to the melting point 1405K (1132°C).

The bcc-structured γ-phase, the highest temperature phase, dissolves the elements that are largest. Therefore, the elements of bcc structures – Hf, Ti, Zr, and Nb – show large solubility in U. The elements of low thermal conductivity commonly show small solubility in U regardless of the Young's modulus.

Mn has only small solubility in U, probably because the bcc phase of Mn is in a very narrow temperature range.

Fig. 13-20 shows the solubility of elements in Mn on the TC-YM diagram.

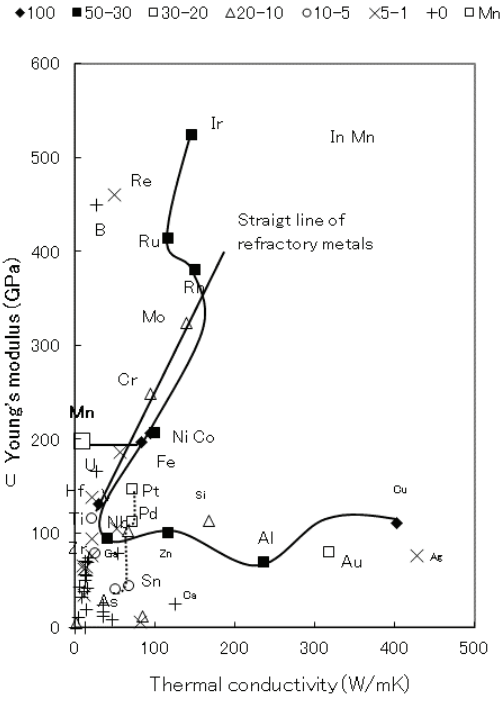

Fig. 13-20 – Solubility of elements in Mn shown on the TC-YM diagram

The α-phase (quasi-bcc structure) of Mn is stable below 1015K (742°C). The β-phase (complicated cubic structure) is stable between 1015K (742°C) and 1368K (1095°C). The γ-phase (fcc structure) is stable between 1368K (1095°C) and 1407K (1134°C). The δ-phase (bcc structure) is stable between 1407K (1134°C) and the melting temperature 1518K (1245°C).

The pattern is similar to those of Ni and Cu in Figs. 13-10 and 13-11. Mn behaves like an fcc-structured element as a base metal for alloying.

U does not resolve into Mn, because U does not have an fcc structure in its allotropic transformations.

In this way, Mn has versatility in crystal structures and solubility behaviors. It stems from its unique location on the TC-YM diagram. Its very low thermal conductivity loosens the bonding of the lattice and makes it easy to transform to other crystal structures. (Its melting point is relatively low.) As a result, Mn dissolves both bcc-structured metals and fcc-structured metals to a large extent. Mn could be called “the amphibious element”.

But Mn has not been used as a base metal for alloying. Its very low thermal conductivity and the resulting multiple allotropic transformations are not applicable for practical use as a base metal.

Fig. 13-21 shows the solubility of elements in Ge on the TC-YM diagram.

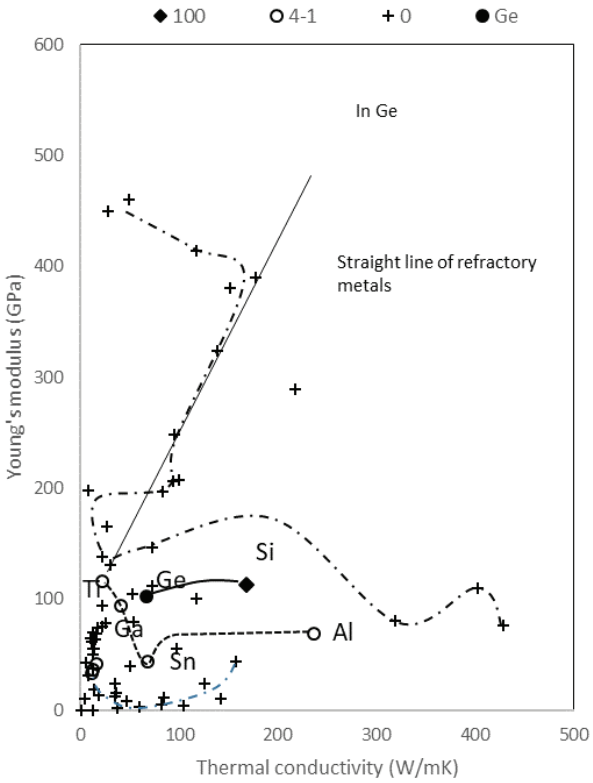

Fig. 13-21 – Solubility of elements in Ge shown on the TC-YM diagram

Ge is a semi-conductor element and adopts a diamond structure. Only Ge and Si among elements adopt diamond structures. Therefore, very limited soluble elements in these elements are expected. Si shows 100 pct solubility, because it has the same crystal structure as Ge. Other elements – Ti, La, Al, Ga, Sn, Ce and Nb – show a few pct solubility. They are located near Ge.

Fig. 13-22 shows the solubility of elements in Si on the TC-YM diagram.

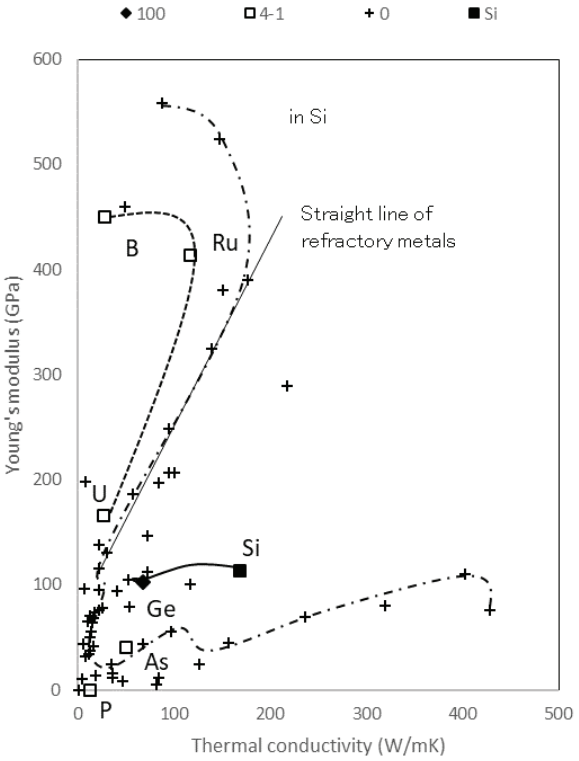

Fig. 13-22 – Solubility of elements in Si shown on the TC-YM diagram

Ge shows 100 pct solubility in Si, because it's the same crystal structure as Si. The elements – B, P, As, Ru and U – show a few pct solubility. They have miscellaneous crystal structures except for Ru. They lie on two kinds of curves.

13.3 Summary

The new rules about the solubility of elements in metals concluded in this chapter are as follows:

1. The crystal structure must be the same as the matrix metal to have large solubility.

2. The elements in the neighborhood of the matrix metal on the TC-YM diagram have large solubility. It means that the binding force of atoms represented by the Young's modulus and the configuration of electrons represented by the thermal conductivity must be similar between the solute atoms and the matrix metals.

3. The capacity of the matrix metals to dissolve other elements decreases with its decreasing Young's modulus and thermal conductivity.

The trends in the crystal structures are followed also after the allotropic transformations. The elements lying between the lowest end of the straight line of refractory metals and the left-most end of the curve of alkali metals tend to transform to bcc structures.

The bcc structure can be thought as the high temperature phase of elements. For refractory metals, their bcc structures are stable down to low temperature, because their binding forces are strong. For Ti, Zr and lanthanide, the bcc structure is unstable at low temperature. Consequently, these elements adopt other structures at low temperature. Room temperature is a high temperature for alkali metals, so they adopt bcc structures at room temperature.

The elements Fe and Co near Ni, and the elements with low thermal conductivity – Mn, Pu, Ce, and La – transform to fcc structures.

The elements with low thermal conductivity – Np, Mn, U, Pu, Ce, La, and Sr – show multiple transformations which transform more than twice and finally to bcc structures.

The conclusions obtained in the previous study [4] that the same crystal structure as the matrix metal and the location near the matrix metal are necessary conditions for large solubility were confirmed to be valid also in the elements which undergo allotropic transformation.

The elements which transform to bcc structures show large solubility in bcc-structured matrix metals. In the same way, the elements which transform to fcc structures show large solubility in fcc-structured matrix metals.

Mn is located in the low thermal conductivity region on the TC-YM diagram, and undergoes multiple transformations. It shows large solubility in both bcc-structured and fcc-structured matrix metals.

This is the reason why the elements with very different thermal conductivity to each other – Cu and Mn – form an unlimited solid solution. Very low thermal conductivity induces the multiple transformations in the elements and the multiple transformation enables an element to be soluble in other elements with high thermal conductivity. The elements of low thermal conductivity expand the application field owing to their multiple transformations.

References

1. D. R. Askeland, The science and engineering of materials, 3rd ed., PWS, Boston, 1994, p. 240.
2. E. C. Subbarao and W. E. Wallace, Science and technology of rare earth materials, Academic Press, New York, 1980, p. 53.
3. K. N. R. Taylor and M. I. Darby, Physics of rare earth solids, Chapman and Hall, 1972, p. 65.
. Y. Mae, What the Darken-Gurry plot means about the solubility of elements in metals, Metall. Mater. Trans. A Vol. 47, Dec. 2016, pp. 6498-6506.

14. COMMERCIAL ALLOYS (WHY THERMAL CONDUCTIVITY AND YOUNG'S MODULUS ARE IMPORTANT)

14.1 Effects of Young's modulus and thermal conductivity on the commercial alloys

As shown in Fig. 4-2, the gulf elements show a good combination of thermal conductivity and Young's modulus. Be has high Young's modulus and good thermal conductivity. But it adopts an hcp structure, because it is located far from both the straight line of refractory metals and the curve of fcc metals. The metals of hcp structures are difficult to be worked due to their limited slip systems. Furthermore, Be is toxic and expensive. Its abundance is small due to its large neutron multiple number, as explained in Chapter 3. Therefore, Fe, Ni and Co are the practical elements which have the highest Young's modulus and highest thermal conductivity among the gulf elements.

Fig. 14-1 shows the heat flow at the contact surface between the work and the tool in machining. The generated heat must be dissipated to avoid adhesion between them.

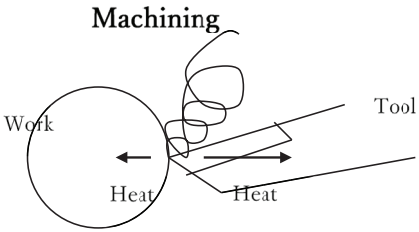

For good machinability, both the work and the tool must have good thermal conductivity.
WC (tungsten carbide) cutting tool has good thermal conductivity. The work also must have good thermal conductivity.

Fig. 14-1 – Heat flow at the machining of materials

As shown in Fig. 14-2, the high Young's modulus and the high thermal conductivity are advantageous to many properties. [1]

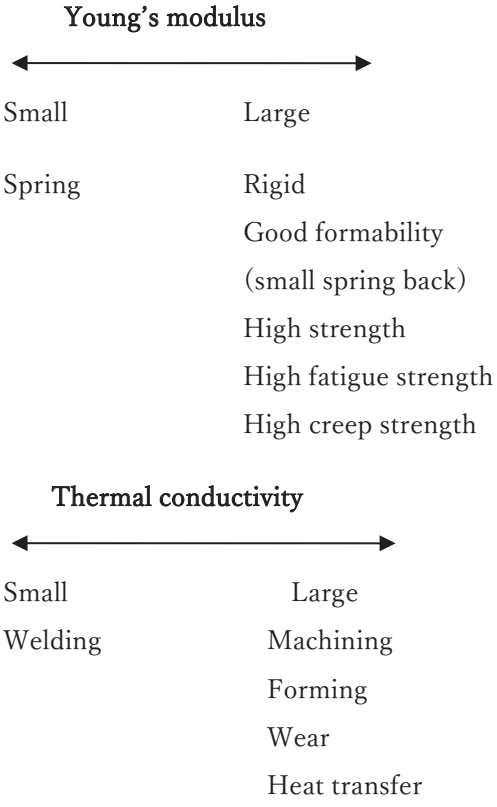

Fig. 14-2 – Upper side: The Young's modulus dependence of the material properties
Lower side: The thermal conductivity dependence of the material properties

From this point of view, Fe is a good material for many applications. The Young's moduli and thermal conductivities of the commercial alloys are shown in Fig. 14-3.

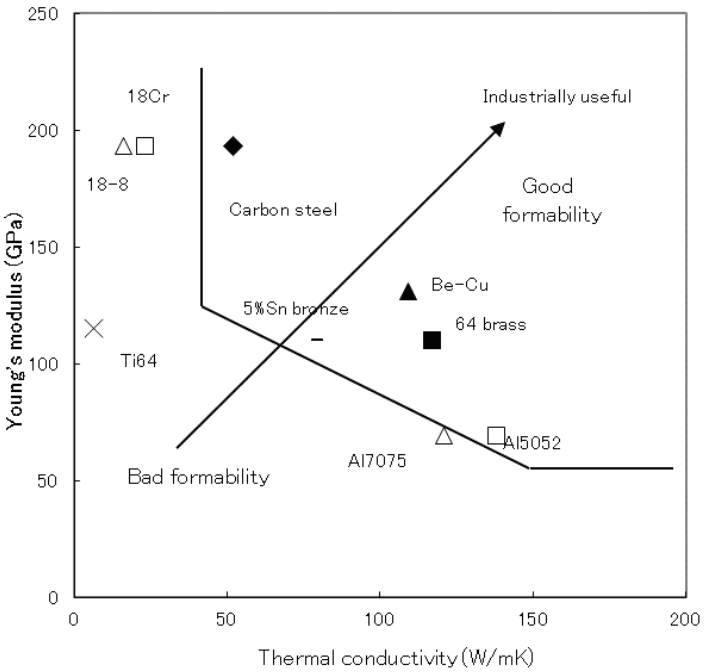

Fig. 14-3 – Distribution of the commercial alloys and the boundary between good formability and low formability on the TC-YM diagram

The alloys of good formability are located in the high Young's modulus and the high thermal conductivity region. The Young's modulus does not change by alloying, but the thermal conductivity changes greatly by alloying. For alloy development, it is important not to lower the thermal conductivity of the alloy.

To avoid adhesion between the material and the tool, the heat conductivity of both the material and the tool must be good to dissipate the heat generated

at the contact surface.

Practically, carbon steels, bronze, brass, and aluminum have good formability mainly because of large thermal conductivity. In contrast, stainless steels and Ti alloys have poor formability mainly because of their low thermal conductivity. The recognition of thermal conductivity and Young's modulus is important to understand the properties of the alloys and to develop the commercial alloys.

The properties of various commercial alloys will be explained in terms of thermal conductivity and Young's modulus below. It will provide new viewpoints about the alloys to the readers.

14.2 Alloying elements in the commercial alloys

It may be useful to know how the alloying elements in the existing alloys distribute on the TC-YM diagram.

(1) Fe alloys

Fig. 14-4 shows the alloying elements in the commercial alloys of Fe.

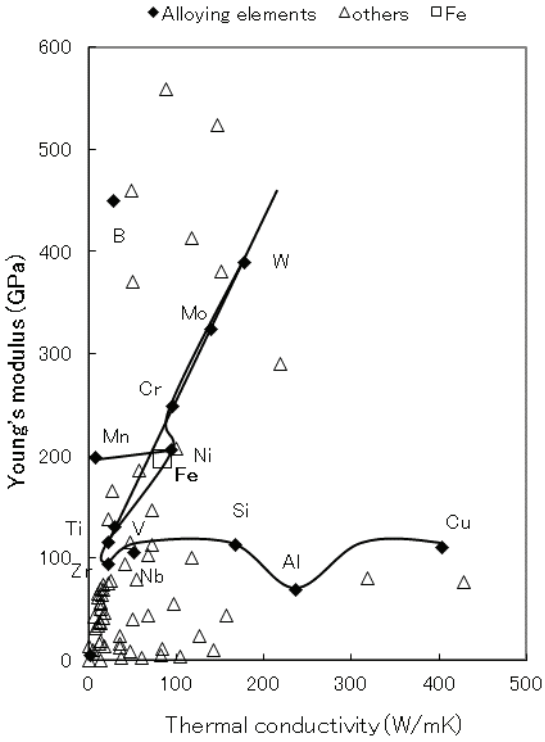

Fig. 14-4 – Alloying elements in the commercial alloys of Fe

It shows a similar pattern to that of the solubility of elements in Fe. As a result of a good combination of thermal conductivity and Young's modulus, Fe has a large abundance in the universe, and good formability, as shown in Figs. 3-3 and 14-2, respectively.

Fe is located near the straight line of refractory metals and Ni. Therefore, Fe adopts a bcc structure and transforms into an fcc structure at high temperature, as shown in Fig. 2-2. Both the bcc structure and the fcc

structure give good formability due to their many slip systems. Moreover, the transformation brings about many advantages.

From the same reason, Fe has many alloying elements. Solution hardening is obtained by many alloying elements. It has been proved that solution hardening is brought about by the same mechanism of diffusion of elements in Fe, as shown in Fig. 12-12. The greatest method of hardening of Fe is martensitic transformation. It also has been proved that martensitic transformation is controlled by the diffusion of elements in the γ-phase of Fe, as shown in Figs. 9-9 and 9-10.

Moreover, Fe has a medium melting temperature similar to other gulf elements, as shown in Fig. 4-3. It is convenient for the smelting of iron ores. The medium melting temperature gave a low temperature of direct reduction of iron and enabled the ancient people to get wrought iron. In this way, Fe is endowed with many fortunate coincidences.

This author believes that the best example of the application of materials science to the metal industry is the development of the Bessemer converter with a basic lining invented by Sidney Gilchrist Thomas. He succeeded to eliminate phosphorous in iron in the Bessemer converter. It is a very intellectual story. It has no relationship with this author's TC-YM diagram but he would like to point out its importance.

(2) Cu alloys

Fig. 14-5 shows the alloying elements in the commercial alloys of Cu.

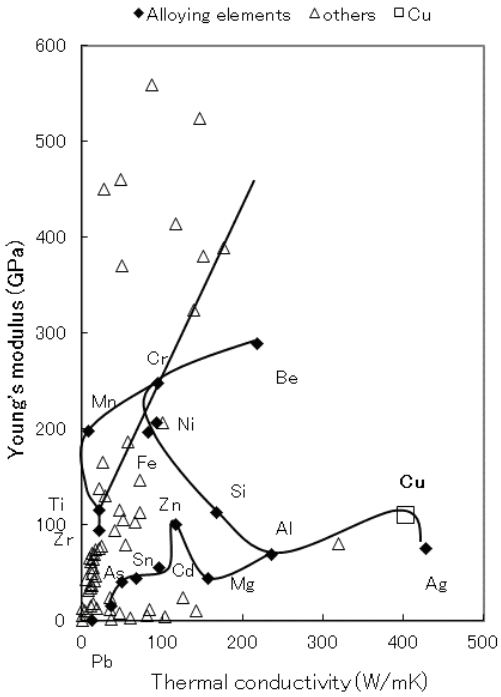

Fig. 14-5 – Alloying elements in the commercial alloys of Cu

It shows a similar pattern to that of the solubility of elements in Cu. The elements of the highest Young's modulus and those of low thermal conductivity are not used.

The greatest characteristic of Cu is in its high conductivity. It is located at the right-most side of the diagram. It has been proved that Cu dissolves many elements due to its high conductivity, as shown in Fig. 13-12.

Cu is included in the gulf elements together with Fe. Therefore, Cu shows similar characteristics to Fe in many points such as atomic radius, melting point, etc. Until now it has been considered that Cu is quite a different metal from Fe, but it is not true. Cu is rather a similar element to Fe.

Cu lies on the curve of fcc metals, and adopts an fcc structure; therefore, it shows good formability. Solution hardening is recognized, as shown in Fig. 12-2. But solution hardening degrades conductivity. Therefore, precipitation hardening is used often in Cu alloys because it does not degrade conductivity so much. Solution treatment before aging is necessary for precipitation hardening. In this point, the solubility of elements in Cu is also important for precipitation hardening.

Cu is used as a conductor of electricity. Therefore, the electrical resistivity increase by the impurities and alloying elements is important. It is found that the electrical resistivity increase of the solvent metal by the solute atoms is proportional to the square of the difference in the valence. This is referred to as the Linde law. [2] Fig. 14-6 shows the resistivity increase of Cu by the impurities as a parameter of the group number in the periodic table.

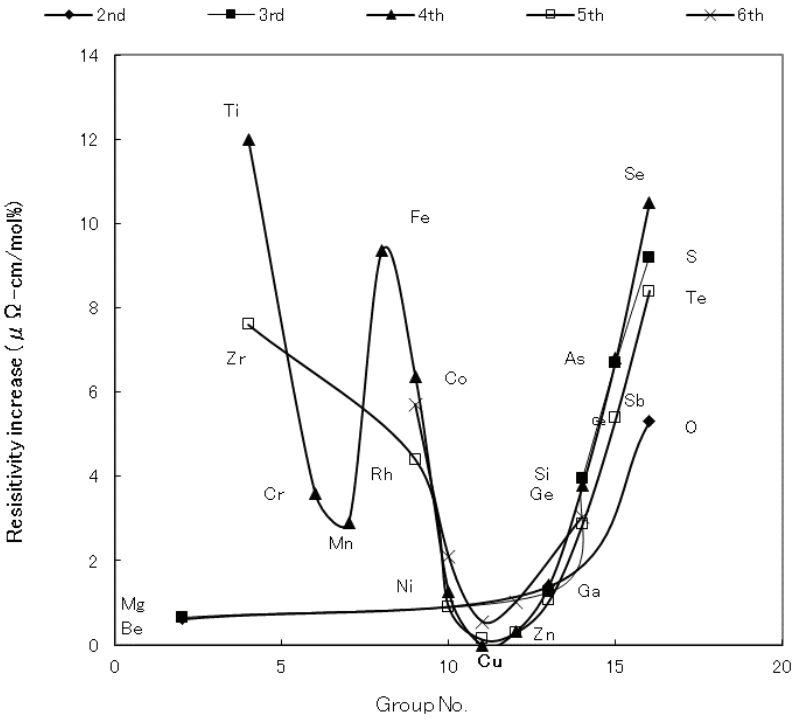

Fig. 14-6 – Resistivity increase of Cu by the impurities as a parameter of the group number

The Linde law is valid in the 4th period, and the same tendency is recognized in other periods. Mg and Be are exceptions.

Fig. 14-7 shows the distribution of the resistivity increase of Cu by the impurity elements on the TC-YM diagram.

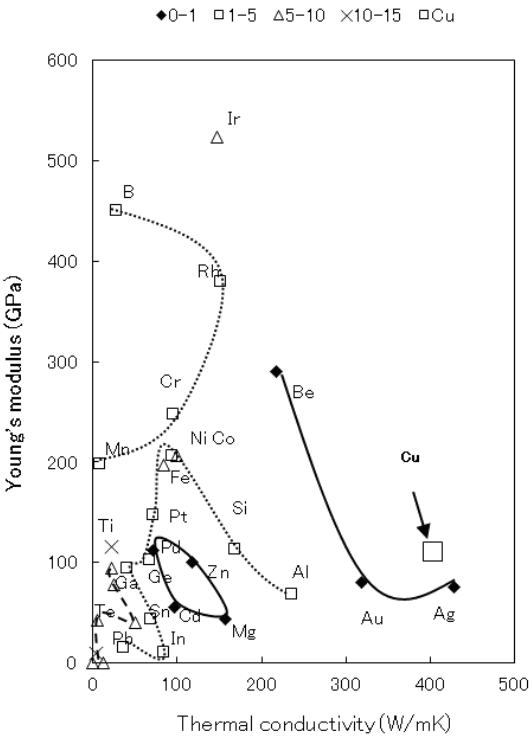

Fig. 14-7 – Distribution of the resistivity increase of Cu by the impurity elements shown on the TC-YM diagram

The elements near Cu – Ag, Au, and Be – show a small resistivity increase. Moving far from Cu, the resistivity increase increases. But, the elements in the area of intermediate thermal conductivity – Mg, Zn, Pd, and Cd – show a small resistivity increase similar to the elements near Cu. Here, an idea is inspired. If an intermetallic compound which has similar values of thermal conductivity and Young's modulus to these elements is added into Cu, what will happen? Is there no chance of strengthening Cu with a minimum

resistivity increase?

The resistivity increase of metals is considered to be caused by the lattice distortion of the matrix metals. The lattice distortion is caused by the repulsive force between matrix atoms and foreign atoms. Therefore, a correlation between the resistivity increase and diffusion coefficients can be speculated.

Fig. 14-8 shows the correlation between the resistivity increase of Cu and the diffusion coefficients of elements in Cu at 1273K.

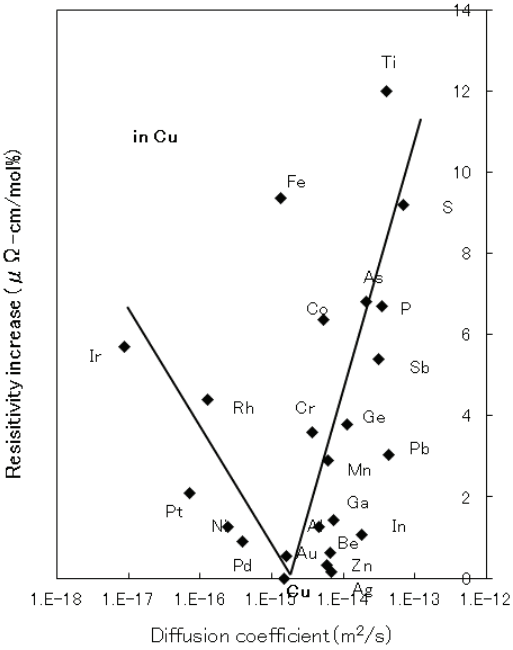

Fig. 14-8 – Correlation between the resistivity increase of Cu and the diffusion coefficients of elements in Cu at 1023K

A moderate correlation can be seen. The elements – Ag, Zn and Be – show an exceptionally small resistivity increase despite their considerable difference in the diffusion coefficient. In contrast, Fe shows a very large resistivity increase despite its small difference in the diffusion coefficient. Its magnetism can be involved.

Except for these elements, the repulsive force theory is valid also in the resistivity increase.

(3) Al alloys

Fig. 14-9 shows the alloying elements in the commercial alloys of Al.

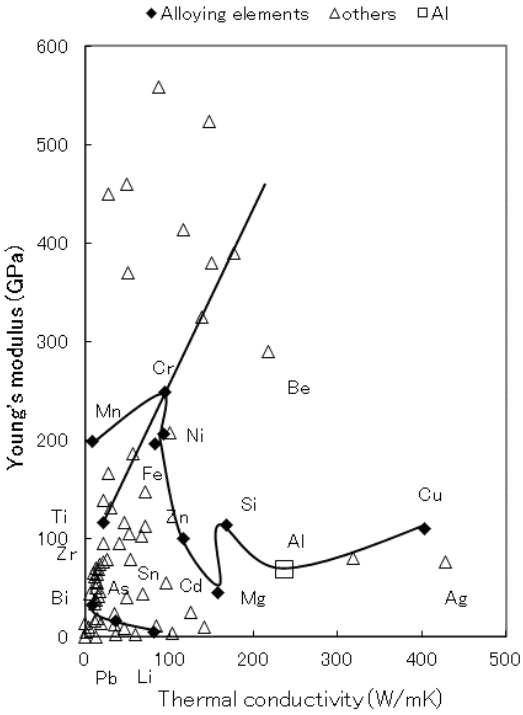

Fig. 14-9 – Alloying elements in the commercial alloys of Al

Al has smaller thermal conductivity than Cu with a similar Young's modulus. Therefore, it shows fewer soluble elements than Cu, as shown in Fig. 13-13. Alloying elements are also fewer than Cu.

Al lies on the curve of fcc metals, and adopts an fcc structure, and therefore, it shows good formability. Solution hardening is not large because of its low Young's modulus. Precipitation hardening is used for large strengthening. Solution treatment before aging is necessary for precipitation hardening. In this point, the solubility of elements in Al is important for precipitation

hardening also.

Precipitation hardening was first discovered in Al by Wilm in1906. In 1911, the first duralumin (Al-3.75%Cu-0.5%Mg-0.5%Mn) was invented.

The dilemma of Al alloys is a conflict between strength and corrosion resistance. As shown in Figure 5.2, Al has low electrode potential, and Cu has high electrode potential. The precipitates containing Cu act as the cathodic points and corrode the Al matrix.

In contrast to this, the Al alloys with the precipitates of Mg_2Si are corrosion resistant as well as pure Al.

Mg and Si have electrode potentials as low as Al, as shown in Fig. 5-2.

Al is also used as a conductor of electricity. Fig. 14-10 shows the resistivity increase of Al by the impurity elements as a parameter of the group number.

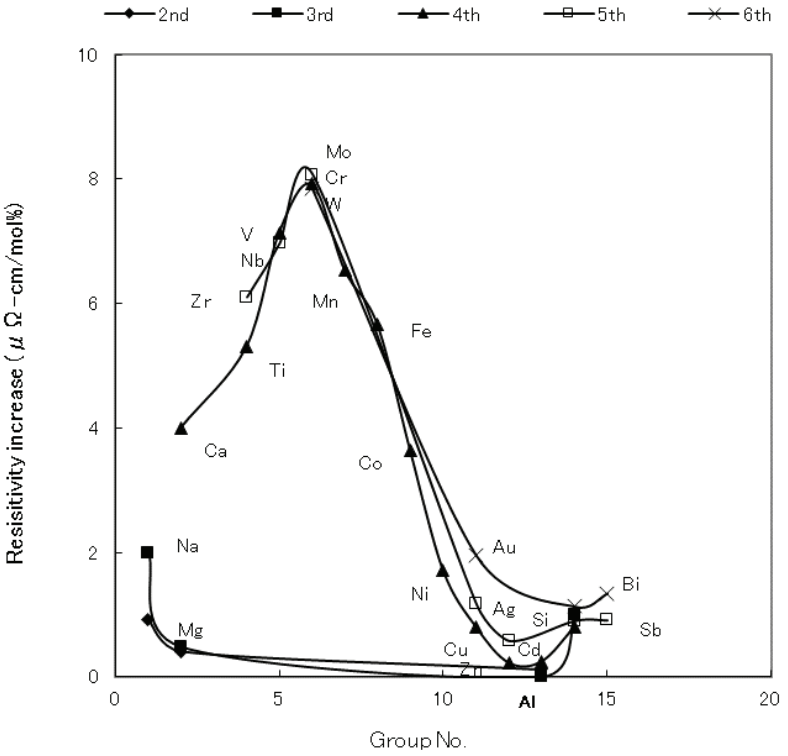

Fig. 14-10 – Resistivity increase of Al by the impurities as a parameter of the group number

The Linde law is valid in the 3rd period, and the same tendency is recognized in other periods. Fig. 14-11 shows the distribution of the resistivity increase of Al by the impurity elements on the TC-YM diagram.

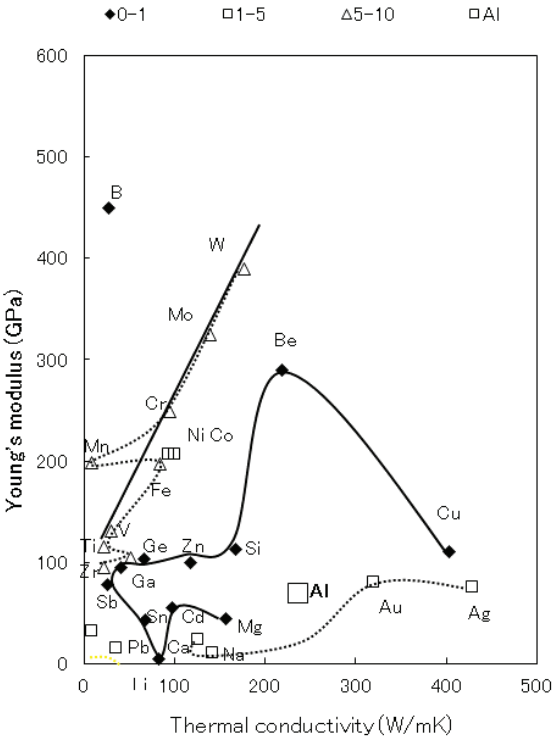

Fig. 14-11 – Distribution of the resistivity increase of Al by the impurity elements shown on the TC-YM diagram

The elements surrounding Al – Cu, Be, Si, Zn, Ge, Ga, Sb, Li, Cd, and Mg – show a small resistivity increase. The elements on the right and lower side of Al – Ca, Na, Au, and Ag – show a larger increase. The elements on the straight line of refractory metals and those along it show the largest increase.

Fig. 14-12 shows the correlation between the resistivity increase of Al and the diffusion coefficients of elements in Al at 773K.

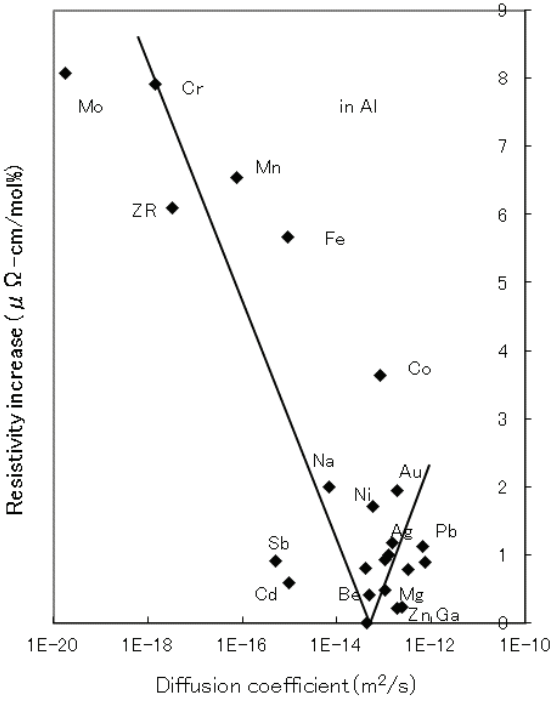

Fig. 14-12 – Correlation between the resistivity increase of Al and the diffusion coefficients of elements in Al at 773K

A moderate correlation can be seen also in Al. The elements – Zn and Ga – exceptionally show a small resistivity increase despite their considerable difference in diffusion coefficient. The elements – Fe and Co – show a very large resistivity increase despite their small difference in diffusion coefficient. Except for these elements, the repulsive force theory is valid in the resistivity increase of Al.

(4) Ni alloys

Fig. 14-13 shows the alloying elements in the commercial alloys of Ni.

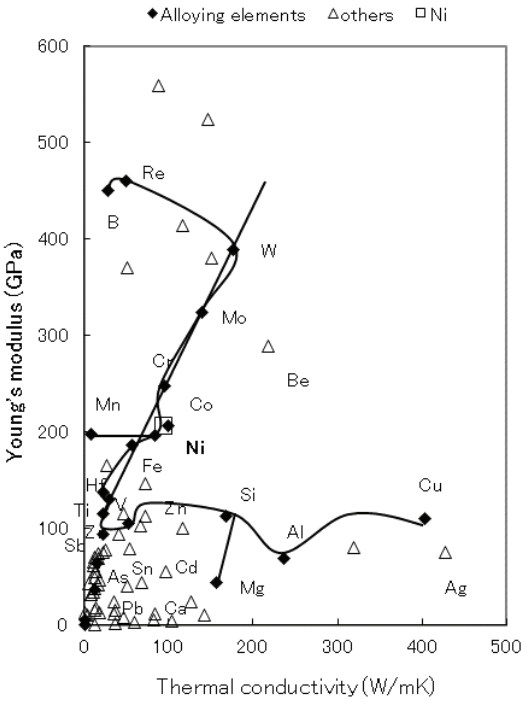

Fig. 14-13 – Alloying elements in the commercial alloys of Ni

Ni lies on the curve of fcc metals, and adopts an fcc structure at all temperatures. Additionally, Ni is located just on the right side of Fe, and near the center of the diagram. Therefore, it shows excellent characteristics in a wide range. Ni shows good corrosion resistance and good heat resistance brought about from the good combination of the thermal conductivity and the Young's modulus.

Ni undergoes no allotropic transformation, and therefore, it shows no hardenability. In place of this, it forms a gamma prime phase $Ni_3(Al, Ti)$ which shows inverse temperature dependence of strength at high temperatures. Ni is the only metal resistant to the alkali. Mo is added for further improvement.

Many alloys have been developed until now for both corrosion resistant use and heat resistant use.

(5) Pb alloys

Fig. 14-14 shows the alloying elements in the commercial alloys of Pb.

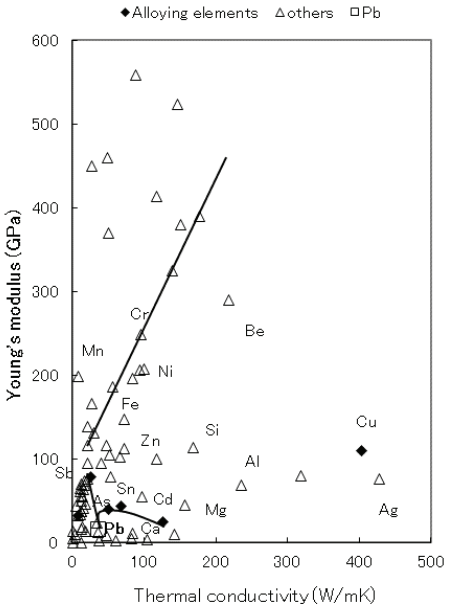

Fig. 14-14 – Alloying elements of the commercial alloys of Pb

Pb lies on the curve of fcc metals. But its thermal conductivity is much lower than that of Al. Therefore, its capacity to dissolve other elements is very small. Alloying elements are limited in the elements in the neighborhood. Pb-Ca alloy has been developed in place of Pb-Sb alloys for maintenance-free batteries for automobiles. Pb and Ca are far away from each other on the periodic table. But Ca is relatively near to Pb on the TC-YM diagram. It is acknowledged that Ca has some solubility in Pb, judging from the position of Ca on the TC-YM diagram.

Pb-Sb alloys were used as grid metals for automobile batteries. The Pb-Sb alloy system is a eutectic system and provides good castability. Fine grids can be cast. But Sb has low hydrogen overvoltage, and generates hydrogen gas by self-discharge. In contrast to this, Ca has high hydrogen overvoltage. Therefore, Pb-Ca alloys are developed for the same use. But the Pb-Ca system is a peritectic system and the castability is not good. Therefore, it is produced by ingot casting and rolling.

(6) Mg alloys

Fig. 14-15 shows the alloying elements in the commercial alloys of Mg.

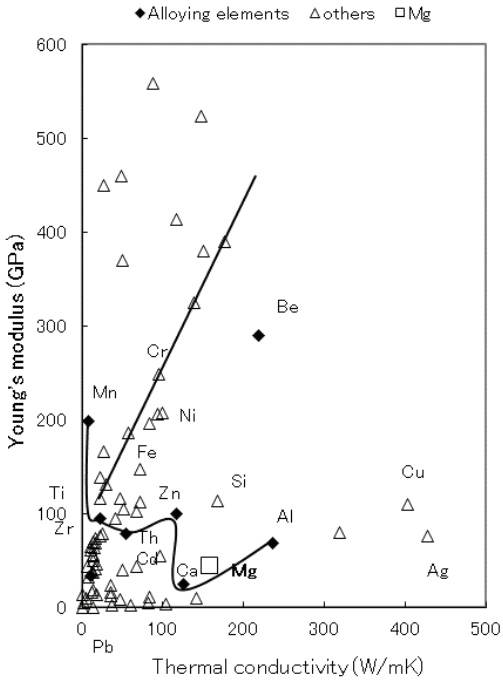

Fig. 14-15 – Alloying elements in the commercial alloys of Mg

Mg is located off the curve of fcc metals and in the region of low Young's modulus and medium thermal conductivity. It is the region of the hcp structure, and therefore, Mg adopts an hcp structure.

One of the defects of Mg is corrosion resistance. As shown in Fig. 5-2, Mg belongs to the element group of the lowest electrode potential. The elements – Cu, Fe, and Ni – degrade the corrosion resistance of Mg. As shown in Fig. 5-2, they show large electrode potentials. As shown in Figure 13.16, they have no solubility in Mg. As a result, they precipitate as particles in the

matrix of Mg. These particles act as the cathodic points and corrode the matrix of Mg. In practice, the contents of these elements are strictly limited.

Mg has an hcp structure, and therefore, it dissolves the lanthanides which adopt hcp structures. Mg dissolves the lanthanides of hcp structures – Gd, Tb, Dy, Ho, Er, Tm, and Lu considerably, and Sm (rhombohedral) and Yb (fcc) a little, while it does not dissolve other lanthanides of double hexagonal structure – La, Ce, Pr, Nd, and Pm, and an element of bcc structure – Eu.

As shown in Fig. 8-1, Mg shows a small neutron absorption cross-section, and was used as a cladding material for nuclear fuel, called Magnox (Al: 1%, Be<0.05%, Ca<0.1%, Mg: balance) in the Calder-Hall type, carbon dioxide cooled nuclear reactor. This alloy was the first alloy that this author melted.

(7) Sn alloys

Fig. 14-16 shows the alloying elements in the commercial alloys of Sn.

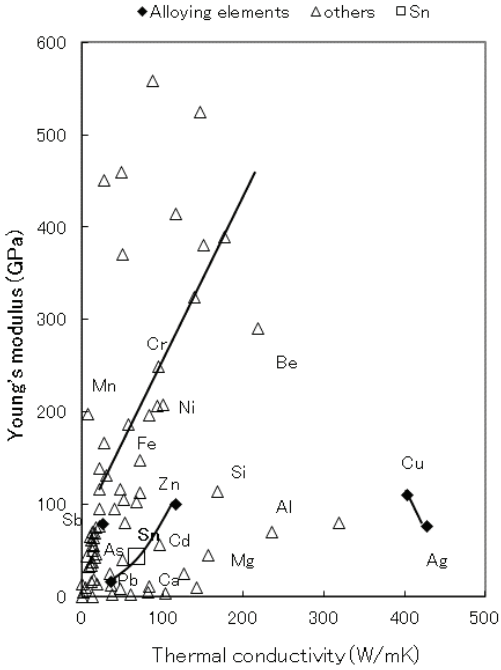

Fig. 14-16 – Alloying elements in the commercial alloys of Sn

Sn is located in the region of a little larger thermal conductivity than Pb. It dissolves the elements in the neighborhood. Sn forms a eutectic system with Pb. It has been used for a long time as solder alloys. But recently, Pb is disliked from the viewpoint of environment, and Sn-based solder alloys have been developed. They contain Zn, Al, Ag, Cu, and Bi.

(8) Ti alloys

Fig. 14-17 shows the alloying elements in the commercial alloys of Ti.

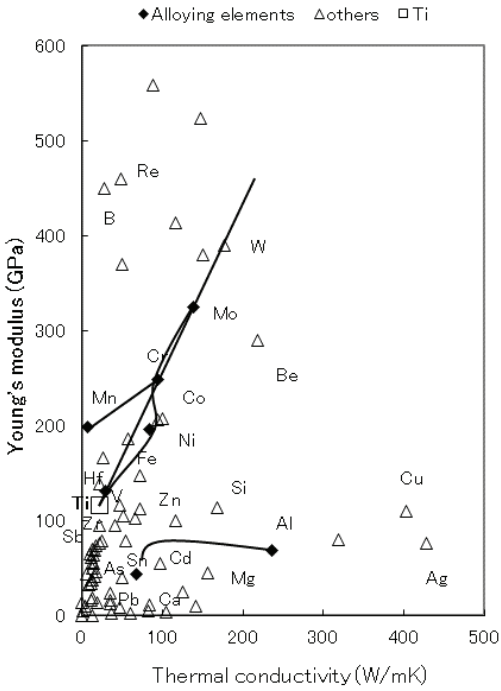

Fig. 14-17 – Alloying elements in the commercial alloys of Ti

Ti is located in the region of low thermal conductivity and low Young's modulus, and at the lower end of the straight line of refractory metals.

As shown in Figs. 13-9 and 13-15, Ti dissolves most of the elements. The most popular alloy is Ti-64 (Ti-6%Al-4%V). Al is soluble in α-Ti, and V is soluble in β-Ti. V is the nearest element to Ti among the elements on the straight line of refractory metals. It is understandable why V was selected as the first β-phase stabilizing element. The farther element – Mo – is a good strengthening element, but it is difficult to be alloyed in Ti because of its

high melting temperature.

Ti is on the extension of the straight line of refractory metals, and therefore, it can be strengthened in spite of its low Young's modulus and low thermal conductivity. Due to low thermal conductivity, wear resistance and machinability are not good. It is very adhesive in both cases. To avoid heat generation at the contact surfaces, low sliding speed is necessary.

Due to its location on the TC-YM diagram, Ti adopts an hcp structure. The hcp structure has large anisotropy in the crystal deformation. In sheet rolling, Ti forms a sharp texture and gives rise to a high r-value. It means that the reduction in thickness of the sheet is difficult and the bendability of the sheet is deteriorated, because in the bending, the deformation is in a plane-strain condition; therefore, the reduction in the thickness direction is essential.

To satisfy these conditions, Ti alloy sheets must be rolled in the temperature range of the β-phase (bcc structure).

Fig. 14-18 shows the effects of the rolling temperature on the tensile properties of Ti-6Al-4V sheets. [3]

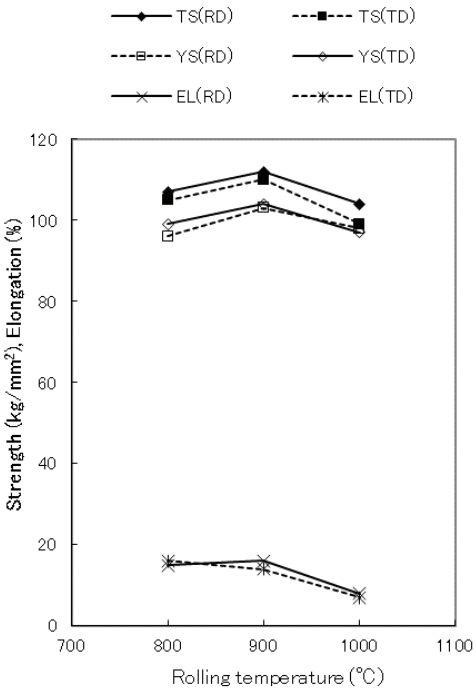

Fig. 14-18 – The effects of rolling temperatures on the tensile strength of Ti64 sheets

The rolling temperature was strictly limited. Ti64 shows all of the β-phase (bcc structure) at 1000℃. It shows 50% of the β-phase (bcc structure) and 50% of the α-phase (hcp structure) at 900℃. It shows almost 100% of the α-phase at 800℃.

In the figure, TS means tensile strength, YS means yield strength, EL means elongation, RD means rolling direction, and TD means transverse direction, respectively.

The sheets rolled at 900℃ without the lowering of temperature during

rolling, show the highest strength and moderate elongation. The most important thing is not to increase the r-values of the sheets. Fig. 14-19 shows the effects of rolling temperature on the r-values of the sheets.

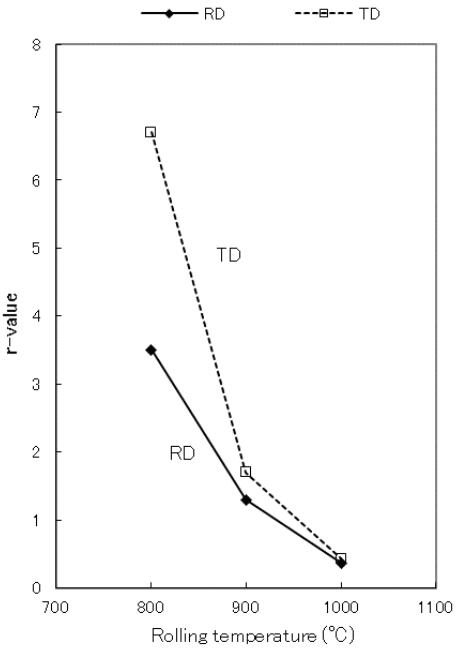

Fig. 14-19 – The effects of rolling temperatures on the r-values of Ti64 sheets

The sheets rolled at 800℃ (100% α-phase) show large r-values (anisotropic). The sheets rolled at 900℃ (50% β-phase) show r-values at nearly one (isotropic). The sheets rolled at 1000℃ (100% β-phase) show r-values smaller than one (anisotropic). High r-values mean difficulty in the reduction of the thickness at bending. In order to obtain sheets with good bendability, the sheets must have r-values near one. Therefore, the rolling temperature is strictly limited to about 900℃.

Where does the dependence of r-values on the rolling temperatures come from?

Fig. 14-20 shows the pole figures of the (0001)-plane of the Ti64 sheets rolled at 800, 900, and 1000°C, respectively.

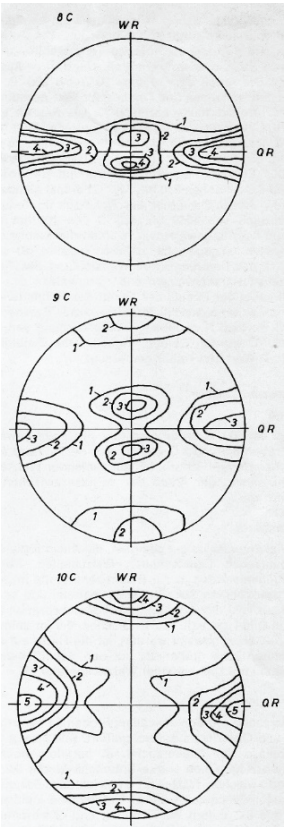

Fig. 14-20 – Pole figures of the (0001)-plane of the Ti64 sheets rolled at 800 (above), 900 (middle), and 1000°C (below), respectively

The sheets rolled at 800°C have the (0002)-plane of the hcp structure in the thickness and transverse directions. The (0002)-plane in the thickness direction gives large r-values. The sheets rolled at 900°C have the (0002)-plane in the rolling and transverse directions in addition to that in the thickness direction. These three concentrations of (0002)-planes are essential in order to obtain the isotropic sheets. The sheets rolled at 1000°C have the (0002)-plane in the rolling and tangential direction and none in the thickness direction. It leads to an inverse anisotropy and the microstructures are coarsened.

What is the mechanism of the formation of the (0002)-plane in the rolling and tangential direction?

It is impossible to measure the textures of the β-phase (bcc structure) at high temperatures. But it is speculated that the (001)[110] texture is formed in the rolling of the β-phase (bcc structure) and it transforms into the α-phase according to the Burgers-relationship (0002)hex.//(001)cub. and [1120] hex.//[111]cub.

Fig. 14-21 shows the (110) poles of the (001)[110] texture of the bcc structure.

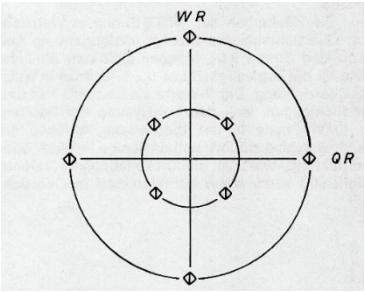

Fig. 14-21 – (110) poles of the (001)[110] texture of the bcc structure

Comparing Fig. 14-21 with Figure 14.20 (middle), it is proved that the texture of Fig. 14-20 (middle) is obtained after the transformation of the (001)[110] texture of the β-phase into the α-phase. This is one of the subjects relating to the transformation of elements, as described in Chapter 13.

As a result, Ti alloy sheets are products of sophisticated theory and a very complicated process. This is attributed to the fact that Ti is located on the extension of the straight line of refractory metals and adopts an hcp structure. In this way, where the element is located on the TC-YM diagram determines the fate of the element and its product.

(9) Zr alloys

Fig. 14-22 shows the alloying elements in the commercial alloys of Zr.

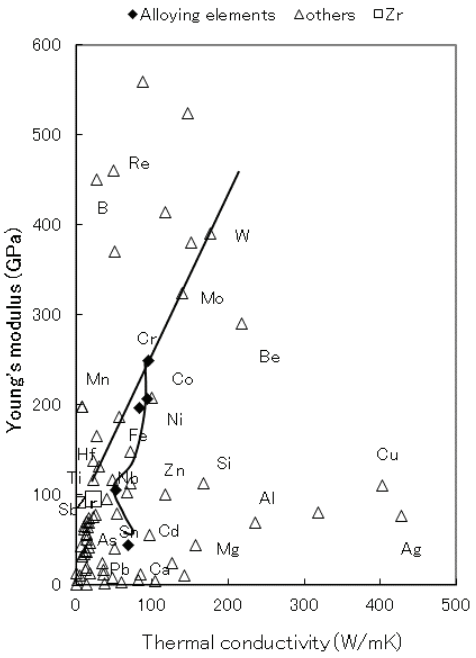

Fig. 14-22 – Alloying elements in the commercial alloys of Zr

Zr is located just under Ti on the diagram. Judging from its position on the TC-YM diagram, Zr has no remarkable features except for its low thermal neutron absorption cross-section. The application of Zr is limited in the cladding material of nuclear fuels; therefore, the alloying elements must have a small thermal neutron absorption cross-section. As shown in Fig. 8-1, the elements with a small absorption cross-section are elements mostly of low Young's modulus. Among them, the elements that can be added to Zr are only Sn and Al. Sn and Al are far away from Zr on the periodic table. But Sn and Al are near to Zr on the TC-YM diagram. In practice, Sn was selected for Zircaloy.

It was said that Sn was added to kill the harmful effect of nitrogen on the corrosion resistance of Zr. As shown in Fig. 5-2, Sn shows the same level of electrode potential as Fe and Cr, while Al shows lower electrode potential similar to W, Be, and Si.

The most remarkable story concerning Zr might be the story about the precipitates in Zr. [4]

The relationship between the Fe/Cr content, the solution treatment temperature, and the weight gain in the corrosion test in 633K water for 15 days was shown in Fig. 8-7.

The specimens that were solution treated at 1123K, containing 30/15 ppm Fe/Cr and 70/40 ppm Fe/Cr, respectively, show no precipitates in the Zr matrix, and show inferior corrosion resistance. In contrast to this, the other specimens show precipitates to a greater or lesser extent in the Zr matrix and show good corrosion resistance. This is due to the fact that the precipitate serves an effective cathodic site during the anodic oxidation of the Zr matrix and enhances the formation of passivation film on the surface.

It is also a fortunate coincidence that the solubilities of Fe and Cr are small in Zr and the electrode potentials of Fe and Cr are higher than that of Zr.

14.3 Summary

Until now, the characteristics of each alloy have been explained separately. In contrast to this, the TC-YM diagrams show the total view over the characteristics of each element schematically.

First, the basic characteristics of the alloys are determined depending upon

where the base metal is located on the TC-YM diagram.

Second, the effects of alloying elements are determined depending upon the relative locations of the alloying elements to the matrix metal on the TC-YM diagram.

References

1. Y. Mae, Anthropic principle observed in the material properties of Fe, J. Mater. Sci. Res. Vol. 6, No. 3, 2017, pp. 11-19.
2. U. Mizutani, The introduction to the electron theory of metals, Cambridge University Press, 2001, p. 228.
3. Y. Takeuchi and Y. Mae, Einfluss von der Hersttellungsbedingunngen auf Texturen und mechanischen Eigenschaften von TIAL6V4-Blechen, Z. Metallkde, Bd. 65, H. 11, 1974, pp. 676-680.
4. T. Isobe, T. Murai, and Y. Mae, Anodic protection provided by precipitates in aqueous corrosion of zircaloy, Zirconium in the nuclear industry, 11th international Symposium, ASTM STP 1295.
5. E. R. Bradley and G. P. Sabol, eds., American Society for Testing and Materials, 1996, pp. 203-217.

15. CONCLUSIONS

According to the experience of this author, when people start to learn about metallurgy, the first barrier might be the crystal structures of elements. Although the bcc-structured refractory metals gather at the 5th and 6th periods, and in the 4th, 5th, and 6th groups of the periodic table, the elements of fcc structures and hcp structures are distributed irregularly on it. Furthermore, the alkali metals of very low melting temperature adopt bcc structures identically to the refractory metals of highest melting temperatures. Under these situations, many beginners tend to give up understanding metallurgy logically. They tend to think that metallurgy is a kind of knowledge of memory.

This author passed a long research life at a company of non-ferrous metals products. Every time the theme was changed, he had to study the different subjects and accept them *a priori*. There were details but no principles across the elements.

On the other hand, the periodic table did not give enough information about the transition metals which are located at the inner side of the periodic table.

From these backgrounds, in order to understand the elements comprehensively, this author has developed the TC-YM diagram to complement the periodic table.

What are the points of the metallic elements?

They are **thermal conductivity and Young's modulus**. Thermal conductivity represents the electron structure in the elements. Young's modulus represents the binding force between atoms.

In every book on metallurgy, material properties such as crystal structure, atomic mass, density, atomic radius, melting temperature, heat capacity, heat of fusion, linear expansion coefficient, thermal conductivity, electrical resistance, Young's modulus, *etc*., are listed. These properties appear to be independent of each other. But it is not true. Most of the characteristics of elements are determined by these two factors. The specific combination of these two factors is a TC-YM diagram. The properties of elements are distributed regularly on the TC-YM diagram. Shortly, they are ruled by both thermal conductivity and Young's modulus.

The unsolved problems of the solid elements can be solved utilizing the TC-YM diagram, as follows:

1. Most of the physical properties of the solid elements are distributed regularly on the TC-YM diagram. Especially, crystal structures of elements are distributed beautifully on the TC-YM diagram. This means that they are controlled by both the electron configuration and the binding force of atoms.

2. The neutron multiple numbers are distributed regularly on the TC-YM diagram. They explain the anomalies in the Oddo-Hankins plot concerning the abundance of elements. They also have a relationship with the thermal neutron absorption cross-section of elements.

3. Even the properties of the lanthanides and actinides are determined by their positions on the TC-YM diagram.

4. The diffusion coefficients and DC ratios of elements in the matrix metals are distributed clearly on the TC-YM diagram. The diffusion coefficient of each element in each matrix metal is determined by the locations of the diffuser element and the matrix element on the TC-YM diagram.

5. The results of the analysis about the mechanisms of fast diffusion and slow diffusion show that the **repulsive force** is generated by the difference in the thermal conductivity and the Young's modulus between the foreign atoms and the matrix atoms. They also show that the atoms of high thermal conductivity and high Young's modulus such as gulf elements possess **hard electron shells** and in contrast to this, the elements of low thermal conductivity and low Young's modulus possess **soft electron shells**. **The combination of the repulsive force and the hardness of the electron shell gives rise to the fast and slow diffusions of foreign elements in metals, decides the solubility of elements in metals, and controls the solution hardening of metals by the alloying elements. It also decides the resistivity increase. This tendency appears in the diffusion of foreign elements in metals most typically.** Consequently, all the phenomena caused by the lattice distortion are apparently related with the diffusion coefficient of the alloying element.

In contrast, the hardenability of steel is directly related with the diffusion coefficient of elements.

In this way, major mysteries of solid elements were solved. But it is worthless if only the past mysteries were solved. The idea must be useful toward the future. A new idea has come to the mind of this author utilizing the idea of the TC-YM diagram. He hopes that various ideas will come to the minds of readers.

INDEX